University of Kentucky Doctoral Dissertations   Graduate School

2011

MICRONEEDLE-ASSISTED TRANSDERMAL DELIVERY OF NALTREXONE SPECIES: *IN VITRO* PERMEATION AND *IN VIVO* PHARMACOKINETIC STUDIES

Mikolaj Milewski
University of Kentucky, mikolajmilewski@wp.pl

Recommended Citation

ABSTRACT OF DISSERTATION

Mikolaj Milewski

The Graduate School

University of Kentucky

2011

MICRONEEDLE-ASSISTED TRANSDERMAL DELIVERY OF NALTREXONE
SPECIES: *IN VITRO* PERMEATION AND *IN VIVO* PHARMACOKINETIC STUDIES

ABSTRACT OF DISSERTATION

A dissertation submitted in partial fulfillment
of the requirements for the degree of Doctor of Philosophy in the
College of Pharmacy
at the University of Kentucky

By

Mikolaj Milewski

Lexington, Kentucky

Director: Dr. Audra L. Stinchcomb, Associate Professor of Pharmaceutical Sciences

Lexington, Kentucky

2011

ABSTRACT OF DISSERTATION

MICRONEEDLE-ASSISTED TRANSDERMAL DELIVERY OF NALTREXONE
SPECIES: *IN VITRO* PERMEATION AND *IN VIVO* PHARMACOKINETIC STUDIES

Naltrexone (NTX) is a drug used primarily in the management of alcohol dependence and opioid dependence. Based on several drawbacks associated with the oral and injectable intramuscular dosage forms of naltrexone currently available on the market, there is substantial interest in delivering naltrexone transdermally. Although naltrexone does not permeate skin at the rate sufficient to reach therapeutic plasma concentrations in humans, novel flux enhancement methods such as microneedles help address this challenge. Earlier work in humans has demonstrated that the use of microneedles achieves plasma concentrations in the lower end of expected therapeutic values. Further flux enhancement is desired to decrease the patch area while increasing drug transport rates. In the present work, several strategies aiming at *in vitro* flux maximization were employed including: formulation optimization, naltrexone salt screening, and naltrexone prodrug design. While naltrexone prodrugs did not reveal any improved permeation characteristics formulation optimization through decrease in vehicle microviscosity allowed a 5-fold increase in the percutaneous transport rates, and naltrexone glycolate salt selection provided an additional 1.5-fold enhancement in flux. One of the key observations was a good correlation (R^2 = 0.99) between vehicle microviscosity and drug transport rates across the microchannel pathway. This finding alone allowed for formulation optimization and, at the same time, provided a potential explanation for the low permeation of high-concentration naltrexone salts and prodrugs. *In vivo* studies were carried out in Yucatan minipigs using a "poke and patch" microneedle method to deliver NTX•HCl. These studies demonstrated that initial plasma concentrations spiked to 2.5 ng/ml but rapidly dropped to a plateau of below 1 ng/ml. This pharmacokinetic profile could be explained by the use of a mathematical model which identified the importance of microchannel closure kinetics on drug transport. Also, an estimate of diffusional resistance of the viable tissue associated with percutaneous NTX•HCl delivery through microchannels was obtained. Its relatively large value suggests that the effect of diffusional resistance of the dermis *in vivo* should not be ignored and must be accounted for in order to obtain a good in *vitro-in vivo* correlation.

KEYWORDS: Transdermal drug delivery, naltrexone, microneedles, prodrugs, mathematical modeling

Mikolaj Milewski

Student's signature

March 23rd, 2011

Date

MICRONEEDLE-ASSISTED TRANSDERMAL DELIVERY OF NALTREXONE
SPECIES: *IN VITRO* PERMEATION AND *IN VIVO* PHARMACOKINETIC STUDIES

By

Mikolaj Milewski

Dr. Audra L Stinchcomb

Director of Dissertation

Dr. Jim Pauly

Director of Graduate Studies

March 23rd, 2011

Date

RULES FOR THE USE OF DISSERTATIONS

Unpublished dissertations submitted for the Doctor's degree and deposited in the University of Kentucky Library are as a rule open for inspection, but are to be used only with due regard to the rights of the authors. Bibliographical references may be noted, but quotations or summaries of the parts may be published only with permission of the author, and with the usual scholarly acknowledgements.

Extensive copying or publication of the dissertation in whole or in part also requires the consent of the Dean of the Graduate School of the University of Kentucky

A library that borrows this dissertation for use by its patrons is expected to secure the signature of each user.

<u>Name</u>   <u>Date</u>

_____

_____

_____

_____

_____

_____

_____

_____

_____

_____

DISSERTATION

Mikolaj Milewski

The Graduate School

University of Kentucky

2011

MICRONEEDLE-ASSISTED TRANSDERMAL DELIVERY OF NALTREXONE
SPECIES: *IN VITRO* PERMEATION AND *IN VIVO* PHARMACOKINETIC STUDIES

DISSERTATION

A dissertation submitted in partial fulfillment
of the requirements for the degree of Doctor of Philosophy in the
College of Pharmacy
at the University of Kentucky

By

Mikolaj Milewski

Lexington, Kentucky

Director: Dr. Audra L. Stinchcomb, Associate Professor of Pharmaceutical Sciences

Lexington, Kentucky

2011

DEDICATION

To my wife and parents

whose enormous support, patience and understanding

allowed me to complete my dissertation

TABLE OF CONTENTS

LIST OF FIGURES

LIST OF ABBREVIATIONS

w/w	weight per weight
w/v	weight per volume
°C	degrees Celsius
µm	micrometer
ACN	acetonitrile
ANOVA	analysis of variance
APCI	atmospheric pressure chemical ionization
AUC	area under the curve
Cl	clearance
cm	centimeter
COX	cyclooxygenase
FDA	Food and Drug Administration
J	flux
h	hour
HCl	hydrochloride
HEC	hydroxyethylcellulose
HEPES	4-(2-hydroxyethyl)-1-piperazineethanesulfonic acid
HPLC	high performance liquid chromatography
IACUC	Institutional Animal Care and Use Committee
IND	Indomethacin
IV	intravenous
kg	kilogram
kHz	kilohertz
LC-MS-MS	liquid chromatography-tandem mass spectroscopy
log $K_{o/w}$	logarithm of octanol-water partition coefficient
logP	logarithm of permeability coefficient
logS_w	logarithm of water solubility
M	molar
MeOH	methanol
mg	milligram
mHz	millihertz
min	minute
ml	milliliter
mm	millimeter
mM	millimolar
MN	microneedle(s)
MP	melting point
MW	molecular weight
n	number
NaOH	sodium hydroxide
ng	nanogram

NMR	nuclear magnetic resonance
NTX	naltrexone free base
NTX•HCl	naltrexone hydrochloride salt
NTXol	6-β-naltrexol free base
NTXol•HCl	6-β-naltrexol hydrochloride salt
PEG 400	Poly(ethylene glycol) 400
PG	propylene glycol
pH	negative logarithm of hydronium ion concentration
pK_a	acid ionization constant
r2	coefficient of determination
SC	stratum corneum
SD	standard deviation
SDS	sodium dodecyl sulfate
TEA	triethylamine
TEWL	transepidermal water loss
TFA	trifluoroacetic acid
UV	ultraviolet

Chapter 1

Statement of the Problem

Alcohol and narcotic addiction are serious societal problems. Over 20 million Americans needed treatment for either alcohol or illicit drug abuse in 2009. Of these, only about 11% received adequate therapy, showing no change in treatment trends as compared to those needing treatment in previous years [1]. Apart from the direct impact on health, illicit drug abuse alone costs society an estimated $181 billion in lost productivity, criminal justice and related areas [2]. Modern approaches to alcohol and opioid addiction treatment usually combine psychotherapy and counseling with medication. A variety of different treatment categories are broadly used including: medical detoxification, long-term and short-term residential programs, outpatient drug-free treatment, agonist maintenance treatment for opiate addicts (methadone) or narcotic antagonist treatment (naltrexone), to name a few. Methadone use is limited due to serious cardiotoxicity, which has been linked to a high number of sudden deaths [3].

From a drug delivery point of view, naltrexone presents several challenging characteristics. Naltrexone (NTX) is a drug used primarily in the management of alcohol dependence and opioid dependence [4]. Our interest in delivering naltrexone transdermally is well-founded and based on several drawbacks associated with the oral and injectable intramuscular dosage forms of naltrexone currently available on the market. These include: significant first-pass effect, gastrointestinal side effects and poor patient compliance [5]. Although NTX does not permeate skin at the rate sufficient to reach therapeutic plasma concentrations in humans, novel flux enhancement methods such as microneedles (MN) can address this limitation [6]. The use of MN can substantially increase the rate of drug delivery through skin and create a great potential

for more effective delivery of drugs, including compounds that previously could not be delivered via this route of administration [7, 8]. Naltrexone's mode of action results in attenuation of euphoric effects of opioids and its effectiveness is well-established [4, 9-13]. The rationale behind NTX treatment is that the repetitive lack of desired alcohol/opiate effects will, over time, result in the decrease of craving thereby breaking the dependence. NTX itself, being an antagonist, does not present a problem of potential misuse [14, 15].

In the United States, naltrexone is currently available under three brand names: ReVia®, Depade® and Vivitrol®. The first two are available in the form of naltrexone hydrochloride 50mg tablets with a daily dosing regimen, the latter is a naltrexone 380mg extended-release intramuscular injection administered monthly. Additionally, low-dose naltrexone is prescribed for other therapeutic indications such as auto-immune disorders (multiple sclerosis). The oral dosing regimen is less than optimal and one of the main issues related to the NTX therapy is poor patient compliance. Moreover, gastrointestinal (GI) tract side effects as well as low and varied interpatient bioavailability (5-40 %) are further disadvantages of this route of administration [5]. In 2004, the Food and Drug Administration (FDA) approved Vivitrol®, which is an injectable formulation that can be used as an alternative. Vivitrol® injection overcomes some of the limitations associated with the oral formulations including the lack of compliance, pharmacokinetics with large daily fluctuations in plasma concentration, and GI toxicity. However, this formulation requires patients to come to a healthcare center to obtain a painful intramuscular injection. Moreover, in August 2008 FDA released an alert notifying healthcare professionals of the risk of adverse injection site reactions in patients receiving Vivitrol®. Serious injection site reactions including abscesses and drainage and cases of tissue necrosis needing surgical intervention have been reported [16]. Additionally, in case of

an emergency pain treatment, when medical opiate administration is necessary patients on Vivitrol® require very high opioid doses to counteract the presence of NTX. Hence, intramuscular injections are not an optimal route of NTX administration either. In general, the major problem associated with naltrexone therapy is noncompliance. A favorable treatment outcome requires effective counseling and careful monitoring of medication compliance.

Transdermal drug delivery represents a novel and alternative route of naltrexone delivery to the existing NTX formulations. Among potential benefits related to this method of drug administration are: elimination of the first-pass effect, lack of pain, prolonged zero-order delivery, transdermal patch self-application and better patient compliance [8, 17]. Typically, drug molecules delivered across skin at desired rates possess a range of favorable physicochemical properties that allow fast passage through the skin barrier. The overall barrier properties of skin (diffusional resistance) towards most xenobiotics can be well approximated by the barrier properties of the stratum corneum (SC) alone [18]. This outermost layer of skin, due to its structure and composition, greatly limits the pool of molecules that can be delivered percutaneously. Low molecular weight (<500 Da), $logK_{o/w}$ value about 2 and low melting point are usually evoked as critical parameters for a good transdermal delivery candidate [19]. Previous studies in our lab showed that NTX does not possess the necessary physicochemical properties for transdermal delivery at satisfying rates to achieve therapeutic concentrations *in vivo* [20]. Modifying NTX's physicochemical properties by the synthesis of its prodrugs and salts can significantly alter transdermal flux values. A prodrug is an inactive precursor of a drug, converted into its active form in the body by normal metabolic processes or chemical hydrolysis. It was shown that some straight-chain ester 3-O-NTX prodrugs afforded superior flux values over the parent drug [21]. These flux

however, were below values that would result in desired plasma levels in humans. Nonetheless, recourse to a new microneedle flux enhancement method proved to significantly improve percutaneous NTX delivery [6]. Microneedle use relies on the creation of transient disruption in the stratum corneum. As a result, the skin barrier properties are compromised and drug permeation is facilitated.

Microneedles offer several advantages over other enhancement methods and can be seen as a hybrid between a traditional transdermal delivery and subcutaneous injections. A great variety of microneedle types have been reported in scientific literature and the increasing number of publications suggests a great potential and interest in this particular technique [22-28]. Typically, "microneedles" denote an array of 200-1000 μm long protrusions fixed on a surface able to perforate the stratum corneum. Among popular types of microneedles are stainless steel solid microneedles [29]. In the most basic mode of application, MN are used to perforate SC and removed; subsequently a transdermal patch is applied – also referred to as a "poke and patch" method. In this way, microchannels (pores) are created in the skin allowing drug molecules to bypass the formidable barrier of SC and diffuse freely through deeper layers of the skin and into the microcirculation. Microneedles offer an advantage of simplicity over other physical enhancement methods and their application is painless [25, 30, 31]. In the case of MN-enhanced transdermal drug delivery, the traditional limitations on the lipophilicity and molecular size of a permeating molecule don't seem to hold. This creates great potential for the delivery of either hydrophilic and/or large molecules. The lack of optimal lipophilicity requirement brings about the option of using ionized, and therefore more water-soluble, molecules. In consequence, the driving force for diffusion can be increased by raising the drug concentration gradient across skin [6]. It has been reported that the application of MN in conjunction with NTX•HCl-containing transdermal patches

on humans afforded plasma concentrations in the lower end of expected therapeutic values [32]. It is the goal of this project to further increase the transdermal delivery of naltrexone (NTX) from a transdermal patch and gain a better understanding of microneedle-enhanced transdermal drug delivery, in terms of critical parameters governing the transport. The development of a mathematical model describing *in vivo* drug transport would facilitate optimization of future drug delivery systems.

Chapter 2

Research hypotheses

The thesis project is based on two major objectives. The first, narrower in scope, is to increase the transdermal delivery rate of naltrexone from a transdermal patch through microneedle-treated (MN-enhanced) skin. The second, wider in scope, is to gain better understanding of microneedle-enhanced transdermal drug delivery in terms of critical parameters governing the transport.

The major hypotheses that have driven this research project are as follows:

Hypothesis 1: Charged naltrexone species with high aqueous solubility and low molecular weight will increase the percutaneous flux through MN-treated skin.

It is commonly recognized that the physicochemical properties of the permeant affect its ability to cross the stratum corneum membrane in traditional passive transdermal drug delivery. Properties such as ionization, molecular weight, lipophilicity as measured by $logK_{o/w}$, hydrogen bonding potential, heat of fusion or melting point determine the solubility and permeability of a given drug. The solubility and permeability, in turn, will determine the maximum flux across skin. With respect to MN-enhanced permeant transport, the critical physicochemical parameters that would allow maximizing the flux have not been explicitly described. It is hypothesized that the presence of molecular charge and low molecular weight will provide high aqueous solubility resulting in high driving force for diffusion. Also, low molecular weight is anticipated to translate into high permeability through microchannel pathway due to its effect on NTX diffusivity in the microchannels.

Hypothesis 2: Non-rate-limiting transdermal formulation of low microviscosity will increase the naltrexone percutaneous flux through MN-treated skin.

Although many literature reports focused on the microneedle effectiveness in the percutaneous drug delivery area, one aspect that lacks extensive examination is the influence of the formulation on the drug transport rates across MN-enhanced skin. In passive transdermal drug delivery the use of permeation enhancers in the formulation has been shown to substantially increase percutaneous flux. However, in the presence of microchannels in the skin it is anticipated that the major diffusional barrier of the stratum corneum will be bypassed and the formulation characteristics may have a radically different effect. It is hypothesized that the selection of a low-microviscosity aqueous-based formulation will provide high mobility for naltrexone and a non-rate-limiting environment for permeation across MN-treated skin. Additionally, it is hypothesized that the elimination of formulation excipients, which can permeate into dermis increasing its diffusional resistance, will allow further improvement of flux.

Hypothesis 3: The analysis of *in vitro-in vivo* correlation in the naltrexone permeation data will elucidate the effect of *in vivo* microchannel closure on the MN-assisted drug delivery and allow calculation of diffusional resistance of dermis separating microchannel from dermal microvasculature.

Typically, in traditional passive transdermal drug delivery the establishment of in *vitro-in vivo* correlation is based on the fact that stratum corneum constitutes the major barrier for drug diffusion. Therefore, accounting for the different skin surface area involved in diffusion alone allows, in many cases, for providing a reasonable link between *in vitro*

and *in vivo* conditions. In the case of MN-assisted transport, several additional factors must be taken into account. The contribution of flux through microchannels as compared to flux across the skin around the microchannels, the diffusional resistance of the dermis and the kinetics of microchannel closure are expected to play a substantial role in establishment of the *vitro-in vivo* correlation. It is hypothesized that the development of mathematical model accounting for the above phenomena will allow for assessment of the role of microchannel closure on drug transport. Specifically, it is hypothesized that the time-dependent changes in microchannel electrical impedance will be mimicked by corresponding changes in microchannel permeability to NTX. Also, it is hypothesized that it will be possible to assess the diffusional resistance of the dermis separating microchannel from dermal microvasculature .

Chapter 3

Research plan

3.1. Development of a mathematical model for *in vitro* microneedle-assisted drug delivery

MN-assisted drug permeation can be analyzed without the use of any mathematical model by comparison of drug apparent permeability coefficients for MN-treated and untreated skin. Such approach allows quick estimation of the "enhancement ratio", which represents the fold-increase in flux (permeability coefficient) as a result of the MN skin treatment. However, this simple analysis lacks insight and is not easily transferable to different experimental conditions. Hence, a mathematical model which accounts for existence of two parallel routes of permeation and individual diffusional resistance of skin layers will be introduced. This model will accommodate the change in the number of microchannels created by microneedles, assign the permeability coefficients to unionized and ionized species permeating through either MN-treated or untreated skin, and account for different skin thickness used in the *in vitro* diffusion experiments.

3.2. Characterization of the formulation physicochemical properties and their influence on the flux of naltrexone hydrochloride across microneedle-enhanced Yucatan minipig skin

The field of transdermal formulation optimization for MN-assisted drug delivery is not well developed and an abundance of literature in the area does not exist. In the presence of microchannels the diffusional resistance of the skin decreases substantially and transdermal formulation is expected to exert an even more pronounced effect on the overall drug transport rate than in passive percutaneous transport. Hence, the effect of

parameters such as micro- and macro-viscosity of the formulation, as well as its osmotic pressure and pH will be examined. A Brookfield DV-III LV programmable cone/plate rheometer with a CPE-40 spindle will be used for measuring viscosity of the donor solutions. All determinations will be carried out at 32°C using a circulating water bath TC-102. Osmotic pressure will be determined through use of a freezing-point osmometer (Micro-Osmette™ from Precision Systems, Inc.). Additionally, pH measurements will be carried out using a pH-meter (Sentron Titan benchtop meter).

3.3. Characterization of the physicochemical properties and determination of *in vitro* microneedle-enhanced transdermal flux of naltrexone prodrugs across Yucatan minipig skin

Physicochemical parameters of the permeant such as ionization, molecular weight, lipophilicity as measured by octanol-water partition coefficient ($logK_{o/w}$), and melting points play an important role in the design of a successful transdermal drug candidate. These parameters affect permeability coefficients and solubility, which in turn determine flux. Additionally, in the case of prodrugs, the chemical and enzymatic stability are critical. A prodrug should possess adequate stability in the formulation but be quickly metabolized to the active form either by chemical or enzymatic processes *in vivo*. The objective of this study is to investigate the stability, solubility and permeation of various groups of naltrexone prodrugs. Prodrug stability studies in donor (0.3M acetate buffer pH 5.0) and receiver solutions (25mM HEPES-buffered Hanks' balanced salt solution pH 7.4) will be initiated by charging a 10 ml volume of hydrolysis media thermostated at 32 °C with ≈1 mg of prodrug, filtering the solution through a 0.45μm nylon syringe filter (Acrodisc® Premium 25mm Syringe Filter) and taking samples of the filtrate over a period of 120 h. Samples will then be diluted with acetonitrile ACN-water 70:30 (v/v) for high-

performance liquid chromatography HPLC analysis. Apparent pseudo-first-order hydrolysis rate constants will be estimated from the slope of the log-transformed amount of prodrug remaining in the medium over time. Prodrugs, which possess adequate stability, will be further tested in *in vitro* permeation studies using MN-treated skin. A PermeGear flow-through (In-Line, Riegelsville, PA) diffusion cell system will be used for permeation studies through MN-enhanced Yucatan minipig skin. The flow rate of the receiver fluid will be set at 1.5 ml hr^{-1} in order to provide sink conditions as well as mimic physiological conditions. HEPES-buffered Hanks' balanced salts solution will be used as receiver solution to preserve tissue viability [33]. The temperature of the diffusion cells will be maintained at 32 °C (the temperature of the skin) with a circulating water bath. The diffusion experiment will be initiated by charging the donor compartment with 250-400 µl of donor solutions. Samples will be collected every six hours and analyzed by HPLC. The cumulative quantity of drug collected in the receiver compartment will be plotted as a function of time. The flux value for a given experiment will be obtained from the slope of the steady-state portion of the cumulative amount of drug permeated vs. time data. In addition, the concentration of the drugs in the skin will be determined after the 48h experiment. Transepidermal water loss (TEWL) will be used to determine the barrier integrity of the skin.

3.4. Characterization of the physicochemical properties and determination of *in vitro* microneedle-enhanced transdermal flux of naltrexone salts across Yucatan minipig skin

In the passive transdermal delivery, the physicochemical parameters of the permeant, such as: ionization, molecular weight, lipophilicity as measured by $logK_{o/w}$, and melting points, play an important role in the design of a successful transdermal drug candidate. These parameters affect permeability coefficients and solubility, which, in turn,

determine flux. The objective of this study is to investigate the pH-dependent solubility and permeation of various naltrexone salts. A naltrexone salt, which possesses the highest aqueous solubility at pH 5.0 will be further tested in *in vitro* permeation studies through MN-treated skin. pH-solubility profiles of naltrexone salts will be determined at 25 °C. At first, excess solids (NTX salts) will be added to glass vials containing 2 ml of water. Solubility at different pH values will be determined by stepwise titration with HCl or NaOH solutions. At each addition of HCl or NaOH, the suspension will be equilibrated for 24 h, the pH value will be recorded, and an aliquot will be removed and spin-filtered for 1 min in VWR centrifugal filters (0.2 μm membrane) at 25 °C. The filtrate will be diluted with an adequate amount of acetonitrile (ACN):water 70:30 (v/v), and resulting solution analyzed by high pressure liquid chromatography (HPLC). A PermeGear flow-through (In-Line, Riegelsville, PA) diffusion cell system will be used for permeation studies through MN-enhanced Yucatan minipig skin. The flow rate of the receiver fluid will be set at 1.5 ml hr^{-1} in order to provide sink conditions as well as mimic physiological conditions. HEPES-buffered Hanks' balanced salts solution will be used as receiver solution to preserve tissue viability. The temperature of the diffusion cells will be maintained at 32 °C (the temperature of skin) with a circulating water bath. The diffusion experiment will be initiated by charging the donor compartment with 250-400 μl of donor solutions. Samples will be collected every six hours and analyzed by HPLC. The cumulative quantity of drug collected in the receiver compartment will be plotted as a function of time. The flux value for a given experiment will be obtained from the slope of the steady-state portion of the cumulative amount of drug permeated vs. time data. In addition, the concentration of the drugs in the skin will be determined after the 48h experiment. Transepidermal water loss (TEWL) will be used to determine the barrier integrity of the skin.

3.5. Development of a mathematical model for *in vivo* microneedle-assisted drug delivery

The mathematical model for *in vitro-in vivo* correlation will include the following three components: a diffusion through the MN-treated skin module, a microchannel closure module, and a compartmental pharmacokinetic module. The first module will be analogous to the mathematical model for *in vitro* microneedle-assisted drug delivery (**3.1**). This module will account for existence of two parallel routes of permeation and diffusional resistance of skin layers. The second module will account for the kinetics of microchannel closure, which has been shown to follow approximately exponential behavior. Finally, the third module, will be a typical compartmental pharmacokinetic model with systemic clearance as a major parameter.

3.6. Determination of plasma pharmacokinetic parameters and *in vivo* MN-enhanced transport of naltrexone hydrochloride in Yucatan minipig

Yucatan minipig skin has been recognized as a good model for human skin [34-36]. Additionally, due to its size Yucatan minipig is expected to be an approximate model of human pharmacokinetics. The pharmacokinetic (PK) parameters of I.V. NTX•HCl will be determined. Data analysis will be carried out using compartmental modeling (WinNonLin, Pharsight®). After gathering the I.V. data, 3-day transdermal studies with a formulation optimized for MN-enhanced transdermal delivery of naltrexone (**3.2**) will be performed. The plasma concentrations of naltrexone will be evaluated with a LC-MS-MS method. In the sample preparation procedure, all standards and samples of volume 200 µl will be extracted with 1ml of acetonitrile:ethyl acetate (1:1, v/v), resulting in protein precipitation. The mixture will be vortexed for 15 s and centrifuged at 12000xg for 20 min. The supernatant will be transferred to a glass tube and evaporated under nitrogen. Then, the residue will be reconstituted in 100 µl acetonitrile, sonicated for 10 min and

13

vortexed for 15 s. Samples will be transferred into low volume inserts in HPLC vials and injected into the LC-MS-MS system. Positive mode atmospheric pressure chemical ionization will be used for detection of naltrexone (APCI+). The analysis of the *in vivo* data will provide evidence regarding the critical factors involved in MN-assisted drug transport in Yucatan minipig. The focal points of interest include: estimating the diffusional resistance of the dermis in *vivo*, kinetics of microchannel closure and the use of the mathematical model (**3.5**) to predict the potential of delivering other drugs via a MN-enhanced skin route.

Chapter 4

Background and literature review

4.1. Introduction

Skin has evolved to provide an efficient barrier at the interface of the external environment and the body. The formidable skin barrier properties greatly limit the permeation of xenobiotics [18, 37]. This protection against toxicological agents makes life in a terrestrial environment possible. However, the same skin structure that is advantageous in terms of the protection against harmful stimuli is also a drawback from the perspective of percutaneous drug delivery. As compared to the traditionally employed oral route of drug delivery, transdermal drug administration can offer several advantages, e.g. avoidance of hepatic first-pass metabolism, time-independent approximately zero-order delivery, the ease of administration, and the possibility of immediate termination of the treatment when needed [8]. However, the aforementioned formidable barrier properties of the skin limit the pool of drugs that can be effectively delivered to the systemic circulation. One of the drugs that does not permeate the skin at a sufficiently high rate to provide therapeutic plasma concentrations *in vivo* is naltrexone. To address this obstacle, permeation enhancement methods can be used [17, 38]. It was demonstrated that with the help of microneedles, which create transient microchannels through the skin barrier, naltrexone transport rates can be increased significantly [6, 32, 39].

In the following paragraphs the structure of the skin will be discussed in more detail and the potential challenges of traditional transdermal drug delivery will be presented. Then, the prevalence of the alcohol and opioid addiction in the U.S.A. will be described and the need for better drug therapies emphasized. Finally, current naltrexone dosage form limitations will be addressed and the employment of transdermal enhancement methods

to overcome the insufficient permeation rate of naltrexone across skin will be discussed further.

4.2. Structure and function of the skin

The skin is the largest organ in the human body. Its primary functions are related to the protection against harmful external conditions and containment of bodily fluids. In an average adult human skin surface area is close to 1.8 m^2 and is the largest organ of the human body [40]. The thickness of skin varies with anatomical site and can be as low as approximately 1 mm up to 4 mm. Typically, it weighs 15 % of the total body weight [41, 42]. The primary protective function is exerted through stratum corneum which provides an interface of significant barrier properties between the organism and its external environment. Not less important is skin's role in preventing water loss and ensuring proper water homeostasis, protecting against ultraviolet radiation, and microbial infection. In one's lifetime skin suffers from multiple physical and chemical insults, however, skin possesses a formidable ability for self-repair. Small flaws in the continuum of the barrier, such as scratches and minor surface wounds, are healed quickly and without any permanent loss of the skin function at the affected site. The rate of wound healing is an area of active research as it is of major clinical and scientific interest [43-46]. Skin's ability to recover from minor insult is of substantial importance for the current work as the viability of the microchannels created by microneedles determines the time window of MN-enhanced drug delivery through a "poke and patch" method and will be briefly addressed in **Chapter 10**. On the other hand, after suffering from a major insult, the skin does not possess the ability to fully restore the original functional state of the barrier. It manifests itself as scar formation – not only the skin's mechanical properties are permanently impaired but also appendages such as hair follicles are never regenerated [18]. Another important function of the skin is related to the temperature

regulation. Under conditions of very cold weather, the peripheral blood flow through skin is diminished with the aim of protection of body organs such as brain and heart that are vital for survival. Conversely, under hot weather conditions peripheral blood flow is increased and eccrine glands produce significant amount of sweat to reduce the body temperature. This temperature regulation exerted by skin is an important contributor to overall body homeostasis. Additionally, biochemical metabolites are also excreted with eccrine glands. The mechanical strength of the skin is a necessary prerequisite for proper functioning in the natural environment and enables to resist physically harmful stimuli [37]. The typical cross-section of human skin reveals the existence of two distinct layers: epidermis and dermis as shown in **Figure 4.1**. The top-most epidermis can be further divided, from outside inward, into stratum corneum, stratum lucidum, stratum granulosum, stratum spinosum and stratum basale. At the interface between epidermis and dermis the basement membrane provides adhesion of the two strata. The dermal layer lies directly above the subcutaneous fat layer.
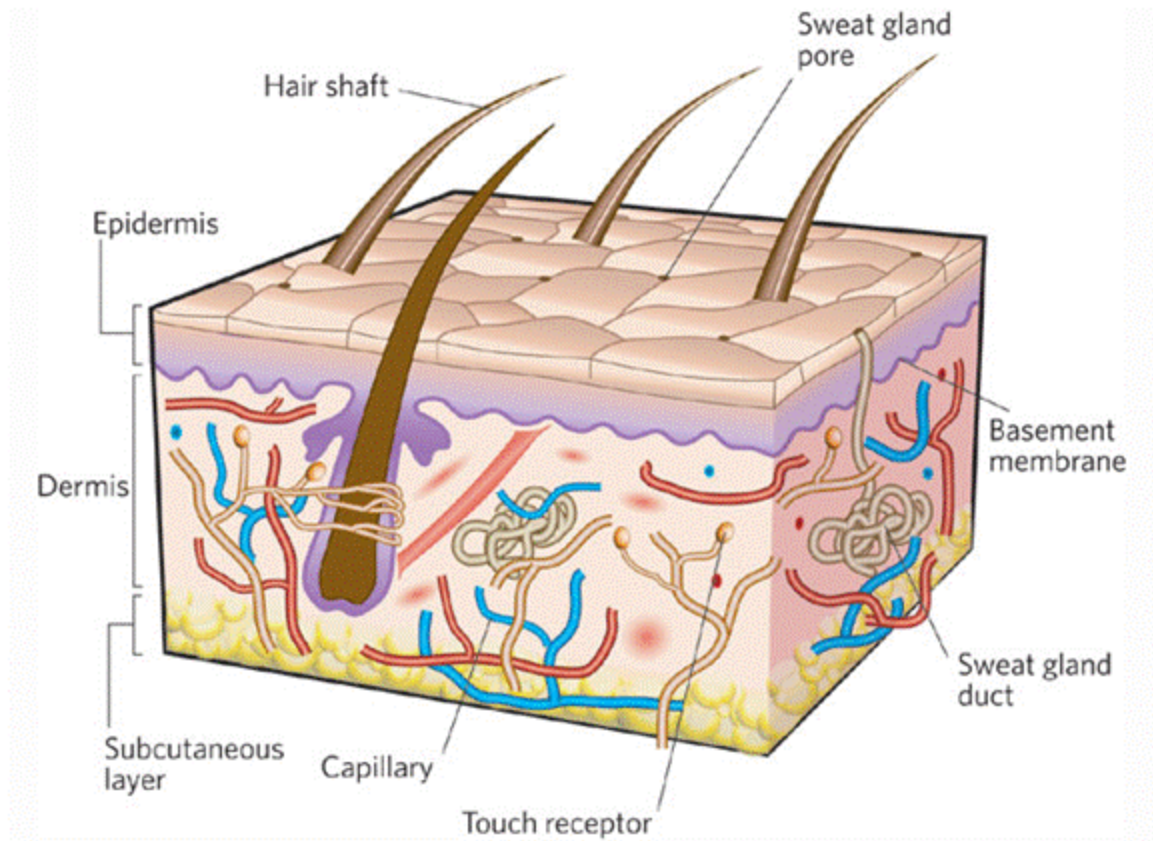
Figure 4.1. A cross-sectional diagram of human skin

Reprinted with permission from Nature 445, 874-880 (22 February 2007)

4.2.1. Stratum corneum

The stratum corneum (horny layer) is the outermost layer of the epidermis. It is also the most distinct layer of the skin in the sense that its composition imparts the barrier properties to the whole skin. The anatomy of stratum corneum is substantially different from all other skin layers. The bulk of this stratum is built of large, flat, and hexagonal cells. At this stage of final differentiation, the cells are dead and fully keratinized. The horny layer undergoes constant renewal through upward migration of the cells from the underlying viable epidermis and shedding off of the topmost cells in the process called "desquamation". The complete turnover of the horny layer takes around two weeks in

healthy humans [37]. An individual corneocyte is composed of keratin which fills up the inside of the cell together with so called "natural moisturizing factor" – a mixture of compounds, amino acids and α-hydroxy acids, that provide the adequate water sorption potential of the stratum corneum. This assures the proper level of hydration (under normal conditions around 20% water) [47]. The outside of the corneocyte forms a cornified envelope and is built of insoluble proteins loricirn and involucrin. Cornified envelopes of neighboring cells are linked together by corneodesmosomes. These structures must be degraded first in order for the outer stratum corneum cells to slough off the surface [48, 49]. The exact thickness of the stratum corneum varies depending on the region of the body. For example, at the friction surfaces of the body such as palm and soles stratum corneum can be up to several hundreds of micrometers thick. Typically, however, around 15-20 corneocytes stacked vertically one upon each other to form the thin layer around 10-20 µm-thick [50]. The overall structure of the horny layer is often referred to as a "brick and mortar" arrangement, with keratinized corneocytes corresponding to bricks and intercellular lipids corresponding to mortar [51, 52]. Stratum corneum possesses a very dense structure that makes its physicochemical properties stand out as compared to all other skin strata. The exceptional lipid composition of the "mortar" built of long chain ceramides, free fatty acids, and cholesterol in approximately equimolar ratio imparts unique lipid phase behavior. Unlike in the phospholipid-based membranes, the horny layer lipids are mainly present in the crystalline phases, with smaller subpopulation of lipids in the liquid phase [53]. Both the crystalline nature and the presence of a 13 nm lamellar strata of lipids between corneocytes are believed to be critical for the proper functioning of the skin barrier. The intercellular lipids are organized in the lipid bilayers with alternating hydrophilic and hydrophobic strata as demonstrated in **Figure 4.2**.
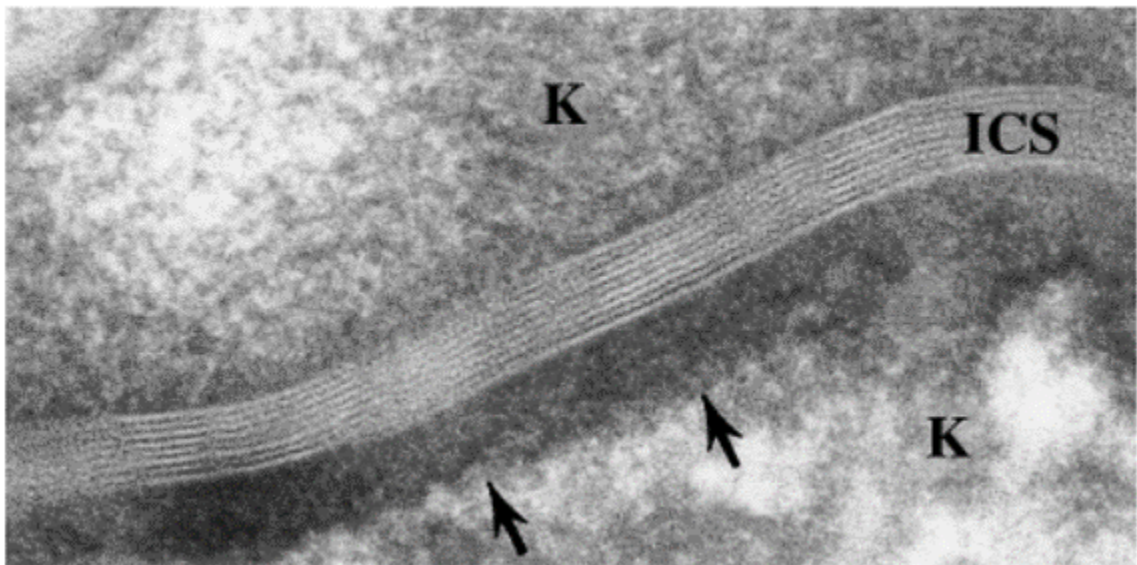
Figure 4.2. Electron micrograph showing the stacked and patterned lamellar membrane sheets in a single intercellular space in mouse SC postfixed with ruthenium tetroxide. The cornified envelope of the lower corneocyte is clearly visible (arrows); ICS, intercellular space; K, keratin contents of the corneocytes bordering the intercellular space. Original magnification x 200,000.

Reprinted with permission from J. Invest. Dermatol. 2003 Aug;121(2):231-41.

Thanks to the unusual composition of the horny layer it is often distinguished as a unique layer of different and very high diffusional resistance as compared to any other portion of the skin. From the drug delivery perspective it means that the horny layer represents the rate-determining step in the diffusion across skin process. In other words, the rate of permeation through the skin can be well-approximated by the permeation across stratum corneum alone. [54]. In its dry state, the intercellular space is filled mostly by lipid matrix accounting for 20 % of the mass while the intracellular space is

predominantly composed of fibrous, 65-70 %, and non-fibrous, 5-10 %, protein [50]. While under normal humidity conditions the stratum corneum absorbs water from the environment to the extent of around 20% of its dry mass, under humid or aqueous conditions the amount of water retained in the stratum corneum may increase several-fold affecting its physical state – skin becomes more pliable – and facilitating the permeation of hydrophilic xenobiotics. On the other extreme, ultra dry conditions cause the dehydration of the stratum corneum and render it more brittle which may manifest itself as chapped lips or windburned skin. It used to be thought that stratum corneum was metabolically inert, and it was treated like a thin lipoidal sheet covering more active viable layers of the epidermis. More recently, however, discoveries illustrating that the biological and chemical activity of the stratum corneum is very intricate and complex have been made [48]. The desquamation involves several enzymes that degrade corneodesmosomes in a specific pattern to facilitate the exfoliation process. Although the exact nature of those processes is not known, it was suggested that water content and pH play a significant role in the activity of these enzymes [55, 56].

4.2.2. Viable epidermis

Viable epidermis is sandwiched between the dead stratum corneum layer and the dermis. It is composed of living cells forming, from outside inward, stratum lucidum, stratum granulosum, stratum spinosum and stratum basale. The thickness of this layer is around 100-200 micrometers [42, 57]. The stratum basale is the bottom-most layer of the epidermis in direct contact with the underlying dermis. This layer of undifferentiated cubical cells constantly proliferate producing new cells through mitosis. This constant production of cells provides basis for turnover of the skin layers. The complete migration of an undifferentiated keratinocyte from the stratum basale to the terminally differentiated

corneocyte of the stratum corneum takes around 30-40 days. Cells that migrate upward across spinosum layer to stratum granulosum and to stratum lucidum undergo gradual differentiation. The processes involved in their differentiation are: elimination of cell nuclei, intensive synthesis of keratin, lamellar bodies development [53], and successive flattening of the cells. At the flat (non-interdigitated) interface of stratum granulosum and stratum corneum the extrusion of lamellar bodies takes place. Polar lipid precursors are enzymatically converted into nonpolar products which then form lamellar structures and become the intercellular "mortar" surrounding corneocytes [57]. On the other hand, the interface between dermis and viable epidermis is highly interdigitated forming many ridges and rivets that increase the interaction surface and provide better adhesion of the these layers. Chemically, keratinocytes of the stratum basale are attached to the basement membranes by proteinaceous hemidesmosomes, which enable anchoring of the cells to the dermal layer. From the histological perspective keratinocytes are predominant and form the bulk of cells present in the viable epidermis. Additionally, Langerhans cells of leukocyte origin are present and exert immunological functions by presenting antigens on their surface [47]. Also, melanocytes can be found at the epidermal-dermal junction. Their role is the production of melanin, the pigment responsible for the darkening of the skin under the control of melanocyte-stimulating hormone and ultraviolet light [18]. Other cells, such as lymphocytes and macrophages are present in smaller quantities and are also involved in immune response. The epidermis is avascular in nature and, in consequence, nutrients and waste products must diffuse across the dermal-epidermal junction in order to provide the necessary exchange for the living epidermal cells. Similarly, xenobiotics applied to the skin must cross the whole epidermis thickness and through the epidermal-dermal junction to be finally swept away by the blood flow in the microvasculature and delivered systemically.

4.2.3. Dermis

The dermis is a skin layer situated between the epidermis and subcutaneous fat. The typical thickness of this layer is around 1 millimeter, although it varies greatly with anatomical site [42, 53, 58]. It may be as thin as 300 micrometers on eyelids and up to 3 millimeters on the back. The dermis, unlike the epidermis, lacks typical lamellar structure although there are fine differences between upper (papillary) dermis and lower (reticular) dermis. The structure of the dermis is composed of a complex meshwork of structural fibers: collagen and elastin, located in a ground substance made out of a mucopolysaccharidic gel. From the perspective of transdermal drug delivery, dermis is often viewed as an aqueous gel-like structure with drug molecular mobility being not less than 1/10 of that seen in water [18]. Krestos et al. suggested that the diffusivity of free drug in dermis is around 3.7-fold lower than in water showing no selectivity with respect to physicochemical properties of the drug [59]. For most drugs this skin layer provides minimal diffusional resistance, although it may change for highly lipophilic drugs, which may experience low solubility in the aqueous environment of the dermis [60]. A variety of structures are present in the dermis, most notably, sensory nerve endings, skin appendages such as hair follicles, sebaceous glands, eccrine glands, and apocrine glands. Eccrine (sweat) glands produce sweat, a slightly acidic dilute salt solution of pH 5, believed to play a crucial role in the protection against the excess microbial growth on the skin surface. These glands are stimulated in response to heat and emotional stress. The sebaceous glands, colocalized with hair follicles, secrete sebum; a lipophilic substance composed mainly of free fatty acids, waxes, and triglycerides, which lubricate the skin surface and help maintain the surface pH at around 5. Although dermis is mostly acellular, fibroblasts responsible for the production of structural fibers and mast cells synthesizing the ground substance can be found. It is noteworthy that skin appendages such as hair follicles and sweat ducts, which extend to the surface of the skin across

stratum corneum, can be seen as offering an alternative permeation pathway for molecules permeating the skin. These shunt routes are thought to play some role in the early times of the permeation process for some polar molecules, but their contribution to the overall permeation is typically negligible because of the very limited area of around 0.1% of total skin surface available for this route [61, 62].

4.2.4. Microvasculature

Cutaneous vasculature originates from deeper-residing arterial vessels and muscles. It forms two separate horizontal plexuses in the dermis, which are connected through vertical vessels [42] as demonstrated in **Figure 4.3**. The superficial (papillary) plexus is located at the interface of the papillary and reticular dermis and nourishes papilla through vertical vascular loops. The arterioles and venules in the hairpin-like loop are connected through dermal capillaries. In the papillary plexus the vessels are represented by 25-μm-in-diameter arterioles and venules to 5-15-μm-in-diameter capillaries. The capillaries are built of a single fenestrated endothelial cell layer followed by a discontinuous outer layer of pericytes and a basement membrane [42]. The deeper (reticular) plexus is located close to the dermal-hypodermal junction and provides nutrients to hair follicles and eccrine glands. Dermal arterioles and venules of the reticular plexus are larger - 50-100 μm in diameter.
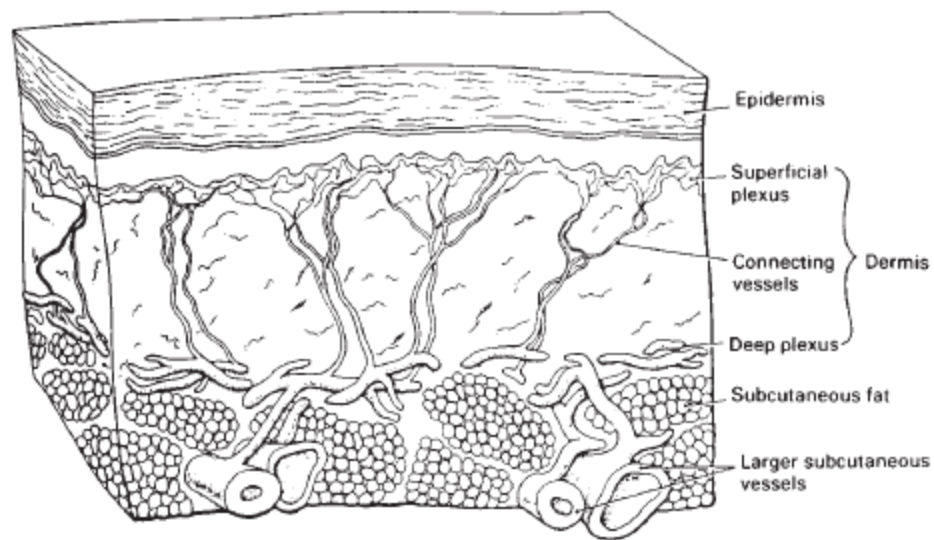
Figure 4.3. Dermal vasculature

Reprinted with permission from Reprinted with permission from Dermatology Nursing.

2005;17(1):62

Capillaries of the superficial plexus are located within approximately 0.1 - 0.2 mm of the

skin surface. The lymphatic system is also present in the dermis and plays an important

role in controlling the pressure of the interstitial fluid, removal of excess fluid and eliciting

immune responses. It originates from blind lymphatic capillaries and forms two plexuses,

similar to the blood vasculature, one superficial and another deep. Lymphatic system

may play a role in the percutaneous transport of large molecules such as interferon [63]

4.3. Transdermal drug delivery

Transdermal drug delivery offers distinct advantages over more ubiquitous oral drug

delivery. Some of the most notable features of this route of systemic delivery are the

avoidance of drug stability issues in the gastrointestinal tract and the first-pass effect, the

ease of application, and approximately zero-order delivery rates that result in steady-

state drug plasma levels [18]. The major challenge often encountered in the field of percutaneous drug delivery is the slow permeation rate across skin [64]. The overall therapeutic effect of the therapy mainly relies on the ability to achieve and maintain the drug plasma levels in the relevant therapeutic window providing desired pharmacological action. The drug plasma levels are controlled by the rate at which the drug is transported into the systemic circulation and the rate at which it is removed. Therefore, there is no general "minimum" permeation rate that would guarantee the therapeutic success as different drugs will possess not only different skin penetration rates, but are also characterized by varied systemic clearance values. While the systemic drug clearance values are determined by a myriad of complex physiological processes typically including renal and hepatic contributions, the drug skin absorption relies mainly on passive diffusion.

4.3.1. Routes of penetration

Upon application of drug formulation to the skin, the permeant must first passively diffuse out of the vehicle. When released from the formulation, it partitions into one of the permeation routes available through the stratum corneum. The main permeation pathway is a function of the physicochemical properties of the drug in question [54]. The pathways available include: appendageal, transcellular, and intercellular. For a moderately lipophilic compound ($logK_{o/w}$ around 0.5 - 3.5) the preferred permeation pathway is the tortuous intercellular route via intercellular lipids, or stratum corneum "mortar" [65]. After diffusing along the preferred stratum corneum permeation pathway the drug molecule partitions into an effectively aqueous milieu of the viable epidermis, which it needs to traverse to ultimately reach the upper portion of the dermis where the microvasculature is located. Next, the drug enters the blood capillaries and is swept away by the bloodstream into the systemic circulation. The driving force for passive

diffusion is the drug concentration (or more precisely activity) gradient across the barrier. It has been shown that for typical, small and moderately lipophilic drugs, that the stratum corneum presents the major diffusional barrier. As mentioned earlier, the horny layer is not homogeneous in nature; rather, its heterogeneity can be represented by a simplified "brick and mortar" model. In this analogy, the lipid domain, or "mortar", was identified as the barrier to drug diffusion across the stratum corneum. Therefore, the rate-determining step in skin permeation would be the permeation through the horny layer alone. The diffusional resistance of the viable epidermis and dermis is typically negligible. Exceptions to this common scenario are known and are dependent on the physicochemical properties of permeants. For very hydrophilic compounds the partitioning into the stratum corneum's lipid domain becomes unfavorable and permeation through a "polar", possibly appendageal, pathway must be taken into account to explain the skin permeation [66]. Also, high molecular weight permeants possess very low diffusion coefficients within the lipid domain and the existence of an alternate permeation route must be accounted for to satisfactorily explain the experimental data. The existence of the "polar", possibly appendageal, permeation pathway is supported by experiments, which showed no dependence of the permeation of hydrophilic and large compounds on their lipophilicity and small dependence on the size of the permeant. Both of these observations suggest a permeation pathway distinct from the intercellular route. On the other hand, for very lipophilic compounds, the low aqueous solubility becomes the limiting factor and the transport through the aqueous layers of the skin such as viable epidermis and dermis is rate determining [66].
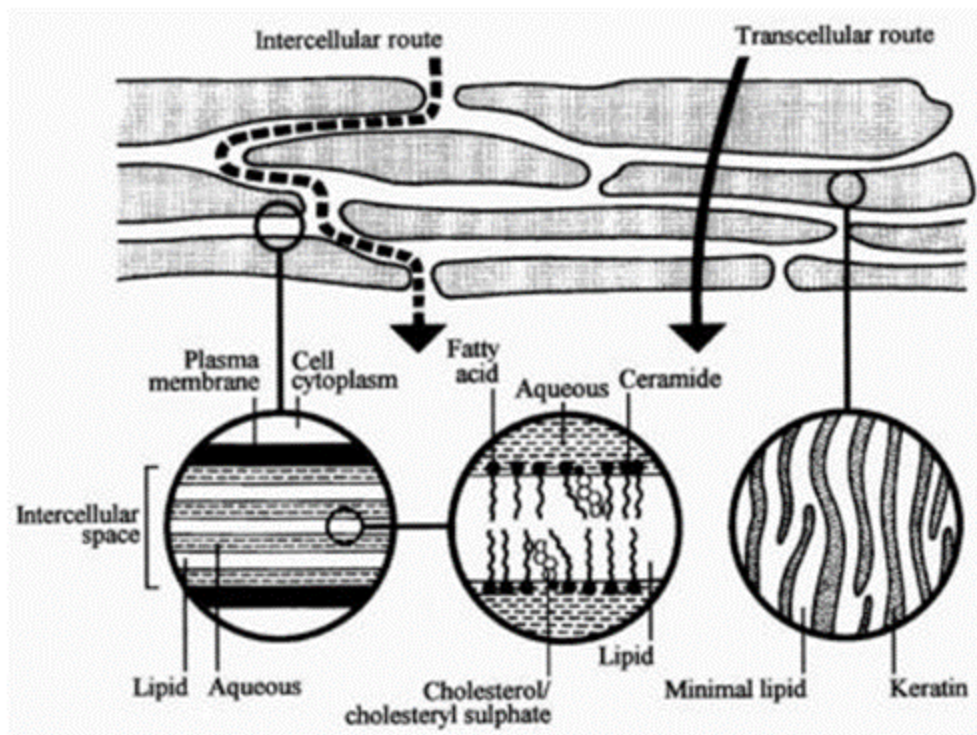
Figure 4.4. A schematic depiction of permeation across stratum corneum via intercellular and transcellular routes. Appendageal route is not depicted.

Reprinted with permission from Eur. J. Pharm. Sci. 14, 101-114

Overall, the three distinct permeation pathways across the horny layer: intercellular, transcellular and appendageal are not mutually exclusive, and xenobiotics may pass through the stratum corneum by a combination of these routes. The schematic depiction of intercellular and transcellular routes is presented in **Figure 4.4**. The relative contribution of each of these pathways to the total flux will depend on the physicochemical properties of the drug. The brief characterization of the three pathways is presented below.

4.3.1.1. Intercellular

The intercellular pathway is commonly believed to be the main pathway by which the low-molecular weight and moderately lipophilic compounds traverse the stratum corneum [58, 67]. It is the only continuous phase of the stratum corneum [51]. The intercellular lipids form large sheets stacked one upon another forming multiple bilayers. The intercellular volume is estimated to be 5 – 30% of the total stratum corneum volume [52] with the thickness of a single bilayer around 13 nm [68]. There are between 4 and 20 such bilayers between two adjacent corneocytes. The permeants diffuse within the lipid domain around corneocytes through a tortuous route, which implies that the actual length of the permeation pathway is not equal to the stratum corneum thickness, but rather is a multiple of it [69].

4.3.1.2. Transcellular

The transcellular pathway involves permeants' diffusion through the transcellular proteinaceous, keratin-filled corneocytes as well as across transcellular lipid domains. This is due to the non-continuous nature of the transcellular environment. Hence, a drug that traversed the stratum corneum by this route would experience multiple partitioning between the aqueous in nature corneocyte interior and the intercellular lipid domain. It is believed that such process would be generally unfavorable and the contribution of this pathway to the overall transport of drugs across the horny layer is minimal with some exceptions [70, 71].

4.3.1.3. Appendageal

The appendageal pathway (shunt pathway) refers to the transport through hair follicles and sweat ducts. Due to the anatomy of skin these appendages can be seen as providing a permeation pathway that bypasses the barrier of the stratum corneum. The

upper portions of hair follicles and sweat ducts extend over the thickness of the horny layer and don't allow the permeant to diffuse across the highly resistive "brick and mortar" structure. Instead, a permeation pathway of lower diffusional resistance becomes available. While in most cases the importance of this route is overridden by the intercellular one there are examples suggesting otherwise for certain hydrophilic compounds. It has been proposed that the appendageal transport is important for large polar molecules and ions that would exhibit low permeation rates across the lipid domain of the horny layer [61]. Shunt pathway transport is characterized by minimal diffusion lag time relative to transport across the stratum corneum lipid domain [72] as can be anticipated based on the lack of shunt tortuosity and higher permeability of the sebum and sweat as compared to the SC's lipid domain. These observations are in agreement with expected high drug diffusivity values in the shunts as compared to the horny layer lipids.

Overall, the significance of this route is, however, limited by the fact that the fractional area of skin area covered by shunts (hair follicles and sweat ducts) is only around 0.1% [61]. Hence, the contribution of this pathway to the total drug flux at steady state is typically minor [62].

4.3.1.4. Clearance by the microvasculature

The presence of the microvascular bed in the dermis is critical from the perspective of transdermal drug delivery. Since the epidermis is an avascular tissue, a xenobiotic to be absorbed systemically must permeate through the whole thickness of the epidermis and top portion of the dermis to reach the blood circulation. The blood flow in the dermis is around 0.05 ml/min per g of skin and the surface area of vasculature available for drug exchange is approximately the same as the surface area of skin subjected to drug permeation (1-2 cm^2/cm^2 skin) [18]. These characteristics typically are sufficient to

provide sink conditions at deeper skin layers. The approach which assumes the existence of an absolute dermal clearance at the skin depth of about 0.2 mm, corresponding to the superficial plexus, has proven to be adequate for a variety of permeants [73]. The cases in which this approach may be unsatisfactory include the use of vasoconstrictive agents [74], pathological states of skin [75], or serious compromise of the stratum corneum barrier [76, 77]. The presence of the lymphatic system may also play a role for absorption of certain xenobiotics. It was shown that the lymphatic flow was a significant factor for the clearance of large molecules such as interferon [63].

4.3.1.5. Mathematics of skin diffusion

The anatomy of human skin is complex, yet in many cases a simple mathematical model for studying drug permeation through skin has been successfully employed [54]. In the modeling of drug absorption across skin *in vitro* several assumptions are typically made. Generally, during permeation experiments drug concentration in the donor solution is maintained constant and receiver solution provides sink conditions throughout the duration of the experiment. Moderately lipophilic solutes permeate SC across lipophilic domain – intercellular pathway. Assuming that steady-state diffusion across a homogenous membrane can approximate steady-state diffusion across stratum corneum the Fick's first law can be employed:

$$\frac{1}{A}\frac{dM}{dt} = J_{SS} = PC$$

where J_{ss} is the steady state flux. It is apparent from the above equation that the permeability coefficient can be treated as a proportionality constant between the drug concentration in the vehicle and flux. Therefore, in an ideal situation, P is a

concentration-independent constant describing the intrinsic ability of a molecule to traverse the stratum corneum barrier. Additionally, P, having units of distance over time can be further broken down into the product of a dimensionless drug partition coefficient between the stratum corneum lipid domain and the vehicle K_m, and drug diffusivity in the lipid domain D divided by the diffusion path length:

$$P = \frac{K_m D}{h}$$

The introduction of the dimensionless partition coefficient K_m is necessary due to the difficulty in the direct estimation of the drug concentration in the top layers of the stratum corneum lipid barrier. The product of the vehicle drug concentration and the partition coefficient K_m provides this estimate [66].

Additionally the steady-state permeation can be also analyzed in terms of the cumulative amount of drug permeating across stratum corneum. The amount appearing at the receiver side of the membrane as a function of time can be expressed as:

$$M = PAC(t - t_{lag})$$

where M is the cumulative amount of drug absorbed, P is permeability coefficient, A is the area involved in the diffusion, C is the drug's concentration in the vehicle, t is time and t_{lag} is the lag time. For a simple, homogeneous membrane the lag time can be related to the diffusivity of the drug in that membrane D, and the membrane thickness h, as follows:

$$t_{lag} = \frac{h^2}{6D}$$

The cumulative amount of drug permeated M, plotted against time is shown in **Figure 4.5**. In this permeation profile, at any time, the flux equals numerically the slope of the line. At late time points, when steady-state is achieved, the slope of the terminal portion of the profile corresponds to the steady-state flux. By back-extrapolation of the steady-state flux to the time axis the estimate for the lag time is obtained.
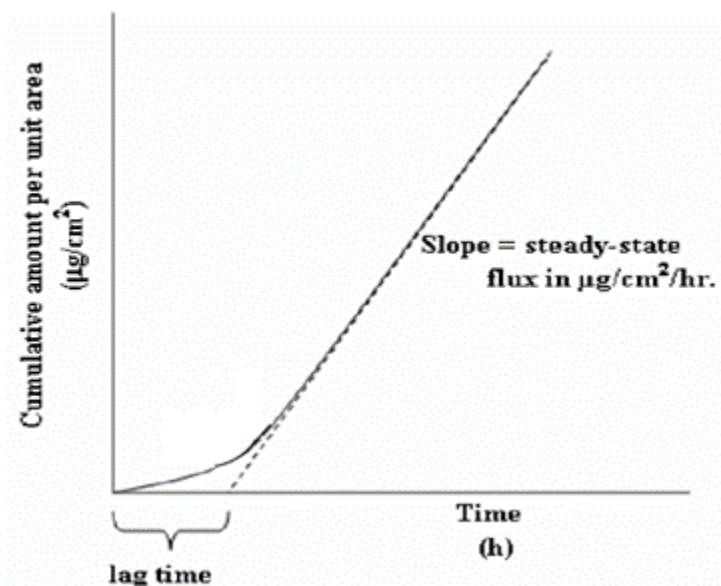
Figure 4.5. A typical permeation profile of a drug diffusing through human skin from a transdermal formulation. Drug concentration remains constant throughout the experiment.

Besides the abovementioned simple, steady-state, conditions the Fick's second law of diffusion can be employed to solve for the time dependence of flux of cumulative amount of solute permeated:

$$\frac{\delta C}{\delta t} = \frac{\delta^2 C}{\delta x^2}$$

where C is permeant concentration in barrier, x is a spatial coordinate, and t is time. In other words, the rate of change in drug concentration with time at a point within a diffusional field is proportional to the rate of change in the concentration gradient at that point. After imposition of the relevant initial conditions and boundary conditions this equation serves as a starting point for resolution of many diffusion problems [78]. For example, the amount of drug leaving the vehicle taken up by the stratum corneum and permeating as a function of time can be calculated as shown in **Figure 4.6** [79].
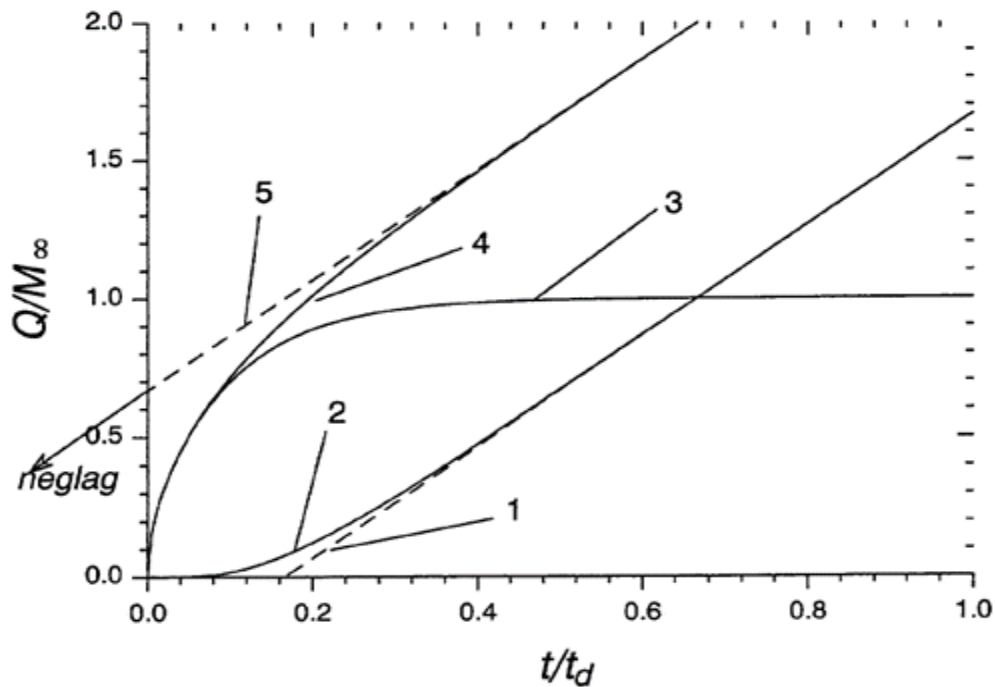
Figure 4.6. Normalized cumulative amount of solute penetrating Q/M$_\infty$ (curve 2); taken up by the stratum corneum (curve 3); and leaving vehicle (curve 4) with normalized time. Curves 1 and 5 represent steady state approximations of the cumulative amount penetrating the stratum corneum and leaving the vehicle with normalized time.

Reprinted with permission from "Percutaneous absorption: drugs-cosmetics—mechanisms-methodology" edited by Robert L. Bronaugh, Howard I. Maibach, 1999

4.4. Naltrexone

Naltrexone is used along with counseling and social support to treat alcohol addiction and opioid addiction. Pharmacologically, naltrexone belongs to opiate antagonists and competes for opioid receptor binding with opiate agonists. The drug exerts its action through decreasing the craving for opiates/alcohol. Naltrexone is reported to be of greatest use in opioid addicts and motivated alcoholics who participate in psychosocial therapy or other compliance-enhancing protocol [80].

4.4.1. Alcohol and opioid addiction prevalence

Opiate and alcohol addiction are societal problems. The scale of the problem is best presented through statistics. A recent National Survey on Drug Use and Health: Volume I. Summary of National Findings [1] showed that: "*Slightly more than half of Americans aged 12 or older reported being current drinkers of alcohol in the 2009 survey (51.9 percent). This translates to an estimated 130.6 million people, which is similar to the 2008 estimate of 129.0 million people (51.6 percent). Nearly one quarter (23.7 percent) of persons aged 12 or older participated in binge drinking at least once in the 30 days prior to the survey in 2009. This translates to about 59.6 million people. The rate in 2009 is similar to the rate in 2008 (23.3 percent). In 2009, during their most recent treatment in the past year, 2.9 million persons aged 12 or older reported receiving treatment for alcohol use, and 1.2 million persons reported receiving treatment for marijuana use. Accordingly, estimates on receiving treatment for the use of other drugs were 787,000 persons for cocaine, 739,000 for pain relievers, 517,000 for stimulants, 507,000 for heroin, 443,000 for hallucinogens, and 421,000 for tranquilizers. In 2009, 23.5 million persons aged 12 or older needed treatment for an illicit drug or alcohol use problem (9.3 percent of persons aged 12 or older). Of these, 2.6 million (1.0 percent of persons aged 12 or older and 11.2 percent of those who needed treatment) received*

treatment at a specialty facility. Thus, 20.9 million persons (8.3 percent of the population

aged 12 or older) needed treatment for an illicit drug or alcohol use problem but did not

receive treatment at a specialty substance abuse facility in the past year. These

estimates are similar to the estimates for 2008 and for 2002.
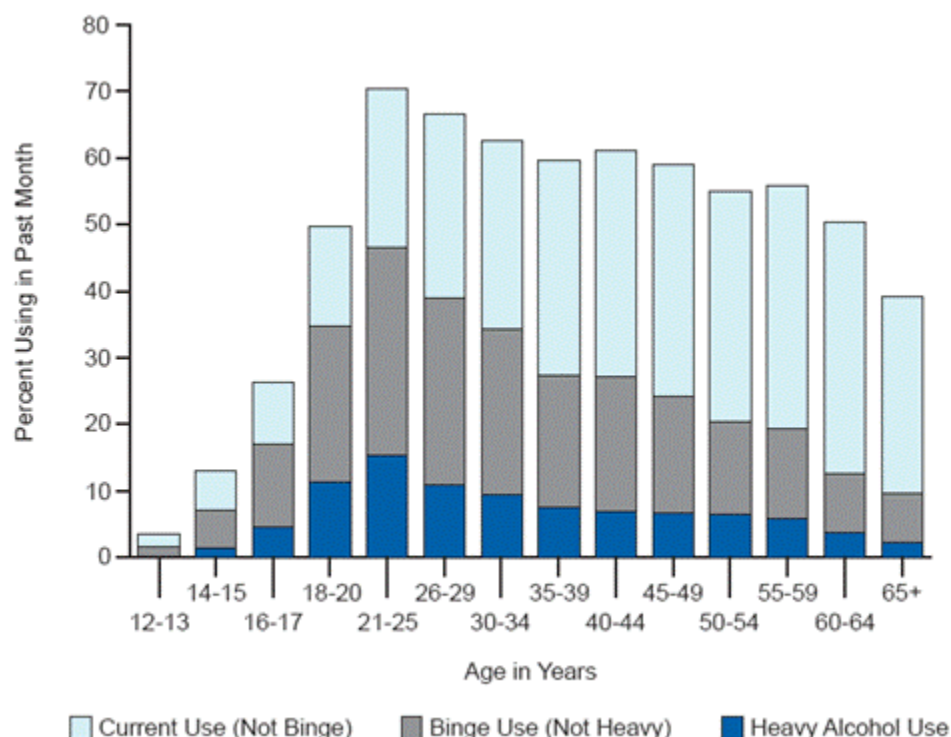
Figure 4.7. Current, Binge, and Heavy Alcohol Use among Persons Aged 12 or

Older, by Age: 2009

Substance Abuse and Mental Health Services Administration. (2010). Results from

the 2009 National Survey on Drug Use and Health: Volume II. Technical

Appendices and Selected Prevalence Tables (Office of Applied Studies, NSDUH

Series H-38B, HHS Publication No. SMA 10-4856Appendices). Rockville, MD.

In 2009, there were 180,000 persons aged 12 or older who had used heroin for the first

time within the past 12 months. The number of heroin initiates was significantly higher

than the average annual number of heroin initiates during 2002 to 2008 (slightly over

100,000). Estimates during 2002 to 2008 ranged from 91,000 to 118,000 per year. The

average age at first use among recent initiates aged 12 to 49 was 25.5 years in 2009,

similar to the average age in 2008. Between 2002 and 2009, the percentage of youths

aged 12 to 17 perceiving great risk declined for the following substance use patterns:

using heroin once or twice a week (from 82.5 to 81.0 percent), trying heroin once or

twice (from 58.5 to 57.0 percent), using cocaine once or twice a week (from 79.8 to

78.5 percent), trying LSD once or twice (from 52.6 to 48.4 percent), and using LSD once

or twice a week (from 76.2 to 71.8 percent).
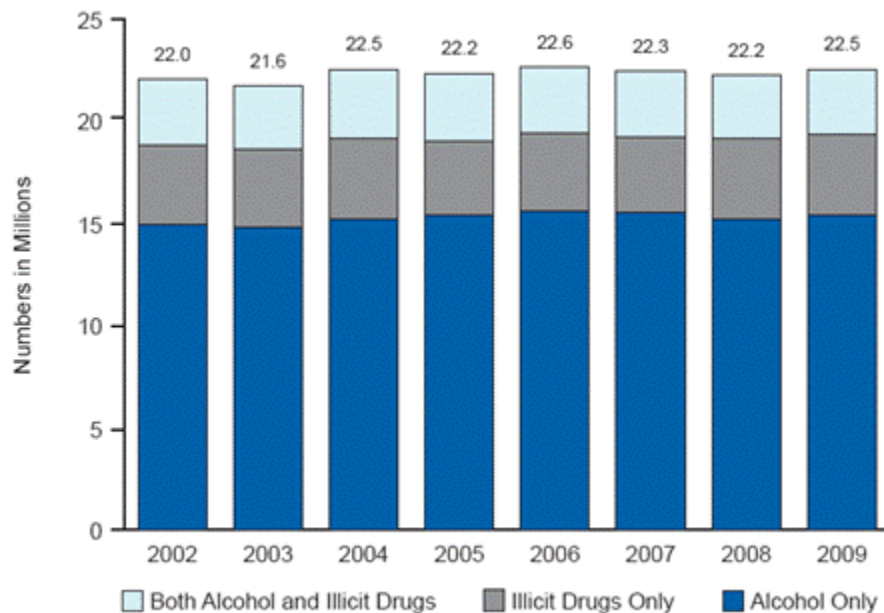
Figure 4.8. Substance Dependence or Abuse in the Past Year among Persons

Aged 12 or Older: 2002-2009

Substance Abuse and Mental Health Services Administration. (2010). Results from

the 2009 National Survey on Drug Use and Health: Volume II. Technical

Appendices and Selected Prevalence Tables (Office of Applied Studies, NSDUH

Series H-38B, HHS Publication No. SMA 10-4856Appendices). Rockville, MD.

Of the 20.9 million persons aged 12 or older in 2009 who were classified as needing substance use treatment but not receiving treatment at a specialty facility in the past year, 1.1 million persons (5.1 percent) reported that they perceived a need for treatment for their illicit drug or alcohol use problem. Of these 1.1 million persons who felt they needed treatment but did not receive treatment in 2009, 371,000 (34.9 percent) reported that they made an effort to get treatment, and 693,000 (65.1 percent) reported making no effort to get treatment. These estimates remained stable between 2008 and 2009."

The alarming magnitude of the problem related to the alcohol and illicit drug abuse calls for better treatment options. The introduction of wider in scope and more effective treatments could help recovering addicts could carry out a more productive and drug-free life. A variety of treatment approaches are used in the management of addictions. While some rely solely on drug-free educational and behavioral programs, others combine them with pharmacotherapy. The pharmacology of addiction is related to the endogenous opioid system.

4.4.2. Endogenous opioid system

Endogenously, the opioid receptor system is involved in signaling of aversive and reinforcing effects. Several receptors have been identified in the central nervous system. Generally, the activation of µ- and δ-receptors is associated with reinforcing effects. Contrarily, selective κ-agonists are typically associated with aversive responses [81]. There are three major classes of endogenous opioid ligands including β-endorphins, dynorphins, and enkephalins, which exert their pharmacological action via binding with the aforementioned µ, δ, and κ opioid receptors [82]. Each class of ligand is characterized by different affinity to the receptors. β-Endorphins have a high affinity for the µ-opioid receptors and, to a lesser extent, for the δ-opioid receptors. Enkephalins have a high affinity for the δ-opioid and, to a lesser extent, for the µ-opioid receptor.

Dynorphins show selectivity mainly for the κ-opioid receptors, although a dynorphin degradation pathway has been described, which generates enkephalin-like peptides that may interact with δ- and μ- receptors [82]. Opioid receptors respond to the administration of exogenous opioids such as heroin. It has been shown that the μ-opioid receptor is involved in the reinforcing effects of heroin and alcohol [11] [83]. The overall mechanisms of craving are not fully elucidated, however, there is evidence implying that the dopamine system is involved in the control of alcohol intake and craving. Both alcohol and opioids seem to induce dopamine release in the nucleus accumbens, through activation of the μ-opioid receptors in the ventral tegmental area, which triggers a cascade of biochemical reactions involved in the brain reward system [11, 13]. In consequence, the potential of substances behaving as opioid receptor antagonists was recognized in the addiction therapies. Multiple studies have shown that opioid receptor antagonists such as naltrexone, naloxone, and nalmefene reduce alcohol consumption in animals and humans. The pharmacological mode of action is believed to be related to the decrease of alcohol-reinforcing effects by inhibiting alcohol-induced dopamine release [84]. It has been suggested that μ-opioid receptors play a major role in this effect [14, 15].

4.4.3. Therapeutic indications

Naltrexone was discovered in the 1970s. In 1984 it was FDA-approved for the purpose of helping heroin or opium addicts. In 1994, after a successful clinical study with an alcohol-dependent population, it was approved for the treatment of alcohol dependence [4]. Since then, several clinical studies have confirmed the effectiveness of naltrexone therapy [10, 12]. Of note, a large multicenter study carried out in 2001-2004 with over 1300 patients evaluated the efficacy of medication, behavioral therapies and their combinations. The outcomes for patients receiving naltrexone, either with or without a

combined behavioral intervention, were significantly better as compared to the placebo group [9]. Currently naltrexone is available in two dosage forms, as an oral 25, 50 and 100 mg tablet (hydrochloride salt) and a 380 mg monthly depot injection (base form). Additionally, low-dose naltrexone is used off-label for treatment of HIV/AIDS, cancer, autoimmune diseases, and central nervous system disorders [85].

4.4.4. Limitations of the current naltrexone dosage forms

Oral 50 mg tablets of naltrexone (ReVia® and Depade®) are, however, related to several limitations. Orally administered, naltrexone is extensively metabolized by the liver through the first pass effect with an estimated bioavailability ranging from 5% to 40% [5]. At high doses, naltrexone causes hepatotoxicity, which limits its use in the alcoholic population often characterized by impaired hepatic function in the first place. Hence, some patients who could benefit from a dose higher than 50 mg, cannot increase the dose due to possible hepatic injury. Additionally, naltrexone is known to cause gastrointestinal side effects such as nausea, vomiting and stomach pain [86]. It has been established that NTX's usage in opioid and alcohol addiction is most effective in highly-motivated individuals [83]. Poor compliance with the daily regimen is a major issue related to NTX therapy [83, 87, 88], which lead to the development of sustained-release injectable Vivitrol® formulation. Vivitrol® was FDA-approved in 2004 as an alternative to oral dosing. Indeed, the new dosage form addressed some of the drawbacks of the oral dosage form. Vivitrol® is a once-per-month, 380 mg, extended-release injectable suspension of naltrexone base. It has been used to treat both alcohol and heroin addiction [89-91]. A clinical study testing two doses of 190 mg and 380 mg injectable NTX has demonstrated a dose-dependent, marked decrease in alcohol consumption [92]. Although the depot injection of NTX eliminates the patient compliance issue, which limited the practical usefulness of the oral dosage form, it creates the necessity of a visit

to a healthcare professional to obtain the injection. Moreover, in 2008, FDA issued a postmarket drug safety warning related to the use of Vivitrol®. A risk of adverse injection site reactions in patients receiving naltrexone was observed including cellulitis, hematoma, and necrosis. Some of the worst injection site reactions required surgical interventions [16]. Other shortcomings related to the depot injectable form include inconsistent drug release from the depot, patients overcoming the narcotic blockade with high doses of opiates and in emergency situations painful surgery to remove a depot in a hospital setting [93, 94].

An alternative to the aforementioned oral and injectable delivery forms is the transdermal route of drug delivery. The potential benefits of designing a transdermal form of NTX are as follows: the convenience of application of a once-per-week transdermal patch, easily-adjustable dose, decreased hepatotoxicity potential (avoidance of the first-pass effect), and the possibility of immediate discontinuation of therapy, if needed. However, NTX does not possess the physicochemical properties to achieve of therapeutically-relevant plasma levels in the presence of high systemic clearance in humans [20, 95, 96]. However, several delivery enhancement strategies have been investigated.

4.5. Enhancement methods in transdermal drug delivery

The following discussion is vastly based on a publication section entitled "Challenges & solutions for overcoming the skin permeation barrier" by M. Milewski in "Challenges and opportunities in dermal/transdermal delivery" by K. Paudel et al. [97]. The microneedle section is partly based on the publication entitled "Current aspects of formulation efforts and pore lifetime related to microneedle treatment of skin" by M. Milewski et al. [98].

Overcoming low skin permeability to xenobiotics is an active field of research and can be achieved by a variety of approaches. Their effectiveness and applicability depends on the physicochemical nature of the compound. Here, a brief overview of the enhancement

41

methods including chemical methods, physical methods and a prodrug approach will be provided. Their applicability to the maximization of percutaneous naltrexone delivery will also be discussed.

4.5.1. Chemical methods

Chemical permeation enhancement is synonymous with the use of chemical permeation enhancers. These substances have the ability to transiently compromise the barrier properties of the horny layer, thus enabling increased transport rates of xenobiotics through skin.

4.5.1.1. Permeation enhancers

Chemical permeation enhancers facilitate drug permeation across the skin by increasing drug partitioning into the barrier domain of the stratum corneum, increasing drug diffusivity in the barrier domain of the stratum corneum or the combination of both [99]. The heterogeneous SC is composed of cross-linked keratin "bricks" and transcellular continuous lipid "mortar" organized in multilamellar strata [51, 100, 101]. Depending on the nature of the drug either of these two environments may be the rate-limiting milieu (barrier domain) of percutaneous transport. As a consequence, it is anticipated that the magnitude of permeation improvement obtained with a given permeation enhancer will vary between lipophilic and hydrophilic drugs. Several mechanisms of action are known: increasing fluidity of SC lipid bilayers, extraction of transcellular lipids, increase of drug's thermodynamic activity, increase in SC hydration, alteration of proteinaceous corneocyte components, and others [102, 103]. Permeation enhancers are conventionally divided into several groups based on their chemical structure rather than the mechanism of action. This is partially due to the difficulty determining a primary or mixed mode of action for many of them. Also, compounds from the same group can exert their effect

through different mechanisms. More than 300 substances have been shown to have skin permeabilization potential and this number is still growing. Most known enhancers fall into the following categories: alcohols (ethanol, pentanol, benzyl alcohol, lauryl alcohol, propylene glycols, glycerol), fatty acids (linoleic acid, valeric acid, lauric acid), amines (diethanolamine, triethanolamine), esters (isopropyl palmitate, isopropyl myristate, ethyl acetate), amides (1-dodecylazacycloheptane-2-one - Azone®, urea, dimethylacetamide, dimethylformamide, pyrrolidone derivatives), hydrocarbons (alkanes, squalen, mineral oil), surfactants (sodium laureate, cetyltrimethylammonium bromide, Brij, Tween, sodium cholate), terpenes (D-limonene, carvone, anise oli), sulfoxides (dimethyl sulfoxide) and phospholipids (lecithin). The importance of water, or hydration of SC, is not to be underestimated. A fully hydrated SC (under occlusion) presents lesser diffusional resistance to xenobiotics than its dehydrated counterpart. However, a common drawback of permeation enhancers is that their efficacy is often closely mimicked by skin irritation. In general, the same mechanisms that are responsible for enhanced drug transport such as disrupting ordered SC lipid bilayers or corneocyte structural organization are also responsible for skin irritation [104]. A possible solution to this concern is to identify mixtures of permeation enhancers that exhibit synergistic effects [105]. Such mixtures allow decreased irritation potential while maintaining high effectiveness. Although the identification of such combinations *a priori* is difficult, Karande et al. successfully used a screening approach to test 5000 binary mixtures of chemicals [106, 107]. Several types of synergistic mixtures were identified such as sodium laureth sulfate (0.35%) and phenyl piperazine (0.15%) or a 1:1 mixture of ethanol and phosphate-buffered saline. Most of the products on the transdermal market rely on the effect of occlusion, which is defined as an enhancement technique acting through the hydration of the SC. Additionally, drugs such as nitroglycerin (Nitro-Dur®, Nitro Disc®, Transderm-Nitro®) use fatty acid esters, and lidocaine (Lidoderm®) urea and

propylene glycol as chemical enhancers. Traditionally, chemical enhancers have been used to increase the delivery of small molecules and showed only limited success in permeation enhancement of macromolecules. Overall, chemical methods, although effective, cannot compete with physical enhancement methods, which provide greater magnitude of skin permeabilization.

4.5.2. Physical methods

The oldest and most by far the most popular way of overcoming the skin barrier physically is the use of hypodermic needles. In many cases it is the only viable method of delivery of poorly absorbable and highly unstable agents. Typically, drug solution is forced under piston pressure directly into bloodstream or tissue (skin and muscle). Such drug administration results in quick delivery of large amounts of drug. If controlled drug delivery over longer periods of time is desired indwelling catheters are used. However, both require mechanical perforation of skin with a needle which causes pain and trauma. According to Hamilton needle phobia is a medical condition that affects at least 10% of the population [108]. This condition is a serious problem in the health care system in the sense that people with needle phobia tend to avoid medical care. To address these drawbacks, several alternative physical skin enhancement methods such as jet injections, dermabrasion, thermal ablation, laser, microneedles, iontophoresis, electroporation, ultrasound and combinations of the above are investigated. These methods aim at developing more user-friendly and flexible delivery systems able to produce bolus-type as well as sustained drug delivery profiles.

4.5.2.1. Jet injections

Jet injections involve the delivery of liquid or solid particles driven by high pressure accelerators across the SC [109]. The concept of drug-delivering jets is not new as first

reports date back to the 1940's; however, first attempts of using this technology translated into limited success. Technology advances in the later decades enabled the construction of more reliable and effective devices based on the compressed helium [110]. It proved its potential in the delivery of insulin to diabetic patients [111]. This method, similar to the hypodermic injection in that it enables rapid delivery of large amounts of drug, has resulted in improved patient compliance [112]. Shortcomings of jet injections include inability to deliver drugs over longer periods of time; however, they seem to be well-suited for vaccination delivery [113].

4.5.2.2. Dermabrasion

Dermabrasion has been traditionally used to treat acne, scars and other dermatologic and cosmetic conditions [114]. Recently the potential of this technique for transdermal drug delivery has been recognized. Mechanistically, crystal microdermabrasion use microcrystals blown onto the skin surface to perform the exfoliating process. Several-fold improvement in the flux of small molecular weight drugs was shown by various researches using this technique [115, 116]. Recent study by Gill et al. investigated the effect of microdermabrasion on SC removal in rhesus macaques and human volunteers *in vivo*. The effectiveness of the skin barrier removal correlated with number of passes of the mobile dermabrasion device and selective removal without damage to the viable epidermis was possible [117].

4.5.2.3. Thermal ablation

Thermal ablation takes advantage of the external source of thermal energy, which propagates into the SC to create microchannels. Heating of the skin surface to hundreds of degrees for a very short period of time allows the thermal damage to be limited to the SC alone without further heat propagation to live epidermal layers. An interesting

publication by Park et al. discussed the effect of heat in skin permeability. Authors pointed out skin permeability changes to a model hydrophilic compound at different temperature ranges. While an intermittent increase in the skin temperatures to 100-150 °C causes moderate increase in the flux of a hydrophilic compound, 150-250 °C translates into one to two-orders of magnitude increase and temperature of over 300 °C add yet another tenfold augmentation in the transdermal flux. Different mechanisms are postulated to be responsible for such change at each temperature range [118]. Althea Therapeutics developed a PassPort™ system that is comprised of a single-use disposable patch and a re-useable handheld applicator. Phase I and II clinical trials have been completed for the delivery of insulin via this enhancement system.

4.5.2.4. Laser ablation

A laser can also be used to thermally ablate parts of the SC creating pores. These pores allow drug molecules applied to the surface of the skin to bypass the diffusional barrier and gain easy access to the vascularized deeper layers of the skin. This method has been able to extract of interstitial fluid to measure glucose levels in diabetic patients as well as effective in augmenting transdermal flux of hydrophilic and hydrophobic molecules [119-121]. A transdermal laser system P.L.E.A.S.E.® (Pantec Biosolutions) has been developed and was granted a European patent in 2009. Furthermore, laser-assisted drug delivery (Norwood Abbey) was developed and the device has been cleared for marketing by the FDA for the delivery of a topically applied local anesthetic. The pitfalls of the laser approach are relatively complicated technology and cost.

4.5.2.5. Iontophoresis

There are several methods that use electric current as means to permeabilize the skin. Iontophoresis relies on the continuous electric current to drive charged drug molecules

across the skin via electrophoresis and electroosmosis [122]. It is commonly stated that iontophoresis mainly provides additional electrochemical driving force for drug transport across skin, rather than increases permeability of the skin. First *in vivo* animal investigation showing effectiveness of this approach was carried out at the beginning of the 20th century. Since then many drug delivery systems were tested for small molecules such as pilocarpine [123] or lidocaine [124], zolmitriptan [125] and large molecules such as calcitonin, insulin, parathyroid hormone or vasopressin [126-130]. Clinical studies, however, have been limited to the small agents such as lidocaine, cortisone or fentanyl [131-133]. Although there have been reports indicating the presence of erythema under electrode application site [134] the irritation correlates well with the current and as long as the current is low adverse effects are not substantial. Both continuous and intermittent delivery of drugs is feasible. A couple of drug delivery systems using iontophoretic devices were approved by the FDA in the past, for example, lidocaine HCl with epinephrine (Iontocaine® and Lidosite® topical system) and fentanyl HCl (IONSYS™) [135]. IONSYS, however, was never marketed in the USA. These products have now been listed as discontinued by the FDA (Iontocaine since 2005, Lidosite topical system since 2006 and IONSYS since 2008). The discontinuation of IONSYS in the USA was affected primarily by the European Medicines Agency's recall of the product and suspension of marketing because of corrosion of a component in the system, which can lead to release of fentanyl without patient activation. The limitations of this delivery method include the relatively high cost of the iontophoretic device.

4.5.2.6. Electroporation

Another method – electroporation – is based on the use of short (micro- to mili-second), high-voltage electrical pulses to create transient disruptions in the structure of the SC [136]. Such disruptions, or pores, facilitate the transport of small and large molecules

otherwise unable to permeate at all. Drug molecules are believed to be transported through skin by electrophoretic movement and diffusion. Examples proving *in vitro* effectiveness of electroporation include small molecules such timolol [137] as well as larger molecules such as oligonucleotides, heparin and IgG antibodies [138].

4.5.2.7. Sonophoresis

Ultrasound skin enhancement (sonophoresis) is achieved by the use of high (MHz) or low (kHz) frequency devices, the latter showing greater percutaneous drug flux improvement. At low frequencies the ultrasound applied to the skin results in the production of cavitational bubbles which by oscillation disrupt the SC structure. *In vitro* experiments have shown substantial increase in the skin permeability to small molecules such as estradiol, aldosterone or lidocaine [139] as well as macromolecules such as insulin, erythropoietin or γ-interferon [140-144]. In 2004 FDA approved an ultrasound system SonoPrep® to accelerate the action of lidocaine for local dermal anesthesia. The same system is intended to be used for delivering vaccines, insulin delivery, blood glucose monitoring, and antibiotic delivery in the future. An interesting feature of the device is real-time skin impedance feedback which stops the sonication procedure when the desired level of conductance has been achieved. This method does not cause pain or irritation when used within certain limitations. A ViaDerm system (TransPharma) has been developed and preclinical trials demonstrated effectiveness of this method of skin enhancement. Moreover, clinical trials involving the ViaDerm system coupled with human parathyroid hormone (1–34) and human growth hormone are underway.

4.5.2.8. Microneedles

Microneedles became one of the major enhancement techniques in the transdermal drug delivery field after advancements in the micro-fabrication techniques in recent years

had been made. Microneedles are a minimally invasive means of assisting the transport of drug molecules across the skin, and several reports have demonstrated that MN treatment is painless and well-tolerated by most patients [30, 31, 145]. There are various ways that microneedles can assist in the transdermal delivery of drugs across the SC, and currently 4 major types of microneedle systems have been described [146]. Solid microneedles pierce the skin and create pores (also referred to as microchannels) in the SC, which can be utilized to increase delivery of a variety of compounds by applying a gel formulation or transdermal patch over the MN-treated skin; this is called the "poke and patch" method [7, 147]. **Figure 4.9** presents two designs of solid steel microneedles.
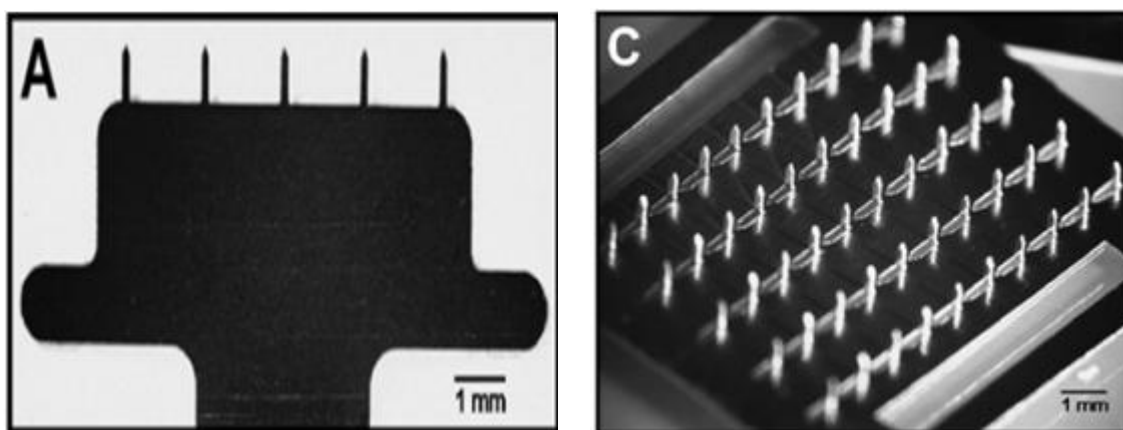
Figure 4.9. Solid steel microneedles: A) "in-plane" row with five microneedles; C)

"out-of-plane" microneedle array with 50 microneedles

Reprinted with permission from Journal of Controlled Release 117 (2007) 227–237

Microneedles can be coated with various drug formulations, which has been used to deliver DNA, proteins, and virus particles; this is referred to as the "coat and poke" approach [7, 147]. Polymeric microneedles have been prepared with encapsulated drug to be inserted, detached and left in the skin, which can be used for either rapid or

controlled release into the skin [146]. Lastly, hollow microneedles have been utilized to deliver drug compounds (insulin, vaccines) by diffusion or pressure-driven flow through the bore of the needle [7, 146, 147]. All of these applications are inherently different and it can be expected that each technique requires separate optimization. There are many factors that affect drug delivery and permeability of the skin with respect to MN application. These include parameters such as mechanical properties of the MN arrays, formulation of drugs to be delivered, and lifetime of the pores following MN application. To date, the mechanical properties of microneedle arrays have been well described in the literature, including parameters such as length, bore, geometry, force of application, and number of microneedles [30, 148-151]. The optimization of these factors affects the strength of the microneedles, the amount of pain associated with application, and the overall permeability of the skin (and therefore efficiency of drug delivery) [146, 151]. Beyond the mechanical properties of the MN arrays, the other factors affecting drug delivery via this route remain largely unexplored, specifically drug formulation and pore lifetime following MN treatment. When it comes to the effectiveness of MN in enhancing the permeability of the skin, Henry et al. showed an increase in the transdermal flux of calcein up to four orders of magnitude [152]. A multitude of other studies proved that microneedles effectively permeabilize skin to drugs [6, 29, 153, 154]. With respect to NTX delivery it has been shown that although the creation of microchannels in the skin after MN treatment did not have a substantial effect on the delivery rates of the neutral (free-base) form of NTX or 6-ß-naltrexol, an improvement in the delivery of positively charged (salt-form) species of these drugs was possible [6]. It was proposed that higher NTX and 6-ß-naltrexol water-solubility at the lower pH range, rather than the presence of a positive charge, was responsible for the observed increase in the transport rates of the salt forms of these drugs [6]. *In vitro* and *in vivo* animal studies proved the utility of the MN method of enhancement showing approximately an order-of-magnitude increase in

50

the transdermal flux of highly water soluble species via MN-assisted delivery over that through untreated skin [6, 155]. Subsequently, a first-in-human MN study demonstrated that the combination of MN skin pretreatment and application of four NTX•HCl patches afforded drug plasma levels in the lower end of the targeted therapeutic range [32]. Currently, several systems based on microneedles are being investigated such as Microstructured Transdermal Systems (3M), Macroflux® (Zosano), MicroCor™ (Corium), or Soluvia™ (Becton-Dickenson) and have shown efficacy in preclinical trials.

Combinations of enhancement techniques have a potential of showing synergistic effects [156]. Some combinations that have been studied include electroporation-ultrasound [157], electroporation-iontophoresis [158, 159] and microneedle–iontophoresis [160]. The observed synergistic effects may be rationalized by different mechanisms by which enhancement methods work, e.g. electroporation disrupts SC barrier structure increasing its permeability to drugs while iontophoresis provides additional driving force for diffusion of charged particles above that of just passive diffusion.

4.5.3. Prodrugs

The design of prodrugs for increasing transdermal delivery must consider: permeation across skin, chemical and enzymatic stability as well as skin irritation potential. While all of these factors need to be considered for a design of a successful prodrug, usually the main reason to recur to this approach is to modify the physicochemical properties of a parent drug so that the flux of the prodrug is increased over that of the parent molecule. A chemical modification of the compound of interest presents great opportunity to alter its ability to cross the SC barrier. In the most conventional case, when the diffusional barrier is represented by the lipid domain of the SC and parent drug is relatively

51

hydrophilic, increasing its lipophilicity can result in the improved percutaneous flux. However, a penalty is paid for the increase in the size of the permeant [60]. By contrast, it has also been possible to improve the flux of extremely hydrophobic compounds (which undergo viable tissue controlled diffusion, in comparison to stratum corneum controlled diffusion) by creating more hydrophilic prodrugs. With respect to NTX, several studies evaluated the potential of employing various prodrug classes to enhance its percutaneous flux [21, 96, 161-164]. Prodrug moieties based on short aliphatic chains in conjunction with carboxylic acid esters proved to be successful in increasing transdermal flux up to 6-fold. More recent literature reports of use prodrugs in transdermal drug delivery include the delivery of ketorolac piperazinylalkyl prodrugs [165], a pilot clinical trial involving prodrugs of levodopa [166], effects of PEGylation on transdermal flux of acetaminophen [167], naltrexone prodrugs [96] and bupropion prodrugs [162]. Currently, there are no transdermal prodrugs available on the market.

Chapter 5

Development of a mathematical model for maximum flux estimation of nonionized drugs across untreated skin

5.1. Introduction

Although the main research objectives of this thesis are related to MN-enhanced transdermal drug delivery (**Chapter 2 and 3**) it is important to develop a general understanding of the drug transport across skin in the absence of microchannels. Not only does drug delivery through intact skin provide a basis for comparison against MN-assisted transport, but it also is an integral part of the delivery through MN-treated skin. This is true because after formation of microchannels the vast majority of the skin surface is still covered with intact stratum corneum. Hence, as long as the formulation is applied on the MN-treated skin area, the intact skin surface will also participate in the overall drug transport. More detailed description of the parallel drug transport across microchannels and intact skin will be presented in **Chapter 6**. Moreover, the relative contribution of either of the parallel pathways to the total flux will be further discussed in **Chapter 7**. In the current chapter the emphasis is placed on the recognition of basic physicochemical characteristics of nonionized permeants that influence the maximum percutaneous flux through untreated skin. The following discussion has been submitted for publication in Molecular Pharmaceutics, and a revision has been requested.

Skin has evolved to provide an efficient barrier at the interface of the external environment and the body. The formidable skin barrier properties greatly limit the permeation of xenobiotics [18, 37]. An advantage in terms of the protection against environmental toxicological agents is also a drawback from the perspective of percutaneous drug delivery. In both respects, the ability to identify the key

physicochemical properties of xenobiotics that determine their skin permeation potential is very attractive.

A large body of literature has been published about skin permeability to drugs. The description of percutaneous transport across skin usually comprises several assumptions about the nature of the barrier and the nature of the drug penetrating this barrier. The barrier properties of the skin for a moderately lipophilic drug are typically well-described by accounting for the barrier properties of stratum corneum (SC) lipid domain alone [49, 57]. While some studies focused on the investigation of the permeability coefficient (P), others emphasized the maximum transdermal flux (J_{max}). From the therapeutic and toxicological point of view it is often the maximum transdermal flux that is of critical importance. Such flux is normally attained by the use of a drug-saturated vehicle.

The purpose of this study is to develop a simple and easy-to-use predictive mathematical model for estimation of the maximum transdermal flux of xenobiotics based on three easily accessible molecular descriptors: logarithm of octanol-water partition coefficient ($logK_{o/w}$), molecular weight (MW) and melting point (MP). Additionally, the usefulness of this model was evaluated using a permeation database comprised of 64 compounds. The model is based on two previously-reported, predictive models estimating drug skin permeability coefficients [168] and aqueous solubility of nonionic compounds (S_w) [169, 170].

5.2. Models estimating permeability coefficients

The permeability coefficient is often seen as a parameter describing the intrinsic, concentration- independent, ability of a molecule to cross the SC barrier. The majority of mathematical models used to estimate drugs' permeability coefficients recognize the importance of drug partitioning into the SC lipids and drug molecular size.

Physicochemical properties frequently used to estimate the permeability coefficients of drugs include MW, $\log K_{o/w}$ and hydrogen bonding potential [58, 168, 171-178]. The direct measurement of a drug concentration in the lipid domain of the SC is not easily obtained and often replaced by a product of a drug aqueous-vehicle concentration and a partition coefficient between the SC lipids and the vehicle ($K_{SC/w}$). In turn, this partition coefficient, can be related through a linear free energy relationship [179-181] to a drug partition coefficient between octanol and water ($K_{o/w}$) e.g. $\log K_{SC/w} = a \log K_{o/w}$. In this equation, "a" stands for a coefficient accounting for the difference in the drug solubilities in SC lipids and bulk octanol, and usually is found to be in the range of 0.7 – 0.9 indicating a somewhat more hydrophilic nature of the anisotropic SC lipids as compared to the isotropic bulk octanol [58, 168, 172, 175]. Additionally, the diffusivity of a drug molecule in the SC lipid domain (D) can be linked to its size through an inverse power function [182, 183] or a free volume theory [60, 184-186]. In the free-volume theory, molecular volume is habitually substituted with MW for simplicity and without loss of prediction accuracy e.g. $D = D_0 * 10^{-\beta * MW}$, where D_0 is the diffusivity of a hypothetical molecule having MW of zero, and β is a coefficient relating the MW to a drug's diffusivity in the SC lipid domain. This relationship predicts a sharp drop in the drug diffusivity within the SC's lipid bilayers with increasing molecular size, where β values typically vary in the range of 0.006-0.012 [58, 168, 171, 173]. The accessibility and ease of interpretation of the $\log K_{o/w}$ and the MW makes them very popular determinants in skin permeability equations. The number of equations estimating permeability coefficient based, among others, on $\log K_{o/w}$ and MW is above 20 and still growing [187]. It is worth noting that most models strive to use a single equation to describe the skin permeability for molecules spanning a broad range of physicochemical properties which implicitly assumes that the same permeation pathway across the SC is involved and no shift in the rate-limiting step in drug transport across skin occurs. One of them, arguably the

most widely used, was derived by Russel Potts and Richard Guy (P&GE) [168]. These authors used a multiple regression analysis of the Flynn permeation database [65] containing human epidermal permeability data of about 90 compounds to obtain the following relationship:

$$logP = -2.72 + 0.71\ logK_{o/w} - 0.0061\ MW \qquad [cm/h] \qquad\qquad (5.1)$$

This model explained 67% of the variability in the dataset [168]. The popularity of this model can be, at least to some extent, explained by the choice of just two easily-accessible determinants: $logK_{o/w}$ and MW.

5.3. Models estimating aqueous solubility of nonelectrolytes

According to Fick's first law of diffusion the maximum flux can be achieved by using a drug-saturated vehicle. Since the P estimates are often obtained with the use of the logarithm of octanol and *water* partition coefficient (as it is in the P&GE), the knowledge of the drug's *aqueous* solubility becomes important for finding the maximum percutaneous flux. A number of equations predicting solubility of nonelectrolytes in non-aqueous [188-191] and aqueous media have been published [169, 170, 192-195]. Many of them take a theory-based approach to the solubility estimation and typically recognize the importance of determinants such as heat of fusion, experimental temperature, MP, heat capacity, cohesive energy density, molecular volume, dispersion forces, dipolar forces and hydrogen bonding potential. However, some of the above properties are not easily accessible and their estimation requires additional experimental or calculation work. One way to circumvent this hurdle is to introduce reliable assumptions about the solute's nature and simplify the model so that it is based solely on more readily accessible determinants. One of the most widely known semi-theoretical models

estimating aqueous solubility of nonelectrolytes which uses only two determinants, MP and $K_{o/w}$, is the General Solubility Equation (GSE) introduced by Samuel Yalkowsky [169, 170]. Parameter values obtained by a multiple regression analysis on the database of 580 nonelectrolytes were found to agree very closely with those derived theoretically and accounted for 97% of the variability in the dataset. The regression form of the model is as follows:

$$\log S_w = -0.0102\ (MP-25) - 1.031\ \log K_{o/w} + 0.424 \quad [mol/l] \tag{5.2}$$

where $\log S_w$ is solute aqueous solubility, MP is solute melting point [°C] and $\log K_{o/w}$ is the logarithm of the solute octanol-water partition coefficient. The first term is derived from the ideal solubility equation. The ideal solubility is solvent-independent and the solubility estimate relies on the knowledge of the enthalpy of fusion, MP of the solute and the experimental temperature [169]. The introduction of a molecular-independent estimate of enthalpy of fusion and a set temperature of 25^0C allows a substantial simplification of the original equation and shows a negative dependence of the aqueous solubility on the MP of the solute. The second term addresses the non-ideality concerns by directly relating solute activity coefficient in water to solute $K_{o/w}$. This transformation reveals a strong inverse relationship between aqueous solubility of a nonelectrolyte and its $\log K_{o/w}$.

5.4. Models estimating maximum percutaneous flux

From the therapeutic and toxicological point of view the J_{max} is usually of higher importance than the P because it correlates directly with the maximum dose deliverable over a given period of time. Relatively few mathematical models have been proposed for the purpose of J_{max} estimation [60, 196, 197]. They employ parameters such as drug

solubility in octanol, S_w, solubility in isopropyl myristate, and MW. Kasting et al. proposed a semi-theoretical model for moderately lipophilic permeants based on the drug octanol solubility and MW [60]. Magnusson et al. found by statistical analysis that MW was the single major determinant of J_{max} in the database tested by the authors. It was shown that the addition of extra determinants such as solute solubility in octanol, MP and hydrogen bonding potential only improved the predictive ability of the model marginally [196]. Also, Sloan et al. postulated a model using drug solubility in isopropyl myristate (or octanol), S_w and MW [197-199]. Each of those models showed reasonable performance in their J_{max} predictive ability. However, drawbacks include the use of parameters that are not easily determined, such as octanol or isopropyl myristate solubility. Also, the statistical model based on MW alone, although extremely simple and user-friendly, lacks theoretical backing. We believe that the introduction of a new semi-theoretical model based solely on easily-accessible molecular descriptors will be useful for the quick estimation of J_{max}. The model reported herein may be seen as a close relative to the one reported by Kasting et al. [60] in which the drug MP and $logK_{o/w}$ are surrogates for drug octanol solubility. Octanol solubility, in turn, approximates drug solubility in the SC lipid barrier.

Generally, the maximum transdermal flux can be obtained by the use of a drug-saturated aqueous vehicle, as long as the aqueous solubility is sufficient to eliminate the possibility of dissolution rate-limited diffusion, and as long as the drug stability is sufficient: $J_{max} = P * S_w$, or

$$logJ_{max} = logP + logS_w \tag{5.3}$$

The model we set forth is based on the combination of two semi-theoretical models – P&GE (**Eq. 5.1**) and GSE (**Eq. 5.2**). The P&GE uses two determinants, $logK_{o/w}$ and MW,

to estimate a compound's skin permeability. Similarly, the GSE uses two determinants, $\log K_{o/w}$ and MP, to estimate the aqueous solubility of a nonionic compound. The direct substitution of **Eq. 5.1** and **5.2** into **Eq. 5.3** and the unit conversion gives:

$$\log J_{max} = 3.704 - 0.321 \log K_{o/w} - 0.0061\ MW - 0.0102\ (MP-25)\ [nmol\ h^{-1}\ cm^{-2}] \qquad (5.4)$$

where $\log K_{o/w}$ is the logarithm of the permeants's octanol-water partition coefficient, MW is the permeants's molecular weight, and MP is its melting point [$^{\circ}$C]. For liquid solutes the term (MP-25) is set equal to zero. Since the $\log K_{o/w}$ is used by both **Eq. 5.1** and **5.2**, **Eq. 5.4** relies on the total number of three determinants: $\log K_{o/w}$, MW and MP.

To assess the predictive ability of this equation it was tested against the skin permeation database (**Table 5.1**) of 64 nonionized compounds (87 entries). The database was obtained from Magnusson et al. "Molecular size as the main determinant of solute maximum flux across the skin" (supplement, originally named "set t") [196] and is compiled in terms of the J_{max} of various solutes obtained from aqueous vehicles. The inclusion criteria for this database were: the use of human SC or epidermal membrane, no organic liquids present either in donor or receiver solutions, no pure liquid permeants applied to the membrane, ionization less than 10% at the experimental pH, and the knowledge of MP, S_w and either J_{max} or P. The compounds included in the database span over a large range of physicochemical properties, $\log K_{o/w}$ (-4.67 – 4.52), MW (18 - 477) and MP (liquids – 293 $^{\circ}$C). The maximum flux was either experimentally measured or calculated from the product of the reported drug aqueous solubility and its permeability coefficient. No theoretically estimated aqueous solubility was allowed for calculation of J_{max} from P, which is critical for evaluation of this model. The database is not complete in the sense that it does not include extremely lipophilic solutes with $K_{o/w}$ greater than 4.6. However, this is should not be seen as a major disadvantage since for

very lipophilic compounds the rate of percutaneous permeation is not SC-limited and they would not be expected to follow the relationship derived here. Additionally, the accurate estimation of the rate of transdermal permeation of such solutes could be very challenging due to limited aqueous solubility in the absence of cosolvents. The compounds included in **Table 5.1** partly overlap with the entries included in the Flynn database [65].

Figure 5.1 shows the $\log J_{max}$ predicted by **Eq. 5.4** plotted against the experimental $\log J_{max}$ reported in the database (**Table 5.1**). The straight line depicts ideal correlation and dashed lines enclose the region of ideal correlation ± 1 log unit. Generally, the predictions fall in a reasonable range of $\log J_{max}$ values, although a trend of overestimating J_{max} in the low-flux region and underestimating J_{max} in the high-flux region is apparent. It is noteworthy that **Eq. 5.4** parameter values were obtained directly from **Eq. 5.1** and **5.2** employing separate databases (training sets), and not through the regression analysis on the database reported here. In the next step, a multiple linear regression analysis on the database (**Table 5.1**) was carried out using the following model:

$$\log J_{max} = a + b \log K_{o/w} + c \, MW + d \, (MP-25) \qquad [\text{nmol h}^{-1} \text{ cm}^{-2}] \qquad (5.5)$$

The initial parameter (a,b,c, and d) estimates were taken directly from **Eq. 5.4**. Since the parameters c and d were found to be highly inversely correlated, the parameter d preceding the (MP-25) term was fixed at 0.0102, the value estimated *a priori* by the GSE. The least-square fitting (Scientist®) yielded the following equation:

$$\log J_{max} = 4.9109 - 0.1666 \log K_{o/w} - 0.0120 \, MW - 0.0102 \, (MP-25) \quad [\text{nmol h}^{-1} \text{ cm}^{-2}] \quad (5.6)$$

An improved correlation devoid of any systematic deviation between calculated and experimental $\log J_{max}$ is demonstrated in **Figure 5.2.** The coefficient of determination (R^2) indicates that the model accounts for 90% of the variability in the dataset with the standard deviation of 0.7145 log unit. The vast majority of the experimentally determined J_{max} values fall in the range of the predicted J_{max} values ± 1 log unit. Moreover, the difference between predicted and experimental $\log J_{max}$'s (residuals) plotted against individual determinants: $\log K_{o/w}$, MW and MP is shown in **Figures 5.3, 5.4 and 5.5**, respectively. As evident from these figures residuals oscillate around the value of zero and there are no apparent trends in residuals as the value of each determinant is varied.

5.5. Discussion

According to **Eq. 5.6** a decrease in a drug's $\log K_{o/w}$, MW or MP implies higher maximum percutaneous flux. While the parameters c and d preceding MW and (MP-25) terms, respectively, retain their original meaning from **Eq. 5.1** and **5.2**, the parameter b preceding the $\log K_{o/w}$ term reflects its influence on both P and S_w. All parameter estimates obtained here (mean ± 95% CI) agree well with previous literature reports. The negative dependence of $\log J_{max}$ on the MW (0.0120 ± 0.0015) is somewhat steeper than that reported by Potts and Guy but falls in the range of values previously reported, such as 0.012 [58], and is justified on the grounds of the free-volume theory. The increase in the MW of 100 Da translates, on average, into a 16-fold drop in the J_{max}. The negative dependence of $\log J_{max}$ on the drug's MP (0.0102, as estimated *a priori* by GSE) can be rationalized by its influence on the aqueous solubility, with an increase in the MP of 100°C translating, on average, into a 10-fold drop in the flux. Finally, the negative dependence of $\log J_{max}$ on the drug's $\log K_{o/w}$ (0.1666 ± 0.0801) arises from its effect on both the drug's permeability coefficient and aqueous solubility. A unit increase in the $\log K_{o/w}$ value causes roughly a 10-fold drop in the aqueous solubility of a nonionic drug.

On the other hand, it also causes around a 7-fold increase in the partitioning into the SC lipids. Overall, the permeant's concentration in the SC lipid barrier drops, on average, around 1.5-fold per unit increase in the $logK_{o/w}$ value. Therefore, the $logK_{o/w}$ effect on J_{max} is opposite from its effect on P. It is also true that $logK_{o/w}$ influence on J_{max}, as compared to MW and MP, is minor since its effects on P and S_w almost cancel out. It could be argued that the presence of the $logK_{o/w}$ parameter in the model is not necessary. However, both the non-zero parameter b estimate found here as well a slight decrease in the Model Selection Criterion from 2.28 to 2.12, when $logK_{o/w}$ is excluded from the model, suggest otherwise. (Model Selection Criterion is a modified Akaike Information Criterion where larger value indicates more appropriate model). Physically, the non-zero parameter b estimate supports the notion of SC lipids being somewhat more polar in nature as compared to the bulk octanol [58, 168, 172, 175].

Although the cosolvent-containing vehicles were excluded from the analysis reported here it is known that drug's solubility in any vehicle (not necessarily aqueous) can be related to its solubility in the SC lipids through a partition coefficient [200]. At saturation, the product of the drug solubility in that vehicle and the vehicle-SC lipids partition coefficient remains constant. Therefore, as long as the vehicle does not affect either drug's solubility or diffusivity in the SC barrier the J_{max} from any saturated vehicle would be expected to be the same and the relationship (**Eq. 5.6**) derived here should hold. At present, however, any solvents other than water were not included in the database due to the concern of potential interaction with the SC barrier.

Limitations of the model proposed here are related to the fact that it uses a single equation to predict the maximum transdermal flux. Therefore, it is implicitly assumed that all permeants cross the skin barrier by the same pathway and no shift in the rate-limiting step of the drug transport occurs. Also, the GSE predicts aqueous solubility of the nonionic compounds at 25°C while *in vitro* skin diffusion experiments are typically carried

out at higher temperature. However, given the different experimental conditions (temperature in the range 22 - 39°C) used by authors whose data is included in the regression database (**Table 5.1**) and for the sake of simplicity of the final model, the temperature difference was not explicitly considered.

5.6. Conclusions

There are several mathematical models that can be used to estimate maximum transdermal flux of xenobiotics. We believe that the major advantage of our model comes from the fact that it requires little or no experimental data. While many models estimating drug skin permeability coefficient use two determinants – $logK_{o/w}$ and MW, with the cost of one additional determinant – MP, the maximum percutaneous flux can be estimated. Also, all three parameters are typically easily accessible and their use can be rationalized based on scientific theory. The model provides simple mechanistic interpretation of the influence of each determinant on J_{max}. When skin permeation measurements are not readily available or a quick screening of a database of compounds is required, this model can readily provide initial estimates of maximum transdermal flux.

Table 5.1. Skin permeation database comprised of 67 compounds, 87 entries. The database was obtained from Magnusson et al. "Molecular size as the main determinant of solute maximum flux across the skin" (supplement, originally named "set t") [196].

#	Compound	$\log J_{max}$ [nmol h^{-1} cm^{-2}]	MW [Da]	$\log K_{o/w}$	MP [°C]*
1	17-alfa-Hydroxyprogesterone	-1.77	330.5	2.89	223
2	2,3-Butanediol	2.75	90.1	-0.99	25
3	2,4,6-Trichlorophenol	2.43	197.5	3.58	69
4	2,4-Dichlorophenol	3.27	163	3	45
5	2-Butanone	4.14	72.1	0.37	25
6	2-Ethoxy ethanol	3.42	90.1	-0.27	25
7	2-Phenylethanol	3.14	122.2	1.36	25
8	3,4-Xylenol	3.17	122.2	2.4	61
9	4-Hydroxybenzyl alcohol	2.03	124.1	0.3	120
10	5-Fluorouracil	0.43	130.1	-0.78	283
11	alfa-(4-Hydroxyphenyl) acetamide	1.63	151.2	-0.29	177
12	Benzene	3.39	78.1	2.22	25
13	Benzoic acid	3.1	122.1	1.9	122
14	Benzoic acid	3.1	122.1	1.9	122
15	Benzyl alcohol	3.38	108.1	1.04	25
16	beta-Estradiol	-0.89	272.4	4.13	176
17	beta-Estradiol	-2.88	272.4	4.13	176
18	beta-Estradiol	-1.2	272.4	4.13	176
19	Betamethasone-17-valerate	-1.65	476.6	3.98	184
20	beta-Naphthol	2.29	144.2	2.71	123
21	Butanol	3.41	74.1	0.88	25

22	Butanol	3.33	74.1	0.88	25
23	Chlorocresol	3.28	142.6	2.89	67
24	Chloroxylenol	2.05	156.6	3.35	116
25	Cortexone	-0.87	330.5	3.41	142
26	Corticosterone	-0.51	346.5	1.76	181
27	Corticosterone	-1.54	346.5	1.76	181
28	Corticosterone	-1.89	346.5	1.76	181
29	Corticosterone	0.17	346.5	1.76	181
30	Cortisone	-2.19	360.5	1.24	222
31	Decanol	1.27	158.3	4.06	25
32	Estriol	-2.23	288.4	2.94	282
33	Estrone	-1.76	270.4	3.69	255
34	Ethanol	4.13	46	-0.19	25
35	Ethyl ether	4.12	74.1	0.98	25
36	Heptanol	2.73	116.2	2.47	25
37	Heptanol	2.66	116.2	2.47	25
38	Hexanol	2.87	102.2	1.94	25
39	Hydrocortisone	-2.64	362.5	1.43	220
40	Hydrocortisone	-2.6	362.5	1.43	220
41	Mannitol	1.95	182.2	-4.67	167
42	Mannitol	1.74	182.2	-4.67	167
43	Mannitol	2.07	182.2	-4.67	167
44	m-Cresol	3.55	108.1	1.94	25
45	Methanol	4.19	32	-0.72	25
46	Methanol	4.7	32	-0.72	25
47	Methyl-4-hydroxy benzoate	2.08	152.1	1.87	128
48	m-Nitrophenol	2.72	139.1	1.93	97
49	Nicotinate, ethyl	3.35	151.2	1.41	25

50	Nicotinate, methyl	3.03	137.1	0.88	43
51	Nonanol	1.77	144	3.53	25
52	o-Chlorophenol	3.75	128.6	2.04	25
53	o-Cresol	3.56	108.1	1.94	30
54	Octanol	2.33	130.2	3	25
55	Octanol	2.4	130.2	3	25
56	o-Phenylenediamine	2.26	108.1	0.05	104
57	p-Bromophenol	3.5	173	2.49	64
58	p-Chlorophenol	3.83	128.6	2.43	44
59	p-Cresol	3.53	108.1	1.94	36
60	p-Cresol	4.38	108.1	1.94	36
61	Pentanol	3.18	88.2	1.41	25
62	p-Ethylphenol	3.15	122.2	2.47	45
63	Phenol	4.23	94.1	1.48	41
64	Phenol	2.12	94.1	1.48	41
65	Phenol	3.83	94.1	1.48	41
66	p-Nitrophenol	2.75	139.1	1.57	114
67	p-Phenylenediamine	1.91	108.1	-0.85	146
68	Prednisolone	-1.56	360.4	1.69	241
69	Pregnenolone	-1.09	316.5	4.52	193
70	Progesterone	-1.37	314.5	4.04	121
71	Propanol	4.35	60	0.34	25
72	Propanol	4.2	60	0.34	25
73	Resorcinol	3.19	110.1	0.76	111
74	Sucrose	1.76	342.3	-3.85	186
75	Testosterone	-1.46	288.4	3.48	155
76	Testosterone	-1.16	288.4	3.48	155
77	Thymol	2.55	150.2	3.28	52

78	Toluene	3.68	92.1	2.68	25
79	Triamcinolone	-3.09	394.5	1.03	270
80	Triamcinolone acetonide	-3.01	434.5	2.6	293
81	Urea	3.4	60.1	-2.11	133
82	Urea	3.24	60.1	-2.11	133
83	Urea	3.13	60.1	-2.11	133
84	Water	4.94	18	-1.38	25
85	Water	4.93	18	-1.38	25
86	Water	4.68	18	-1.38	25
87	Water	4.44	18	-1.38	25

*For liquid permeants the MP was set to 25 °C

Figure 5.1.
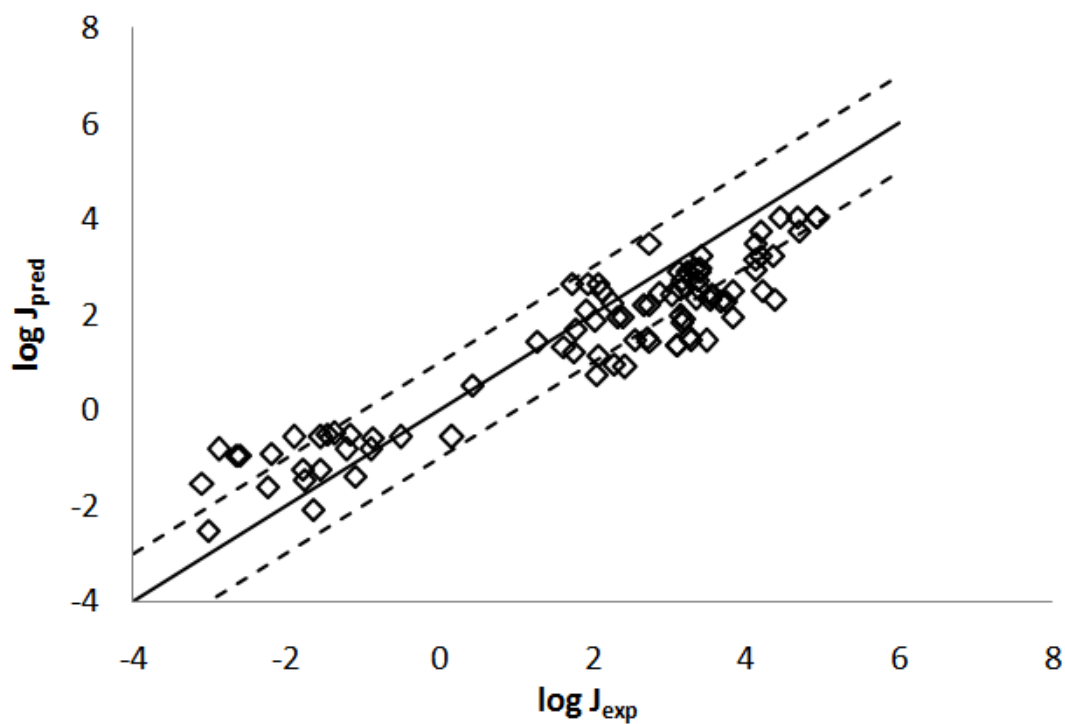
Maximum transdermal flux calculated from Eq. 4 (J_{pred}) plotted against the experimental maximum transdermal flux (J_{exp}) of solutes included in the permeation database (Table 5.1). The solid line indicates ideal correlation while dashed lines enclose the region of ideal correlation ± 1 log unit.

Figure 5.2.
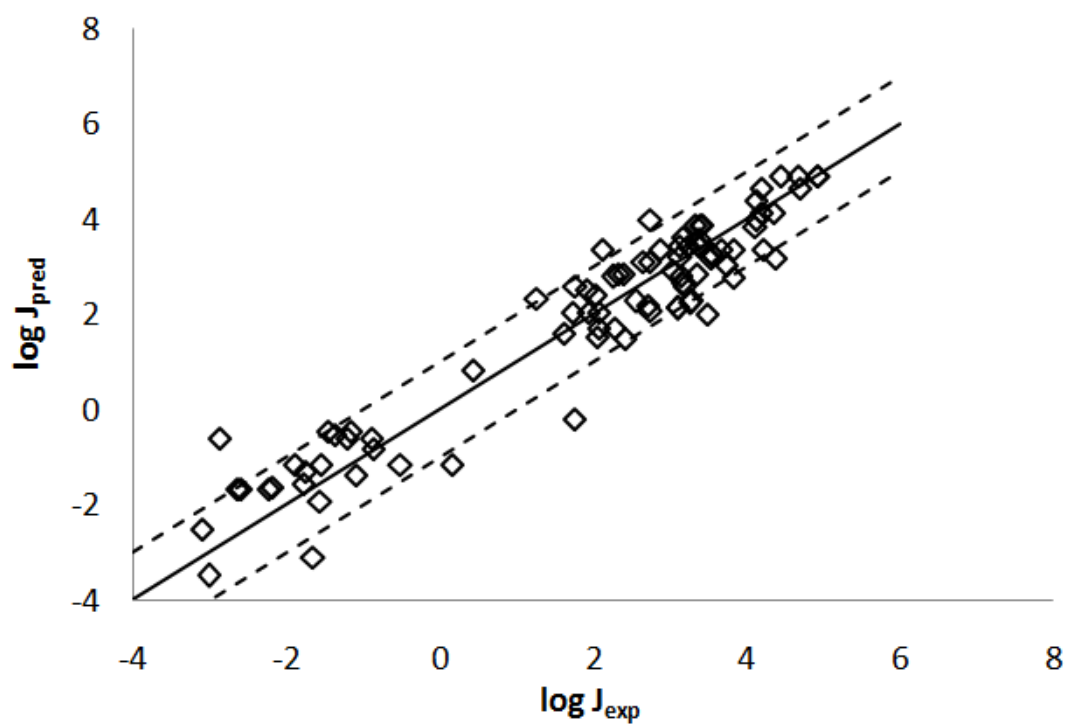
Maximum transdermal flux calculated from eq. (6) (J_{pred}) plotted against the experimental maximum transdermal flux (J_{exp}) of solutes included in the permeation database (Table 1). The solid line indicates ideal correlation while dashed lines enclose the region of ideal correlation ± 1 log unit.

Figure 5.3.
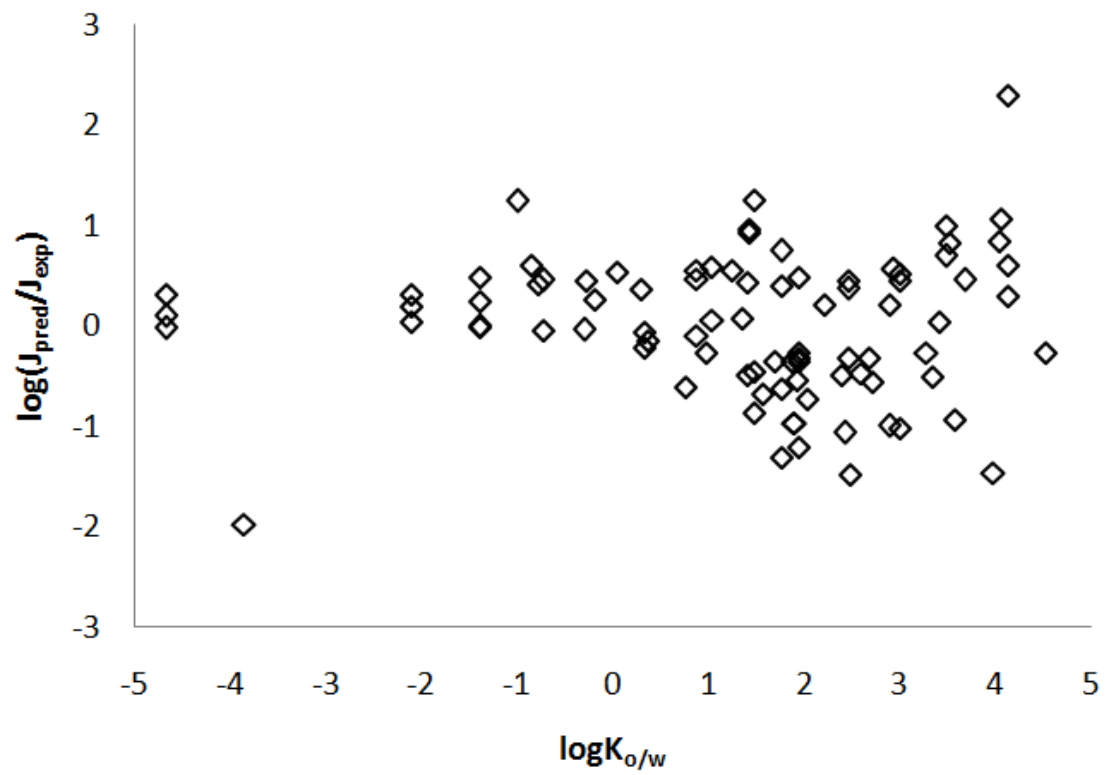
Regression analysis residuals log(J_{pred}/J_{exp}) plotted against logK$_{o/w}$ of permeants

Figure 5.4.
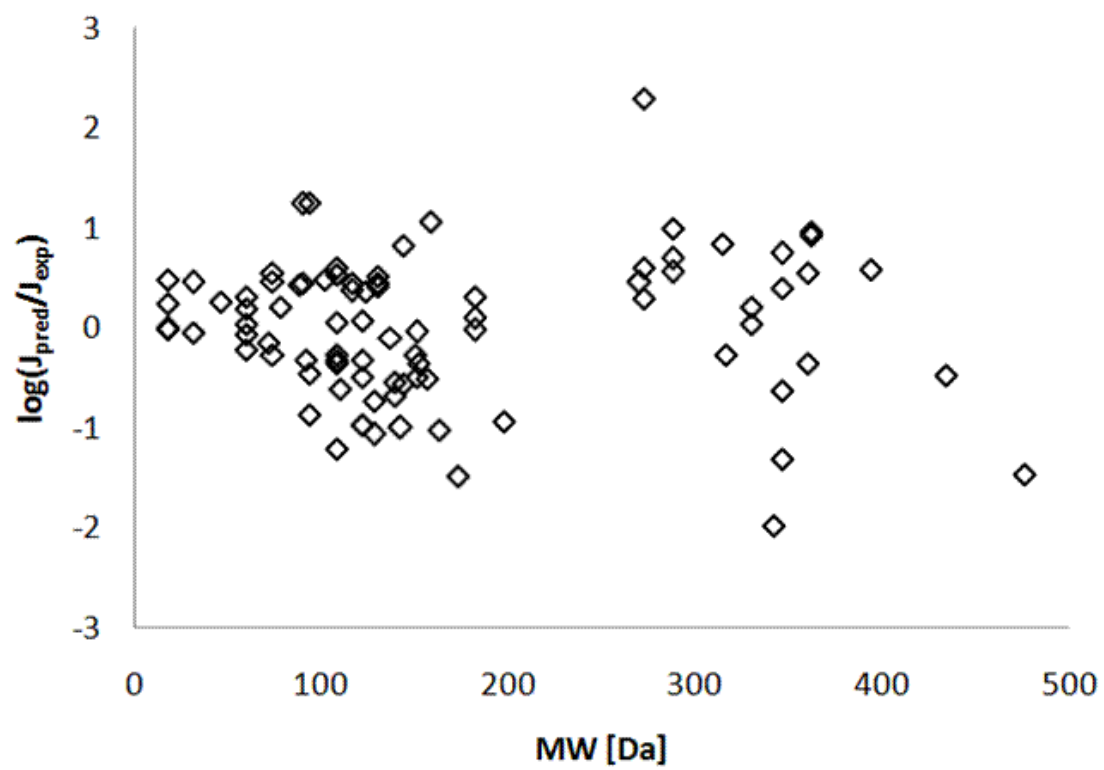
Regression analysis residuals log(J$_{pred}$/J$_{exp}$) plotted against MW of permeants

Figure 5.5.
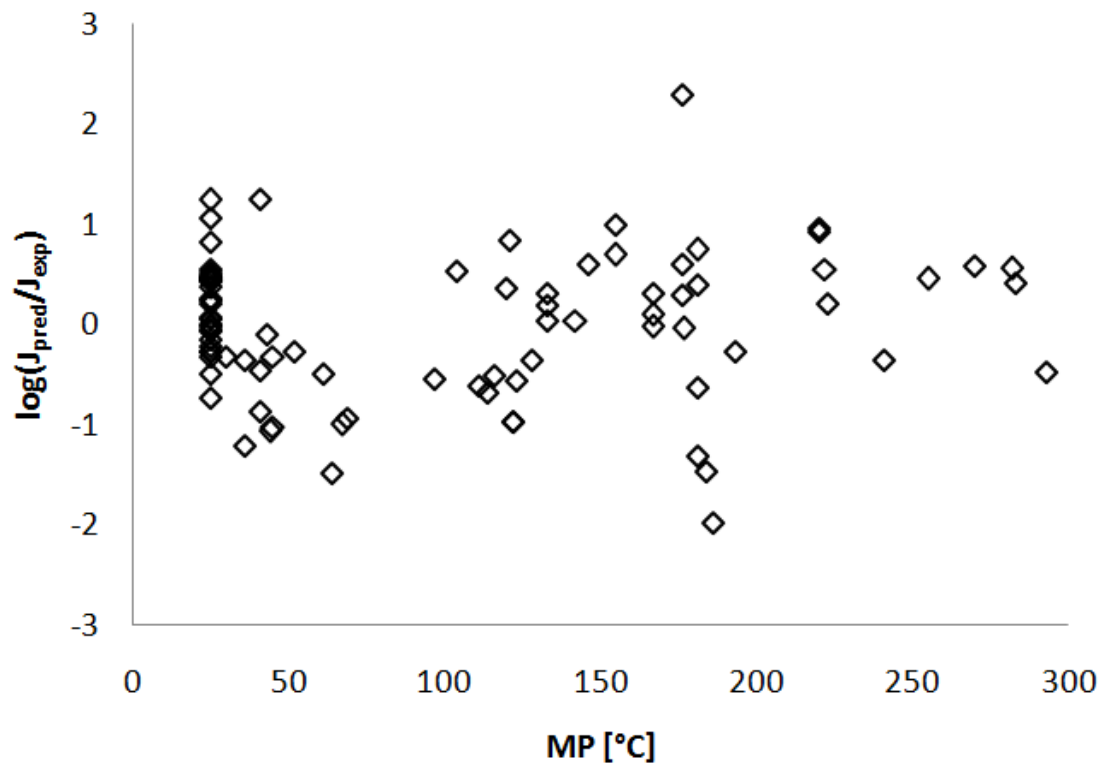
Regression analysis residuals log(J_{pred}/J_{exp}) plotted against MP of permeants

Chapter 6

Development of a mathematical model for characterization of drug transport across microneedle-treated skin

6.1. Introduction

The aim of this chapter is to introduce a simple mathematical model for analysis of the drug permeation data across MN-treated skin in fulfillment of the **research goal 3.1**. Although permeation data can be analyzed without use of any mathematical model by comparison of drug apparent permeability coefficients for MN-treated and untreated skin, such analysis lacks insight and is not easily transferable to different experimental conditions. Therefore, a simple mathematical model, which accounts for existence of two parallel routes of permeation – microchannel pathway and intact skin pathway – and the diffusional resistance of individual skin layers will be introduced. This model will accommodate the change in the number of microchannels created by microneedles, assign the permeability coefficients to unionized and ionized species permeating through either MN-treated or untreated skin, and account for different skin thickness used in the *in vitro* diffusion experiments. Fragments of the following discussion related to conceptual model development have been published in Pharmaceutical Research [39].

6.2. Classical transdermal transport

The description of percutaneous transport across untreated skin usually comprises several assumptions about the nature of the barrier and the nature of the drug penetrating this barrier. Often the barrier properties of the skin can be well-described by accounting for the barrier properties of SC alone. Despite its heterogeneous nature, the SC is frequently assumed to be a thin layer of skin that is lipoidal in nature. Current marketable drugs that are passively delivered through the skin into systemic circulation

73

are uncharged, small and moderately lipophilic compounds [8]. It is believed that these drugs traverse the SC mainly through continuous intercellular lipids, which becomes the rate-limiting step in transport across skin. Hence, the transdermal delivery of fairly lipophilic drugs through intact skin is usually described by the following equation:

$$J_{ISP} = P_{ISP} * \Delta C = K_{SC/veh} * \frac{D_{SC}}{h_{SC}} * \Delta C \qquad\qquad (6.1)$$

where J_{ISP} is flux, P_{ISP} is permeability coefficient, $K_{SC/veh}$ is partition coefficient between SC lipid domain and vehicle, D_{SC} is the diffusivity of the drug in SC, h_{SC} is effective thickness of the SC; and ΔC is the drug concentration difference across SC. The subscript "ISP" refers to the "intact skin pathway" or the only pathway available for drug diffusion across untreated skin. A good understanding of the above parameters and the role they play in transdermal delivery permits recognition of potential drug candidates and optimization of delivery systems.

Many studies have found that the partitioning between SC lipids and aqueous vehicle, although relatively hard to be determined directly, can be estimated by use of the octanol-water partition coefficient $K_{oct/w}$. The character of the octanol microenvironment, although isotropic in nature, was found to be similar to the microenvironment of anisotropic SC lipids and they can be correlated through a linear free energy relationship [179, 180]. On the other hand, the diffusivity of a drug molecule in SC lipids can be linked to its size through a free volume theory. Habitually molecular volume is substituted with molecular weight for simplicity and without large loss of prediction accuracy. This relationship predicts a sharp drop in the drug diffusivity within the SC's lipid bilayers with increasing molecular size [60, 168]. Also, the effective thickness of the SC differs from the real SC thickness. The microstructure of the SC shows keratinocytes

being surrounded by a continuous phase of lipid bilayers in a "brick and mortar"-like arrangement [51, 100, 101]. The actual pathway along which a drug molecule diffuses using intercellular lipid domain across the SC is longer than just its thickness [51, 201-204]. Lastly, transdermal flux is affected by the concentration (more precisely activity) gradient across the SC. When sink conditions are maintained on the receiver side of skin then the concentration gradient is simply the drug concentration in the donor solution. Therefore, the upper limit of the transdermal delivery rate can be attained by using saturated donor solutions. Moreover, having the same drug saturated in different solvents corresponds to the same (maximum) activity of the drug in those solvents [205]. Thus, transdermal flux values obtained from such donor solutions should be the same, as long as the solvent does not significantly affect the permeability of the skin. This is the basis for a generalization that a certain percent solubility of a drug in different solvents will provide approximately the same percutaneous flux. This is expected to be true only if transport across skin is occurring through the intercellular lipid domain of SC and there is no effect of the solvent used on the barrier properties of SC.

6.3. MN-enhanced transdermal transport

Transdermal transport characteristics change dramatically when MN are used as an enhancement method. MN create transient aqueous channels through the upper skin layers thus providing a new route of transport. This new pathway bypasses the SC barrier and continues through microchannels directly into deeper layers of skin. Transport across microchannels, therefore, is not expected to be SC-limited. A diffusing drug molecule needs to traverse several layers in series before it reaches the receiver solution (*in vitro* experiments) or the microvascular bed (*in vivo* experiments). Although this scenario is analogous to delivery across intact skin, one important difference needs to be taken into account. For untreated skin, the diffusional resistance of the SC is

typically orders of magnitude larger and overrides that coming from vehicle, epidermis and dermis [18, 54, 59]. In the context of this thesis, MN-enhanced delivery was limited to the use of MN in skin pretreatment and subsequent application of the drug-containing formulation on the treated area resulting in zero-order drug delivery. Other applications of MN, such as hollow MN with drug, coating MN with drug, using self-dissolving drug-containing MN etc. were not considered for development of this mathematical model. In the case of the microchannel pathway (MCP), corresponding to the channels and underlying dermis, the resistance from SC is eliminated and diffusional resistances from the microchannel and the dermis beneath the microchannel become important. Also, transport is not dependent on partitioning between two distinct hydrophilic and lipophilic phases. The relative contributions of individual layer resistances to the total resistance will determine a new rate-determining step in skin transport. The individual layer resistance depends on drug diffusivity in that layer as well as on its thickness. G. Flynn reported that drug diffusivities in viable tissue (epidermis and dermis) are typically no more than 10 times lower than in bulk water and are without great molecular selectivity [18] while Kretsos et al. calculated the free drug diffusivities in the viable tissue to be about 3.7-fold lower than their diffusivities in water [206]. The thickness of the viable tissue used in *in vitro* diffusion experiments can be controlled by using either different length MN or different thicknesses of skin. In the following studies the thickness of the microchannel layer was typically about half the thickness of the underlying dermis layer (0.6 mm and 1.2 mm, respectively). Hence, it is anticipated that the dermis layer would present a higher resistance to a diffusing drug molecule as compared to the microchannel itself. Nevertheless, the difference between these two layers is not expected to be anywhere close to that between SC and viable tissue seen in delivery through untreated skin. Another crucial difference in transport via the microchannel pathway is the absence of a lipoidal layer that separates vehicle from viable tissue. By

creating microchannels in the skin and bypassing the SC an aqueous pathway is formed for transport which connects an aqueous vehicle through interstitial fluid to the aqueous milieu of viable tissue. As expected, the partition coefficients between aqueous vehicle and dermis for a variety of drugs are close to 1 [18] (and authors unpublished data). Moreover, aqueous vehicles are miscible with interstitial fluid within the microchannels. These conditions sharply contrast those met in the delivery across intact skin. An equation that can describe the steady-state flux through the microchannel pathway is as follows:

$$J_{MCP} = P_{MCP} * \Delta C = \left(\frac{1}{R_{MC} + R_{VT}}\right) * \Delta C = \left(\frac{1}{\frac{h_{MC}}{D_{MC}} + \frac{h_{VT'}}{D_{VT}}}\right) * \Delta C \qquad (6.2)$$

where J_{MCP} is flux, D_{MC} is diffusivity of the drug in the microchannel, D_{VT} is diffusivity of the drug in the viable tissue, h_{MC} is thickness of the microchannel, $h_{VT'}$ is thickness of the underlying viable tissue, and ΔC is the drug concentration difference across skin. The terms in this equation no longer relate to SC as it is not involved in the transport. Instead, two individual resistance terms from the microchannel and the underlying viable tissue are included. One important realization is that, contrary to intact skin, transport through microchannels no longer revolves around SC-oriented optimization of the physicochemical parameters of a drug molecule. A commonly reported $\log K_{o/w}$ value around 2 provided favorable drug partitioning into the lipid domain of the SC lipids and a small molecular volume assured that diffusivity of the drug across SC would be sufficiently high to provide desired transdermal flux. These physicochemical parameters of the drug molecule seem to be no longer critical.

Drug diffusivity in the bulk solution doesn't follow the relationship described by the free volume theory used for SC. Rather, it obeys the Stokes-Einstein equation:

$$D = \frac{kT}{6\pi\eta r} \qquad\qquad\qquad (6.3)$$

Where: k is the Boltzmann constant, T is the absolute temperature, η is the viscosity of the medium and r is the hydrodynamic radius of the solute. Although this equation predicts the decrease of diffusivity with increasing molecular size of the drug molecule, the magnitude of this effect is much smaller. It has been shown by McAllister et al. that MN-enhanced transdermal flux values for a variety of compounds of different sizes correlated well with prediction based on the Stokes-Einstein eq. [27]. It suggests that diffusivity of drug molecules in the microchannels will resemble that in the bulk solution rather than in the SC lipid bilayers. The thicknesses of layers that a diffusing molecule has to traverse in series in an *in vitro* diffusion experiment depend on several factors. In contrast to the SC, the effective thicknesses of the microchannel layer and underlying dermis layer are expected to resemble closely their real thicknesses. Dermis, for the purpose of diffusion studies, is a highly aqueous, gel-like phase with a meshwork of collagen fibers surrounded by a proteoglycan matrix. Molecular motion in this milieu is not restricted to a large extent, and drug molecules can diffuse relatively unhindered along the concentration gradient.

Upon piercing the skin with MN, a new route of delivery is created. This new microchannel pathway (MCP) is in parallel with the intact skin pathway (ISP), which was originally the only route available before the MN treatment. Assuming independence of these two routes, percutaneous flux can be described according to the equation:

$$J_{TOT} = J_{MCP} + J_{ISP} = (f_{MCP} * P_{MCP} + f_{ISP} * P_{ISP})\Delta C \qquad\qquad (6.4)$$

where J_{TOT} is the total flux through MN-treated skin, J_{MCP} is the microchannel pathway flux, J_{IS} is the intact skin pathway flux, f_{MCP} is the fractional skin surface area of the microchannel pathway, P_{MCP} is the apparent permeability coefficient of the microchannel pathway, f_{ISP} is the skin surface fractional area of the intact skin pathway, P_{IS} is the apparent permeability coefficient of the intact skin pathway and ΔC is the drug concentration difference across skin. In other words, the flux values coming from two independent parallel routes are additive. The relative importance of each pathway for a given drug molecule depends on that pathway's distinct features, reflected in the respective permeability coefficient, and the fractional area of skin each pathway covers. A MN treatment produces numerous microchannels; however, the fractional area occupied by them is typically very low. For example, McAllister et al. estimated that in their *in vitro* experimental set-up the fractional area of microchannel pathway was on the order of 0.001 or 0.1% [27]. Consequently, as a result of the MN-treatment the fractional area of intact skin pathway decreases only by 0.1% to 99.9% of the original value. In the *in vitro* diffusion experiments described in the following chapters of this thesis, typically a skin area of 0.95 cm^2 was treated with MN to obtain the total of 100 microchannels. Assuming the diameter of a single microchannel opening is around 50 μm, 100 microchannel openings translate into 0.2 % of the total skin surface area. This allows a simplification to be introduced. Since $f_{ISP} \approx 1$ (100%) the $f_{ISP}*P_{ISP}$ term can be well-approximated by the value of P_{ISP} alone. Additionally, from a practical point of view, the exact knowledge of f_{MCP} is not necessary as long as it remains very small.

In the experiments involving MN, it is sometimes assumed that intact skin is impermeable to drug and flux is ascribed to the microchannel pathway exclusively. This premise may or may not be sound depending on the drug being used and particular experimental conditions and is further discussed in **Chapter 7**. Additional experiments

with untreated skin allow determination of the value of J_{ISP} (P_{ISP}) independently which then can be used to calculate J_{MCP} ($f_{MCP}*P_{MCP}$) from J_{TOT} (P_{TOT}).

MN-enhanced transport permits the use of ionized drug molecules and increases the maximum achievable driving force for diffusion through the use of highly water soluble, charged molecules. The question whether charged molecules can permeate through SC becomes important because the majority of skin surface area after MN-treatment is still intact SC and this pathway may contribute to the total flux. The area of transdermal research dealing with transport of charged molecules across SC is not extensively developed and less understood. There are reports that indicate that the transport of small charged molecules is possible through a polar route in SC [207, 208]. Transport via this polar route is not expected to obey the relationships discussed earlier for classical transdermal delivery. In most cases, the treatment of ionic equilibria in percutaneous transport evokes the pH-partition theory which states that the neutral form of a drug molecule traverses membranes far more readily than its ionized counterpart [66]. Therefore, the correction introduced to solutions containing partly ionized drug is to multiply the total drug concentration by the fraction of uncharged drug. While this approach works, it is important to realize that although the SC permeability of charged species is low, their solubility might be much higher. Consequently, while working with saturated donor solutions at different pH's, the experimental results may be somewhat counterintuitive as evoked by Hadgraft showing higher transdermal flux of ibuprofen in its charged form through intact skin as compared to its uncharged form. These results suggest that, in this particular case, lower permeability of the charged species is more than compensated for by its increased solubility [209]. Another relevant question is how the diffusivity of a molecule in bulk solution changes as its charge varies. It has been shown that the ionization of molecules typically doesn't change their bulk diffusivity much, if at all [54]. In the case of small molecules, the diffusivity of charged species may

drop slightly due to solvation effects and the resulting increase in the hydrodynamic radius. Those effects are not expected to play an important role with regard to larger molecules. Therefore, as long as the microchannel environment can be properly described by bulk solvent properties, one would expect that diffusional resistance of the microchannel should be similar for both charged and uncharged species.

6.4. *In vitro* skin diffusion studies

Full-thickness hairless guinea pig skin was harvested from the dorsal region of euthanized animals. Animal studies were approved by the University of Kentucky IACUC. Subcutaneous fat from skin samples was removed with a scalpel. Such skin samples were immediately placed in a plastic bag and frozen until use (-20 °C). Before the permeation study, skin samples were allowed to thaw for about 30 min. Skin used for MN treatment was placed on a wafer of polydimethylsiloxane polymer, which mimicked the naturally occurring mechanical support of underlying tissue because of its comparable structural elasticity. MN which were obtained from Dr. Prausnitz's laboratory were fabricated by laser cutting of stainless steel sheets as reported previously [210]. MN were solid metal, two-dimensional "in-plane" rows each containing five MN oriented with their axis parallel to the steel sheet. This design is characterized by the following MN dimensions: 750 µm long, 200 µm wide and 75 µm thick. The insertion of MN into skin was carried out manually by applying gentle finger pressure followed by their instantaneous removal. The diffusion area of skin (0.95 cm^2) was pierced 20 times with a row containing five MN (i.e., to make a total of 100 individual and non-overlapping piercings) before mounting the skin in the diffusion cell. If any damage to MN was observed a new array was used. Untreated skin samples were placed directly into the diffusion cells. Three to four cells were used per donor solution composition per case (untreated or MN-treated skin) (n = 3-4). A PermeGear flow-through (In-Line,

Riegelsville, PA) diffusion cell system was used for the *in vitro* diffusion studies. Normal saline with 10% ethanol was used as the receiver solution. The flow rate of the receiver fluid was set at 1.5 ml/h to maintain sink conditions. Skin samples in the diffusion cells were kept at 32°C using a circulating water bath. The diffusion experiments were initiated by charging the donor compartment with 0.3 ml of the donor solution. Samples were collected from the receiver compartment in 6 h increments over 48 h. All samples were stored at 4°C until processed by HPLC. The permeation data were plotted as the cumulative amount of NTX•HCl collected in the receiver compartment as a function of time. The flux value for a given run was calculated from the terminal slope of the cumulative amount plotted vs. time.

Quantitative analysis of indomethacin concentrations was carried out by HPLC. The HPLC system consisted of a Waters 717 Plus autosampler, a Waters 600 quaternary pump, and a Waters 2487 dual wavelength absorbance detector with Waters Empower™ software. A Brownlee (Wellesley, MA, USA) C-18 reversed phase Spheri-5 µm column (220×4.6 mm) with a C-18 reversed phase guard column of the same type (15×3.2 mm) by Perkin Elmer[®] was used with the UV detector set at a wavelength of 254 nm. The mobile phase consisted of 60% methanol and 40% 0.03 M KH_2PO_4 buffer (pH 7.0). Samples were run at a flow rate of 1.5 ml/min with a run time of 8 min. The injection volume used was 100 µl. The retention time of NTX•HCl was 5.0 ± 0.1 min. Samples were analyzed within a linear range of the NTX•HCl standard curve from 100 – 10000 ng/ml.

The statistical analysis of data was carried out with student t-test at significance level α = 0.05 using SIGMA-STAT (SPSS, Inc., Chicago, IL, USA) software.

6.5. Indomethacin permeation

Indomethacin was chosen as a model drug for model testing due to its physicochemical characteristics. Its molecular weight 357.8 Da resembles that of naltrexone 341.4 Da. Indomethacin lipophilicity, as measured by $logK_{o/w}$, is 3.1 and higher as compared to naltrexone's $logK_{o/w}$ of 1.8. Finally, indomethacin is an acid with pK_a of 4.5 while naltrexone behaves as a base at acidic to neutral pH with pK_a of 8.2. Hence, with careful selection of experimental conditions meaningful comparisons between the ionized and unionized species, their solubility and permeability through intact skin and through microchannels can be made.

In the current experimental design two sets of *in vitro* diffusion experiments – with untreated and MN-treated skin – and at two pH values of 2.5 and 8.0 were performed. The absence or existence of microchannels in skin translated into the absence or existence of the microchannel pathway, respectively, in addition to the intact skin permeation pathway, according to **Eq. 6.4**. Next, the pH control allowed influencing the ionization state of indomethacin. At pH of 2.5 (2 units below pK_a) the species predominantly present in the solution were unionized while at pH 8.0 (over 2 units above pK_a) the predominant species were negatively charged. Also, the pH affects the total solubility of indomethacin. At pH 2.5 the saturation solubility in propylene glycol:water (PG:water) 1:3 solution was measured to be 5.1 mg/ml while at pH 8.0 it was 182.3 mg/ml. By performing studies which employ untreated skin at two pH values it is possible to estimate J_{ISP}, and using the experimental drug concentration in the donor solution (equal to saturation solubility) calculate P_{ISP} according to **Eq. 6.1**. On the other hand, carrying out the studies with MN-treated skin provided estimates for J_{TOT} and P_{TOT} from which J_{MCP} and P_{MCP} can be calculated according to **Eq 6.4**. The permeation profiles of indomethacin are presented in **Figure 6.1**. The first striking feature of the comparison is that the flux of indomethacin from a pH 8.0 donor solution and through MN-treated skin

is by far the highest. All other cases resulted in much lower flux. In simple terms, the flux enhancement ratio as result of MN skin treatment at pH 8.0 is around 8-fold. However, at the same time at pH 2.5 this enhancement ratio is only about 1.4-fold. These enhancement ratios are a quick way to estimate the benefit of employing MN in drug delivery but do not provide much insight of the drug transport process. It is difficult to judge why such change in the enhancement ratio is observed as a function of pH. Also, it is difficult to predict what critical parameters govern the permeation through MN-enhanced skin. On the other hand, by **Eq. 6.1** and **6.4** the flux and permeability coefficients corresponding to the intact skin pathway and microchannel pathway can be calculated. The analysis of these parameters provides much more informative comparison. As presented in **Figures 6.2** and **6.3** the total flux J_{TOT} is composed of J_{ISP} and J_{MCP}. However, at pH 2.5 the relative contribution of J_{MCP} to the J_{TOT} is small while at pH 8.0 the contribution of J_{MCP} to the J_{TOT} is overwhelming. To explain this experimental observation it is necessary to recall that at low pH indomethacin is predominantly unionized which makes it a relatively good transdermal permeant through untreated (intact) skin. Thus, the flux across intact skin around microchannels is relatively high and the formation of microchannels increases total flux only by around 40 %. Conversely, at high pH indomethacin is negatively charged which makes it a poor permeant across intact skin. In this scenario, the formation of microchannels in skin brings about a substantial increase in the total flux of around 800 %. Ionized species are not disfavored at permeation through microchannel pathway because there is no requirement of crossing highly resistive barrier of stratum corneum lipids. Thus, the recourse to the nature of the permeant and barrier of the intact skin pathway and microchannel pathway can satisfactorily explain experimental observations. Interestingly, it should be noted that in terms of indomethacin permeation through the intact skin alone, the highly soluble but poorly permeating ionized species provide higher flux over poorly soluble but highly

permeating neutral species. This demonstrates that the drop in the indomethacin permeability coefficient caused by ionization (**Figure 6.4**) is more than compensated for by the increase in the donor solution solubility. Even more interesting is the evaluation of ability of the ionized and neutral species to permeate through the microchannel pathway. **Figure 6.4** shows that the permeability coefficients of negatively charged and neutral species are statistically equal (t-test p>0.05). This finding suggests that the intrinsic ability of indomethacin to permeate across microchannel pathway is independent of the molecular charge. Since the length of the microchannel h_{MC} and underlying dermis $h_{VT'}$ are experimental constants, the comparisons of permeability coefficients can be interpreted as changes in drug diffusivity. Such observation is in good agreement with the fact that diffusivity of the molecule in bulk solution is independent of or barely affected by its electronic state [54]. Also, since the permeability coefficients of negatively charged and neutral species were found to be the same it implies that the drug diffusivity in the whole microchannel pathway – including underlying dermis – is independent of the molecular charge. This bears an important consequence on the overall understanding of drug delivery through MN-treated skin. First, the current data suggests that high aqueous solubility, irrespective of the permeant's charge, will result in the elevated flux though microchannel pathway. In reality, for many permeants high aqueous solubility is achieved through the presence of molecular charge. Second, the apparent enhancement ratios obtained as a consequence of MN skin treatment at different pH values will primarily depend on the permeant's ability to cross the untreated (intact) skin as its ability to permeate through the microchannel pathway remains the same irrespective of the ionization state. Finally, the direct comparison of total permeability coefficients P_{TOT}, which can be done without use of the mathematical model presented herein (**Figure 6.4**), is meaningless because P_{TOT} contains confounded information about overall permeation and does not discriminate between intact skin and microchannel pathways.

Hence, no differences in the nature of the barriers are recognized and properly addressed by such comparison.

Furthermore, **Figure 6.4** reports the P_{MCP} values multiplied by fraction of skin surface area available for microchannel pathway f_{MCP}. This approach allows a direct comparison between the magnitude of indomethacin flux between 100 microchannels used in the present study (microchannel pathway) and 1 cm^2 of intact skin. To obtain a comparison between the relative ease at which indomethacin permeates the same area of microchannel pathway and intact skin pathway a correction accounting for the surface of the area taken by the microchannel pathway f_{MCP} needs to be made. Assuming a 50 μm opening of a single microchannel a f_{MCP} of 0.2 % can be calculated. Numerically, P_{MCP} is expected to closely mimic the permeability coefficient that would be obtained by employing SC-devoid skin in *in vitro* diffusion experiments. At pH 2.5, unionized indomethacin has a P_{MCP} of 8.77 10^{-3} cm h^{-1} and P_{ISP} of 4.07 10^{-5} cm h^{-1}. This translates into approximately 200-fold increase in the ease of permeation through microchannel pathway as compared to the intact skin pathway. On the other hand, at pH 8.0, ionized indomethacin has a P_{MCP} of 1.71 10^{-2} cm h^{-1} and P_{ISP} of 4.93 10^{-6} cm h^{-1}. This translates into approximately 3500-fold increase in the ease of permeation through microchannel pathway as compared to the intact skin pathway. The difference in these values, again, is reflective of the change in the ability of ionized and unionized species to permeate through intact skin pathway and not their ability to permeate through microchannel pathway which remains unchanged. Also, the influence of number of microchannels present in the skin on the flux is accounted for by f_{MCP}. It was found that flux increases proportionally with the increase in the number of microchannels in accordance with **Eq. 6.4** (unpublished data). Lastly, the influence of the thickness of the microchannel layer (its length) and the thickness of the underlying dermis on steady-state flux is also

incorporated in the model. An increase in the barrier thickness causes inversely proportional drop in the flux. This topic will be further discussed in the **Chapter 10**.

A reasonable doubt can be expressed about the statistical equivalency of the microchannel pathway permeability coefficients presented in **Figure 6.4**. The error related to the P_{MCP} estimate at pH 2.5 is large and makes the power of comparison with P_{MCP} at pH 8.0 less than desirable. However, it should be noted that the attainment of P_{MCP} estimate at pH 2.5 with narrow margin of error is extremely difficult. This is due to the fact that it is calculated from the difference of P_{TOT} and P_{ISP} which is numerically very small. Despite of the reasonable errors associated with both P_{TOT} and P_{ISP} estimates the error associated with the difference between these values becomes large. The only way to address this issue is the collection of extremely precise estimates of P_{TOT} and P_{ISP}. At present, the comparison reported herein between P_{MCP} at pH 2.5 and 8.0 is deemed acceptable, however, more precise estimates would be very helpful in strengthening the conclusions.

6.6. Naltrexone and 6β-naltrexol permeation

The permeation of naltrexone and 6β-naltrexol across MN-treated skin had been extensively studied [6, 32, 155, 211]. *In vitro* diffusion experiments of similar design to these described above for indomethacin showed that the highly water-soluble ionized species in combination with microneedle skin treatment afforded the highest transdermal flux. On the other hand, the effect of microchannels on the permeation of unionized species was much less pronounced. In other words, the overall behavior of naltrexone and 6β-naltrexol seems to follow the trend seen for indomethacin [6]. Noteworthy, the ionized species of naltrexone and 6β-naltrexol possess positive charge unlike negatively charged indomethacin.

6.7. Conclusions

A simple mathematical model was developed for analysis of steady-state permeation data through MN-treated skin. The distinct feature of the model is that it recognizes the microchannels as a separate permeation pathway in parallel to the intact skin permeation pathway. Since the fractional skin surface area taken by the microchannel openings is very small the formation of microchannels does not significantly affect the intact skin pathway. Hence, MN-treatment can be seen as a method of providing an additional permeation pathway through skin without affecting an already existing one. *In vitro* diffusion studies with indomethacin demonstrated that the formation of microchannels increases percutaneous drug transport. The magnitude of flux enhancement depends on the drug donor solution solubility and permeability through both: intact skin pathway and microchannel pathway. The interplay between these factors determines the overall benefit of using MN. Former studies carried out with naltrexone and 6β-naltrexol provided similar results. This mathematical model provides a simple framework for analysis of *in vitro* permeation data presented in **Chapters 7,8 and 9**.

Figure 6.1.
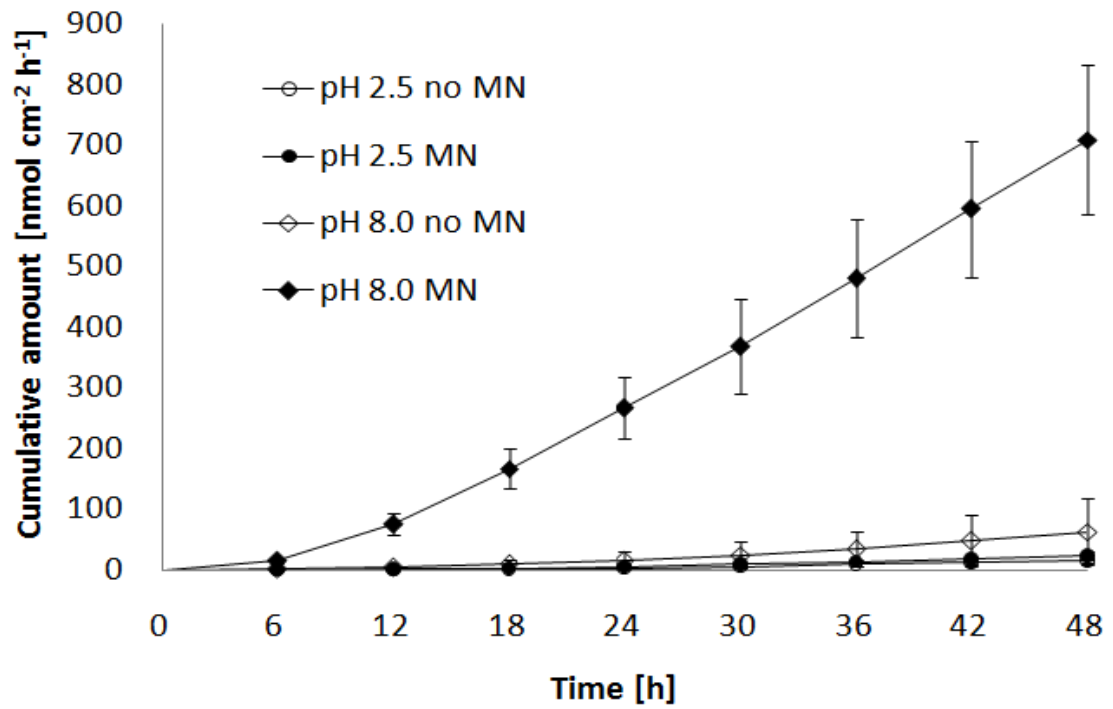
Permeation of indomethacin across untreated and MN-treated guinea pig skin at two different pH values 2.5 and 8.0. Mean ± SD (n = 3-4).

Figure 6.2.
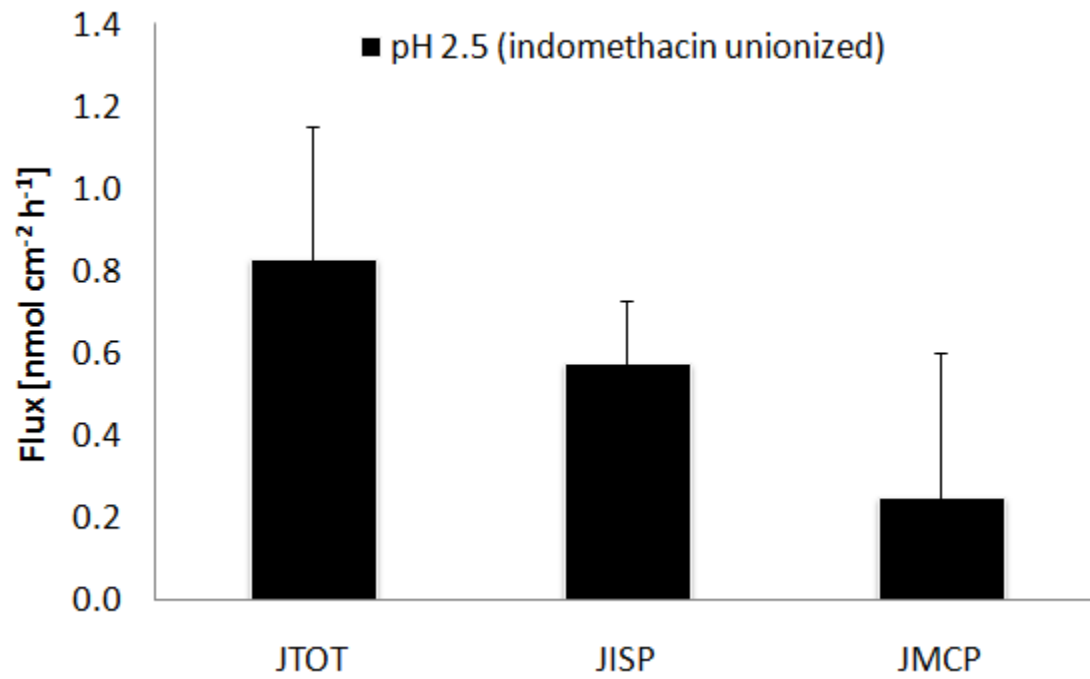
Indomethacin flux at pH 2.5 across MN-treated guinea pig skin (J_{TOT}), intact skin pathway (J_{ISP}) and microchannel pathway (J_{MCP}). Mean ± SD (n = 3-4).

Figure 6.3.
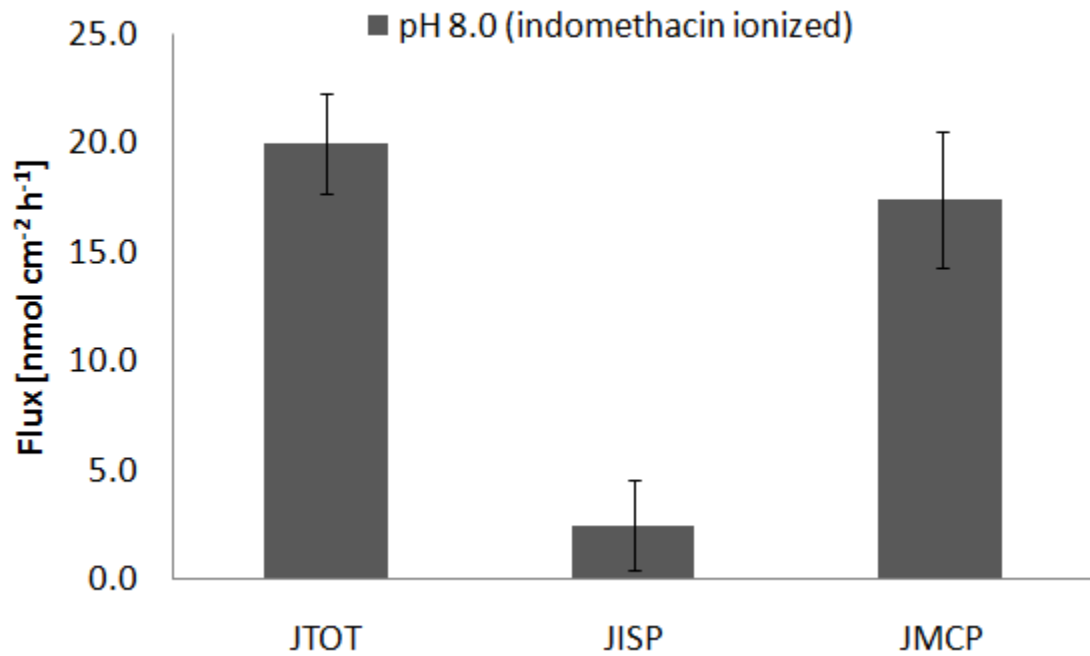
Indomethacin flux at pH 8.0 across MN-treated guinea pig skin (J_{TOT}), intact skin pathway (J_{ISP}) and microchannel pathway (J_{MCP}). Mean ± SD (n = 3-4).

Figure 6.4.
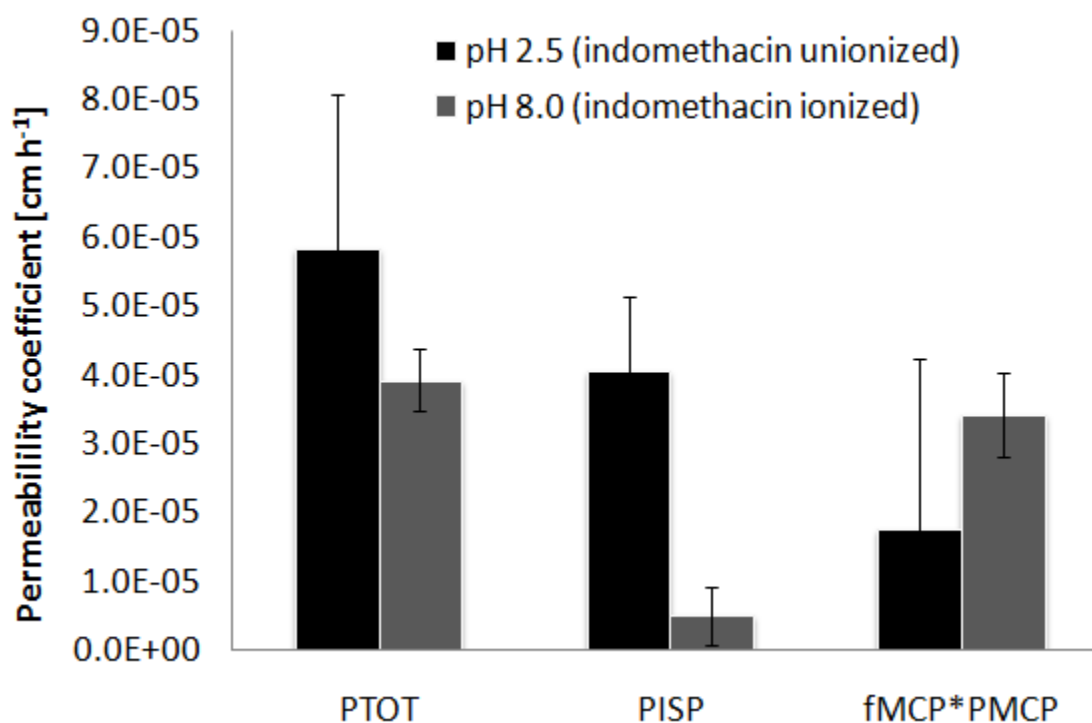
Indomethacin permeability coefficients at pH 2.5 and 8.0 across MN-treated guinea pig skin (P_{TOT}), intact skin pathway (P_{ISP}) and microchannel pathway (P_{MCP}). Mean ± SD (n = 3-4). P_{ISP} at two pH values is statistically different (t-test $p<0.05$), while $f_{MCP}*P_{MCP}$ at two pH values is not statistically different (t-test $p>0.05$).

Chapter 7

Formulation effects on the *in vitro* permeation of naltrexone hydrochloride across untreated and microneedle-treated skin

7.1. Introduction

The purpose of this chapter is to present the formulation optimization efforts to maximize the delivery of naltrexone hydrochloride through MN-treated skin. As stated in the **research plan 3.2** there is a literature gap with respect to examination of preferred formulation characteristics for MN-enhanced drug transport. Oftentimes, diffusion studies involve a direct application of an aqueous drug solution to the treated skin area. This approach works well in *in vitro* conditions. However, in *in vivo* studies the application of drug-containing aqueous solution although not impossible [212], is highly inconvenient and without prospect of being ultimately developed into a practical transdermal patch. It is the intent of this chapter to first analyze the influence of the propylene glycol, a ubiquitous thickening cosolvent excipient in percutaneous drug delivery, on the flux of NTX•HCl in an aqueous system. Then, the application of other cosolvents will be examined. Finally, gel systems will be investigated and the application of gels and hydrocolloids in *in vivo* studies will be briefly discussed. Fragments of the following discussion related to the use of propylene glycol have been published in Pharmaceutical Research [39].

The SC possesses formidable barrier properties that prevent most xenobiotics from permeating through the skin. Since the pool of molecules possessing necessary physicochemical properties to cross this barrier is limited, the amount of drugs that can be delivered percutaneously at therapeutically relevant rates is also low [17, 18, 141]. Increasing drug permeation rates across skin represents a great challenge. MN offer a method of substantially increasing the transdermal delivery of drugs by transiently

compromising the barrier properties of SC. The use of MN enables the formation of microchannels that extend over upper layers of skin and allow drug molecules to diffuse directly into deeper layers of skin. In general, this process results in up to several orders-of-magnitude enhancement of transdermal transport of drugs [6, 27, 152, 213].

Naltrexone is a potent, competitive opioid receptor antagonist. It is used to treat opioid and alcohol addiction [83]. This drug undergoes an extensive first-pass effect and is characterized by low and varying bioavailability ranging from 5 to 40% [214, 215]. The currently marketed oral ReVia® and Depade® are not well-suited for long-term therapy as they produce gastrointestinal side effects and result in poor patient compliance. On the other hand, injectable Vivitrol® affords effective plasma levels for as long as 30 days but necessitates in reporting to a healthcare professional upon administration [80]. Also, it cannot be easily discontinued, if needed, without painful surgical removal. It would, therefore, be advantageous to use the transdermal route of delivery for this drug. A transdermal patch would allow eliminating some of the drawbacks related to either oral or injectable alternatives. Since naltrexone itself does not possess the physicochemical properties that would result in percutaneous transport at therapeutically relevant rates an enhancement method is needed [20]. Previous studies showed that a prodrug strategy resulted in increased percutaneous transport of NTX, however, observed flux values were still below expectations [21, 96, 164]. Alternatively, MN were used to improve the delivery of the highly-soluble hydrochloride salt form of NTX. Initial *in vitro* and *in vivo* animal studies proved the utility of the MN method of enhancement showing approximately an order-of-magnitude increase in the transdermal flux over that through non-MN treated skin [6]. Subsequently, the first published human MN study demonstrated that skin pretreatment with MN and subsequent application of four NTX patches afforded drug plasma levels in the lower end of the therapeutic range targeted [216]. The results of these studies validated the interest put into the development of MN

techniques for increased transport of drugs across skin. Although a large number of articles focusing on the engineering aspects of MN use and their effectiveness has been published there is little systematic work done in the area of the formulation influence on the rate of MN-enhanced transdermal delivery of drugs. Recent publications report the efforts to combine liposomes with skin MN pretreatment to further increase drug delivery rates [28, 217]. Y. Qiu et al. studied the combined strategy of using conventional and elastic liposomes with MN skin pretreatment for the delivery of poorly water-soluble docetaxel through porcine skin. The results indicated that this approach afforded superior flux values from both liposomal drug formulations as compared to the saturated docetaxel solution alone. Additionally, the elastic liposomes produced shorter lag times as compared to conventional liposomes. Another study by M.M. Badran et al. focused on the effect of the microneedle length and flexible liposomal formulation on the transport of a model hydrophilic compound, mannitol, through human skin. It was shown that the flexible liposomal formulation delivered a larger fraction of the dose applied in the donor compartment as compared with the aqueous mannitol solution. Moreover, the effect of MN length on flux values was more pronounced in liposomal formulations. These examples illustrate that adequate formulation choice may have a substantial effect on the delivery through MN-enhanced skin.

PG is a very common, generally recognized as safe (GRAS), non-irritating cosolvent widely used in topical formulations [218]. It is fully miscible with water and as such is often used to increase the solubility of poorly water soluble compounds in formulations. Its effect on the transdermal delivery of drugs has been the subject of many studies. In the ideal case when the vehicle does not affect the integrity and barrier properties of the SC, flux values from saturated solutions of a given drug should be the same as suggested by Higuchi [205]. Therefore, the presence of PG in an aqueous formulation of a saturated drug solution should not translate into a different flux. However, it rarely is

the case. B.W. Barry examined the PG-human skin interactions and implied that this cosolvent can act as a skin permeation enhancer by solvating keratin and occupying hydrogen-bonding sites as well as promoting drug partitioning into the skin [219]. Similarly, Michael Goodman et al. suggested that the effect of PG on human skin may be related to the solvation effects on keratin in the corneocytes [220]. Later, N.A. Megrab, A C. Williams and B.W. Barry showed that saturated PG-rich donor solutions afforded higher flux values of estradiol through human epidermal membranes as compared to their water-rich counterparts [221]. Authors explained the outcome in terms of increased solubility of estradiol in SC which was not offset by somewhat decreased apparent diffusivity of the drug in the barrier. On the other hand, L. Trottet et al. studied the depletion of PG from topical drug-containing formulations *in vitro*. It was found that the permeation enhancement effect on human cadaver skin showed time-dependence that correlated with PG levels in the formulation [222]. In another study, Christophe Herkenne et al. investigated the effect of PG on ibuprofen absorption on into human skin *in vivo*. Authors found that PG enters SC increasing ibuprofen's solubility in the barrier but does not affect the drug's diffusivity in the barrier [223]. Moreover, R.M. Watkinson et al. studied the influence of the PG concentration on the permeation of ibuprofen *in vitro*. The experiments were analyzed in terms of thermodynamic (partitioning) and kinetic (diffusivity) parameters. In accordance with the above studies it was concluded that the effect of PG on the human epidermis had little effect on the drug diffusivity in the barrier but had a substantial influence on the partitioning from the vehicle into the SC [224]. In other words, it seems that the predominant effect on the PG on the human skin is reflected in the increased solubility of lipophilic drugs in the PG-altered SC but little effect, if any, on the drug diffusivity in this rate-limiting environment. These are a few examples illustrating that PG affects and modifies dermal permeation rates of drugs through intact skin.

No published studies to date have focused on the investigation of the PG effect on the MN-enhanced transdermal delivery of drugs. Since PG is ubiquitous in the area of topical formulation, understanding its influence on transport could provide some insights into formulation optimization for this new enhanced route of delivery. The present study is an evaluation of the effect of different PG-water donor solution compositions on the rate of delivery of NTX•HCl through MN-treated skin.

7.2. Materials and methods

Chemicals

NTX hydrochloride was purchased from Mallinckrodt (St. Louis, MO, USA). Water was purified using NANOpure Diamond^{TM}, Barnstead water filtration system. 1,2-Propanediol, Hanks' balanced salts modified powder, and sodium bicarbonate were purchased from Sigma (St. Louis, MO). 4-(2-Hydroxyethyl)-1-piperazineethanesulfonic acid (HEPES), gentamicin sulfate, trifluroacetic acid (TFA), triethylamine (TEA), 1-heptane sulfonic acid sodium salt, and acetonitrile (ACN) were obtained from Fisher Scientific (Fairlawn, NJ). Reagent-grade chemicals were obtained from Sigma Chemical Company (St. Louis, MO).

Donor solution preparation

Adequate volumes of deionized water and PG (total 5 ml) were pipetted into a disposable plastic beaker and stirred magnetically until well-mixed. Seven donor solution PG-water binary mixtures with the following compositions were prepared: 0-100, 10-90, 25-75, 40-60, 75-25, 90-10 and 0-100 % (v/v). To each of these donor solutions NTX•HCl was added to obtain the concentration of 110 mg/ml. The solutions were placed in glass vials, closed tightly with a plastic cap, sonicated for 15 min and left in the shaking water bath at 32 °C overnight before use to ensure all the drug is dissolved.

NTX•HCl solubility

The apparent solubilities of NTX•HCl in different composition PG-water binary mixtures were obtained by equilibrating excesses of NTX•HCl with these mixtures. Each slurry was continuously shaken in a tightly closed glass vial in a shaking water bath at 32 °C. Samples were taken at 24h, 48h, 72h and 96h, filtered using a 32°C prewarmed syringe and VWR syringe filter with a 0.2 µm membrane, and diluted with the adequate amount of acetonitrile-water 70:30 (v/v) to be analyzed by HPLC. Long equilibration time proved to be necessary for PG-rich donor solutions for which the attainment of equilibrium was slow. The solubility determination was repeated twice for each sample (n = 2).

Viscosity measurements

A Brookfield DV-III LV programmable cone/plate rheometer with a CPE-40 spindle was used for measuring viscosity of the donor solutions. The sample volume was 0.5 ml. All determinations were carried out at 32^0C using a circulating water bath TC-102. Each donor viscosity measurement was taken three times at low, medium and high instrument torque value in the range of 10-100% (n = 3). Results are reported as mean and standard deviation.

In vitro diffusion studies

Full-thickness Yucatan minipig skin (approximately 1.8 mm thick) was harvested from the dorsal region of a euthanized 6-month-old animal. Animal studies were approved by the University of Kentucky IACUC. Subcutaneous fat from skin samples was removed with a scalpel and sparse hair shaved. Such skin samples were immediately placed in a plastic bag and frozen until use (-20 °C). Before the permeation study, skin samples were allowed to thaw for about 30 min. Skin used for MN treatment was placed on a

wafer of polydimethylsiloxane polymer, which mimicked the naturally occurring mechanical support of underlying tissue because of its comparable structural elasticity. MN which were obtained from Dr. Prausnitz's laboratory were fabricated by laser cutting of stainless steel sheets as reported previously [210]. MN were solid metal, two-dimensional "in-plane" rows each containing five MN oriented with their axis parallel to the steel sheet. This design is characterized by the following MN dimensions: 750 µm long, 200 µm wide and 75 µm thick. The insertion of MN into skin was carried out manually by applying gentle finger pressure followed by their instantaneous removal. The diffusion area of skin (0.95 cm^2) was pierced 20 times with a row containing five MN (i.e., to make a total of 100 individual and non-overlapping piercings) before mounting the skin in the diffusion cell. If any damage to MN was observed a new array was used. Untreated skin samples were placed directly into the diffusion cells. Three to four cells were used per donor solution composition per case (untreated or MN-treated skin) (n = 3-4). A PermeGear flow-through (In-Line, Riegelsville, PA) diffusion cell system was used for the *in vitro* diffusion studies. Isotonic HEPES-buffered Hanks' balanced salts solution (pH 7.4) was used as the receiver solution. The flow rate of the receiver fluid was set at 1.5 ml/h to maintain sink conditions. Skin samples in the diffusion cells were kept at 32 °C using a circulating water bath. The diffusion experiments were initiated by charging the donor compartment with 0.3 ml of the donor solution. Samples were collected from the receiver compartment in 6h increments over 48h. All samples were stored at 4 °C until processed by HPLC. The permeation data were plotted as the cumulative amount of NTX•HCl collected in the receiver compartment as a function of time. The flux value for a given run was calculated from the terminal steady-state portion of the graph. Permeability coefficients can be calculated from Fick's first law of diffusion:

$$\frac{1}{A}\left(\frac{dM}{dt}\right) = J_{SS} = P * \Delta C \qquad\qquad\qquad (7.1.)$$

where, J_{ss} is the steady-state flux, M is the cumulative amount of NTX•HCl permeating the skin [nmol], A is the area of the skin [0.95 cm^2], P is the effective permeability coefficient [cm h^{-1}], and ΔC is the concentration difference [nmol cm^{-3}] of the drug in donor and receiver solutions. Since sink conditions prevail under constant flow of the receiver solution ΔC is well-approximated by the drug donor concentration alone.

Quantitative analysis

Quantitative analysis of NTX•HCl concentrations by HPLC was carried out using a modification of the assay described by Hussain et al. [225]. The HPLC system consisted of a Waters 717 plus autosampler, a Waters 600 quaternary pump, and a Waters 2487 dual wavelength absorbance detector with Waters Empower™ software. A Brownlee (Wellesley, MA, USA) C-8 reversed phase Spheri-5 μm column (220×4.6 mm) with a C-8 reversed phase guard column of the same type (15×3.2 mm) by Perkin Elmer® was used with the UV detector set at a wavelength of 215nm or 278nm. The mobile phase consisted of 70:30 (v/v) ACN:(0.1% TFA with 0.065% 1-octane sulfonic acid sodium salt, adjusted to pH 3.0 with TEA aqueous phase). Samples were run at a flow rate of 1.5 ml/min with a run time of 4 min. The injection volume used was 100 μl. The retention time of NTX•HCl was 2.3 ± 0.1 min. Samples were analyzed within a linear range of the NTX•HCl standard curve from 100 – 10000 ng/ml. The standard solutions exhibited excellent linearity over the entire concentration range employed in the assays.

Hydrogel preparation

Commercially available AquaSite® (Derma Sciences, Princeton, NJ) hydrogel sheets were cut into circular discs, 0.9 cm in diameter. Next, a solution of benzyl alcohol 1%, ethanol 5%, propylene glycol 10% and water for injection 84% (v/v) was prepared and NTX•HCl was dissolved to obtain a concentration of 110 mg/ml. A four-fold excess of NTX•HCl solution, with respect to the weight of the hydrogel, was equilibrated with the discs for 48 h. The equilibrium NTX•HCl concentration in the hydrogel discs was determined by HPLC to be 90 mg/g. Drug-loaded hydrogel discs were applied on the MN-treated skin areas.

Statistical analysis

The statistical analysis of data was carried out with one-way ANOVA using SIGMA-STAT (SPSS, Inc., Chicago, IL, USA) software. $P < 0.05$ was considered statistically significant.

7.3. Propylene glycol

The aim of this study was to investigate the influence of PG-water donor solution composition on the MN-enhanced transdermal flux of naltrexone hydrochloride *in vitro*. In order to do so, a series of seven donor solutions containing equal concentrations of NTX•HCl 110mg/ml were prepared. This subsaturation concentration was chosen to avoid potential problems related with the use of saturated solutions with excess solid such as obstruction of microchannel openings or deposition of solid drug in the microchannels. These donor solutions consisted of binary mixtures of PG and water. One set of *in vitro* experiments aimed at evaluating transdermal NTX•HCl flux with the use of MN, the other employed untreated (no MN) skin.

Naltrexone pK_a values at 32 °C calculated with the help of the Van't Hoff's equation are 8.20 and 9.63 [226]. The first pK_a corresponds to the dissociation of the protonated

101

aliphatic nitrogen proton and the second to the dissociation of the phenolic proton. The pH of a 110 mg/ml aqueous solution of NTX•HCl was found to be 4.95. Hence, in this solution NTX is expected to be positively charged.

Figure 7.1 shows a representative diffusion profile of NTX•HCl through MN-treated skin and untreated skin. The steady-state is reached quickly for MN-treated skin but less rapidly for untreated skin. This is consistent with a previous report which showed decreased lag times upon pretreatment with MN [6]. Transdermal flux values were obtained from the slope of the linear, terminal portion of the graph. Individual flux values obtained from each donor solution composition were collected and plotted against the increasing concentration of PG in the donor solution. **Figure 7.2** shows the summary of data derived from two sets of experiments. The first set of experiments evaluated the permeation of NTX•HCl through MN-enhanced skin. Transdermal flux values varied greatly with the highest flux of 30.9 ± 4.4 µg cm^{-2} h^{-1} obtained from a pure aqueous solution and the lowest flux 0.8 ± 0.3 µg cm^{-2} h^{-1} corresponding to a pure PG solution. The gradual drop in the transdermal flux was a non-linear function of the PG content in the donor solution with the greatest effect seen in water-rich solutions. The magnitude of the flux difference obtained from MN-treated skin is as much as ≈40 fold and indicates how great the influence of the formulation on this route of delivery can be. Additionally, the same set of experiments was repeated with the intact, non-MN-treated skin. The results revealed that for all donor solutions tested the flux values were much lower ranging from 0.3 ± 0.02 to 3.4 ± 1.0 µg cm^{-2} h^{-1}. Initially, the increase in the PG content in the donor solution resulted in a slight rise in the flux, but between 10% and 40% PG-water (v/v) the flux values leveled off and finally dropped from PG-rich solutions. The maximum flux was measured from a 25% (v/v) PG-water donor solution. Although there is a qualitative trend in the data showing that water-rich donor solutions provide higher flux over PG-rich donor solutions, this trend doesn't mimic the one seen with MN-treated

102

skin. Hence, the effect of donor solution composition is different and had a much more pronounced effect on MN-treated skin as compared to the untreated skin.

The same data can be presented in terms of the flux enhancement calculated as the flux through MN-treated skin over that through untreated skin. **Figure 7.3** shows such enhancement as a function of the donor solution composition. Clearly, the enhancement obtained by piercing the skin with MN is not the same for all formulations and equals ≈17 for the pure aqueous donor but drops to only ≈3 for PG-rich donors. Therefore, it seems that the flux enhancement, although providing a quick measure of the efficacy of skin MN-treatment, may be of limited practical use as it varies with formulation.

7.4. Viscosity influence on drug diffusivity

In order to examine in more detail the possible reason for seeing a non-linear rise in the MN-enhanced flux with increasing donor solution water content the viscosities of PG-water binary mixtures were measured and are presented in **Table 7.1**. The donor solutions' viscosities seem to be inversely related to the flux obtained from experiments with MN-enhanced skin. Such a relationship may be described by the Stokes-Einstein equation (**Eq. 6.3**). To better visualize the interrelation between flux and donor viscosity, the original data is plotted as NTX•HCl flux versus its calculated diffusivity in the donor solution. The diffusivity of NTX in water was calculated using the Stokes-Einstein equation using an experimentally determined viscosity value of 1.03 cP and assuming the hydrodynamic molecular radius is 4.6 Å yielding a value of $4.7 \ 10^{-6} \ cm^2 \ s^{-1}$ [227]. Other diffusivity values of NTX in PG-containing donors were obtained by employing the experimentally determined viscosity of the relevant donor solution. In **Figure 7.4** two data sets correspond to the experiments performed with MN-enhanced and untreated skin and the third set results from the treatment of data according to **Eq. 6.4**. The experiments carried out with MN-treated skin provided transdermal flux corresponding to

J_{MCP} and J_{ISP} while those with untreated skin produced flux corresponding to J_{ISP} alone. By simple subtraction, the value of the microchannel pathway flux is obtained. It is worth noting that in **Figure 7.4** the data points corresponding to PG-rich solutions are situated to the left of the graph, unlike any other table of figure reported here.

It can be noted that J_{ISP} doesn't show linear dependence on diffusivity of the donor solution. This is not surprising, as in the presence of SC one would expect that it will provide a major diffusional resistance. If the drug molecule traverses SC by partitioning into intercellular lipids and diffusing along its tortuous route, then in the ideal case, the transdermal flux should correlate with percent saturation of the donor solution. The apparent solubility of NTX•HCl in donor solutions is summarized in **Table 7.2.** There is a qualitative agreement between percent saturation in donor solution and observed flux. Furthermore, PG is known to be a weak permeation enhancer and may affect SC characteristics adding additional complexity to the interpretation of data from intact skin experiments.

On the other hand, J_{MCP} correlates with NTX diffusivity in the donor solution. The fact that a very good linear correlation ($R^2 = 0.99$) was observed for microchannel pathway flux is interesting because it indicates that although the diffusivity calculations in **Figure 7.4** account for the changes of the donor solution exclusively, it seems that they reflect drug diffusivity changes in the whole microchannel pathway. A possible explanation for this observation is that PG diffuses out of donor solution into MN-treated skin affecting its diffusional properties. To test that hypothesis a calculation accounting for changes in drug diffusivity in the microchannel and underlying dermis was carried out. In the first case (**Figure 7.5**), it was assumed that PG enters the microchannels, which causes a decrease in NTX diffusivity in this region but no changes in NTX diffusivity in the underlying dermis are observed. In the second case (**Figure 7.6**), it was assumed that not only PG enters the microchannels, which causes a decrease in NTX diffusivity in this

region, but also it decreases NTX diffusivity in the underlying dermis. The calculations assumed the changes in diffusivity can be well-described by Stokes-Einstein equation (**Eq. 6.3**), effective f_{MCP} of 2%, and the following NTX diffusivity values for microchannels and dermis unaffected by PG: 4.7 10^{-6} [cm s^{-1}] and 3.4 10^{-6} [cm s^{-1}], respectively. In the first case, the overall diffusional resistance is controlled mainly by the resistance of the viable tissue and only in the PG-rich region the diffusional contribution of the microchannels comes into play. On the other hand, in the second case, the total diffusional resistance is practically equal to the resistance of the viable tissue throughout the whole range of vehicle composition tested. When these resistance values are used to calculate steady-state microchannel pathway flux, the profiles shown in **Figure 7.7** are obtained. The experimental data closely follows the pattern outlined by the prediction based on the second case calculations. Considering the above, it seems that it is not reasonable to assume that by varying the propylene glycol-water composition of the donor solution, only the properties of the vehicle and microchannel but not dermis are affected. In such case, in water-rich solutions transport through the microchannel pathway would likely be controlled by diffusion through viable tissue underlying the microchannel. Therefore, transdermal flux would not be expected to correlate with viscosity of the donor solution until the viscosity of the donor solution would be high enough to produce microchannel resistance that would overcome the resistance of the underlying dermis. The prediction based on the first case reveals insensitivity of microchannel pathway flux to the changes in composition of water-rich donors, but their dependence on the donor composition in the PG-rich region. The experimental data obtained in the current study clearly shows that this is not the case. Conversely, the experimental profile correlated well with prediction based on the second case and can be explained by the influence of propylene glycol on the diffusional properties of both

microchannel and underlying dermis through the relationship predicted by the Stokes-Einstein equation.

The J_{TOT} obtained from MN-treated skin experiments also seems to follow the linear correlation with NTX donor solution diffusivity calculated from viscosity determinations (R^2 = 0.98). The likely reason for this is that the contribution of J_{ISP} to the J_{TOT} in water-rich donors is minor. As shown in **Figure 7.8**, the contribution of J_{ISP} to the total flux is of most importance in the PG-rich donors where it accounts for around 40% of J_{TOT} but diminishes to less than 10% in water-rich donors. **Figure 7.4** obscures the region corresponding to the PG-rich solutions which could reveal difference between behavior of J_{MCP} and J_{TOT} as their values diverge in this area. In order to have a closer look at the difference between J_{TOT} and J_{MCP} the original data set was transformed by normalization of transdermal flux on the basis of viscosity. Since it was observed that viscosity of donor solutions seems to affect transdermal flux in MN-treated skin in accordance to the Stokes-Einstein equation, viscosity influence on flux can be cancelled out by multiplying the observed flux by individual viscosities of donor solutions according to the equation:

$$J^{'} = J * \eta \qquad\qquad\qquad\qquad (7.2)$$

where: J' is the viscosity-normalized flux, J is the flux and η is the viscosity of the donor solution. Such viscosity-normalized flux values are presented in **Figure 7.9.** The viscosity-normalized flux values correspond to a donor viscosity of 1 cP which is close to the value obtained for aqueous solutions. It can be noted that the viscosity-normalized flux values remain relatively constant both for the microchannel pathway alone and for the microchannel and intact skin pathways combined (MN-treated skin total flux) irrespective of the donor composition used. Statistical analysis (ANOVA) revealed no statistically significant difference between viscosity-normalized flux values within either

of the two data sets at $\alpha = 0.05$. Because of large uncertainty in viscosity-normalized flux values in PG-rich donor solutions it is impossible to discriminate between J_{TOT} and J_{MCP}. Nevertheless, **Figure 7.9** suggests that while J_{MCP} flux shows no trend as donor solution composition is varied the J_{TOT} shows a slightly decreasing trend with increasing PG content in the donors. This observation is in accordance with the expectation that only the microchannel pathway resistance closely correlates with donor solution composition. Total flux, besides J_{MCP}, also incorporates J_{ISP} which doesn't depend greatly on the viscosity of the donor solution. Overall, the behavior of viscosity-normalized J_{MCP} indicates that accounting for viscosity of the donor solution can very well predict the microchannel pathway transdermal flux. It is important to note that in the experimental set-up used in the present work the concentration of NTX•HCl in all donor solutions was maintained at a constant value, and therefore the relationship shown here between flux and viscosity is exactly the same for corresponding permeability coefficients and viscosity.

Since from the practical point of view one is often interested in the maximum flux attainable it is interesting to look at the apparent solubility of NTX•HCl in different donor solutions and their viscosities. As reported in **Table 7.2**, the addition of PG to an aqueous donor gradually increases NTX•HCl solubility up to the donor solution composition of PG-water 90-10 after which a sharp drop is observed. Simultaneously, higher NTX•HCl concentration causes elevated viscosity of the donors. The data show that increased solubility is more than compensated for by elevated viscosity, and therefore saturated and PG-containing solutions of NTX•HCl do not deliver the drug at higher rates though MN-treated skin as compared to purely aqueous, saturated donor solution (data not shown).

7.5. Other common excipients

At the next stage of investigation, the main question to be addressed was whether the apparent viscosity effect on flux seen in the propylene glycol study can be generalized to other cosolvents and excipients. This information is valuable from the perspective of optimization of formulations designed for MN-enhanced skin. Besides viscosity, some other factors that might come into play are the difference in the osmotic pressure between the donor and receiver solutions. This could drive the water flow across microchannels in the opposite direction and interfere with drug permeation. Other possibilities are related to the pH-gradients across skin and possibility of convectional flow through microchannels. To address these possibilities collectively in a qualitative manner an experiment was designed in which the viscosity of the donor solutions containing NTX•HCl and excipients at different concentrations was kept constant. Other parameters such as osmotic pressure and pH varied. By comparing the experimental results to the viscosity-predicted conclusions were drawn.

The selection of excipients involved: propylene glycol (PG), poly(ethylene glycol) 400 (PEG 400), sucrose and hydroxyethylcellulose (HEC). All four were compared to the NTX•HCl permeation from an aqueous donor solution alone. For all donor solutions the NTX•HCl was kept constant at 90 mg/g.

Figure 7.10 demonstrates experimental NTX•HCl steady-state flux obtained from five different donor solutions. Also, flux is compared to the viscosity-based prediction calculated from Stokes-Einstein equation (**Eq. 6.3**). It is important to realize the flux values collected in this study are total flux through MN-treated skin and not microchannel pathway flux values since no experiments were performed with untreated skin. It is implicitly assumed that the contribution of flux through the intact skin pathway is small at all times. Hence, it is expected that some error will be introduced by such simplification. For example, for PG based on **Figure 7.5**, an error of around 20 % can be expected.

Table 7.3 summarizes the physicochemical properties of the formulations including excipient concentration, solution viscosity, osmotic pressure, and pH. As evident from **Figure 7.10** flux values obtained from donor solutions containing PG, PEG 400 and sucrose agree reasonably well with the predictions based on the viscosity donor solution changes (pair-wise t-test between experimental and predicted values show no difference at α = 0.05). Flux obtained from donor solution containing HEC does not (the means are statistically different at α = 0.05). First, it is interesting to analyze the PG-containing donor solution which is characterized by osmotic pressure approximately 4-fold higher than either solution containing PEG 400 or sucrose. It could be expected that the flow of water in the opposite direction to the drug flux could slow down the apparent permeation of NTX•HCl from a high-osmotic-pressure donor solution. However, no evidence of such behavior is observed. The flux values obtained from the first three solutions are approximately the same and there is no trend corresponding to the varying osmotic pressure of the donor solutions. The same holds true for the apparent pH effects. However, a major striking feature of **Figure 7.10** is the disagreement between the experimental and predicted flux value seen for HEC-based donor solution. The experimental flux is statistically equal (p > 0.05) to the flux obtained from purely aqueous solution. No drop in the transport rate is observed even though the viscosity of the donor solution is 2.45 cP. A plausible explanation to this apparent discrepancy is related to the fact that HEC is the only high-molecular-weight polymer used in the study. It can be envisioned that the diffusion of 720 kDa molecules into the microchannel will be very slow due to is low aqueous diffusion coefficient. Moreover, its mobility may be further limited in dermis if it ever reaches that skin layer. As a result it could be anticipated that the diffusional properties of the skin will not be altered. At the same time the molecular mobility of NTX•HCl in the HEC solution is not expected to be lowered as the macroviscosity measured experimentally does not mimic microviscosity of the solution.

The concept of micro- and macro-viscosity applies to gel systems and the diffusion coefficients of low-molecular-weight drugs will be related to the microviscosity only. In case of large compounds such as proteins microviscosity may not correlate well with a diffusion coefficient as hindrance coming from gel meshwork can no longer be ignored. According to Zhao and Chen the discrepancy between the macro- and micro-viscosity for a HEC solution at 0.13% (w/w) used in this study is approximately 2.5-fold [228]. In consequence, the microviscosity of the HEC solution is close to 1cP, or, the viscosity of the aqueous solution. This finding rationalizes the equivalent flux from HEC and aqueous donor solutions.

7.6. Gel systems

The findings of the preceding section are directly applicable to the development of a gel-based transdermal system. Gels offer the advantage of relatively sturdy structure and easy-to-use formulation form. In the following study, the effect of increasing concentration of the HEC in the NTX•HCl-containing donor solution was evaluated. HEC gellified aqueous donor solutions at the concentration of 1% (w/w) reached a macroviscosity of approximately 1000 cP, while the microviscosity only increases to about 1.03 cP [228]. Higher HEC concentrations provide gels of even higher macroviscosity, which slows down the gel flow and makes their use *in vivo* more convenient. NTX•HCl at 90 mg/ml in aqueous solution, 2% HEC, 3% HEC, and 4% HEC were used as donor solutions. The flux through MN-treated skin was recorded and is presented in **Figure 7.11**. As demonstrated experimentally, indeed, the flux drops only marginally as a result of the increase of the HEC in the donor solution from 0 to 4%. Hence, it was confirmed that for a gel system the macroviscosity does not correlate with the flux through MN-treated skin.

7.7. Sheet hydrogels and hydrocolloids

Despite the encouraging results from gel formulations presented in the proceeding section additional improvement of the formulation was desired. The main reason for further formulation optimization is not related to the rate of NTX•HCl percutaneous transport but to the fact that amorphous gels, although a major step forward as compared to aqueous solutions, still presented practical challenges when applied *in vivo*. One of the main problems was the containment of the gel in a custom-made covering patch over the experimental duration of several days. Amorphous gel had a tendency to leak from beneath the prototype patch and out of the MN-treated skin area. Another challenge was related to the fact that gels based solely on aqueous solutions with no cosolvents present (PG or PEG 400) tended to collapse during *in vivo* experiments due to the water evaporation at elevated skin temperature of 32 °C. To address these two major concerns the suitability of commercially available wound dressings as vehicles for MN-assisted drug delivery were evaluated. Two distinct classes of dressings: sheet hydrogel and hydrocolloids were selected.

Sheet hydrogels, besides the benefit of providing a vehicle from which NTX•HCl could be delivered through MN-enhanced skin at the rate similar to the one obtained from aqueous solution, also provided additional benefit of improved formulation sturdiness. As the name implies the sheet hydrogels are not amorphous, but rather formed in a disc or square-shape and don't flow. That allowed full control over the application area and addressed the first containment problem. Of three commercially available sheet hydrogels tested: AquaFlo™ (Kendall), AquaClear® (Hartmann), and AquaSite® (Derma Sciences), the latter was found to have the properties that best suited *in vivo* study needs. As for the second problem, the addition of 10% highly-hygroscopic PG to the formulation allowed several-day use of hydrogels without collapse or drug precipitation.

A price, however, is paid in an approximate 25% decrease in the flux due to the microviscosity increase.

The sheet hydrogel formulations were prepared by 48 h equilibration of the commercial product with the excess solution of NTX•HCl at 100 mg/ml in 10% PG aqueous solution. The hydrogel absorbs loading solution with the end result of increase in the hydrogel mass about 4-fold. Such prepared formulations were tested in an *in vitro* diffusion experiment across MN-treated skin and compared to the loading solution alone, and the gel formulation used previously in the first-in-human MN study [216]. The following flux values at 48 h were obtained: new AquaSite®-based hydrogel formulation 74.5 ± 6.7 nmol cm^{-2} h^{-1}, loading solution 71.6 ± 13.1 nmol cm^{-2} h^{-1}, and former gel formulation 11.9 ± 0.5 nmol cm^{-2} h^{-1} (courtesy of Priyanka Ghosh). In conclusion, formulation optimization resulted in a 6-fold increase in *in vitro* flux and an improved, more user-friendly hydrogel sheet form.

Apart from the sheet hydrogels, another group of wound dressing products that was selected for testing were hydrocolloid dressings. These dressings possess lower water content than hydrogels, but also absorb aqueous solution to a great degree and additionally possess acrylate adhesives which facilitate adhesion to skin. Two commercial products were evaluated: Tegaderm^{TM} hydrocolloid dressing (3M^{TM}), and Cutinova Hydro (Smith&Nephew). The experimental procedure involved the preloading of hydrocolloid dressing by equilibration with a drug-containing loading solution. However, the hydrocolloid performance in *in vitro* diffusion studies was less than satisfactory. The non-steady-state flux at 48 h was only 17.8 ± 3.7 nmol cm^{-2} h^{-1} and the altered structure of the fully-hydrated dressing made it impossible to provide appropriate intimate adhesion to the MN-treated skin surface (courtesy of Priyanka Ghosh).

7.8. Conclusions

Overall, it is possible that factors other than the viscosity of the donor solution can influence MN-enhanced percutaneous flux. One example is the case of drugs with lipid binding and protein binding potential in dermis. Low binding to immobile cell-membrane dermal lipids as well as low-mobility albumins would be expected to elongate lag times, but not to affect steady-state flux values. However, in the case of drugs extensively bound to albumin the diffusivity of the drug-albumin complex would need to be considered and could translate into lower-than-expected permeation rates.

In conclusion, this work investigated the influence of donor solution composition on the rate of transdermal transport of NTX•HCl through MN-enhanced skin. It was found that flux correlated well with changes in drug diffusivity caused by donor viscosity variations. Also, it is likely that the microchannel pathway flux rather than total flux (combined microchannel pathway and intact skin pathway flux) correlates with viscosity changes of donor solution through the Stokes-Einstein equation. Moreover, this work indicates that percutaneous flux of charged species across intact skin may become important when a large skin area is exposed to the drug formulation. In broader context, the findings of this work may help improve the design of delivery systems for MN-enhanced skin. In classical percutaneous delivery the vehicle plays a critical role in the appearance and delivery rates of a drug. Excipients impart the desired rheological character to the dosage form. Also, they determine physical properties of the vehicle and its ability to modify stratum corneum, the rate-limiting barrier to transport of most drugs. PG, PEGs and other viscous cosolvents are common excipients used in topical dosage forms. Changes in the physicochemical characteristics may promote drug partitioning from a topically applied formulation into the barrier as well as diffusion of drug molecules through the barrier. Based on the results from current work it seems reasonable to state that when maximum flux through MN-treated skin is sought, then the viscosity of the

formulation should be kept as low as possible. However, that restriction does not hold with respect to high molecular weight polymeric systems which do not seem to increase the diffusional resistance of the microchannel pathway. The selection of a water-rich sheet hydrogel formulation proved the most successful in conjunction with MN-assisted transdermal drug transport.

Table 7.1. Viscosities of NTX•HCl (110 mg/ml) in PG-water binary mixtures (n = 3)

NTX•HCl 110mg/ml in PG-water % (v/v)	0-100	10-90	25-75	40-60	75-25	90-10	100-0
Viscosity [cP] ± SD	1.03 ± 0.01	1.48 ± 0.03	2.47 ± 0.01	4.01 ± 0.01	14.40 ± 0.00	28.43 ± 0.12	46.33 ± 1.01

Table 7.2. Apparent NTX•HCl solubility and corresponding viscosity in binary mixtures of PG-water (n = 2 for solubility determinations and n = 3 for viscosity determinations)

PG -water %(v/v)	0-100	10-90	25-75	40-60	75-25	90-10	100-0
NTX•HCl solubility [mg/ml] ± SD	121 ± 1	148 ± 24	159 ± 1	189 ± 22	222 ± 12	301 ± 3	130 ± 5
Viscosity [cP] ± SD	1.09 ± 0.00	1.70 ± 0.02	2.94 ± 0.01	5.20 ± 0.01	20.97 ± 0.06	61.00 ± 0.53	51.57 ± 0.25

Table 7.3. The summary of physicochemical properties of the donor solutions containing NTX•HCl at 90 mg/g and the excipient listed in the first column of the table. Concentrations of excipients vary but the donor solution viscosity remains approximately constant 2.7 cP. Osmotic pressure (∏) and apparent pH describe the characteristics of the donor solutions while the difference in the osmotic pressure (Δ∏) and the difference on the apparent pH refer to the difference between donor and receiver solutions.

Donor solution	MW [Da]	Concentration [% (w/w)]	Concentration [mol/l]	Viscosity [cP]	∏ [mOsm]	Δ∏ [mOsm]	pH_{app}	ΔpH
PG	76	29.7	3.91	2.66	4222	3922	3.35	4.05
PEG 400	400	22.1	0.55	2.67	1277	977	3.15	4.25
sucrose	342	27.4	0.80	2.98	1346	1046	5.40	2.00
HEC	720 000	0.13	1.8×10^{-6}	2.45	311	11	5.04	2.36
DI water	n/a	n/a	n/a	0.98	312	12	5.31	2.09

Figure 7.1.
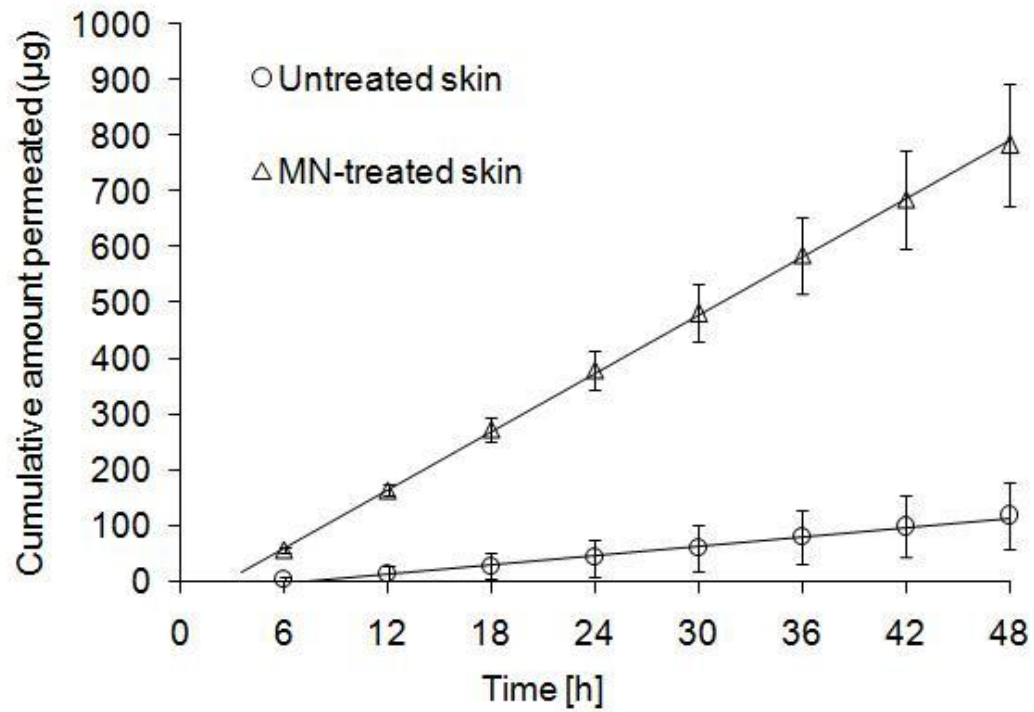
Representative diffusion profile of NTX•HCl through MN-treated Yucatan minipig and intact skin (PG-water 25:75 v/v) (n=3).

Figure 7.2.
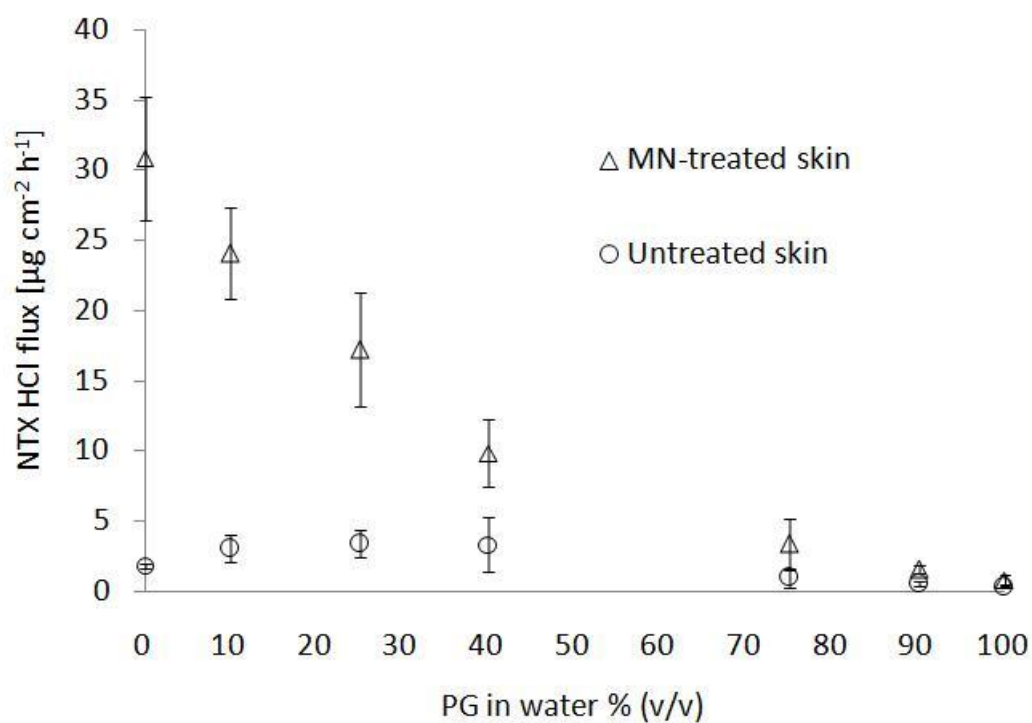
Steady-state flux values of NTX•HCl permeating through untreated and MN-treated Yucatan minipig skin as a function of the donor solution composition. The concentration of NTX•HCl is constant 110 mg/ml for all donors, while the amount of PG increases to the right of the graph (n = 3–4).

Figure 7.3.
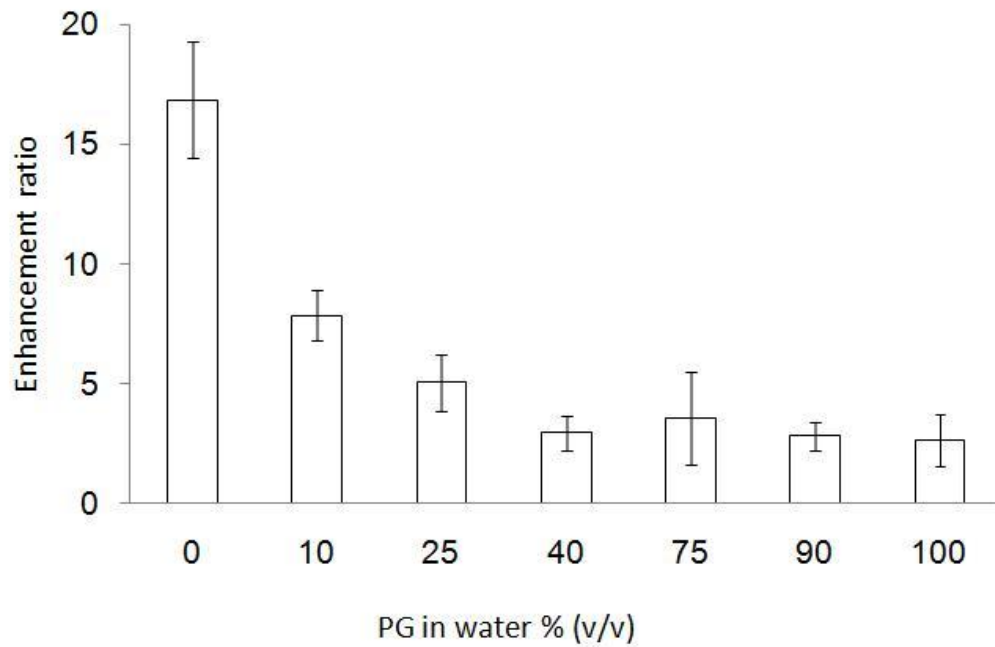
NTX•HCl flux enhancement as a result of MN-treatment of the Yucatan minipig skin (n = 3–4).

Figure 7.4.
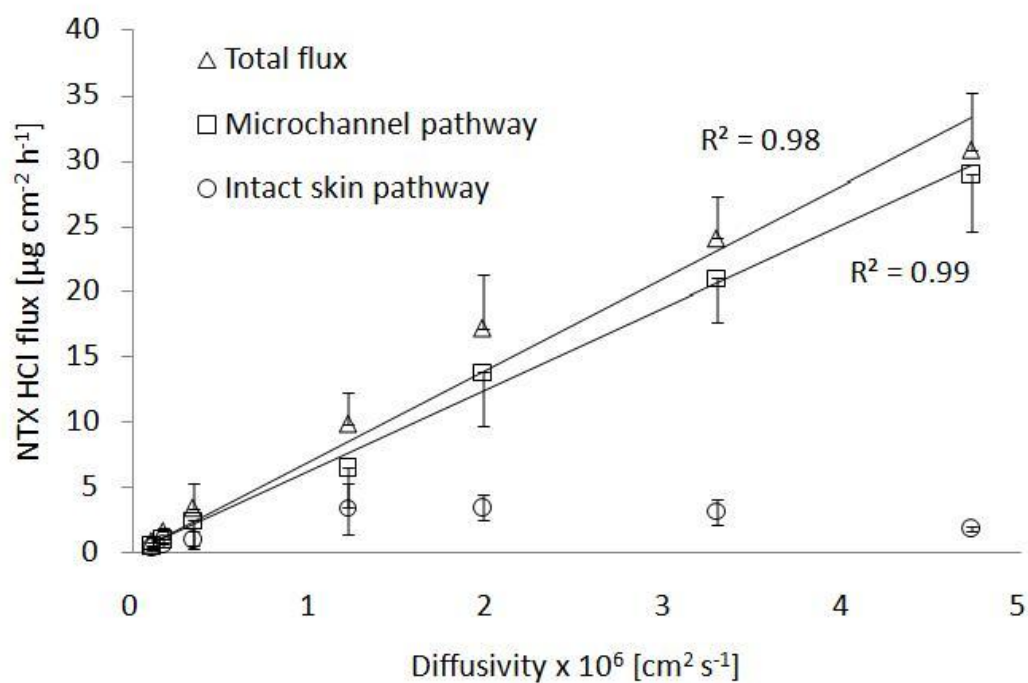
Steady-state flux values of NTX•HCl for intact skin pathway, microchannel pathway, and the sum of both plotted against calculated diffusivity of NTX in the donor solution. Low diffusivity on the left of the graph corresponds to the PG-rich donors (n = 3–4).

Figure 7.5.

Legend: ■ Microchannel pathway flux □ Intact skin pathway flux

X-axis: 0, 10, 25, 40, 75, 90, 100

PG in water % (v/v)
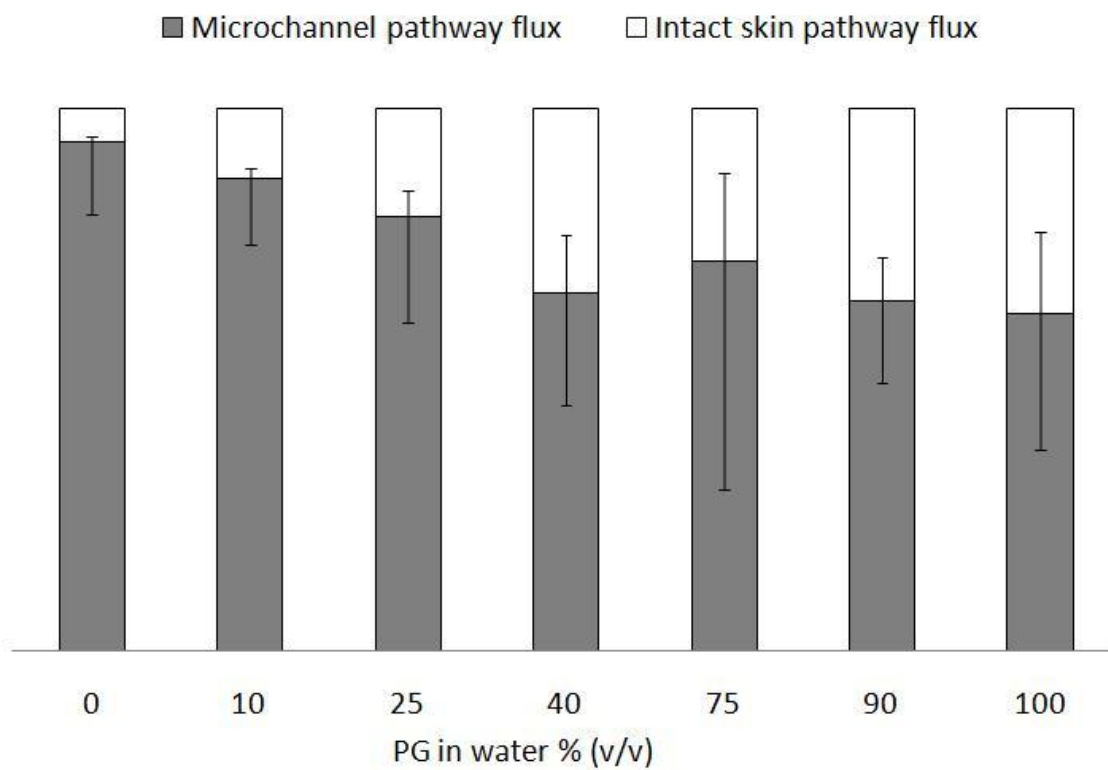
Relative contribution of microchannel pathway flux and intact skin pathway flux to the total transdermal flux of NTX•HCl. Calculated according to Eq. 6.4. (n = 3–4).

Figure 7.6.
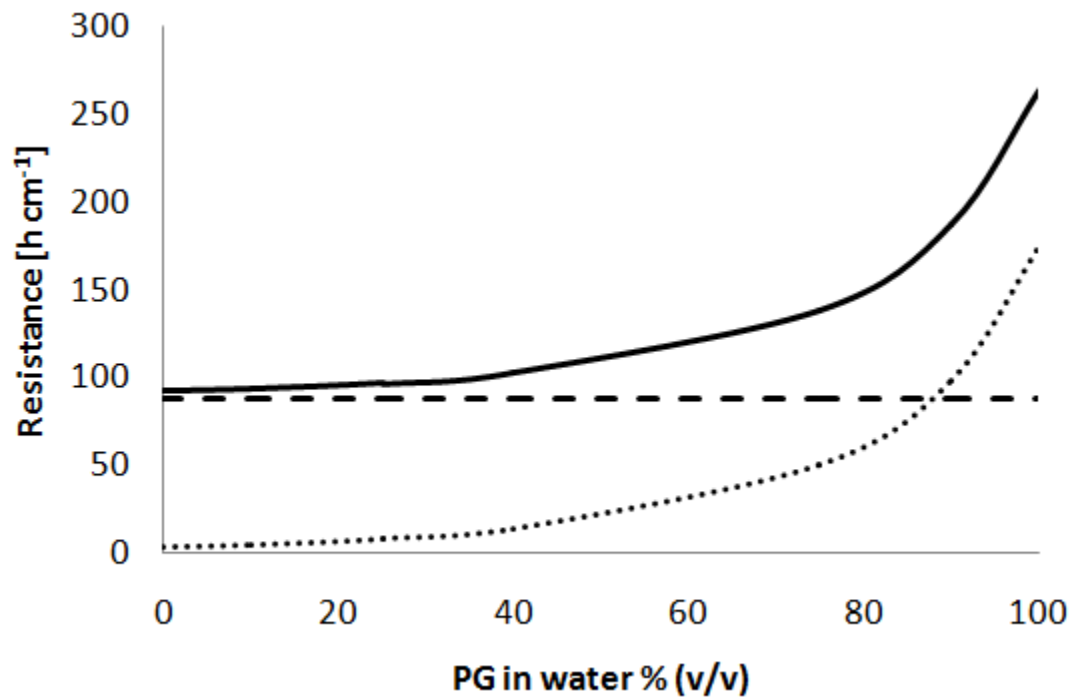
Case 1. Propylene glycol assumed to increase the diffusional resistance of the microchannel but **not** the underlying dermis. Dotted line (•••) corresponds to the resistance of the microchannel, dashed line (---) corresponds to the resistance to the underlying dermis (viable tissue), and solid line (——) corresponds to the total resistance of the microchannel pathway.

Figure 7.7.
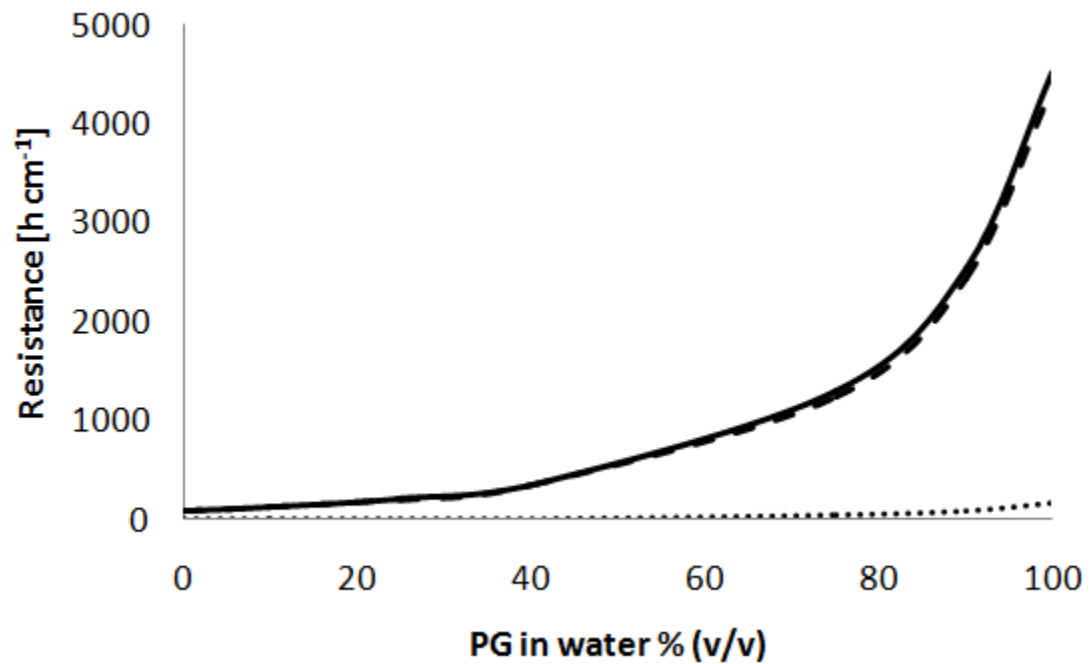
Case 2. Propylene glycol assumed to increase the diffusional resistance of the microchannel <u>and</u> the underlying dermis. Dotted line (•••) corresponds to the resistance of the microchannel, dashed line (---) corresponds to the resistance to the underlying dermis (viable tissue), and solid line (—) corresponds to the total resistance of the microchannel pathway.

Figure 7.8.
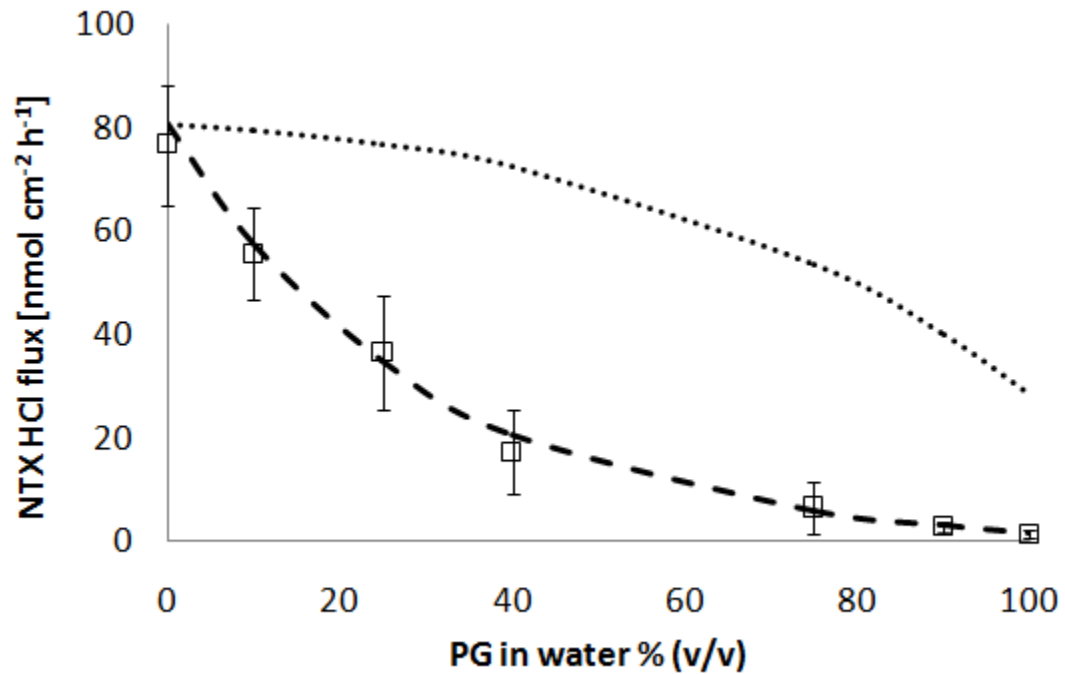
Microchannel pathway flux predictions based on the Case 1 (dotted line) and Case 2 (dashed line) assumptions plotted against experimentally obtained flux (unfilled boxes). Experimental data presented as mean ± SD (n = 3-4)

Figure 7.9.
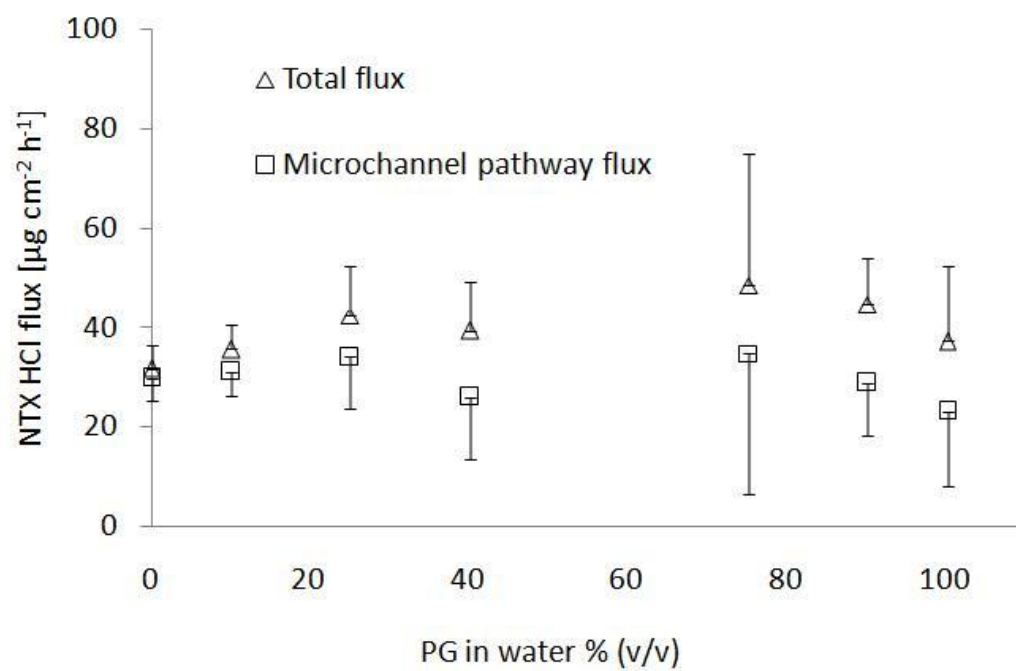
Viscosity-normalized flux of NTX•HCl through Yucatan minipig MN-treated skin calculated according to Eq. 7.2. (n = 3–4)

Figure 7.10.
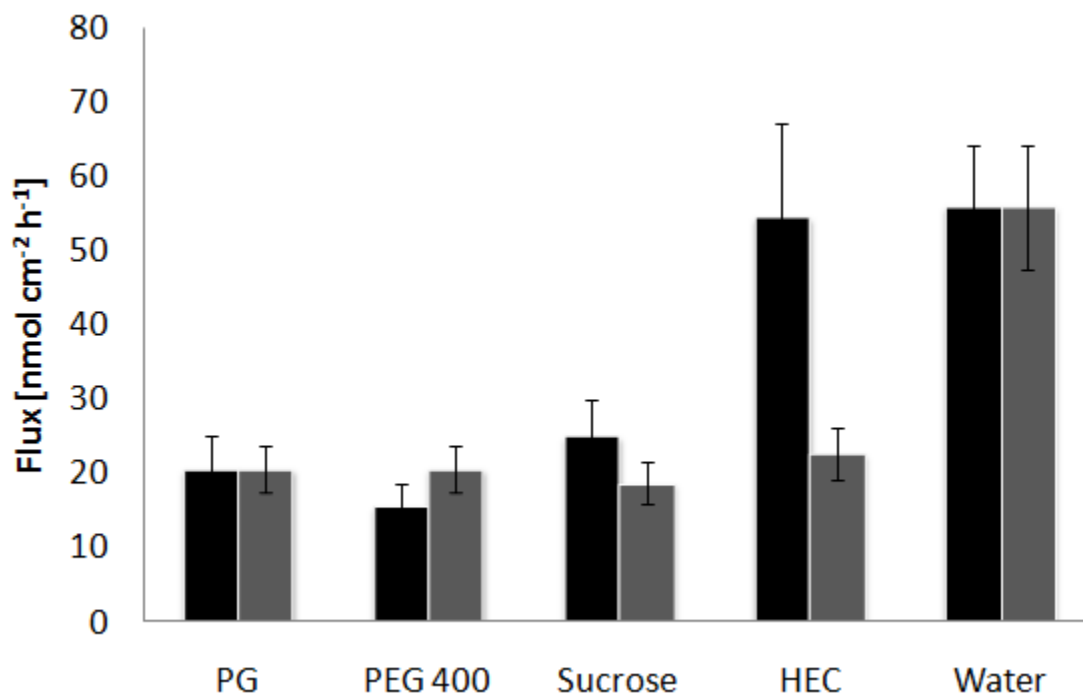
Steady-state flux (black bars) from donor solutions containing NTX•HCl at 90 mg/g. The first four donor solutions also contained the following excipients: propylene glycol (PG), poly(ethylene glycol) 400 (PEG 400), sucrose, and hydroxyethylcellulose (HEC). The concentration of excipients varied and was adjusted so that the viscosity of the donor solution equals approximately 2.7 cP. The last donor solution contained no excipient and its viscosity was approximately 1 cP. Gray bars correspond to the flux predictions calculated based on the viscosity change of the donor solution according to Eq. 6.3. All data presented as mean ± SD (n = 4).

Figure 7.11.
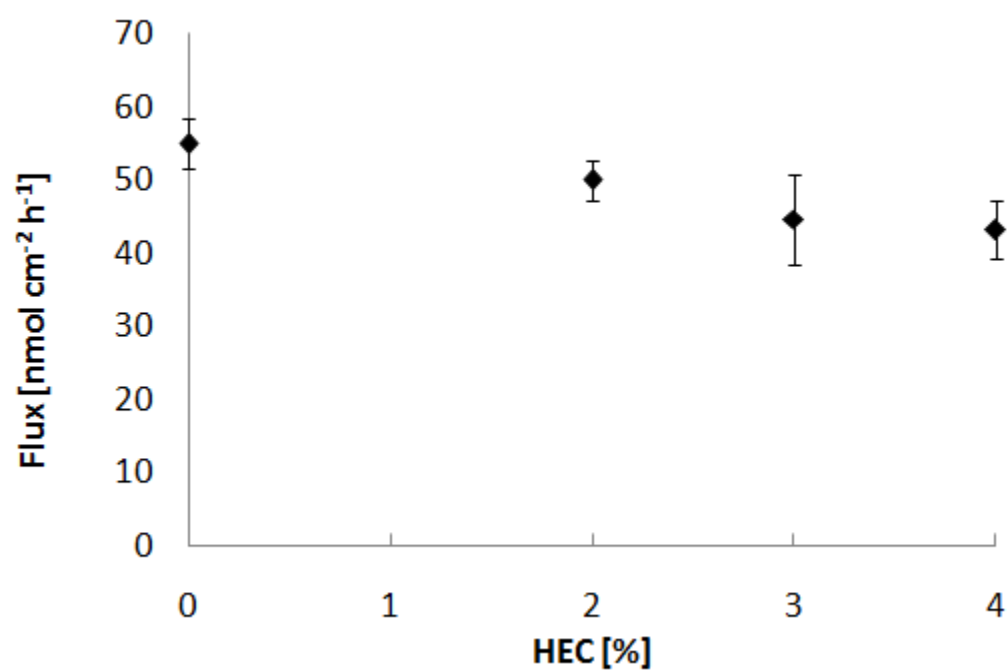
The flux of NTX•HCl across MN-treated Yucatan minipig skin as a function of increasing HEC concentration in the donor solution. Data presented as mean ± SD, n = 3.

Chapter 8

***In vitro* permeation of naltrexone prodrugs across microneedle treated skin**

8.1. Introduction

The aim of this chapter is to present the potential of naltrexone prodrugs to be used in conjunction with MN-treated skin. In order to fulfill the **research goal 3.3** a variety of naltrexone prodrugs from different chemical classes were synthesized in Dr. Crooks' laboratory. Prodrug structures underwent rigorous examination with respect to the hydrolytic stability (at physiologically-relevant skin surface pH of 5.0 and tissue and blood pH of 7.4) as well as solubility. Only a few prodrugs were deemed suitable for *in vitro* permeation testing. First, a PEGylated ester 3-O'-naltrexone prodrug stability and solubility will be described in detail followed by permeation through MN-treated skin. Then, other prodrug classes and the challenges associated with them will be outlined. The contents of the following chapter besides point 8.7 have been published in Journal of Controlled Release [229].

The restrictions in percutaneous drug delivery are largely governed by skin anatomy. Skin has evolved to provide an adequate interface between the external and internal body environment, to minimize water loss, and to impede the penetration of xenobiotics. This evolutionary hurdle results in very low skin permeability to most foreign substances [55, 57, 230]. The barrier property of the skin for most compounds lies in the stratum corneum (SC) extracellular matrix of lipid bilayers [51, 101]. The pool of molecules possessing the necessary physicochemical properties to cross this barrier is limited, and the number of drugs that can be delivered transdermally at therapeutically relevant rates is also low [17]. To overcome this challenge, a variety of different techniques can be used [8, 22]. One of the most promising and effective approaches involves the use of microneedles (MN). Micrometer-size needles were shown to be long enough to

penetrate the skin effectively breaching the SC barrier, but at the same time being short enough to minimize pain sensation. In general, this process results in up to several orders-of-magnitude enhancement of drug transdermal transport [8, 152].

Naltrexone (NTX) is a potent, competitive opioid receptor antagonist used to treat opioid and alcohol addiction [83]. The percutaneous delivery of this agent could bear substantial advantages over currently available dosage forms: i.e. oral tablet and intramuscular controlled-release injection [20, 231]. Although neither NTX, nor its active metabolite, 6-ß-naltrexol, permeate through skin at clinically relevant rates from reasonably-sized patches [20, 231], the use of MN proved to significantly improve transport [6]. Studies have shown that although the creation of microchannels in the skin after MN treatment did not have a substantial effect on the delivery rates of the neutral (free-base) form of NTX or 6-ß-naltrexol, an improvement in the delivery of positively charged (salt-form) species of these drugs was possible [6]. It was proposed that higher NTX and 6-ß-naltrexol water-solubility at the lower pH range, rather than the presence of a positive charge, was responsible for the observed increase in the transport rates of the salt forms of these drugs [6]. *In vitro* and *in vivo* animal studies proved the utility of the MN method of enhancement showing approximately an order-of-magnitude increase in the transdermal flux of highly water soluble species via MN-assisted delivery over that through untreated skin [6, 155]. Subsequently, a first-in-human MN study demonstrated that the combination of MN skin pretreatment and application of four NTX•HCl patches afforded drug plasma levels in the lower end of the targeted therapeutic range [216]. Furthermore, an increase in flux would be expected to translate into higher plasma levels, as well as allow a decrease in the number of patches needed.

It is known that PEGylation, or the process of covalent attachment of polyethylene glycol polymer chains to another molecule can substantially increase aqueous solubility of hydrophobic drugs and proteins [232, 233]. Besides improved water-solubility,

PEGylation is commonly used in the field of pharmaceutics to serve other purposes, such as enhancing stability, modifying pharmacokinetics, shielding labile molecules from proteolytic enzymes, or eliminating protein immunogenicity [234-236]. In the field of transdermal drug delivery, PEGylation has been employed to alter the physicochemical properties of prodrugs to enhance delivery across non-MN-treated skin. Overall, these attempts translated into limited success for passive transdermal delivery. An elevated aqueous solubility was postulated to contribute to a moderate increase in flux observed for some derivatives. All these studies involved drug delivery through non-MN-treated skin [64, 167, 237].

Based on the experiments by Banks et al. [6], it could be anticipated that an aqueous solubility increase achieved through PEGylation of NTX would favorably affect flux through MN-enhanced skin. No previous peer-reviewed literature reports have described the transdermal potential of PEGylated drug molecules used in conjunction with MN skin treatment. The aim of this work was to evaluate the *in vitro* transport of a PEGylated NTX prodrug through MN-treated skin, as a function of concentration in the donor solution.

8.2. Materials and methods

Chemicals

Naltrexone was purchased from Mallinckrodt (St. Louis, MO, USA). Water was purified using a NANOpure Diamond^{TM} Barnstead water filtration system. Hanks' balanced salts modified powder, and sodium bicarbonate were purchased from Sigma (St. Louis, MO). 4-(2-Hydroxyethyl)-1-piperazineethanesulfonic acid (HEPES), gentamicin sulfate, trifluoroacetic acid (TFA), triethylamine (TEA), 1-heptane sulfonic acid sodium salt, and acetonitrile (ACN) were obtained from Fisher Scientific (Fairlawn, NJ). 1-Octane sulfonic acid sodium salt was obtained from ChromTech (Apple Valley, MN, USA).

Synthetic procedure for the preparation of the naltrexone PEGylated prodrug (PEG-NTX). The following synthetic procedure was carried out by Dr. Reddy Thirupathi from Dr. Crooks' laboratory.

The detailed synthetic procedure for the preparation of 3-O-[3-(2-(2-hydroxyethoxy)ethoxy)propanoyl]naltrexone prodrug has been reported in Bioorganic & Medicinal Chemistry Letters [238]. Briefly, to a mixture of naltrexone (0.341 g, 0.001 mol), DMAP (0.146 g, 0.0012 mol), and dicyclohexylcarbodiimide (DCC, 0.247 g, 0.0012 mol) in chloroform (30 ml), 3-(2-(2-hydroxyethoxy)ethoxy)propanoic acid (0.178 g, 0.001 mol) in chloroform (5 ml) solution was added dropwise over a period of 5-10 min under an argon atmosphere at ambient temperature. The solution was stirred at ambient temperature for 24 hrs, then it was cooled to 0-5 °C, and the precipitated dicyclohexyl urea by-product filtered-off. The filtrate was washed with ice-cold water (20 ml), ice-cold brine solution (20 ml), dried over Na_2SO_4, and the solvent evaporated *in vacuo*. The resulting residue was purified by column chromatography (silica gel, eluted with 3% v/v methanol in chloroform) to obtain pure 3-O-[3-(2-(2-hydroxyethoxy)ethoxy)propanoyl]naltrexone (0.42 g, 85% yield) as a colorless oil.

Solubility

The apparent solubilities of the PEG-NTX prodrug and NTX in 0.3M acetate buffer (pH 5.0) were obtained by equilibration of an excess quantity of prodrug/drug in 6ml of buffer. After addition of prodrug/drug, the pH of the resulting slurry was adjusted to pH 5.0, if this was found to be necessary. The PEG-NTX prodrug slurry was continuously shaken in a tightly closed glass vial in a shaking water-bath at 32°C for 12h. A relatively short equilibration time was chosen, due to the hydrolytic instability of the prodrug. The NTX slurry was continuously shaken in a tightly closed glass vial in a shaking water bath at

32°C for 24h. At the end of the equilibration time, samples were transferred to prewarmed plastic centrifuge vials and centrifuged for 10 min at 12000 x g at 32°C. The supernatant was sampled, filtered using a 32°C prewarmed syringe containing a 0.2 μm membrane syringe filter (VWR 28145-491), diluted with an adequate amount of ACN-water 70:30 (v/v), and resulting solution analyzed by high pressure liquid chromatography (HPLC). Solubility determinations were repeated twice (n = 2).

Prodrug stability

For the purpose of determining the pH-rate profile, several 20mM buffers were prepared and adjusted to the constant ionic strength of I = 0.1 with NaCl: i.e. pH 2.0 (phosphate buffer), pH 3.3 (citrate buffer), pH 4.4 (formate buffer), pH 5.4 (acetate buffer), pH 5.9 (citrate buffer), pH 6.9 (phosphate buffer) and pH 8.7 (ammonium buffer). A stock solution of PEG-NTX was obtained by dissolving about 40mg of the prodrug in 2 ml ACN. Then, 100μl of the stock solution was transferred to 10ml of buffer thermostated at 32°C, vortexed and filtered through a 0.45μm nylon syringe filter (Acrodisc® Premium 25mm Syringe Filter). Multiple samples were drawn over a period of 140h. Next, prodrug stability studies in donor (0.3M acetate buffer pH 5.0) and receiver solutions (25mM HEPES-buffered Hanks' balanced salt solution pH 7.4) were initiated by charging a 10ml volume of hydrolysis media thermostated at 32°C with ≈1mg of prodrug, filtering the solution through a 0.45μm nylon syringe filter (Acrodisc® Premium 25mm Syringe Filter) and taking samples of the filtrate over a period of 120h. Samples were then diluted with ACN-water 70:30 (v/v) for HPLC analysis. All PEG-NTX-prodrug hydrolysis studies showed pseudo-first-order kinetic behavior. Apparent pseudo-first-order hydrolysis rate constants, k_{app}, were estimated from the slope of the log-transformed amount of PEG-NTX prodrug remaining in the medium. All stability studies were carried out in duplicate (n = 2).

Donor solution preparation

Acetate buffer (0.3M, pH 5.0) containing prodrug at saturation (629mM) was diluted with 0.3M acetate buffer, pH 5.0 to obtain solutions at 10, 20, 40, 70 and 90% solubility. Solutions were vortexed and used immediately in *in vitro* diffusion studies.

NTX was added to 0.3M acetate buffer, pH 5.0 to obtain concentrations of 25, 50, 75, 178 and 338mM and the pH of the solutions adjusted to 5.0, if necessary. Solutions were vortexed and used immediately in *in vitro* diffusion studies immediately.

Viscosity measurements

A Brookfield DV-III LV programmable cone/plate rheometer with a CPE-40 spindle was used for measuring the viscosity of the donor solutions. The sample volume was 0.5 ml. All determinations were carried out at 32 ^{0}C maintained by a circulating water-bath TC-102. Each donor viscosity measurement was taken three times at low, medium and high torque value in the range of 10-100% of the instrument specifications (n = 3).

In vitro diffusion studies

Full-thickness Yucatan minipig skin was harvested from the dorsal region of a euthanized 6-month-old animal. Animal studies were approved by the University of Kentucky IACUC. Subcutaneous fat from skin samples was removed with a scalpel and sparse hair clipped. Such skin samples were immediately placed in a plastic bag and frozen until use (-20°C). The effect of freezing on skin viability [239-241] and permeability to xenobiotics [241-244] has been the subject of multiple studies. The presence [241-243] or absence [244] of freezing-induced increased skin permeability is related to factors such as skin type, nature of the permeant, freezing conditions and time of storage. Our experience indicates no major detrimental effect is caused by Yucatan

minipig skin freezing up to one year of storage for the purpose of use in *in vitro* drug permeation studies. Before the permeation study, skin samples were allowed to thaw for about 30 min. Skin used for MN treatment was first dermatomed to a thickness of about 1.7mm and then placed on a wafer of polydimethylsiloxane polymer, which mimicked the naturally occurring mechanical support of underlying tissue because of its comparable structural elasticity. In the context of studies described in this article "MN" refer to microneedle rows obtained from Dr. Prausnitz's laboratory. They were fabricated by laser cutting of stainless steel sheets as reported previously [29]. MN were solid metal, two-dimensional "in-plane" rows each containing five microneedles oriented with their axis parallel to the steel sheet. This design is characterized by the following microneedle dimensions: 750 µm long, 200 µm wide, 75 µm thick and 1.35 mm inter-needle spacing. The insertion of MN into skin was carried out manually by applying gentle finger pressure followed by their instantaneous removal. The diffusion area of skin (0.95 cm^2) was pierced 20 times, with a row containing five microneedles, gradually advancing the MN application area to obtain 100 non-overlapping piercings before mounting the skin in the diffusion cell. If any damage to the MN was observed a new array was used. Three to four cells were used per one drug/prodrug concentration (n = 3-4). A PermeGear flow-through (In-Line, Riegelsville, PA) diffusion cell system was used for the *in vitro* diffusion studies. Isotonic HEPES-buffered Hanks' balanced salts solution (25mM, pH 7.4) was used as the receiver solution. Additional experiments were carried out to ascertain that the receiver flow rate of 1.5 ml/h was sufficient to maintain sink conditions. An increase in flow rate to 7.5ml/h did not change the amount of drug permeating over time, and a lower 1.5ml/h flow rate was used for all experiments for practical convenience. Skin samples in the diffusion cells were maintained at 32°C using a circulating water bath. The diffusion experiments were initiated by charging the donor compartment with 0.4 ml of the donor solution. Samples were collected from the receiver compartment in 6h

increments over 48h. All samples were stored at 4°C until HPLC analysis, which was carried out within 24 hours.

Transepidermal water loss (TEWL) measurements

TEWL was used to assess the integrity of the skin barrier using a DermaLab® TEWL probe (CyberDerm Inc.). MN-treatment, by itself, increases TEWL and detection of possible barrier compromise due to vehicle alone under such conditions would be difficult at best. Therefore, a separate diffusion experiment was carried out to evaluate the effect of the drug-free donor solution (0.3M acetate buffer) on the barrier properties of the untreated skin. The TEWL values for uncompromised minipig skin are known, and are generally equal or less than 10 g m^{-2} h^{-1} [245-247]. Measurements were taken after 30 min. equilibration of the untreated skin with the receiver solution in the diffusion apparatus before charging the donor chamber with the drug-free 0.3 M pH 5.0 acetate buffer. Another measurement was obtained after removal of the buffer from the donor chamber after 48 h, and 30 min equilibration.

Prodrug skin disposition

After the completion of the diffusion experiment, skin samples were rinsed three times with distilled water to remove residual formulation and then dismounted from the diffusion cells. A circular section of the skin corresponding to the diffusion area was excised with a scalpel and weighed. Next, the skin sample was placed in a glass vial containing 10 ml of ACN, the vial closed tightly and left in a shaking water bath thermostated at 32°C for 12 h. Solutions were then sampled, diluted with ACN and analyzed by HPLC. The PEG-NTX prodrug and NTX content was normalized by skin weight and reported as the concentration in the skin.

Quantitative analysis

Quantitative analysis of NTX and the PEG-NTX prodrug by HPLC was carried out using a modification of the assay described by Hussain et al. [225]. The HPLC system consisted of a Waters 717 plus autosampler, a Waters 600 quaternary pump, and a Waters 2487 dual wavelength absorbance detector with Waters Empower™ software. A Waters YMC™ CN column (2.0mm × 150mm) with a CN guard column of the same type (2.0mm × 20mm) was used with the UV detector set at a wavelength of 278nm. The mobile phase consisted of 70:30(v/v) ACN:0.1% TFA containing 0.065% 1-octane sulfonic acid sodium salt, adjusted to pH 3.0 with TEA aqueous phase. Samples were run at a flow rate of 1.5 ml/min with a run time of 4.5 min. The injection volume was 100 µl, and the retention times of PEG-NTX and NTX were 3.2 min and 3.5 min, respectively. Samples were analyzed within a 100–5000ng/ml linear range of the PEG-NTX prodrug and NTX standard curves. Standard solutions exhibited excellent linearity over the entire concentration range employed in the assays.

The permeation data were plotted as the cumulative amount of PEG-NTX and NTX collected in the receiver compartment as a function of time. The steady-state flux value for a given run was calculated from the terminal slope of the cumulative amount plotted against time. The permeability coefficient was obtained from Fick's first law of diffusion:

$$\frac{1}{A}\left(\frac{dM}{dt}\right) = J_{SS} = P \times \Delta C \tag{8.1}$$

where, J_{ss} is the steady-state flux, M is the cumulative amount of drug permeating the skin [nmol], A is the area of the skin [0.95 cm^2], P is the effective permeability coefficient [cm h^{-1}], and ΔC is the concentration difference [nmol cm^{-3}] of the drug in donor and

receiver solutions. Since sink conditions prevail under constant flow of the receiver solution, ΔC is well-approximated by the drug donor concentration alone.

Statistical analysis

The statistical analysis of the data was carried out by one-way ANOVA with post-hoc Bonferroni's analysis using SIGMA-STAT software (SPSS, Inc., Chicago, IL, USA).

8.3 Stability and solubility of PEGylated naltrexone prodrug

The structures of both parent drug (NTX) and its PEGylated prodrug (PEG-NTX) are presented in **Figure 8.1**. A short, two ethylene-glycol unit side chain is attached through a hydrolytically labile carboxylate ester linkage to the 3-O position of the NTX molecule. Before the *in vitro* evaluation of the prodrug permeation through the MN-treated skin was carried out, its stability was studied at different pH values. A wide pH range was investigated with the aim of identifying the pH-dependency for slow and fast chemical hydrolysis. The prodrug stability studies at all pH values showed pseudo first-order degradation behavior. Apparent pseudo first-order rate constants (k_{app}) were obtained from the slope of the log-transformed amount of prodrug remaining plotted against time. **Figure 8.2** summarizes the pH stability in the form of a U-shaped pH-rate profile. At pH values around 3-5, the PEG-NTX prodrug is most stable. Lower pH values reveal acid-catalyzed hydrolysis while higher pH values demonstrate base-catalyzed hydrolysis. Specifically, in the pH region 7-9, the slope reaches a value of unity, indicating that hydroxide ion-catalyzed hydrolysis is the predominant mechanism of hydrolysis in this pH range. Since under normal conditions, the surface pH of the skin oscillates around 4.5 – 6.0, a donor solution of pH 5.0 was chosen for diffusion experiments to closely mimic the physiological milieu [248, 249]. This pH value also provides the best stability for the PEG-NTX prodrug, as indicated by the pH-rate profile. On the other hand, the

receiver solution was buffered to the physiologically relevant pH 7.4, reflecting the environment of the deeper layers of skin and bodily fluids [250, 251]. Because the actual composition of the donor and receiver solutions differed from buffers used in the stability determination, an additional hydrolysis study was carried out to evaluate PEG-NTX stability in those media. It was found that the prodrug's k_{app} in the donor solution was $1.93 \cdot 10^{-3}$ h^{-1}, which translates into a t_{90} of about 54 h, while in the receiver solution k_{app} equaled $2.88 \cdot 10^{-2}$ h^{-1} or a t_{90} of about 4 h. In other words, by chemical hydrolysis alone, PEG-NTX would be expected to degrade releasing the parent drug 15 times faster in the receiver solution as compared to the donor solution. Overall, the t_{90} of over 48 h (the duration of diffusion experiment) was deemed to be sufficient to ensure that only a small portion (<10 %) of NTX coming from prodrug in the donor solution would be formed, and would not substantially affect the interpretation of the data. Besides stability, the second key parameter of interest was solubility. The main purpose for designing a PEGylated NTX prodrug was to achieve increased water-solubility of the drug in the donor solution. The apparent aqueous solubility values for the parent drug and prodrug were 338 mM and 629 mM, respectively, showing nearly a 2-fold increase in apparent aqueous solubility of the prodrug compared to that of NTX.

8.4. Permeation and simultaneous bioconversion

The potential detrimental effect of the acetate buffer (present in donor solution) on skin was evaluated in a separate experiment involving transepidermal water loss (TEWL) measurements before and after charging the donor chamber with the drug-free donor solution over 48 h. Typical readings for untreated minipig skin were equal to or less than 10 g m^{-2} h^{-1} [245-247]. The experimental TEWL values for untreated skin remained low and increased from 2.2 ± 0.4 to 3.1 ± 0.2 g m^{-2} h^{-1} over 48 h, suggesting no damage to the barrier had occurred. All *in vitro* diffusion experiments used MN-pretreated Yucatan

minipig skin. Minipig skin is a well-established model for human skin in transdermal drug delivery as it possesses the characteristics similar to those of the human skin [34, 35]. However, as every model, it has some limitations [36] and results reported here should not be extrapolated to human skin without caution. Differences in the structure of the dermis may translate into different diffusional resistance of that tissue and, therefore, affect the flux values obtained from MN-enhanced permeation experiments. The diagram of the experimental set-up used to investigate the transport of PEG-NTX prodrug across MN-treated skin is presented in **Figure 8.3**.

The transdermal permeation through MN-enhanced skin was evaluated at 6 concentrations for PEG-NTX: i.e. 10, 20, 40, 70, 90 and 100 % saturation, or 63, 126, 252, 440, 566 and 629 mM. The saturated solution did not contain any undissolved prodrug to ensure that potential interference between excess prodrug and microchannels, such as obstruction of the microchannel opening, presence of the undissolved prodrug in the microchannels, etc., would not affect the results. Since the prodrug possesses much lower chemical stability at elevated pHs, its diffusion across MN-treated skin is accompanied by simultaneous chemical hydrolysis and possibly enzymatic bioconversion. As a result, two species, the prodrug itself and NTX generated from hydrolysis of the prodrug, are detectable in the receiver solution. Prodrug permeation from donor solution at either concentration tested resulted in steady-state conditions after a relatively short lag time. A representative permeation profile is presented in **Figure 8.4** and permeation data is summarized in **Table 8.1**. The total flux was obtained by summation of prodrug flux and NTX-from-prodrug flux, and can be seen as a measure of overall performance of the prodrug. Steady-state total flux values plotted as a function of PEG-NTX concentration in the donor are shown in **Figure 8.5**. (Note that **Table 8.1** reports flux of unhydrolyzed (intact) PEG-NTX prodrug and NTX-from prodrug separately while **Figure 8.5** sums them up to obtain total PEG-NTX

prodrug flux (filled circles) which is contrasted with the flux of NTX alone obtained from a separate experiment).

8.5. Deviations from ideal behavior

While in the lower concentration range (63–252 mM) the increase in the flux is roughly proportional to the increase in concentration, at higher concentrations (440–629 mM) the flux is independent, if not inversely related, to the donor concentration. The behavior in the low concentration range can be well predicted by using Fick's first law of diffusion and a concentration-independent permeability coefficient. However, the deviation from ideal behavior is substantial in the higher concentration range. Additionally, **Figure 8.5** illustrates the permeation of the parent drug alone from data obtained from a separate experiment. NTX alone provides higher flux as compared to the PEG-NTX prodrug at any corresponding concentration. The permeability coefficient of the prodrug is expected to be somewhat lower than the permeability coefficient of the parent drug, due to its higher molecular weight. In bulk solution (as in microchannels), the Stokes-Einstein equation can be used to inversely relate solute diffusivity to the cubic root of the size of a molecule, $D \sim MW^{-0.33}$. On the other hand, in dermis, Kretsos et al. found that the Wilke-Chang relationship, which predicts a steeper drop in diffusivity as a function of increasing molecular weight, $D \sim MW^{-0.6}$, correlated well with their experimental data [59]. However, other functional relationships including that predicted by the Stokes-Einstein equation were not excluded. In other words an increase in the molecular weight from 341 Da (parent drug) to 502 Da (PEG-NTX prodrug) would be expected to decrease prodrug diffusivity by about 12% (by the Stokes-Einstein equation) or about 20% (by the Wilke-Chang relationship). Furthermore, the hydrodynamic radius of the PEG-NTX prodrug may be actually larger than that calculated from the molecular weight alone due to the association of water molecules with the PEG chain. Overall, superior

prodrug solubility, even with a somewhat decreased diffusivity, but in the absence of non-ideal behavior, should result in improved transdermal flux through MN-treated skin.

8.6. Viscosity influence on prodrug diffusivity

It has been suggested that the viscosity of the donor solution may have a vital effect on drug delivery rates through MN-treated skin [39]. The relationship between the viscosity (η) of the diffusion medium and the diffusion coefficient is given by the Stokes-Einstein equation:

$$D = \frac{kT}{6\pi\eta r} \qquad\qquad (8.2)$$

where k is Boltzmann's constant, T is absolute temperature, and r is the radius of the diffusant (assuming it can be represented by a spherical particle). Specifically, it was shown that the NTX•HCl flux through microchannels and underlying dermis correlated well with the decrease in the calculated drug diffusivity in the donor solution. Additionally, the flux through microchannels using aqueous drug solutions was found to be well approximated by the flux through MN-enhanced skin (the contribution of flux through skin around microchannels was low). To test the hypothesis that an increase in the viscosity of the prodrug-containing donor solution may explain low PEG-NTX flux at high concentrations, the donor solution viscosity values were measured. It is known that at sufficiently high solute concentration, solvent viscosity can be altered, exerting a secondary effect on the solute's own diffusivity [54]. **Figure 8.6** shows that donor solution viscosity increases in an exponential fashion as a function of the prodrug concentration, and demonstrates approximately a 3-fold increase between the lowest and highest concentrations tested. A simple log-linear empirical equation in the form of:

$$\log \eta = a \times C + b \tag{8.3}$$

was used to describe this trend for later flux calculations, where C is concentration [mM] and a and b are fitted parameters [252]. The experimental data can be transformed by normalizing either flux or permeability coefficient for apparent viscosity effect. Multiplication by viscosity of a given donor solution affords the viscosity normalized parameter, e.g.

$$J' = J \times \eta \tag{8.4}$$

or

$$P' = P \times \eta \tag{8.5}$$

where J' is the viscosity-normalized flux, J is the experimentally measured flux and η is the viscosity of the donor solution, and the P' is the viscosity-normalized permeability coefficient and P is the experimentally determined permeability coefficient. Such correction results in flux or permeability coefficient values corresponding to a viscosity value of unity. If the hypothesis is valid, it would be expected that the viscosity-normalized flux will correlate linearly with the prodrug concentration in the donor solution over the whole concentration range tested. A plot of viscosity-normalized flux is presented in **Figure 8.7**, which shows a reasonable linear correlation (R^2 = 0.96). Moreover, from the slope of this graph, an average viscosity-normalized permeability coefficient P'_{ave} of $23.01 \cdot 10^{-5} \pm 2.57 \cdot 10^{-5}$ (mean ± 95% CI) was estimated. Individual

viscosity-normalized permeability coefficients (P') are reported in **Table 8.2**. Apart from the P' for the 63 mM concentration which is somewhat higher than the average, the normalized permeability coefficients are concentration-independent over the range of prodrug concentrations tested (one way ANOVA with post-hoc Bonferroni's analysis reveals a statistically significant difference at $\alpha = 0.05$ between the P' at 63 mM and P' at 629 mM). In other words, the changes in MN-enhanced percutaneous flux of the PEG-NTX prodrug can be satisfactorily explained by changes in the viscosity of the donor solution.

Assuming that most prodrug molecules permeate through microchannels and into the dermis below, rather than through skin around microchannels, a two-ply membrane concept incorporating the microchannel and underlying dermis can be used to rationalize the data. In the experimental set-up used in the current study the thickness of the dermis below the microchannel exceeds the length of the microchannel, and the diffusion coefficients of drugs in the dermis are known to be approximately 3.7-fold lower as compared to those in the bulk aqueous solutions [59]. Based on the above, it can be expected that the major diffusional resistance lies in the dermis layer. Therefore, flux should not depend on the viscosity of the donor solution unless it changes the properties of the barrier (dermis). It is possible that the prodrug-containing, elevated-viscosity donor solution alters the microenvironment of the dermis by increasing its diffusional resistance. Assuming this effect is similar to that seen in the bulk solution, flux through microchannels and dermis below would be inversely related to the viscosity of the donor solution. In other words, the results from the current study imply that changes in the prodrug diffusivity in the donor solution are reflective of prodrug diffusivity changes in the whole skin barrier. Using the previously estimated average viscosity-normalized permeability coefficient (P'_{ave}) and the viscosity of the donor solution at any given concentration, an expected flux (J_{calc}) can be calculated from:

$$J_{calc} = \frac{P'_{ave}}{\eta} \times C \qquad\qquad (8.6)$$

which, after incorporation of **Eq. 3**, becomes:

$$J_{calc} = \frac{P'_{ave}}{10^{(0.000807 \times C\ -\ 0.097641)}} \times C \qquad\qquad (8.7)$$

where C is the prodrug donor concentration [mM]. **Figure 8.8** presents experimental data and compares it to the predicted total flux for the PEG-NTX prodrug. A reasonable agreement between experimental and calculated values lends practical utility to this approach. Finally, prodrug skin disposition studies at the end of the diffusion experiment were carried out. Both prodrug and NTX-from-prodrug were detected in the skin. **Table 8.3** shows the amount of each as a function of changing concentrations in the donor solution. The extent of prodrug metabolism, calculated as fraction of prodrug converted to NTX, does not differ substantially and remains constant at 37 ± 10%. This value is somewhat higher that its counterpart (29 ± 9%) obtained from flux values (**Table 8.1)**, and likely reflects extra degradation that occurred during sample processing time and skin extraction procedures. A lack of decline in the fraction of prodrug metabolized with an increase in concentration suggests either chemical hydrolysis alone or chemical hydrolysis accompanied by non-saturable enzymatic hydrolysis is the primary mechanism for PEG-NTX hydrolysis in skin.

8.7. Other prodrugs and codrugs for MN-enhanced drug delivery

A multitude of other naltrexone and 6β-naltrexol prodrugs and codrugs were synthesized by Dr. Crook's group. Most of them were evaluated with respect to the hydrolytic stability

in the aqueous vehicle at pH 5.0 and with respect to the hydrolytic stability at pH 7.4. A list of structures possessing a variety of prodrug moieties and different chemical linkers are presented in **Table 8.4**. It was decided that chemical stability at pH 5.0 should be at least enough to provide less than 10% prodrug degradation over the duration of the *in vitro* diffusion experiment. This translated into a pseudo first-order hydrolytic rate constant of less than 2.2×10^{-3} h^{-1}. As evident from a stability summary in **Figure 8.9** many prodrugs did not fulfill this requirement. The lack of adequate formulation stability was the single major issue related to prodrug use. Some of the comparisons, among the tested compounds, are instructive. The hydrolytic stability between compounds of the same chemical linker containing minor modification at the side chain situated far from the reaction center is similar (YTR-NTX-20 vs. YTR-NTX-43 and YTR-NTX-28 vs. YTR-NTX-63). Everything else being the same, carbamate esters hydrolyzed 2-fold slower than carboxylate esters (YTR-NTX-20 vs. YTR-NTX-28 and YTR-NTX-43 vs. YTR-NTX-63). NTX prodrugs containing an electron-withdrawing oxygen atom situated close, β, to the reaction center hydrolyzed about 16–fold faster as compared to the structures possessing an oxygen atom in the farther γ position (YTR-NTX-29 or YTR-NTX-31 vs. YTR-NTX-43), which can be rationalized on the basis of facilitating the nucleophilic attack at the carbonyl. A carboxylate carbohydrate prodrug hydrolyzed much faster than its PEGylated counterparts (YTR-NTX-69 vs. YTR-NTX-29 or YTR-NTX-31). A cholyl carbonate prodrug of NTX hydrolyzed at a similar rate to the PEGylated carboxylate prodrugs of NTX with oxygen in the β position (YTR-NTX-100 vs. YTR-NTX-29 or YTR-NTX-31). The NTX-cytisine codrug (JAE-1) is characterized by very high chemical stability (no hydrolysis observed over the stability study duration) as can be expected from a disubstituted carbamate linker [253]. Finally, with respect to the reactivity of the 3O' and 6O' hydroxide groups of NTX and NTXol; the reactivity of the phenolic –OH is much greater as can be expected from a better leaving group character. The pK_a of a

146

phenolic group is around 10 while the pK_a of an aliphatic hydroxide group is around 14. This difference is readily observed while comparing the hydrolytic rates of 3O' NTX and 6O' NTXol amino acid prodrugs (Val-3O'-NTX and Leu-3O'-NTX vs. Val-6O'-NTXol and Leu-6O'-NTXol). Also, the duplex carbonate NTXol codrug (YTR-NTXol-89) hydrolyzed slowly as could be expected based on the lower reactivity of the 6O' hydroxyl group and steric hindrance provided by two bulky NTXol molecules in the direct vicinity of the reaction center. In order to increase the stability of some prodrugs the change in aqueous vehicle composition was investigated. The addition of a cosolvent, such as PG, to unbuffered water was found to dramatically influence the rate of hydrolysis. The increase in the abundance of PG caused a decrease in the hydrolysis rate. The magnitude of this effect was different for carboxylate and carbamate esters as shown in **Figure 8.10** and **Figure 8.11**. However, the practical utility of this approach is limited due to the effect that a cosolvent exerts on flux through MN-treated skin as described in **Chapter 7.**

The stability at pH 7.4, was typically at least one order of magnitude lower as compared to pH 5.0, which was expected and advantageous from the perspective of systemic drug delivery. The notable exception was the JAE-1 codrug, which was very stable under both pH values. This observation is in agreement with a different, and extremely slow, mechanism which is involved in the hydrolysis of disubstituted carbamates [253].

The fulfillment of the stability prerequisites was not interpreted as a warrant for progressing to the *in vitro* diffusion studies. In addition to the adequate stability a produg/codrug must possess high solubility so that the driving force for diffusion is high. An example of a codrug which possessed desired stability but failed to demonstrate high solubility is YTR-NTXol-89. Despite promising formulation stability the solubility at relevant pH of 5.0 was very low (**Figure 8.12**) and no permeation studies were carried out with this molecule.

8.8. Conclusions

The current study explored the *in vitro* permeation of a PEGylated NTX prodrug across MN-treated skin as a function of its concentration in the donor solution. It has been found that the flux did not proportionally increase when high concentrations of the prodrug in the donor solution were utilized. In other words, the apparent permeability coefficient (calculated as a ratio of flux over drug concentration in the donor solution) is not a concentration-independent proportionality constant between flux and drug concentration. It was hypothesized that this non-linearity was caused by elevated viscosity of the donor media. Calculations based on the Stokes-Einstein equation afford a reasonable explanation of the experimental data. Interestingly, if this reasoning is correct, a clear decline in flux would be expected with further increases in prodrug concentrations in the donor solution. It was not possible to investigate this with the present PEG-NTX prodrug, due to its limited solubility. Overall, it cannot be excluded that other formulation characteristics besides viscosity of the donor solution may also alter transport rates through MN-treated skin. Apart from kinetics considerations, a decrease in the thermodynamic chemical potential of the diffusant at high concentrations may also contribute to deviation from ideal behavior. Nevertheless, in the present study, accounting for changes in viscosity alone provided a rational interpretation for the data obtained. Obviously, the generalization of the results obtained from the current study will require further investigation. It is not expected that the type of behavior seen in the present study will be universal for all MN-involving transport experiments as different methods of MN application, MN design and formulation characteristics play a significant role in the drug transport across MN-treated skin [254]. In consequence, the generality of the present *in vitro* findings may be limited to the studies involving, among others, water-based formulations, MN-pretreated skin with microchannels having similar nature to those obtained in this study and permeants which cross the skin mainly through

microchannels and underlying dermis, rather than through the intact skin around microchannels. Overall, it is very likely that the prodrug approach to increase aqueous solubility of a poorly soluble lipophilic parent drug could be successful in increasing flux across microchannel pathway. However, in the present study, charged NTX possesses already high water solubility and further increase seems not to translate into any practical benefit due to deviations from ideal behavior. If the above reasoning is correct, the maximum flux for a compound permeating across microchannel pathway would occur where the ratio of donor solution concentration to donor solution viscosity is the highest.

Table 8.1. Summary of the *in vitro* permeation of the PEG-NTX prodrug through MN-treated Yucatan minipig skin from donor solutions containing prodrug at different concentrations. Simultaneous diffusion and hydrolysis of the prodrug resulted in the detection of both: prodrug itself and NTX-from-prodrug in the receiver phase. Each value represents the mean ± SD (n = 3-4).

Prodrug concentration in donor solution [mM]	Prodrug		NTX-from-prodrug		Fraction of prodrug converted ± SD [%]	n
	Flux ± SD [nmol cm^{-2} h^{-1}]	Lag time ± SD [h]	Flux ± SD [nmol cm^{-2} h^{-1}]	Lag time ± SD [h]		
63	17.9 ± 5.3	5.8 ± 0.7	6.8 ± 2.5	10.5 ± 1.1	28 ± 12	3
126	22.9 ± 5.7	8.4 ± 2.6	9.0 ± 2.5	9.5 ± 2.2	28 ± 10	4
252	37.9 ± 7.3	7.8 ± 1.0	14.1 ± 2.8	8.6 ± 1.1	27 ± 7	4
440	45.0 ± 4.1	7.7 ± 0.6	20.5 ± 2.3	12.0 ± 1.7	31 ± 4	3
566	40.8 ± 13.8	4.2 ± 2.3	17.0 ± 4.8	8.6 ± 1.5	29 ± 11	4
629	35.5 ± 10.1	3.5 ± 2.7	14.6 ± 3.6	7.8 ± 2.9	29 ± 9	4
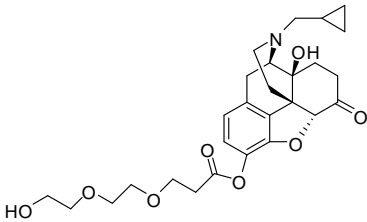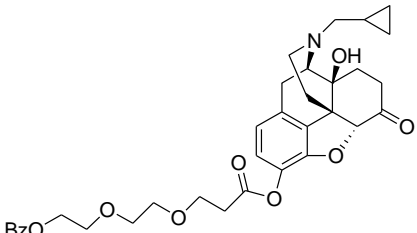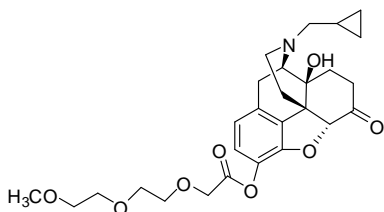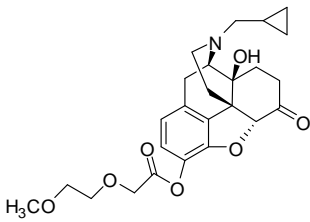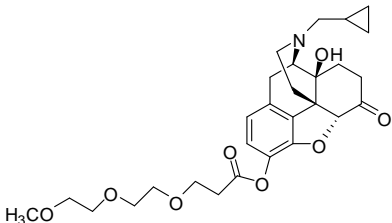
Table 8.2. Summary of individual permeability coefficients (P) and viscosity-normalized permeability coefficients (P') as a function of the prodrug concentration in the donor solution. Permeability coefficients were normalized per viscosity according to Eq. 5. Each value represents the mean ± SD (n = 3-4).
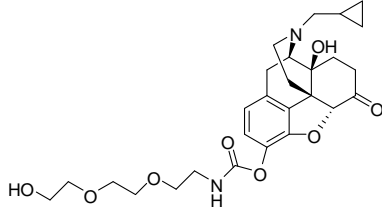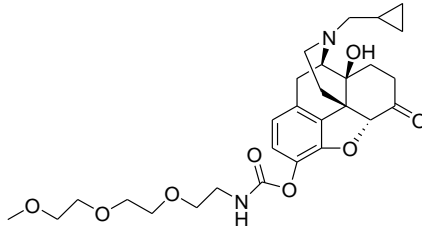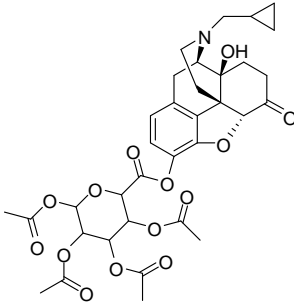
Prodrug donor concentration [mM]	63	126	252	440	566	629
n	3	4	4	3	4	4
P x 10^5 ± SD [cm h^{-1}]	39.3 ± 9.3	25.4 ± 4.9	20.7 ± 3.1	14.9 ± 1.1	10.2 ± 2.6	8.0 ± 1.7
P' x 10^5 ± SD [cm h^{-1}]	36.1 ± 8.6	25.4 ± 4.9	25.9 ± 3.9	26.5 ± 1.9	23.2 ± 5.9	21.0 ± 4.5
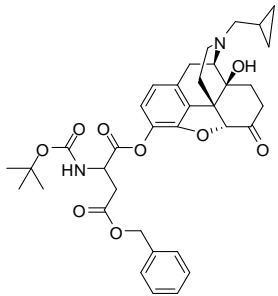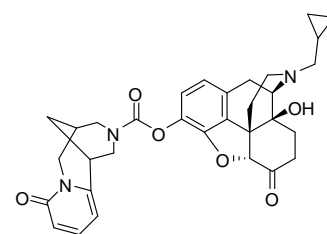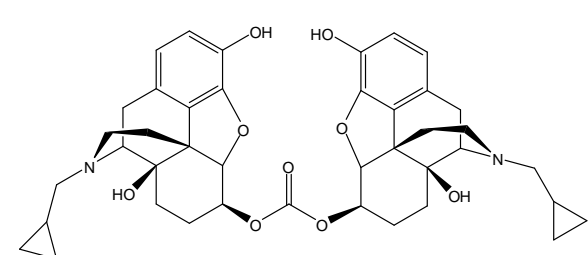
Table 8.3. Summary of the drug skin disposition at the end of the 48 h diffusion experiment involving MN-treated Yucatan minipig skin. Both the PEG-NTX prodrug and NTX-from-prodrug were detected in the skin. Each value represents the mean ± SD (n = 3-4).
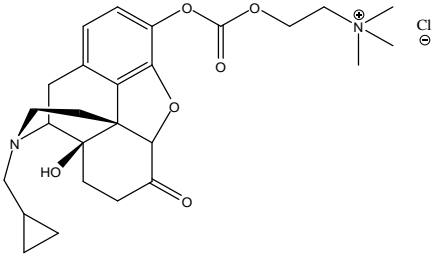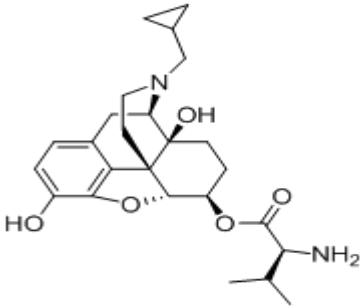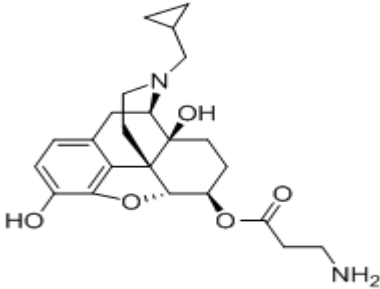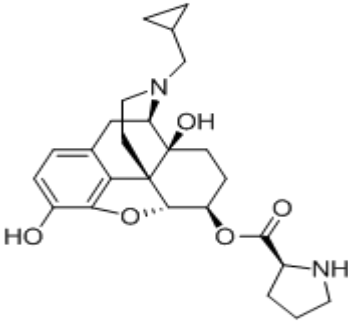
Prodrug donor concentration [mM]	63	126	252	440	566	629
n	3	4	4	3	4	4
Prodrug amount ± SD [nmol/g skin]	367 ± 127	597 ± 214	850 ± 306	1445 ± 123	1352 ± 125	1459 ± 236
NTX from prodrug amount ± SD [nmol/g skin]	253 ± 54	404 ± 129	504 ± 189	752 ± 68	749 ± 68	784 ± 87
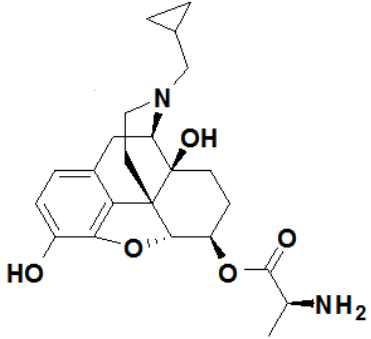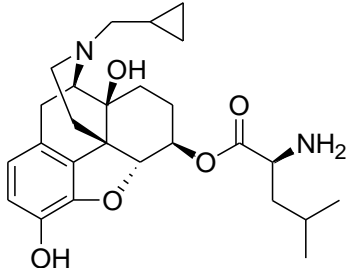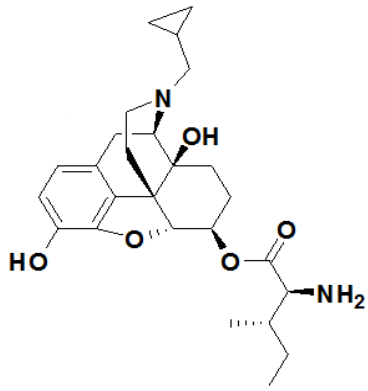
Table 8.4. A list of prodrug and codrug structures of naltrexone and 6β-naltrexol tested for hydrolytic stability at pH 5.0 and pH 7.4. Name, molecular weight, estimated log $K_{o/w}$ (ChemDraw® 8.0), and chemical structure are reported.
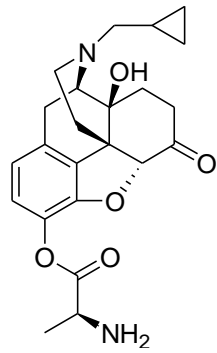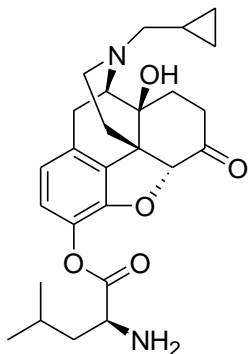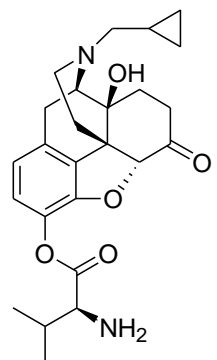
CARBOXYLATE PEGYLATED PRODRUGS			
Name	MW	logK$_{o/w}$	Structure
YTR-NTX-20	502	0.08	
YTR-NTX-21	606	2.21	
YTR-NTX-29	502	0.15	
YTR-NTX-31	458	0.30	
YTR-NTX-43	516	0.44	

CARBAMATE PEGYLATED PRODRUGS

Name	MW	logK$_{o/w}$	Structure
YTR-NTX-28	517	-0.12	
YTR-NTX-63	530	0.24	

CARBOXYLATE CARBOHYDRATE PRODRUGS

Name	MW	logK$_{o/w}$	Structure
YTR-NTX-69	685	-0.4	

CARBOXYLATE AMINO ACID PRODRUG PRECURSORS			
Name	MW	logK_{o/w}	Structure
JAE-2	647	2.82	
CARBAMATE CODRUGS			
Name	MW	logK_{o/w}	Structure
JAE-1	558	0.19	
CARBONATE DUPLEX PRODRUGS OF 6-β-NALTREXOL			
Name	MW	logK_{o/w}	Structure
YTR-NTXol-89	712	N/A	

CHOLYL CARBONATE PRODRUG OF NALTREXONE			
Name	MW	logK$_{o/w}$	Structure
YTR-NTX-100	507	N/A	
AMINO ACID ESTER PRODRUGS OF 6β-NALTREXOL			
Name	MW	logK$_{o/w}$	Structure
6-O-valinyl-naltrexol ester	443	2.04	
6-O-β-alanyl-naltrexol ester	414	1.15	
6-O-prolinyl-naltrexol ester	441	1.82	

6-*O*-alanyl-naltrexol ester	414	0.81	
6-*O*-leucinyl-naltrexol ester	456	2.04	
6-*O*-isoleucinyl-naltrexol ester	457	2.11	

AMINO ACID ESTER PRODRUGS OF NALTREXONE

Name	MW	logK$_{o/w}$	Structure
3-*O*-alanyl-naltrexone ester	412	0.21	
3-*O*-leucinyl-naltrexone ester	454	1.44	
3-*O*-valinyl-naltrexone ester	440	1.09	
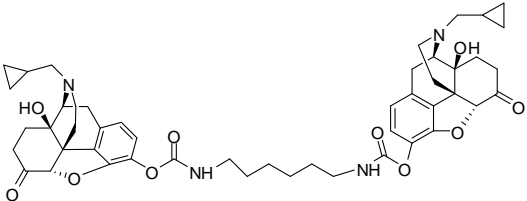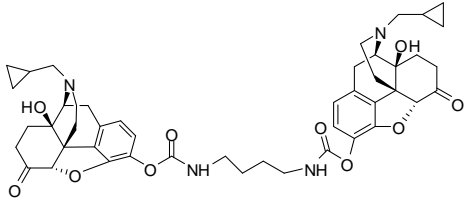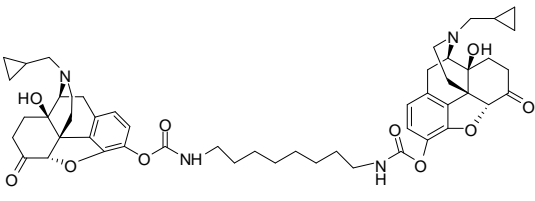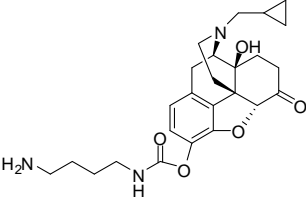
DUPLEX CARBAMATE PRODRUGS			
Name	MW	logK$_{o/w}$	Structure
AVR-11	851	-	
AVR-13	823	-	
AVR-15	879	-	
AMINO PRODRUG			
Name	MW	logK$_{o/w}$	Structure
AVR-14	456	0.37	

159
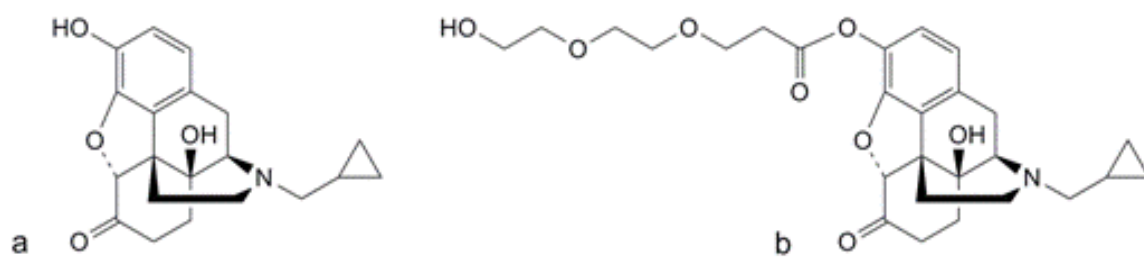
Figure 8.1.

Structures of (a) naltrexone and (b) its PEGylated prodrug.

Figure 8.2.
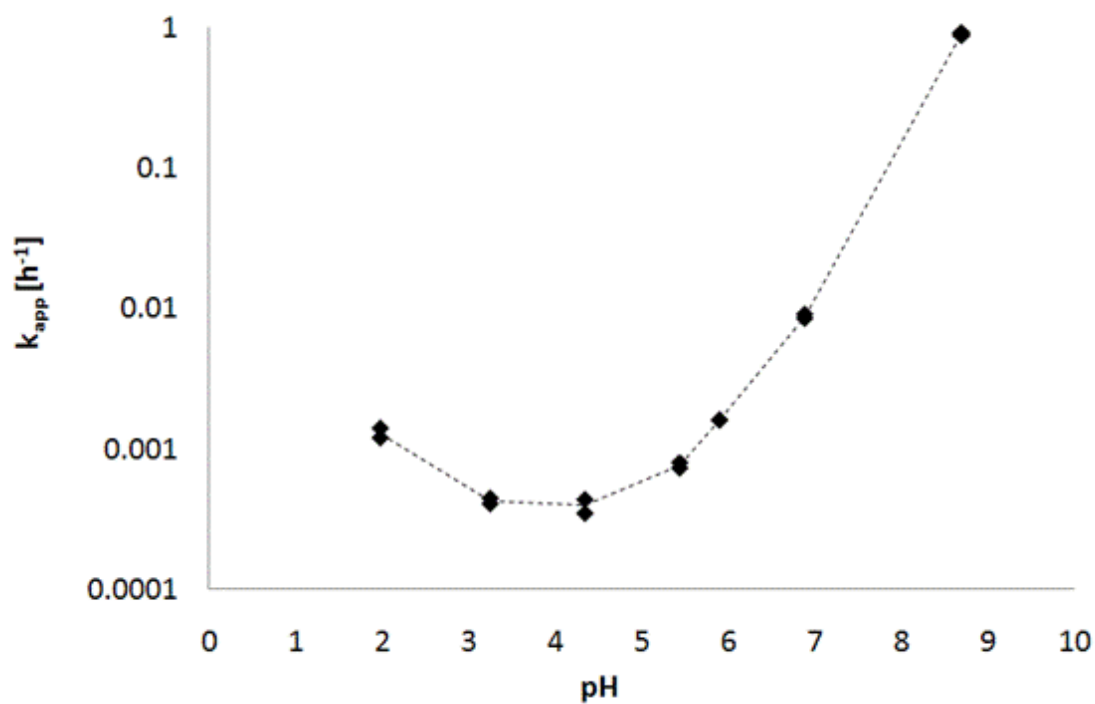
pH-rate profile for the hydrolysis of the PEG-NTX prodrug ester bond in 20mM buffers, I = 0.1 at 32°C. Points indicate apparent rate constants for the degradation of the prodrug (n = 2).

Figure 8.3.
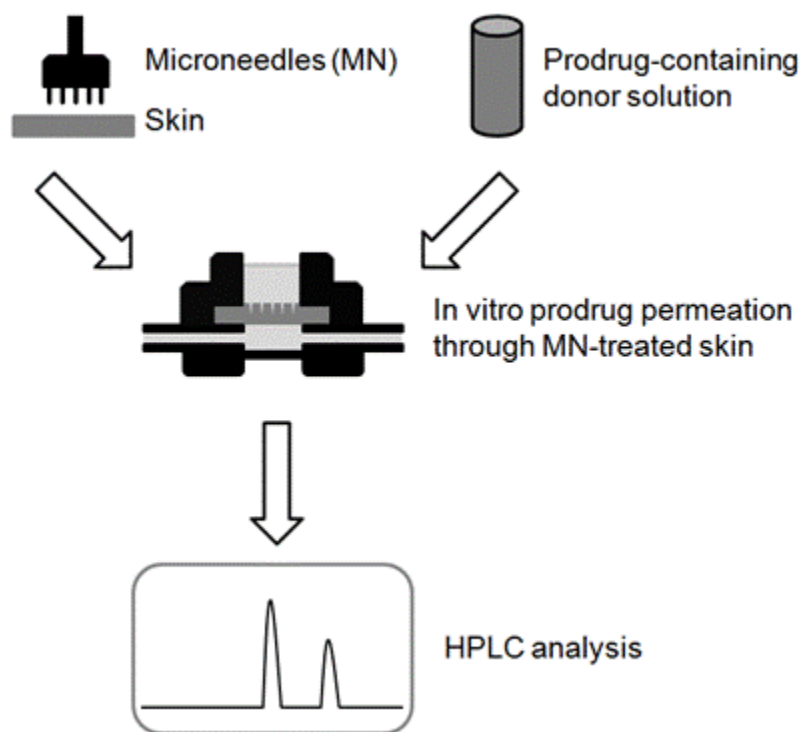
Diagram of the *in vitro* experimental set-up used to study the permeation of the PEG-NTX prodrug. Yucatan minipig skin was treated with MN to obtain 100 microchannels and mounted into a diffusion cell. Six different concentrations of the prodrug solution (pH 5.0) were prepared and placed in diffusion cell donor compartments to initiate the permeation experiment. Fractions of the receiver solution composed of the isotonic HEPES-buffered Hanks' balanced salts solution (pH 7.4) were collected every 6h over the 48h duration of the experiment. They were analyzed by HPLC for the presence of the PEG-NTX prodrug (intact prodrug) and the NTX-from-prodrug (parent drug generated from prodrug).

Figure 8.4.
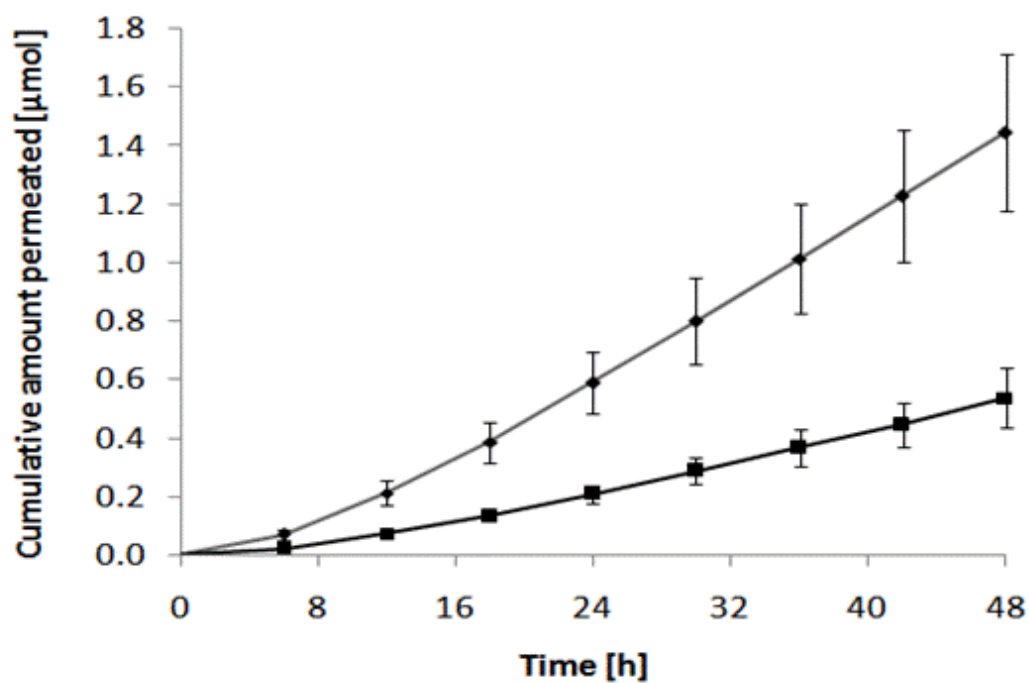
Representative *in vitro* permeation profile of the PEG-NTX prodrug through MN-treated Yucatan minipig skin. The cumulative amount of PEG-NTX prodrug itself (♦) and NTX generated from the prodrug (■) detected in the receiver phase are plotted against time. Each point represents the mean ± SD (n = 4).

Figure 8.5.
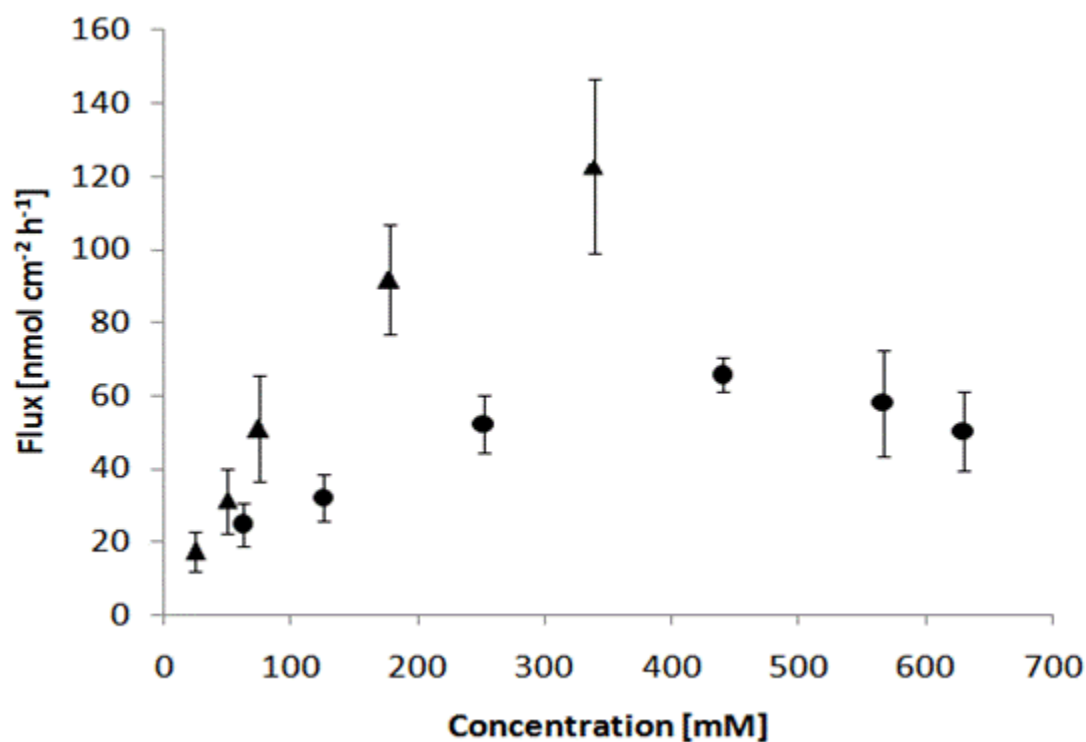
Summary of the drug permeation data presented as a total flux plotted against drug concentration in the donor solution. Two independent plots correspond to two separate experiments which used either: PEG-NTX prodrug (●) or NTX (▲) as the permeant in the donor solution. MN-treated Yucatan minipig skin was employed. Each point represents the mean ± SD (n = 3-4).

Figure 8.6.
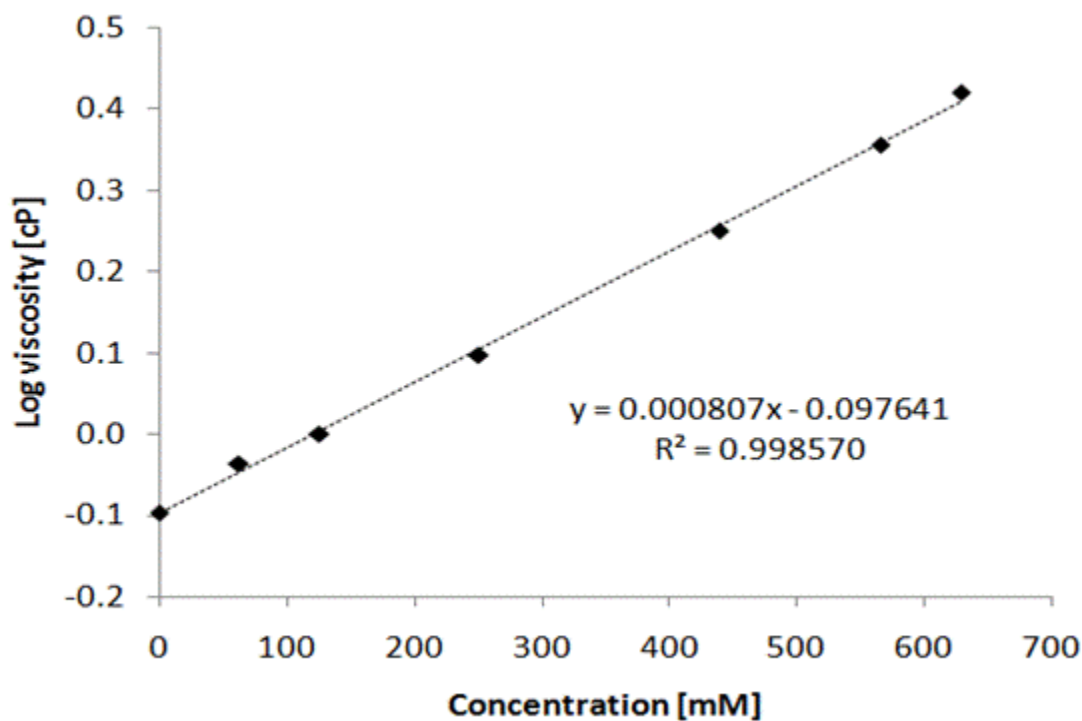
Viscosity of the prodrug-containing donor solutions as a function of PEG-NTX prodrug concentration. Points indicate experimentally measured viscosity values while dashed line represents the least-squares fit to the log-linear empirical Eq. 3. Each point represents the mean of three determinations (n = 3), standard deviation is smaller than the size of the symbols.

Figure 8.7.
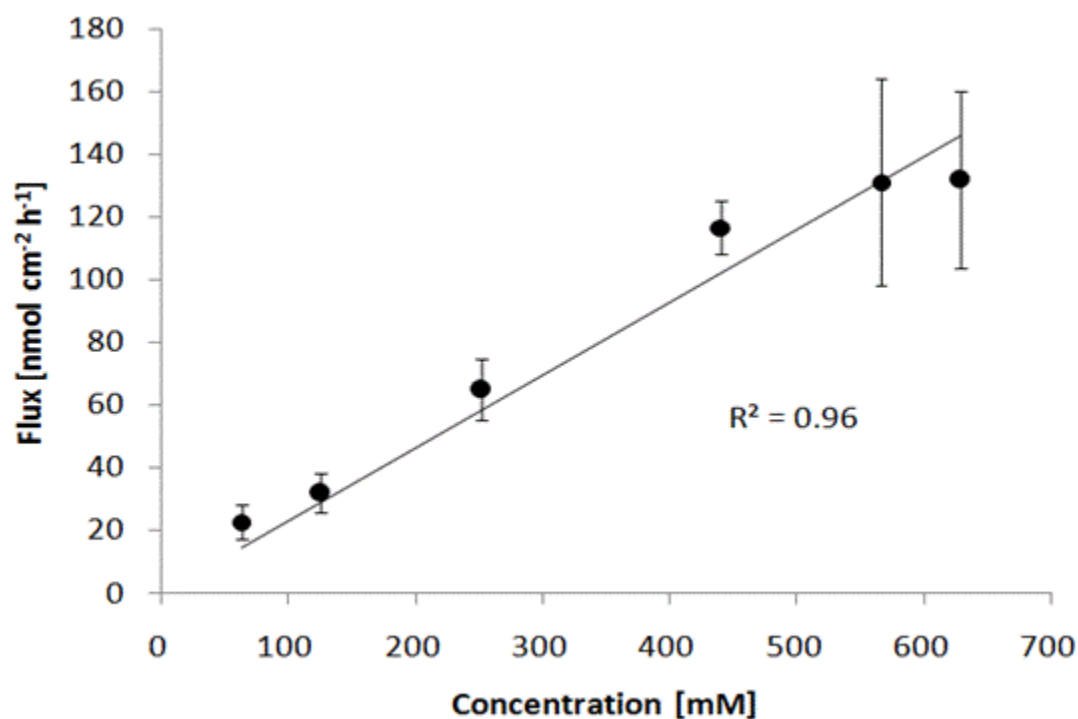
Total flux of the PEG-NTX prodrug through MN-treated Yucatan minipig skin normalized per viscosity of the donor solution according to Eq. 4. Points indicate calculated viscosity-normalized total flux values and solid line represent the least-square fit to a linear equation with zero Y-intercept. Each point represents the mean ± SD (n = 3-4).

Figure 8.8.
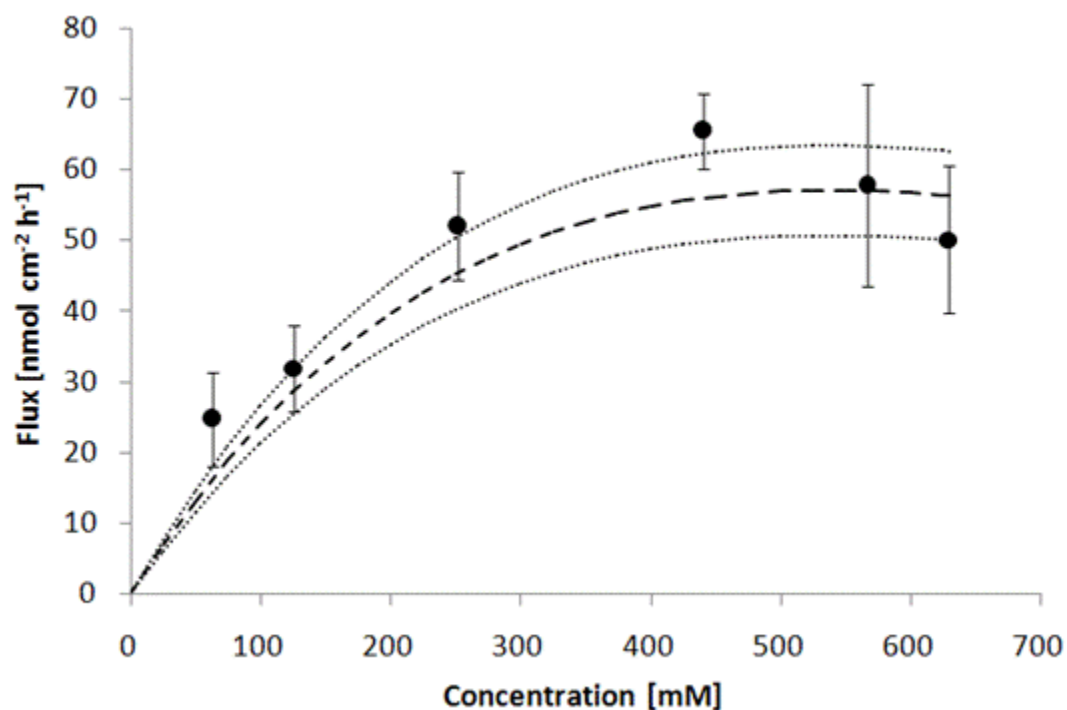
Comparison of the experimental total prodrug flux through MN-treated Yucatan minipig skin to the flux calculated according to the Eq. 7. Points indicate experimentally measured mean flux values ± 95% CI (n = 3-4) and dashed line denotes the calculated mean flux value ± 95% CI as outlined by dotted lines.

Figure 8.9.

YTR-NTX-20	1.93E-03
YTR-NTX-43	1.84E-03
YTR-NTX-28	9.83E-04
YTR-NTX-63	1.11E-03
YTR-NTX-69	5.30E-01
YTR-NTX-21	5.00E-04
YTR-NTX-29	2.93E-02
YTR-NTX-31	2.83E-02
YTR-NTXol-89	6.45E-05
YTR-NTX-100	2.76E-02
JAE-1	0.00E+00
JAE-2	4.00E-02
beta-Ala-6O'-NTXol	7.80E-04
Val-6O'-NTXol	8.50E-04
Ala-6O'-NTXol	1.07E-02
Leu-6O'-NTXol	4.69E-03
Ile-6O'-NTXol	3.05E-04
Pro-6O'-NTXol	2.05E-02
Val-3O'-NTX	6.82E-02
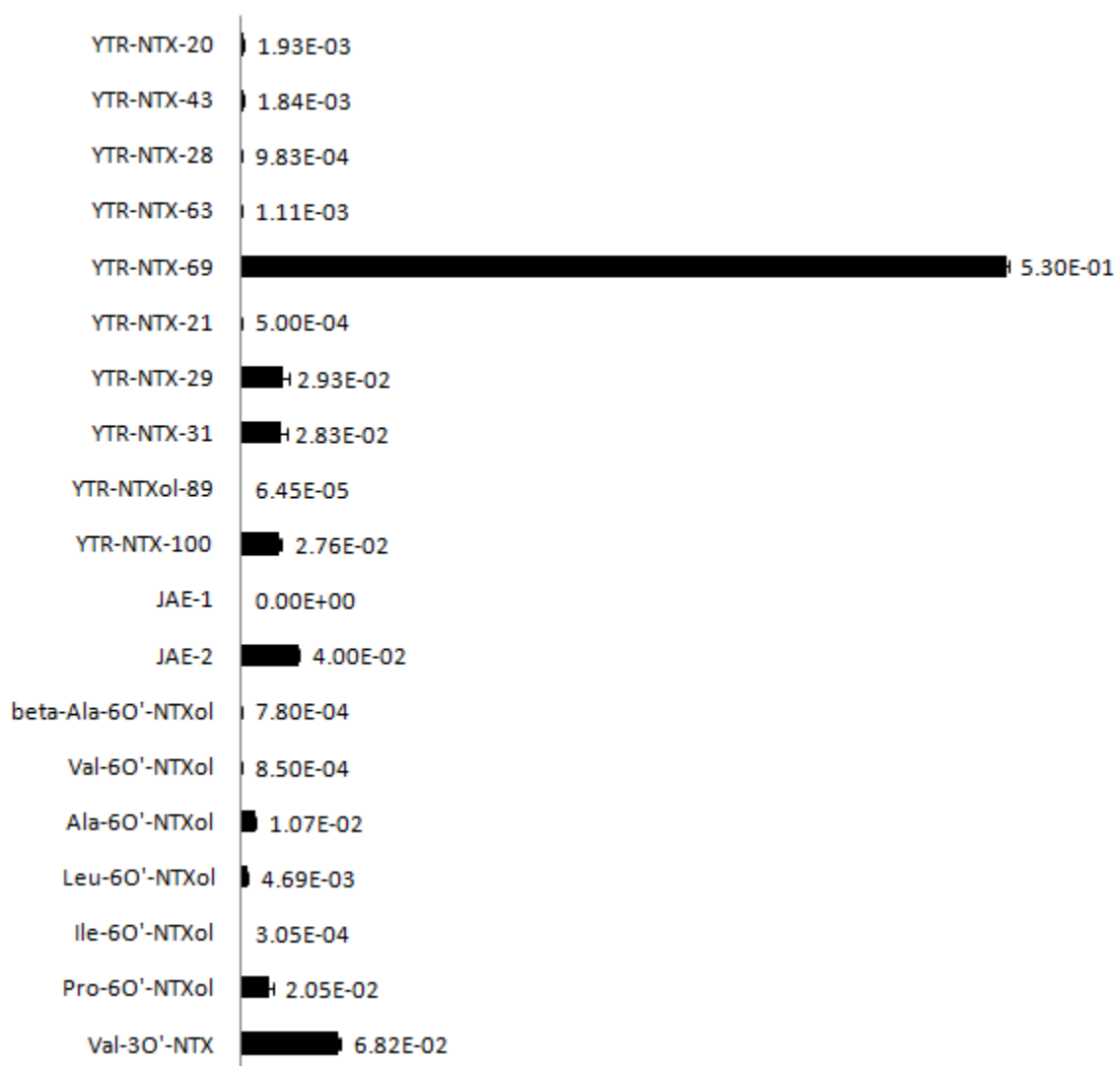
The pseudo first-order hydrolytic rate constants (k) for NTX and NTXol prodrugs and codrugs at pH 5.0. Additionally, Ala-3O'-NTX and Leu-3O'-NTX, which are not included in the graph, degraded extremely fast giving k values of 4.74 and 2.32 h^{-1}, respectively.

Figure 8.10.
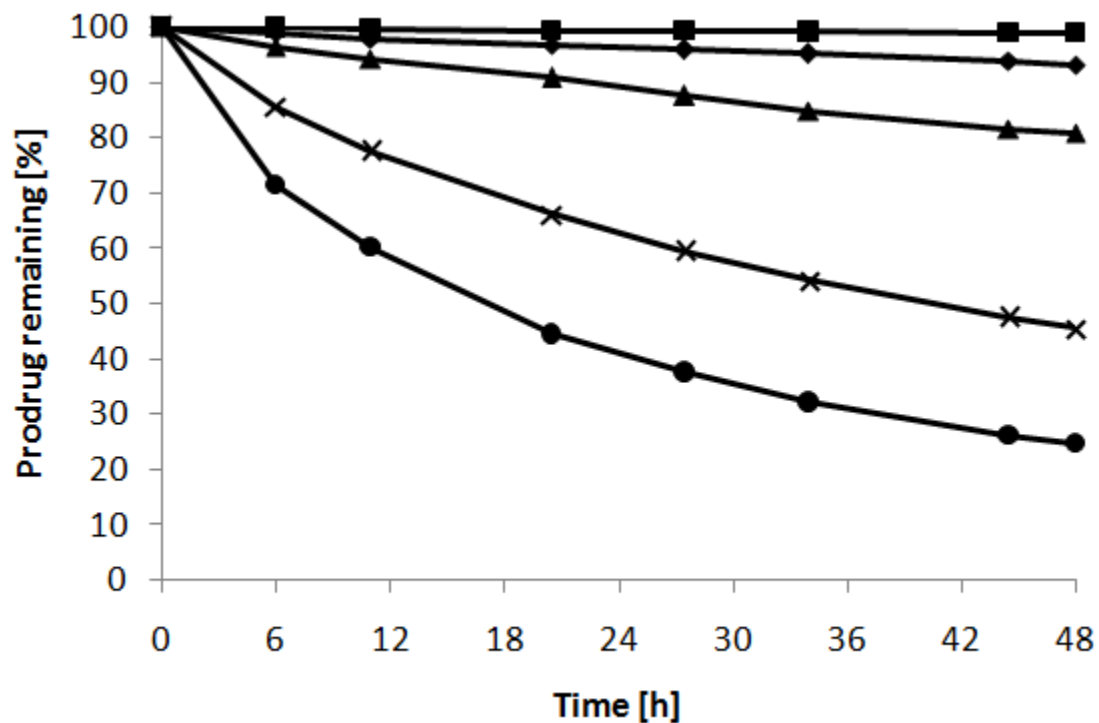
YTR-NTX-20 carboxylate prodrug hydrolysis as a function of PG concentration in the aqueous medium. Higher PG content corresponds to lower prodrug degradation rates. Circles – 25% PG, crosses – 50% PG, triangles – 75% PG, rhomboids – 90% PG and squares – 100% PG.

Figure 8.11.
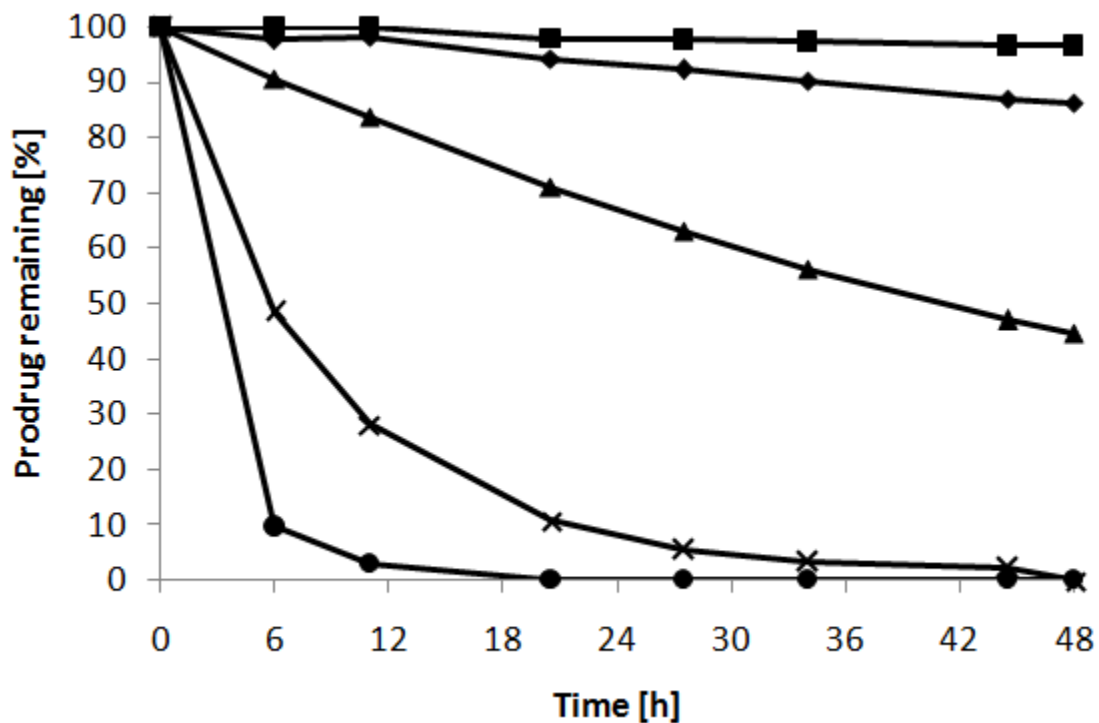
YTR-NTX-28 carbamate prodrug hydrolysis as a function of PG concentration in the aqueous medium. Higher PG content corresponds to lower prodrug degradation rates. Circles – 25% PG, crosses – 50% PG, triangles – 75% PG, rhomboids – 90% PG and squares – 100% PG.

Figure 8.12.
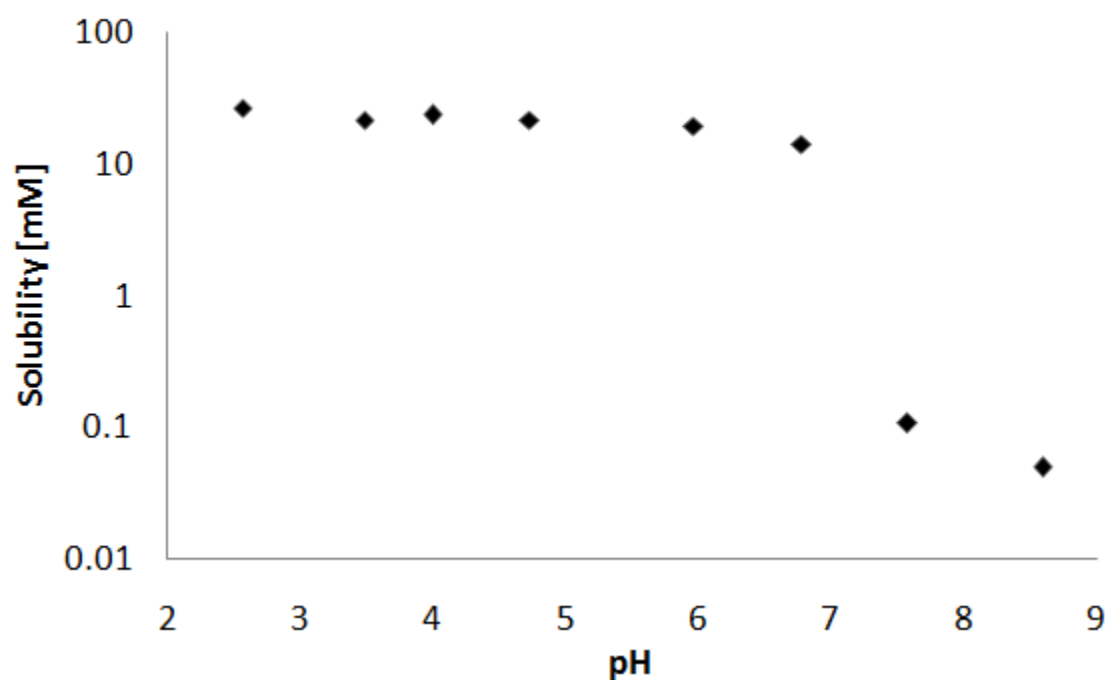
The pH-solubility profile of the YTR-NTXol-89 codrug. Even at the high solubility range at low pH values, the absolute solubility is low as compared to NTX and NTXol.

Chapter 9

In vitro permeation of naltrexone salts across microneedle treated skin

9.1. Introduction

The goal of this chapter is to present the potential of using naltrexone salts in conjunction with MN-treated skin. In order to fulfill the **research goal 3.4** several naltrexone salts were synthesized by Dr. Reddy Pinninti. First, pH-solubility profiles were established. Next, permeation of highest water-soluble salt – NTX glycolate – across MN-treated skin was evaluated. Finally, the skin irritation potential of NTX glycolate, lactate and hydrochloride were assessed in hairless guinea pig model. The contents of the following chapter have been submitted for publication to Journal Investigative Dermatology.

The effectiveness of transdermal drug delivery depends on the ability of transporting a drug across skin in a quantity sufficient to elicit a therapeutic effect. A single major challenge in the percutaneous drug delivery field is low permeability of the human skin. For most xenobiotics, it is the very high diffusional resistance of the stratum corneum (SC) that imparts barrier properties to the whole skin and results in low drug transport rates [55, 57]. The spectrum of drugs possessing the necessary physicochemical properties to cross this barrier at a relevant rate is limited, and the number of drugs that are successfully delivered percutaneously is relatively low [17]. To address this challenge, a variety of skin permeability enhancement techniques are used [8, 22]. Microneedles (MN) represent one of the physical enhancement methods that have been shown to produce substantial increase in the transdermal drug flux. Physically, microneedles typically refer to the arrays of micrometer-size protrusions long enough to penetrate and breach the SC barrier, but at the same time short enough to minimize pain

sensation [25, 30, 31]. Transient microchannels created by the application of MN provide a path of the least diffusional resistance for permeating drug.

Naltrexone (NTX) is a potent, competitive opioid receptor antagonist approved for treatment of opioid and alcohol addiction [83]. Its transdermal delivery could bear substantial advantages over currently available dosage forms: e.g. oral tablet and intramuscular controlled-release injection [20]. The percutaneous rates of passive transport of NTX and its active metabolite, 6-ß-naltrexol, from reasonably-sized patches are therapeutically insufficient. However, the use of MN proved to significantly improve transport. *In vitro* diffusion studies have shown that the creation of microchannels in the skin had limited effect on the delivery rates of the neutral (free-base) form of NTX and 6-ß-naltrexol, but an improvement in the rate of delivery of positively charged (salt-form) species of these drugs was observed [6]. It was hypothesized that elevated NTX and 6-ß-naltrexol water-solubility, rather than the presence of a positive charge, was responsible for the observed increase in the transport rates of the salt forms of these drugs [6]. As an extension of this thought, a study evaluating a highly-soluble PEGylated prodrug form of naltrexone was carried out [229]. However, it was observed that the improved solubility of the prodrug did not translate into superior flux as compared to the parent drug. Besides increased molecular size, a highly non-linear relationship between prodrug donor solution concentration and percutaneous flux was noted and rationalized based on the accompanying vehicle viscosity changes [229].

Generally, for NTX•HCl, *in vitro* and *in vivo* animal studies showed that MN use resulted in an approximate 10-fold enhancement in the transdermal flux over that through untreated (no MN) skin [6, 155]. Importantly, a first-in-human pharmacokinetic MN study demonstrated that the combination of MN skin pretreatment and application of four NTX•HCl patches afforded drug plasma levels in the lower end of the targeted therapeutic range [32]. To improve this prototype drug delivery system an increase in the

flux is desired. An enhanced transport rate through MN-treated skin would allow higher plasma levels and a decrease in the number of patches needed.

In the absence of non-ideal behavior, and in accordance with Fick's first law of diffusion, an increase in the drug concentration translates directly into augmented transdermal flux. We have observed a substantial deviation from the ideal behavior while evaluating the permeation of a highly water-soluble PEGylated naltrexone prodrug across MN-treated skin [229]. As a result, a prodrug approach produced no enhancement in the transport rates of naltrexone species. In the present work, another approach involving naltrexone salt selection is investigated. The aim of this study was to identify a naltrexone salt that would a) provide an elevated *in vitro* percutaneous drug transport rate across microneedle-treated skin as compared to that of naltrexone hydrochloride and b) prove non-irritating to the skin *in vivo.*

9.2. Materials and methods

Chemicals

Naltrexone and naltrexone hydrochloride was purchased from Covidien Mallinckrodt (St. Louis, MO, USA). Hanks' balanced salts modified powder, and sodium bicarbonate were purchased from Sigma (St. Louis, MO). 4-(2 Hydroxyethyl)-1-piperazineethanesulfonic acid (HEPES), gentamicin sulfate, trifluoroacetic acid (TFA), triethylamine (TEA), 1-heptane sulfonic acid sodium salt, and acetonitrile (ACN) were obtained from Fisher Scientific (Fairlawn, NJ). 1-Octane sulfonic acid sodium salt was obtained from ChromTech (Apple Valley, MN, USA). Hydroxyethyl cellulose (HEC) Naltrosol® grade 250MR was purchased from Aqualon (Wilmington, DE, USA) and propylene glycol (1,2-propanediol) from Sigma-Aldrich. Water was purified using a NANOpure Diamond™ Barnstead water filtration system.

Synthesis procedure of naltrexone salts

The synthesis was carried out by Dr. Reddy Pinninti.

Naltrexone free base was dissolved in about 10 volumes of anhydrous acetonitrile. An equimolar amount of acid (acetic, glycolic, lactic, fumaric or citric) was added and the reaction mixture was heated until the salt precipitated out. The crystals obtained were filtered and washed three times with dichloromethane to remove the unreacted free base. The resulting salt was dried under vacuum to give white crystals of salts (acetate, glycolate, lactate, fumarate and citrate).

Chemical identity of NTX salts was confirmed by NMR analysis. All the ^{1}HNMR and ^{13}C NMR spectra were recorded as δ values in $CDCl_3$ with reference to tetramethylsilane (TMS) as internal standard on Varian mercury instrument (300 MHZ).

Naltrexone Acetate:

^{1}H NMR (300 $CDCl_3$) δ 0.13 (m,2H), 0.47-0.49 (m,2H), 1.28-1.32 (d,1H), 1.41-1.50 (t,1H), 1.73-1.82 (m,2H), 1.89-2.12 (m,2H), 2.32-2.37(m,4H),2.62-2.66 (d,1H), 2.86-3.00 (m,3H), 3.12-3.13 (d,1H), 3.44 (bs,3H), 4.75-4.76 (d,1H), 6.48-6.59 (m,2H)

^{13}C NMR (300 $CDCl_3$) δ 4.41, 4.60, 10.03, 21.92, 22.97,26.80, 31.02, 31.96, 36.62, 41.13, 44.09, 51.02, 59.14, 62.12, 70.46, 90.09, 117.85, 119.66, 123.98, 130.06, 139.97, 144.03, 172.61,209.22

Naltrexone Glycolate:

^{1}H NMR (300 $CDCl_3$) δ 0.15 (m, 2H), 0.47-0.51 (2H), 0.88 (m,1H), 1.30-1.34 (d,1H), 1.46-1.51 (t,1H), 1.76-1.79(d,1H), 2.20-2.11 (m,2H), 2.37-2.56 (m,5H), 2.66-2.70 (d,2H), 2.89-3.03 (m,2H), 3.18-3.20 (d,1H), 3.85 (d,1H), 4.76 (d,1H), 4.87 (bs, 3H), 6.49-6.58 (m,2H)

^{13}C NMR (300 $CDCl_3$) δ 4.37, 4.72, 9.74, 23.05, 30.78, 31.93, 36.56, 44.34, 50.90, 59.02, 60.49, 62.12, 70.47, 90.01, 117.94, 119.75, 123.76, 129.94, 140.08, 144.06, 174.81, 209.14

Naltrexone Citrate:

^{1}H NMR (300 CDCl$_3$) δ 0.33 (m,2H), 0.60 (m,2H), 1.06 (m,2H), 1.47-1.50 (m,2H), 1.90 (m,1H), 2.11-2.15 (d,1H), 2.31 (m2H), 2.59-2.74 (m,7H), 2.90 (m,5H), 3.35 (bs,1H), 3.67 (m,1H), 4.46-4.87 (d,1H), 6.56-6.64 (m,2H), 9.36 (bs,1H)

^{13}C NMR (300 CDCl$_3$) δ 3.87, 5.48, 7.77, 19.39, 23.49, 29.11, 31.52, 35.95, 43.70, 44.63, 45.86, 49.93, 56.80, 58.13, 62.04, 70.49, 72.29, 89.50, 118.44, 120.26, 122.19, 128.96, 140.49, 144.10, 171.83, 176.75, 208.38

Naltrexone Fumarate:

^{1}H NMR (300 CDCl$_3$) δ 0.20 (m,2H), 0.50-0.53 (m,2H), 0.91 (m,1H), 1.32-1.36 (d,1H), 1.47 (m,1H), 1.79 (d,1H), 2.08-2.13 (m,2H), 2.37-2.44 (m,3H), 2.57-2.73 (m,3H), 2.91 (m,1H), 3.02-3. 08 (d, 1H), 3.31 (1H, m), 4.10 (bs, 3H), 4.79-4.83 (d, 1H), 6.54-6.62 (m, 4H)

^{13}C NMR (300 CDCl$_3$) δ 4.20, 4.96, 9.00, 23.21, 30.14, 31.79, 36.33, 44.85, 50.53, 58.70, 62.09, 70.46, 89.83, 118.12, 119.93, 123.16, 129.59, 135.02, 140.23, 144.07, 167.19, 208.90

Thermal Analysis

Differential scanning calorimetry (DSC) was used to characterize natrexone salts. All thermal analysis were carried out using a TA Instruments DSC 2920 (TA Instruments, New Castle, DE) differential scanning calorimeter. Around 5 mg of each sample was placed in a flat crimped aluminum pan and heated at a rate of 5 °C/min under N$_2$ purge (50 ml/min). Potential changes in drug substance, such as hydration state and melting were monitored. Additionally, all melting points were confirmed by MelTemp$^®$ model 1201D (Barnstead International, IA, USA) (n = 3).

pH-solubility profile determination

pH-Solubility profiles of naltrexone salts were determined at 25 °C. At first, excess solids (NTX salts) were added to glass vials containing 2 ml of water. Solubility at different pH values were determined by stepwise titration with HCl or NaOH solutions. At each addition of HCl or NaOH, the suspension was equilibrated for 24 h, the pH value was recorded, and an aliquot was removed and spin-filtered for 1 min in VWR centrifugal filters (0.2 μm membrane) at 25 °C. The filtrate was diluted with an adequate amount of acetonitrile (ACN):water 70:30 (v/v), and resulting solution analyzed by high pressure liquid chromatography (HPLC). The number of samples obtained for each salt solubility determination is as follows: NTX•HCl (n = 19), NTX acetate (n = 18), NTX glycolate (n = 12), NTX lactate (n = 18), NTX fumarate (n = 10), and NTX citrate (n = 17).

Donor solution preparation

Eleven donor solution concentrations for *in vitro* permeation experiments were prepared. NTX•HCl was dissolved in water at 32 °C to obtain the following concentrations: 40, 80, 119, 159, 212, 265 and 291 mM. NTX glycolate was dissolved in water at 32 °C to obtain the following concentrations: 365, 645, 946 and 1272 mM. The pH of all donor solutions was adjusted to 5.0 with a 3M HCl solution. 291 mM is the saturation solubility of the NTX•HCL at pH 5.0 at 32 °C while 1272 mM is the saturation solubility of the NTX glycolate at pH 5.0 at 32 °C. All donor solutions were prepared immediately before launching *in vitro* permeation experiments. Three to four cells were used per single naltrexone salt concentration (n = 3-4).

Viscosity measurements

A Brookfield DV-III LV programmable cone/plate rheometer with a CPE-40 spindle was used for measuring the viscosity of the donor solutions. The sample volume was 0.5 ml.

All determinations were carried out at 32 ^{0}C maintained by a circulating water-bath TC-102. Each donor viscosity measurement was taken three times at low, medium and high torque value in the range of 10-100% of the instrument specifications (n = 3).

In vitro diffusion studies

Full-thickness Yucatan minipig skin was harvested from the dorsal region of a euthanized 6-month-old animal. Animal studies were approved by the University of Kentucky IACUC. Subcutaneous fat from skin samples was removed with a scalpel and sparse hair clipped. Skin samples were immediately placed in a plastic bag and frozen until use (-20 °C). Before each permeation study, skin samples were allowed to thaw for about 30 min. Skin used for MN treatment was first dermatomed to a thickness of about 1.9 mm and then placed on a wafer of polydimethylsiloxane polymer, which mimicked the naturally occurring mechanical support of underlying tissue because of its comparable structural elasticity. In the context of *in vitro* studies described in this article "MN" refer to microneedle rows obtained from Dr. Prausnitz's laboratory. They were fabricated by laser cutting of stainless steel sheets as reported previously [210]. MN were solid metal, two-dimensional "in-plane" rows each containing five microneedles oriented with their axis parallel to the steel sheet. This design is characterized by the following microneedle dimensions: 750 µm long, 200 µm wide, 75 µm thick and 1.35 mm inter-needle spacing. The insertion of MN into skin was carried out manually by applying gentle finger pressure followed by their instantaneous removal. The diffusion area of skin (0.95 cm^2) was pierced 20 times, with a row containing five microneedles, gradually advancing the MN application area to obtain 100 non-overlapping piercings before mounting the skin in the diffusion cell. If any damage to the MN was observed a new array was used. Three to four cells were used per each naltrexone salt concentration (n = 3-4). A PermeGear flow-through (In-Line, Riegelsville, PA) diffusion cell system was

used for the in vitro diffusion studies. Isotonic HEPES-buffered Hanks' balanced salts solution (25 mM, pH 7.4) was used as the receiver solution. Skin samples in the diffusion cells were maintained at 32 °C using a circulating water bath. The diffusion experiments were initiated by charging the donor compartment with 0.4 ml of the donor solution. Samples were collected from the receiver compartment in 6 h increments over 48 h. All samples were stored at 4 °C until HPLC analysis, which was carried out within 24 hours.

Quantitative analysis

Quantitative analysis of NTX salts by HPLC was carried out using a modification of the assay described by Hussain et al. [225]. The HPLC system consisted of a Waters 717 Plus autosampler, a Waters 600 quaternary pump, and a Waters 2487 dual wavelength absorbance detector with Waters Empower™ software. A Perkin Elmer® Brownlee Spheri-5 VL 5 µm (220 x 4.6 mm) C18 column with a guard column of the same type was used with the UV detector set at a wavelength of 278 nm. The mobile phase consisted of 70:30 (v/v) ACN:0.1% TFA containing 0.065% 1-octane sulfonic acid sodium salt, adjusted to pH 3.0 with TEA aqueous phase. Samples were run at a flow rate of 1.5 ml/min with a run time of 4.5 min. The injection volume was 100 µl, and the retention times of all NTX salts were 2.2 min. Samples were analyzed within a linear range of NTX salts concentrations 100 – 10,000 ng/ml.

The permeation data were plotted as the cumulative amount of NTX collected in the receiver compartment against time. The steady-state flux value for a given run was calculated from the slope of the terminal portion of the graph, according to:

$$Q/A = J_{ss}(t - t_{lag})$$ (9.1)

where Q is the cumulative amount of permeant, A is the area of diffusion, J_{ss} is the steady-state flux defined as mass transport per area, t is time, and t_{lag} is the lag time for diffusion.

In vivo NTX salts skin irritation potential study

Three Charles River hairless guinea pigs were used in the skin irritation studies (n = 3). Five treatment sites were assigned to each guinea pig dorsal region. Four of them corresponded to the formulations under scrutiny and the fifth one was a negative control. The following treatments were employed:

- placebo gel: sterile water:PG 90:10 (v/v) and 3% hydroxyethylcellulose (HEC) (w/v), pH 6.5

- NTX•HCl gel: 250 mM NTX•HCl in sterile water:PG 90:10 (v/v) and 3% hydroxyethylcellulose (HEC) (w/v) , pH 5

- NTX lactate gel: 700 mM NTX lactate in sterile water:PG 90:10 (v/v) and 3% hydroxyethylcellulose (HEC) (w/v), pH 5

- NTX glycolate gel: 700 mM NTX glycolate in sterile water:PG 90:10 (v/v) and 3% hydroxyethylcellulose (HEC) (w/v), pH 5

- Control: no gel

The formulation composition selection was based on former and present findings about the percutaneous transport of the NTX species and skin irritation potential of the excipients. PG and HEC are common, generally recognized as safe (GRAS) excipients widely used in topical formulations and are not skin-irritating [218]. HEC has been successfully used in earlier studies as a thickening agent. The inclusion of 10% PG in the formulation is dictated by its beneficial influence on the physical stability of the gel under *in vivo* conditions where, as a strongly hygroscopic excipient, it prevents water

evaporation and collapse of the gel (unpublished observations). The concentrations of NTX species in gels were selected to approximate the concentrations that provided highest *in vitro* NTX flux through MN-treated skin.

Protective patch fabrication

The occlusive protective patches were fabricated by sandwiching a rubber ring (inner diameter 2 cm) between an ARcare® 7396 adhesive and an impermeable backing laminate (Scotchpak™ #1109 SPAK 1.34 MIL Heat Sealable Polyester Film) fixed on one side of the rubber ring creating a reservoir able to contain a gel formulation. The protective patch was placed on a release liner composed of Scotchpak™ 9742 until the application on animals.

Application of treatments

For *in vivo* studies "MN" refer to two-dimensional "out of plane" 50 MN arrays. The arrays were manufactured with needles cut into the plane of the stainless steel sheet and subsequently bent at 90° out of the plane [210]. MN arrays were obtained from Dr. Prausnitz's laboratory. In each guinea pig, four treatment sites (about 2 cm in diameter) were treated with MN arrays twice to obtain the total of 100 microchannels per site. Next 0.3 g of the gel (placebo, NTX•HCl, NTX lactate or NTX glycolate) was applied to each of the treated sites once and covered with a protective patch. The fifth site (control) was not treated with MN, nor was the gel or protective patch applied. Protective patches were secured on the guinea pig dorsal region by the use of a Bioclusive transparent dressing for the 4-day duration of the experiment. The length of the experiment was chosen based on the *in vivo* drug delivery goals. After 4 days the protective patches and gels were removed.

Biophysical skin assessment

Colorimetry and TEWL measurements were carried out immediately prior to the application of the treatments and 45 min, 3 h, 6 h, 24 h and 48 h after the removal of the treatments.

Colorimetry (a* parameter)

The inflammation of the skin can be evaluated by assessing the degree of erythema. Skin color was measured by the use of a Minolta colorimeter (Chroma Meter CR-400, Konica Minolta, Japan). The instrument records color reflectance in three-dimensional scale L*a*b, where L* value (luminance) expresses the relative brightness; a* corresponds to the red-green axis with +100 expressing full red and -100 full green; and b* corresponds to the yellow-blue axis. The colorimeter was calibrated before use against a white plate provided by Konica Minolta in the study environment. To perform a measurement the head of the instrument was gently placed on the skin treatment area.

Transepidermal water loss (TEWL)

The skin barrier integrity was evaluated by TEWL. The head of a DermaLab$^{®}$ TEWL probe (CyberDerm Inc.) was gently placed on the skin treatment area to perform a measurement. Besides skin barrier compromise, skin hydration and MN-treatment are both known to contribute to increased TEWL values. The detection of possible barrier compromise due to a given NTX salt alone under such conditions would be difficult. However, the inclusion of the treatments with MN and placebo gel allows for examination of these two factors independently.

Statistical analysis

Linear least-square fitting of viscosity-normalized data was performed using Scientist[®] software (MicroMath). The statistical analysis of the skin irritation data was carried out by step-wise t-test at α = 0.05 using SIGMA-STAT software (SPSS, Inc., Chicago, IL, USA).

9.3. pH-solubility profiles

Former studies focused on the skin permeation potential of NTX and 6-β-naltrexol in conjunction with MN [6, 155, 255]. The maximum transdermal flux of NTX was found to be limited by the saturation solubility of NTX•HCl in the donor solution [229, 255]. In this work, five naltrexone salts: acetate, glycolate, lactate, fumarate (1:1) and citrate (1:1) were synthesized and their pH-solubility profiles were evaluated. An increased solubility at the physiologically-relevant skin surface pH of 5.0 gives the theoretical basis for expecting improved transport rates through MN-enhanced skin.

Naltrexone possesses two pK_a values; one basic corresponding to the protonation of the tertiary aliphatic nitrogen atom (pK_{a1} = 8.30), and the other acidic corresponding to the dissociation of the phenolic proton (pK_{a2} = 9.80) [226]. Thus, depending on the pH, it can act as a base or as an acid. At low pH values, naltrexone is positively charged and can form salts with acids, while at high pH values it is negatively charged and can form salts with bases. At the intermediate pH values the naltrexone molecule exists predominantly as an uncharged species. **Figure 9.1** shows the distribution of the naltrexone species as a function of pH.

The total solubility (S_{tot}) of naltrexone at any pH is the sum of solubilities of the unionized and ionized forms:

$$S_{tot} = [N^-] + [NH] + [NH_2^+] \qquad\qquad (9.2)$$

where the $[N^-]$, $[NH]$ and $[NH_2^+]$ correspond to the negative, neutral and positive species of naltrexone, respectively. When the neutral naltrexone species is in equilibrium with the solid, the solubility in the aqueous solution can be written as:

$$S_{tot} = [NH]_s(1 + 10^{pK_{a1}-pH} + 10^{pH-pK_{a2}}) \tag{9.3}$$

where the subscript "s" refers to the saturation species. This equation describes the pH-solubility profile at the intermediate pH values. Of note, since two pK_a's are numerically close to each other there is no pH value at which the intrinsic solubility of the uncharged NTX species could be determined directly. On the other hand, at low pH values where the salt form is the equilibrium species, and the amount of the negatively charged NTX species is negligible, the total solubility can be described by the following equation:

$$S_{tot} = [NH_2^+]_s(1 + 10^{pH-pK_{a1}}) \tag{9.4}$$

where the subscript "s" refers to the saturation species. The maximum solubility for any NTX salt occurs at the pH_{max}, or the pH at which the two curves described by **Eq. 9.3** and **Eq. 9.4** intersect [256]. For all salts tested the pH-solubility curve portion described by **Eq. 9.3** is the same as the unionized form of NTX and is identical for all NTX salts. However, at lower pH values individual salt solubility profiles diverge and plateau at different levels in the cases of NTX•HCl, acetate, glycolate and lactate; or demonstrate more complicated behavior in the cases of NTX fumarate and citrate. **Figure 9.2** presents the pH-solubility profiles of NTX•HCl, acetate, glycolate and lactate. At pH 5.0, relevant for percutaneous drug delivery, the solubility of the NTX salts ranks as follows: NTX glycolate ≥ NTX lactate ≥ NTX acetate >> NTX•HCl. Therefore, all three NTX salts under scrutiny demonstrate superior solubility as compared to the NTX•HCl reference.

(Noteworthy, at pH values less than 4, the addition of hydrochloric acid for pH control converts all three naltrexone salts back to the hydrochloride salt. This was inferred by the converging solubility profiles converge in this region, which cannot be accounted for by **Eq. 9.4**). The intrinsic solubilities of the ionized and nonionized NTX forms are summarized in **Table 9.1** together with experimentally determined melting points and calculated pH_{max} values. **Figure 9.3** shows the pH-solubility profiles of NTX•HCl, fumarate and citrate. The non-plateau region observed for fumarate and citrate salts at the lower pH values may be a consequence of formation of multiple equilibrium species as a result of the use of di- and tri-carboxylic acids and cannot be described by **E. 9.4**). Since the solubility of NTX fumarate and citrate around pH 5.0 did not show a substantial improvement over NTX•HCl these two salts were excluded from further examination.

9.4. Permeation across MN-treated skin

Next, *in vitro* permeation studies were carried out with the most water-soluble NTX salt – NTX glycolate. While the saturation solubility of NTX•HCl at pH 5.0 (32 °C) is below 300 mM, NTX glycolate saturation solubility approaches 1300 mM. Several donor solutions containing either NTX•HCl (<300mM) or NTX glycolate (>300 mM) were prepared. The saturated donor solutions did not contain any excess solid to ensure that potential interference between excess NTX salt and the microchannels would not affect the results, such as obstruction of the microchannel opening, or presence of the undissolved drug in the microchannels, etc. The drug permeation from all donor solutions resulted in steady-state conditions after a relatively short lag time. A representative permeation profile is presented in **Figure 9.4**. Permeation of the two NTX salts as a function of the donor solution concentration is summarized in **Figure 9.5**.

9.5. Deviations from ideal behavior

For NTX•HCl, the increase in the donor solution concentration corresponded to the increase in the flux through MN-enhanced skin. This increase, however, was not linear. For NTX glycolate, further increase in the drug concentration produced a parabolic relationship between the flux and drug donor solution concentration, with a maximum corresponding to a concentration of ≈700 mM. The maximum flux obtained with the use of NTX•HCl was 121 ± 16 nmol cm^{-2} h^{-1} (291 mM donor solution), while the maximum flux obtained with the use of NTX glycolate was 178 ± 43 nmol cm^{-2} h^{-1} (645 mM donor solution). In other words, at the cost of roughly doubling the drug concentration and switching from NTX•HCl to NTX glycolate a 50% increase in the percutaneous flux can be achieved. The behavior in the lower concentration range can be well described by Fick's first law of diffusion and a concentration-independent permeability coefficient. However, the deviation from ideal behavior is substantial at the intermediate and high concentration ranges. Noteworthy, there is no discontinuity in the flux-concentration profile at the NTX concentration where the counterion is swapped from HCl to glycolate. This suggests lack of major counterion effect on the diffusivity of NTX as could be expected given the MW of counterions is substantially smaller than that of NTX.

9.6. Viscosity influence on drug diffusivity

It has been suggested that the viscosity of the donor solution may have a vital effect on drug delivery rates through MN-treated skin [229, 255]. The relationship between the viscosity (η) of the diffusion medium and the solute diffusion coefficient is given by the Stokes-Einstein equation:

$$D \; = \; \frac{kT}{6\pi\eta r} \tag{9.5}$$

where k is Boltzmann's constant, T is absolute temperature, and r is the radius of the diffusant (assuming it can be represented by a spherical particle). Specifically, it was shown that the NTX•HCl flux through microchannels and underlying dermis correlated well with the decrease in the calculated drug diffusivity in the donor solution. The viscosity of the donor solution was controlled by addition of propylene glycol to the aqueous vehicle. Also, the flux through microchannels alone was found to be well-approximated by the total flux through MN-enhanced skin for the aqueous donor solution. In other words, the contribution of flux through intact skin around microchannels was low as shown in **Chapter 7**. Herein, it will be assumed that the contribution of NTX glycolate flux through intact skin pathway was also very low (e.g. <5%) as compared to the microchannel pathway. It seems a reasonable approximation given the experimental results obtained from NTX•HCl studies. It is also corroborated by the fact that neither NTX•HCl or NTX glycolate salts caused skin irritation, which could be indicative of increased flux through skin around microchannels. Furthermore, the permeation of a PEGylated NTX prodrug correlated with the viscosity changes of the prodrug-containing donor solution as shown in **Chapter 8** [229]. In that study, viscosity changes in the donor solution were caused by the prodrug itself. It is known that at sufficiently high solute concentration, solvent viscosity can be altered, exerting a secondary effect on the solute's own diffusivity [54]. Hence, although the donor solution viscosity changes in the above two studies were caused by different mechanisms the end result was the same – increased viscosity of the donor solution correlated with decreased transdermal flux through MN-treated skin.

In the current study the lowest concentration of NTX•HCl (40 mM) produced a donor solution viscosity of 0.81 cP while the highest NTX glycolate concentration (1272 mM) produced a donor solution viscosity of 6.46 cP. Hence, there is almost an 8-fold

difference between these extreme values. The experimental data can be transformed by normalizing flux by the apparent viscosity effect. According to Fick's first law of diffusion:

$$J_{ss} = PC = \frac{D}{h}$$ (9.6)

where J_{ss} is the steady-state flux, P is permeability coefficient and C is the permeant concentration in the donor solution when sink conditions in the receiver solution prevail. For solute transport through microchannels the permeability coefficient, P, is defined as the ratio of solute diffusivity (D) in the barrier to the barrier thickness (h) [39]. The substitution of **Eq. 9.5** into **Eq. 9.6** demonstrates the inverse relationship between steady-state flux and viscosity of the barrier. Hence, the ratio of two flux values, uncorrected (J) and corrected (J') for viscosity effect, is given by:

$$\frac{J}{J'} = \frac{\eta'}{\eta}$$ (9.7)

where J' is flux obtained from a donor solution having viscosity η' while J is the flux obtained from a donor solution having viscosity η. Assuming that η' represents a low-viscosity donor solution and η represents a high-viscosity donor solution, an expected flux at elevated viscosity can be calculated by:

$$J = J'\frac{\eta'}{\eta}$$ (9.8)

Alternatively, having an experimental flux value available from a high-viscosity donor solution, the expected flux value for a low-viscosity solution would be:

$$J' = J \frac{\eta}{\eta'}$$
(9.9)

If it is further assumed that ŋ' equals 1 cP, which is a fair approximation for low drug concentration donor solutions, the viscosity-normalized flux (J') is the product of the experimental flux (J) and the corresponding viscosity (ŋ) of the donor solution. Such normalization yields flux values that correspond to a viscosity value of unity. The above discussion equates the viscosity of the donor solution with the microviscosity of the diffusion barrier – dermis underlying the microchannels. It had been hypothesized that donor solution composition can directly alter the properties of the dermis, thus, affecting the diffusion of drugs through this barrier [229, 255]. If the hypothesis is valid, it would be expected that the viscosity-normalized flux will correlate linearly with the drug concentration in the donor solution over the whole concentration range tested. A plot of viscosity-normalized flux is presented in **Figure 9.6**, which shows a reasonable linear correlation ($1/Y^2$ weighted R^2 = 0.93). Therefore, the results seem to support the hypothesis.

To gain more insight about the diffusion process across MN-treated skin a two-ply membrane concept incorporating the microchannel and underlying dermis can be used. In the experimental set-up used in the current study the thickness of the dermis below the microchannel exceeds the length of the microchannel, and the diffusion coefficients of drugs in the dermis are known to be typically 3-10 times lower as compared to those in the bulk aqueous solutions [18, 59]. Based on the above, it can be expected that the major diffusional resistance lies in the dermis layer. Therefore, flux should not depend on the viscosity of the donor solution unless donor solution changes the properties of the dermis barrier. It is possible that the naltrexone salt containing, elevated-viscosity donor solution alters the microenvironment of the dermis by increasing its diffusional

resistance. Assuming this effect is similar to that seen in the bulk solution, flux through microchannels and dermis below would be inversely related to the viscosity of the donor solution. In other words, the results from the current study imply that changes in the drug diffusivity in the donor solution are reflective of drug diffusivity changes in the whole skin barrier.

By analogy to **Eq. 9.9**, permeability coefficients can also be normalized by viscosity. The slope of the line in **Figure 9.6** corresponds to the average viscosity-normalized permeability coefficient P'_{ave}. Applying $1/Y^2$ weighting to the viscosity-normalized flux values (Scientist[®]), the least-square estimate of P'_{ave} is 47.8×10^{-5} cm h^{-1}, 95% confidence interval (41.1, 54.5) x 10^{-5} cm h^{-1}. This average value, in combination with individual donor solution viscosity, η, and drug concentration in the donor solution, C, can be used to calculate the expected transdermal flux, J_{calc}, across MN-treated skin:

$$J_{calc} = PC = P'_{ave} \frac{\eta'}{\eta} C \qquad (9.10)$$

Figure 9.5 presents flux calculated according to **Eq. 9.10** as compared to the experimental data. A reasonable agreement between experimental and calculated values lends practical utility to this approach. Overall, the selection of NTX glycolate over NTX•HCl permits augmented flux through the MN-treated skin. At the cost of roughly doubling the saturation solubility of NTX•HCl in the aqueous formulation, by means of using NTX glycolate, a 50% increase in the percutaneous flux can be achieved.

9.7. Guinea pig skin irritation study

Finally, a prerequisite for any successful transdermal drug is the lack of or minimal skin irritation potential. Of the three NTX salts that showed increased solubility as compared

to NTX•HCl, NTX glycolate and lactate were further tested for skin irritation potential. α-hydroxy acids, such as glycolic acid and lactic acid, have a long history of being used in cosmetology. Their use typically relates to counteracting skin aging and reduction of wrinkles through increased skin exfoliation [257]. Also, Lac-Hydrin® is a prescription medicine containing 12% lactic acid neutralized with ammonium hydroxide employed for treatment of ichthyosis vulgaris and xerosis. Hence, it was anticipated that NTX salts of these two α-hydroxy acids may have a safe, non-irritating profile. The skin irritation potential of NTX glycolate, NTX lactate and NTX•HCl (as a reference), was evaluated *in vivo* in a hairless guinea pig model. Skin irritation is defined as a reversible damage to the skin following the application of a test substance. It can manifest itself through local inflammation, edema and compromised skin barrier function. Hairless guinea pigs are commonly employed for this type of testing because of their histo-anatomical similarities to the human skin [258-260]. It has been shown that this model ranks skin irritation potential of chemicals in the same order as human studies do, although it is more sensitive. As a consequence, the negative skin irritation results obtained from the hairless guinea pig model imply no irritation to the human skin; however, positive results do not necessarily predict intolerability in humans [259]. The current study protocol involved MN treatment of the designated dorsal sites and application of drug-containing and drug-free gels. Also, one control site with no MN treatment and no gel application was included. After 4 days the gels were removed and skin irritation potential of NTX salts was evaluated by transepidermal water loss (TEWL) and colorimetry measurements (Chroma Meter CR-400, Konica Minolta, Japan). **Figure 9.7** shows the change in the a* value with time in different treatments applied to hairless guinea pigs. The increase in the a* colorimetric value is indicative of erythema, which in turn correlates with local inflammation. Before the application of the treatments, a* values oscillated in the range of 9-10. After the completion of the 4-day experiment and the

removal of gels the a* value was somewhat elevated (up to 12.6) for all the gel treatments, over that of the control, but dropped back to baseline levels over the next 48 hours. The fact that the augmented a* value was observed in naltrexone-containing gels, as well as in the placebo gel suggests that the MN treatments and gel application themselves caused a mild redness. Literature reports indicate that a* values of around 16 [259] are observed following the application 1% sodium lauryl sulfate as a positive control for skin irritation. Our experience (unpublished data) indicates a rise to a value of 18 and higher with sodium lauryl sulfate treatment. Hence, the magnitude of increase in the a* value seen in the current study is not of considerable practical importance. The inclusion of the NTX species in the gels did not produce any additional increase in the erythema. This was also corroborated by visual inspection of the treatment sites.

Complimentary to the colorimetry data, **Figure 9.8** presents the treatment-induced TEWL changes as a function of time. The baseline water loss ranged from 3 to 6 $g\,m^{-2}\,h^{-1}$ in accordance with typical literature reports [259]. Shortly after the removal of the gels, at 45 min, TEWL values were elevated (up to about 20 $g\,m^{-2}\,h^{-1}$) only to drop back to the baseline values within a few hours. The initial increase in the water loss was due to the hydration of the skin resulting from prolonged occlusion. However, an additional contribution coming from the potential existence of the microchannels at that time cannot be ruled out. The lack of augmented TEWL readings at later time points implies no severe reaction to the NTX salts species and maintenance of proper barrier function of the skin.

A previous first-in-human MN study by Wermeling et al. showed that a 3-day application of NTX•HCl formulated in a topical gel ranked from non-irritating to mildly-irritating to the human skin [32]. The present skin irritation study findings suggest that both naltrexone lactate and glycolate performed similarly to NTX•HCl. Consequently, both salts are viable candidates for further *in vivo* investigation. Moreover, *in vitro* diffusion studies

demonstrated that NTX glycolate (and possibly NTX lactate and acetate) increased aqueous solubility can be translated into elevated transdermal flux through MN-treated skin. That increase, although modest, is of practical importance for maximizing the delivery of NTX species through the MN-enhanced skin.

9.8. Conclusions

The present study evaluated permeation and skin irritation potential of several NTX salts. Three NTX salts (acetate, lactate and glycolate) demonstrated improved aqueous solubility that of NTX•HCl at a relevant skin surface pH of 5.0 over. Increased solubility of NTX glycolate, despite the non-ideal flux behavior, can be used to achieve increased permeation across MN-treated skin. Moreover, the skin irritation-potential of naltrexone glycolate and lactate were found to be not greater than that of NTX•HCl or placebo gel in the guinea pig model. Overall, a new naltrexone glycolate (and possibly lactate) salt appears to be a promising candidate for further testing and inclusion in an *in vivo* transdermal drug delivery system in conjunction with microneedle skin treatment.

Table 9.1. Summary of physicochemical properties of naltrexone salts. $[NH]_s$ is the saturation solubility of the neutral naltrexone species in equilibrium with the solid. $[NH_2^+]_s$ is the saturation solubility of the positive naltrexone species in equilibrium with the solid. pH_{max} is the pH corresponding to maximum salt solubility. MP is experimentally determined melting point.

Naltrexone salt	$[NH]_s$ [1] mean (95% CI)	$[NH_2^+]_s$ [1] mean (95% CI)	pH_{max}	MP [°C]
hydrochloride	1.23 (0.95, 1.51)	221 (210, 232)	6.05	275
acetate	1.23 (0.95, 1.51)	804 (746, 861)	5.48	196
lactate	1.23 (0.95, 1.51)	927 (842, 1011)	5.42	221
glycolate	1.23 (0.95, 1.51)	1125 (885, 1365)	5.34	223
fumarate	1.23 (0.95, 1.51)	n/a	n/a	231
citrate	1.23 (0.95, 1.51)	n/a	n/a	208

[1] The concentration units are [mM]

Figure 9.1.
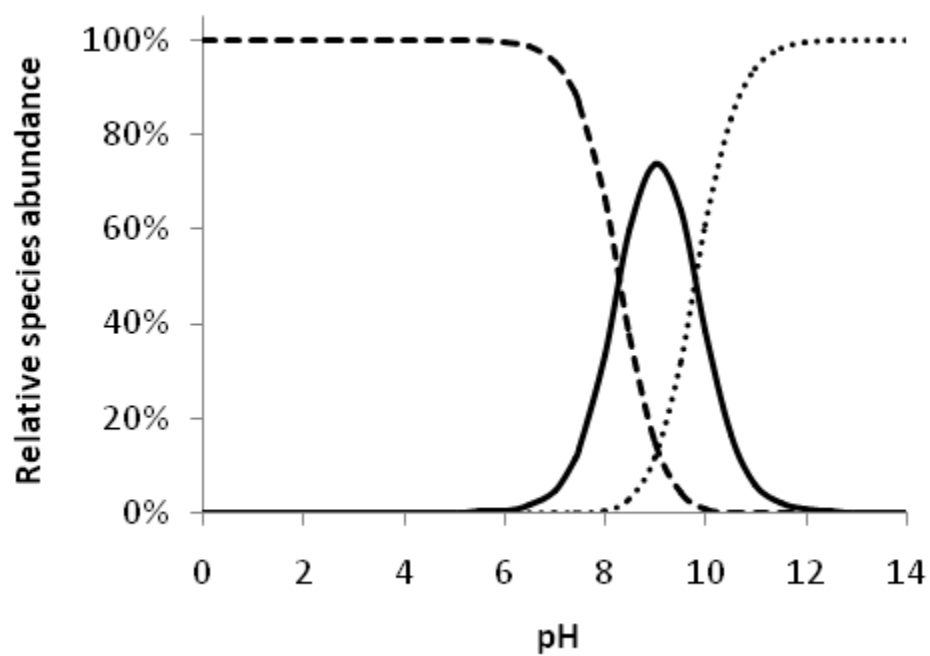
Naltrexone speciation as a function of pH. Dashed line (---) corresponds to positive NTX species [NH_2^+], solid line (—) corresponds to the neutral NTX species [NH], and dotted line (•••) corresponds to the negative naltrexone species [N^-].

Figure 9.2.
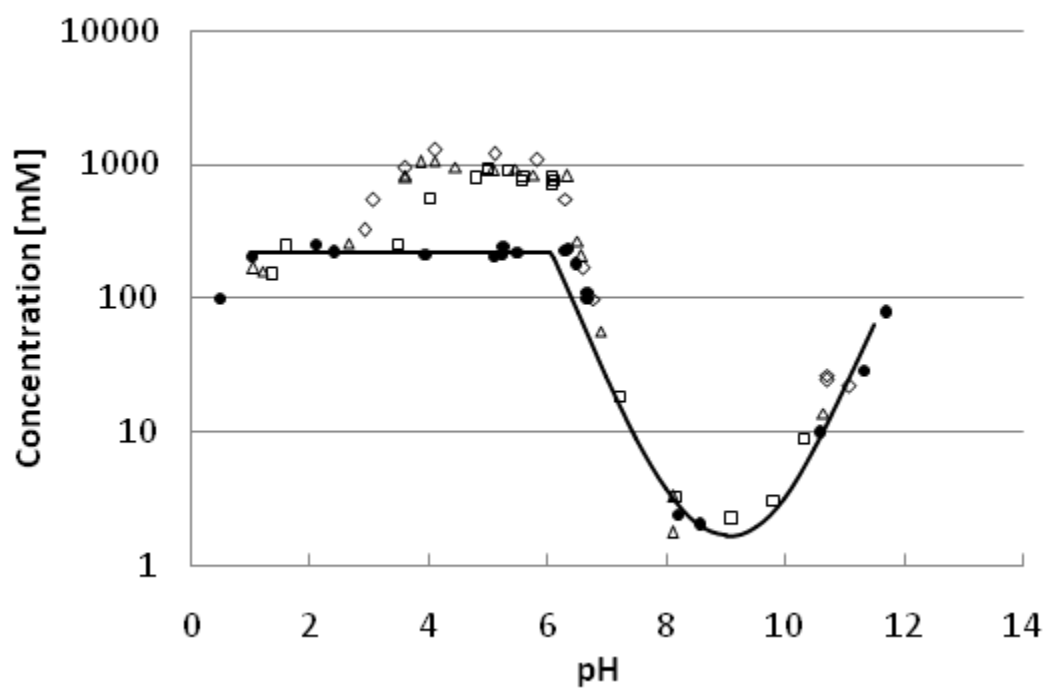
pH-solubility profiles of the hydrochloride (•), acetate (□), lactate (△), and glycolate (◊) naltrexone salts. Solid line represents a least-square fit to Eq. 9.3 and Eq. 9.4 for NTX•HCl.

Figure 9.3.
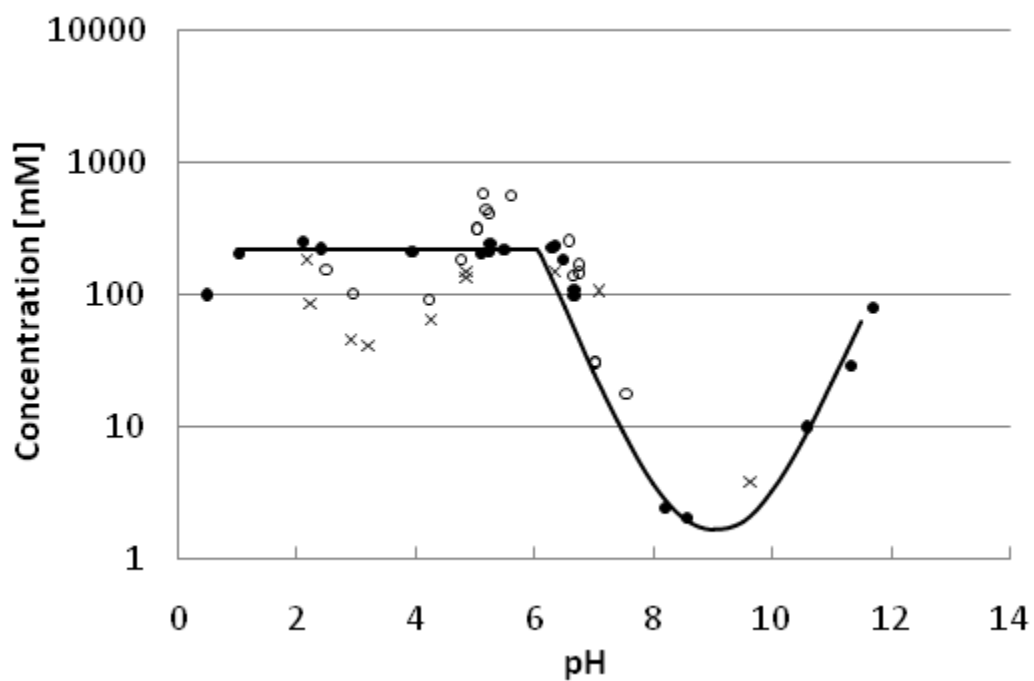
pH-solubility profiles of the hydrochloride (●), fumarate (x), and citrate (○) naltrexone salts. Solid line represents a least-square fit to Eq. 9.3 and Eq. 9.4 for NTX•HCl.

Figure 9.4.
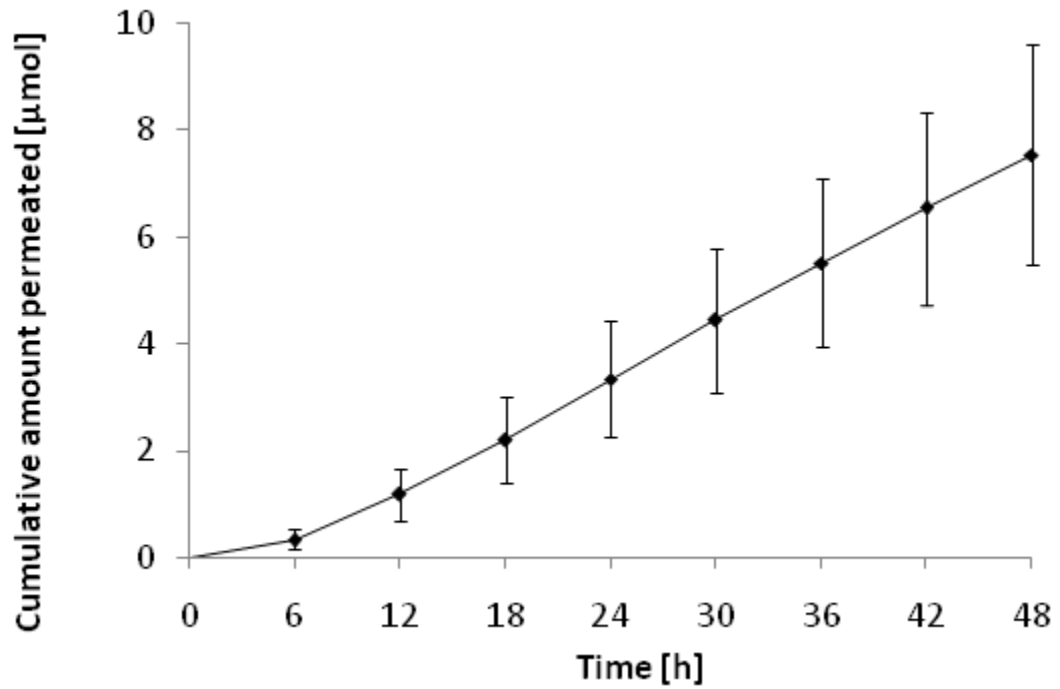
Representative *in vitro* permeation profile of naltrexone glycolate through MN-treated Yucatan minipig skin. The cumulative drug amount is plotted against time. Each point represents the mean ± SD (n=4).

Figure 9.5.
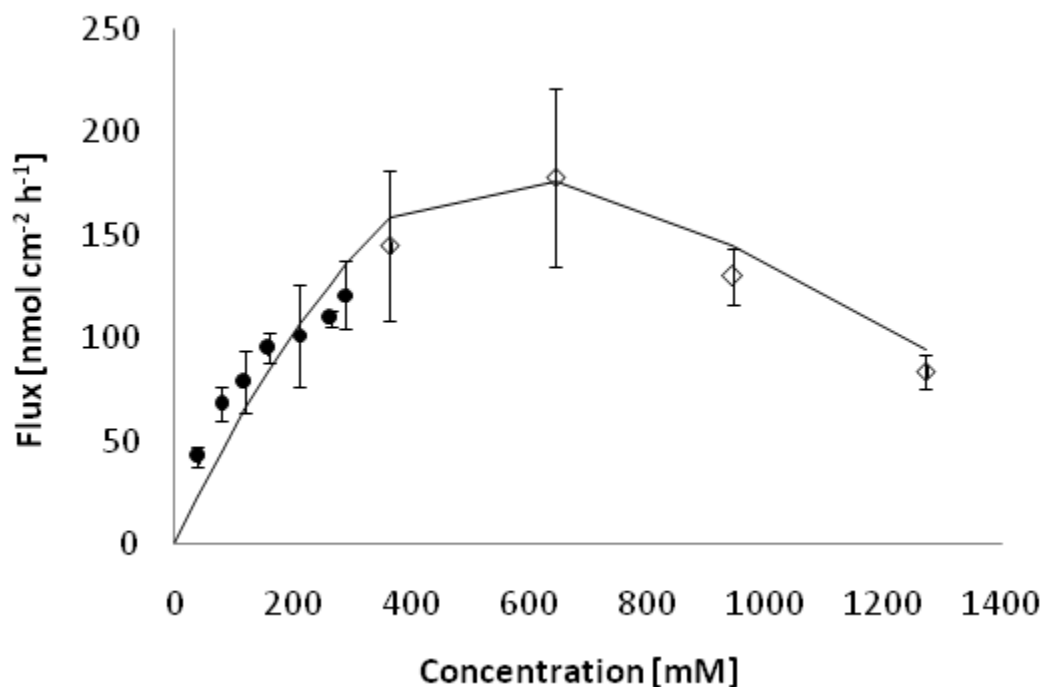
Comparison of the experimental flux of naltrexone hydrochloride (●) and naltrexone glycolate (◊) through MN-treated Yucatan minipig skin to the flux calculated according to the Eq. 9.10. Points indicate experimentally measured mean flux values ± SD (n = 3-4) and the solid line denotes the calculated mean flux value according to Eq. 10.9.

Figure 9.6.
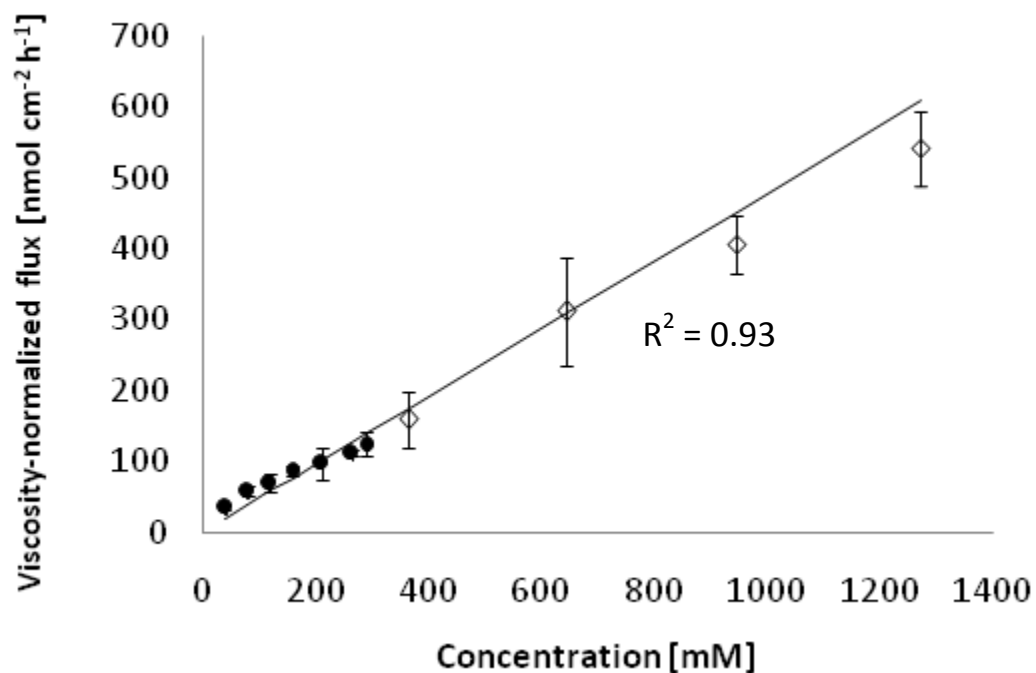
Flux of naltrexone hydrochloride (●) and naltrexone glycolate (◊) normalized per viscosity of the donor solution according to Eq. 9.9. Points indicate calculated viscosity-normalized flux values and solid line represent the $1/Y^2$ weighted least-square fit to a linear equation with zero Y-intercept. Each point represents the mean ± SD (n = 3-4).

Figure 9.7.
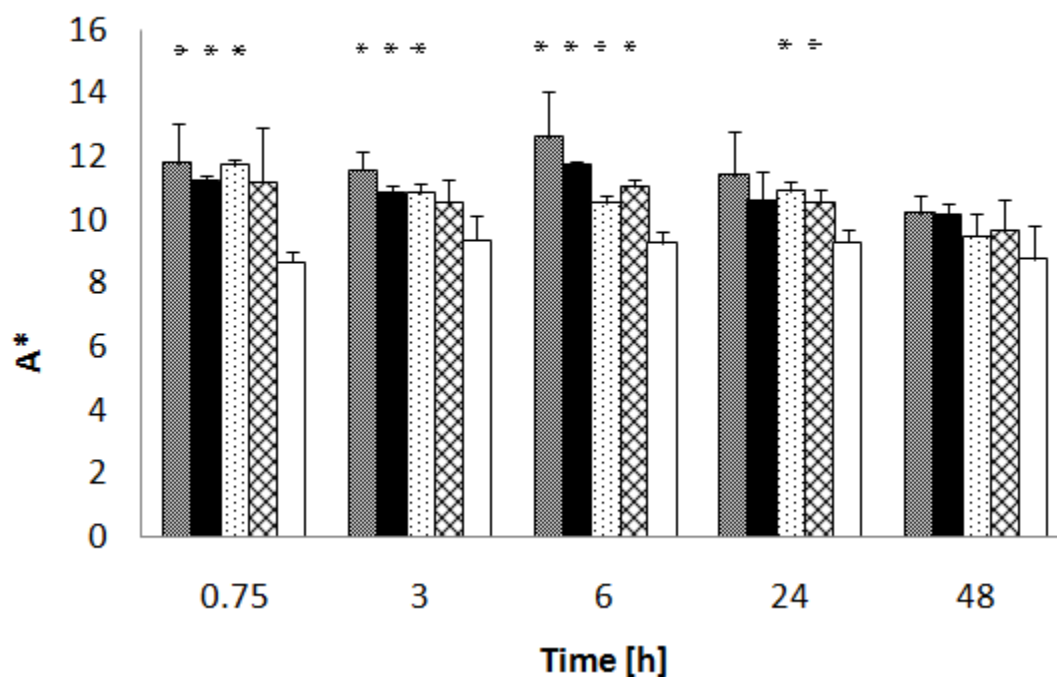
In vivo skin redness, reported as a* value, in guinea pigs after application of the following treatments: placebo gel (gray filling), NTX•HCl gel (black filling), NTX lactate gel (dotted filling), NTX glycolate gel (checked filling), and control (white filling). All results are mean ± SD (n = 3). Of note, readings indicate the time after removal of the treatments. * denotes statistically significant difference (p < 0.05) between the mean control reading as compared to individual treatment mean.

Figure 9.8.
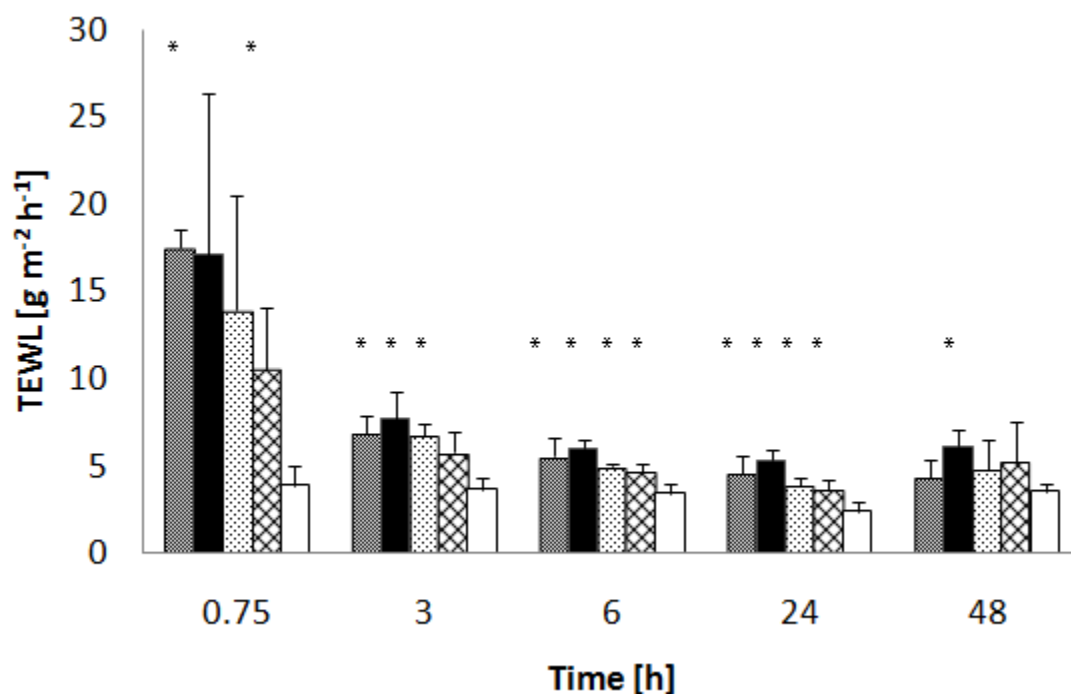
In vivo transepidermal water loss in guinea pigs after application of the following treatments: placebo gel (gray filling), NTC HCl gel (black filling), NTX lactate gel (dotted filling), NTX glycolate gel (checked filling), and control (white filling). All results are mean ± SD (n=3). Of note, readings indicate the time after removal of the treatments. * denotes statistically significant difference (p < 0.05) between the mean control reading as compared to individual treatment mean.

Chapter 10

In vivo MN-assisted permeation and pharmacokinetics of naltrexone

hydrochloride in Yucatan minipig

10.1. Introduction

The purpose of this chapter is to fulfill the **research goals** specified under points **3.5** and **3.6**. All the studies reported so far in previous chapters related to *in vitro* drug delivery with special emphasis on maximization of NTX flux across MN-treated skin. The key question the present chapter attempts to address is: "how can the knowledge obtained so far be used to predict *in vivo* drug delivery with a 'poke and patch method'"? Besides all the topics covered earlier, *in vivo* drug delivery requires the discussion of at least a few additional subjects: microchannel closure and its effect on drug transport, drug disposition in the body and elimination from the body. Only the simultaneous consideration of all the above factors can provide some insight into the behavior of plasma concentration profiles of NTX *in vivo* after MN-assisted transdermal delivery.

There is an abundance of publications related to drug delivery through MN-enhanced skin *in vitro* [6, 24, 213, 217, 229, 255, 261-263]. The number of literature reports on the *in vivo* drug delivery with a "poke and patch" method is limited. A few examples include naltrexol base and hydrochloride delivery in hairless guinea pigs [155], naltrexone hydrochloride delivery in hairless guinea pigs [264], naltrexone hydrochloride delivery in humans [216], ketoprofen delivery in rats [265], and nicardipine hydrochloride delivery in hairless rats [212]. The outcomes of the above studies showed differences in effectiveness of MN skin treatment, and shapes of drug plasma profiles, depending on specific experimental conditions. Additionally, the microchannel closure process was the

topic of several literature reports [23, 155, 211, 266, 267]. The conclusions with respect to the timeframe of microchannel closure varied according to experimental conditions and methods used for making the assessment. However, there is no study that incorporated the concepts of MN-enhanced transdermal drug transport, the microchannel closure process, drug disposition, and elimination *in vivo* in a quantitative manner. In the present study, the delivery of naltrexone hydrochloride in Yucatan minipig using a "poke and patch" method, and the disposition and elimination after IV bolus administration are investigated. The purpose of this work is to develop a mathematical model for description of drug transport across MN-treated skin *in vivo,* and to establish an *in vitro-in vivo* correlation. Previous studies provided some insight into MN-enhanced percutaneous *in vitro* NTX transport [39], which will be used and expanded upon to accommodate the rate of microchannel closure, drug disposition and elimination *in vivo*.

10.2. Materials and methods

Chemicals

NTX hydrochloride was purchased from Mallinckrodt (St. Louis, MO, USA). Water was purified using NANOpure Diamond^{TM}, Barnstead water filtration system. 1,2-Propanediol, Hanks' balanced salts modified powder, and sodium bicarbonate were purchased from Sigma (St. Louis, MO). 4-(2-Hydroxyethyl)-1-piperazineethanesulfonic acid (HEPES), gentamicin sulfate, trifluroacetic acid (TFA), triethylamine (TEA), 1-heptane sulfonic acid sodium salt, and acetonitrile (ACN) were obtained from Fisher Scientific (Fairlawn, NJ). Reagent-grade chemicals were obtained from Sigma Chemical Company (St. Louis, MO).

In vitro diffusion study – estimation of naltrexone diffusivity in dermis

NTX•HCl was added to water to obtain the concentration of 110 mg/ml. The solutions were placed in glass vials, closed tightly with a plastic cap, sonicated for 15 min and left in the shaking water bath at 32°C overnight before use to ensure all the drug is dissolved.

Full-thickness Yucatan minipig skin was harvested from the dorsal region of a euthanized 6-month-old animal. Animal studies were approved by the University of Kentucky IACUC. Subcutaneous fat from skin samples was removed with a scalpel and sparse hair shaved. Such skin samples were immediately placed in a plastic bag and frozen (-20°C) until use. Before each permeation study, skin samples were allowed to thaw for about 30 min. Skin was dermatomed by removing whole epidermis and varying thickness of dermis so that a range of dermis thicknesses were obtained from 0.8 – 2.2 mm. Dermis thickness was evaluated with calipers. A PermeGear flow-through (In-Line, Riegelsville, PA) diffusion cell system was used for the *in vitro* diffusion studies. Isotonic HEPES-buffered Hanks' balanced salts solution (pH 7.4) was used as the receiver solution. The flow rate of the receiver fluid was set at 1.5 ml/h to maintain sink conditions. Skin samples in the diffusion cells were kept at 32°C using a circulating water bath. The diffusion experiments were initiated by charging the donor compartment with 0.7 ml of the donor solution. Samples were collected from the receiver compartment in 6 h increments over 48 h. All samples were stored at 4 °C until processed by HPLC. The permeation data were plotted as the cumulative amount of NTX•HCl collected in the receiver compartment as a function of time. Fourteen diffusions cells were employed (n = 14).

IV bolus injection preparation

NTX•HCl was dissolved in sterile saline to obtain a drug concentration of 40 mg/ml. Solution for IV injection was filtered through a sterile 0.22 μm filter into a sterile scintillation vial under a laminar biosafety hood. Syringes were prefilled to deliver a desired dose: 1 mg/kg, 9 mg/kg or 10 mg/kg.

Transdermal patch preparation

Commercially available AquaSite® (Derma Sciences, Princeton, NJ) hydrogel sheets were cut into circular discs, 4 cm in diameter. Next, a solution of benzyl alcohol 1%, ethanol 5%, propylene glycol 10% and water for injection 84% (v/v) was prepared and NTX•HCl was dissolved to obtain a concentration of 110 mg/ml. A four-fold excess of NTX•HCl solution, with respect to the weight of the hydrogel, was equilibrated with the discs for 48 h. The equilibrium NTX•HCl concentration in the hydrogel discs was determined by HPLC to be 90 mg/g. Next, the transdermal formulation was autoclaved at high pressure saturated steam at 121°C for 15 min (verified for chemical stability by HPLC). Sterile and drug-loaded hydrogel discs were applied on the MN-treated skin areas and covered with protective patches to prevent dislocation throughout the duration of the experiment. The protective patches (4 cm internal diameter) were prepared by sandwiching a rubber ring to create a reservoir between a drug-impermeable backing membrane and an adhesive around the edge of a rubber spacer. After application to Yucatan minipig back treatment sites patches were further secured in place by applying Bioclusive® tape over prototype patches.

Animal Studies

Male and female Yucatan minipigs (Sinclair Bio-Resources; Columbia, MO) weighing approximately 40 kg were used for *in vivo* studies. These animals underwent surgical procedure at Sinclair Bio-Resources to cannulate the jugular veins and implant Vascular Access Ports (VAPs) (Access Technologies; Skokie, IL). All animal studies were in accordance with institutional guidelines approved by the University of Kentucky IACUC.

IV bolus injections: NTX•HCl bolus was administered via VAP through a controlled infusion over 3.5-5 min. Three independent experiments (n=3) were carried out with three different NTX•HCl doses of 1 mg/kg, 9 mg/kg or 10 mg/kg. Blood samples were collected prior to drug treatment (baseline). After dosing, VAP was flushed with sterile heparinized saline. Blood samples (2 ml) were drawn from VAP at scheduled time intervals for 55 h after the intravenous dose. The blood samples were immediately centrifuged at 10 000 g for 3 min; plasma was separated and stored at -70 °C until analyzed.

Transdermal studies: For transdermal delivery studies, 4 sites were designated on the dorsal region of Yucatan miniature pig and treated with MN (400 each). NTX•HCl hydrogels were applied to the sites and covered with patches and Bioclusive® transparent dressing. A jacket was placed on the pig to protect the patches. Three independent experiments (n=3) were carried out. Blood samples were collected prior to drug treatment (baseline). After application of patches, blood samples were obtained over 72 h followed by patch removal and blood sampling for another 24 h. The blood samples were immediately centrifuged at 10 000 g for 3 min. Plasma was separated and stored at -70 °C until analyzed.

Quantitative analysis - HPLC

Quantitative analysis of NTX•HCl concentrations from *in vitro* study was carried out by HPLC using a modification of the assay described by Hussain et al. [225]. The HPLC system consisted of a Waters 717 plus autosampler, a Waters 600 quaternary pump, and a Waters 2487 dual wavelength absorbance detector with Waters Empower™ software. A Brownlee (Wellesley, MA, USA) C-8 reversed phase Spheri-5 µm column (220×4.6 mm) with a C-8 reversed phase guard column of the same type (15×3.2 mm) by Perkin Elmer® was used with the UV detector set at a wavelength of 215 nm or 278 nm. The mobile phase consisted of 70:30 (v/v) ACN:(0.1% TFA with 0.065% 1-octane sulfonic acid sodium salt, adjusted to pH 3.0 with TEA aqueous phase). Samples were run at a flow rate of 1.5 ml/min with a run time of 4 min. The injection volume used was 100 µl. The retention time of NTX•HCl was 2.1 ± 0.1 min. Samples were analyzed within a linear range of the NTX•HCl standard curve from 100 – 10000ng/ml. The standard solutions exhibited excellent linearity over the entire concentration range employed in the assays.

Quantitative analysis – LC-MS-MS

Plasma samples obtained from *in vivo* Yucatan minipig studies were quantified by a LC-MS-MS method.

Calibration standards: Stock solutions of naltrexone hydrochloride (NTX•HCl) and 6-ß-naltrexol hydrochloride (NTXol•HCl) in acetonitrile were prepared at 100 ng/ml concentration. Working solutions were prepared by serial dilution of the stock solutions. Calibration standards of NTX•HCl and NTXol•HCl at concentrations 1, 2, 3, 5, and 10 ng/ml in Yucatan minipig plasma were prepared fresh daily by spiking Yucatan pig

plasma with 20 µl of NTX•HCl and NTXol•HCl working solutions at adequate concentrations.

Sample extraction procedure: All standards and samples of volume 200 µl were extracted with 1ml of acetonitrile:ethyl acetate (1:1, v/v), resulting in protein precipitation. The mixture was vortexed for 15 s and centrifuged at 12000 g for 20 min. The supernatant was transferred to a glass tube and evaporated under nitrogen. Then, the residue was reconstituted in 100 µl acetonitrile, sonicated for 10 min and vortexed for 15 s. Samples were transferred into low volume inserts into HPLC vials and injected onto the LC-MS/MS system.

LC-MS-MS conditions: Waters Atlantis Hilic Silica 5 µm, 2.1x150 was used as the chromatographic column with a mobile phase consisting of methanol with 0.1% acetic acid:buffer 95:05 (v/v). The aqueous buffer consisted of 20 mM ammonium acetate and 5% methanol. The injection volume was 40 µl. Liquid chromatography was carried out in the isocratic mode at the flow rate of 0.5 ml/min with a total run time of 4 min. The retention times for NTX•HCl and NTXol•HCl were as follows: 2.2 and 2.1 min, respectively. The LC-MS/MS system consisted of a HPLC Waters Alliance 2695 Separations Module, Waters Micromass® Quattro Micro™ API Tandem Mass Spectrometer and Masslynx Chromatography software with Waters Quanlynx (V. 4.1) analysis software. Positive mode atmospheric pressure chemical ionization was used for detection of both compounds (APCI+). Multiple reaction monitoring (MRM) was carried out with the following parent to daughter ion transitions for NTX•HCl and NTXol•HCl: m/z 341.8→323.8, m/z 343.8→325.8, respectively. The corona voltage was 3.5 µA, cone voltage 25 V, extractor 2 V, RF lens 0.3 V, source temp 130 °C, APCI probe temperature 575 °C. The collision gas was 20 eV. Nitrogen gas was used as a nebulization and drying gas at flow rates of 50 and 350 l/h, respectively. Calibration plots were prepared

by the linear regression analysis of the standard peak areas versus nominal drug concentration.

Lower quantification limits (LLOQ): based on the coefficient of variation (CV) < 20 % criterion the following limits of quantification were estimated: NTX•HCl 0.5 ng/ml, NTXol•HCl 0.5 ng/ml.

Statistical analysis

The statistical analysis of data (95% confidence intervals determination) was carried out with the use of Scientist$^®$ software (Micromath).

10.3. Model development

The aim of this work was to develop a mathematical model that would adequately describe *in vivo* NTX•HCl plasma profile after a "poke and patch" method application. This was approached through the use of a combined diffusion-compartmental model. The critical elements incorporated into the model are as follows: recognition of two parallel pathways for drug permeation after MN skin treatment (intact skin pathway and microchannel pathway), the barrier thickness-dependant diffusional resistance of microchannel pathway, direct relationship between electrical admittance of the microchannels and their permeability to drugs, and pharmacokinetic compartmental module for description of drug disposition and elimination from the body. The schematic diagram of the model is shown in **Figure 10.1**, and can be divided into 3 modules:

Module 1 – Skin diffusion

One-dimensional diffusion model accounts for diffusion of drug molecules from a formulation across skin to a certain hypothetical skin depth where an absolute clearance exists (sink conditions). The drug concentration on surface of the skin is assumed to remain constant at all times. This is typically true for skin controlled-diffusion where flux is not sufficiently high to deplete drug from the formulation over study duration. In the present study it was confirmed experimentally by observing no change in NTX•HCl concentration from beginning to the end of the *in vivo* transdermal study (data not shown). For untreated skin only one permeation pathway – intact skin pathway – is recognized. The barrier nature of intact skin pathway is well-approximated by the barrier properties of the mono-layered stratum corneum alone. This was experimentally confirmed *in vitro* by comparing the rate of NTX•HCl permeation through untreated skin against skin devoid of stratum corneum, which resulted in hundreds-fold increase in transport rate (data not shown). After MN-treatment another permeation pathway – microchannel pathway – is formed. The barrier nature of this pathway is bi-layered, the first layer corresponds directly to the microchannel and the second to the viable tissue (dermis) between microchannel and hypothetical skin depth at which an absolute clearance exists (sink conditions). However, since NTX diffusivity in the dermis is much lower, as compared the microchannel interior, it is assumed that all diffusional resistance will come primarily from the viable tissue. Thus, a mono-layered membrane model is used for simplicity. Fractional skin surface area is assigned to each pathway which describes relative contribution of each flux to the total flux through MN-treated skin. At any time the total flux, J_{TOT}, equals:

$$J_{TOT} = f_{ISP}J_{ISP} + f_{MCP}J_{MCP} \tag{10.1}$$

where f_{ISP} is the fractional skin surface area of intact skin pathway, J_{ISP} is the flux through intact skin pathway, f_{MCP} is the fractional skin surface area of microchannel pathway, and J_{MCP} is the flux through microchannel pathway. Assuming homogenous nature of skin layers: stratum corneum and viable tissue, the cumulative amount-time profiles can be derived by solving Fick's second law of diffusion:

$$\frac{\partial C_m}{\partial x} = D_m \frac{\partial C_m}{\partial x^2} \tag{10.2}$$

where C_m is drug concentration in the membrane, D_m is drug diffusion coefficient in the membrane, and x is spatial coordinate. After imposing the following initial conditions:

$$C_m(x, 0) = 0 \tag{10.3}$$

and boundary conditions:

$$C_m(0, t) = C_v \tag{10.4}$$

$$C_m(h_m, t) = 0 \tag{10.5}$$

it was shown [78] that the solution is terms of cumulative amount of drug exiting the membrane is:

$$Q(t) = -D_m A \int_0^t \frac{\partial C_m}{\partial x}\Big|_{x=h_m} dt = A C_v h_m \left[\frac{t}{t_d} - \frac{1}{6} - \frac{2}{\pi^2} \sum_{n=1}^{\infty} \frac{(-1)^n}{n^2} \cdot e^{\left(-\frac{t}{t_d}\pi^2 n^2\right)} \right] \quad (10.6)$$

where the diffusion time, t_d is:

$$t_d = \frac{h_m^2}{D_m} \quad (10.7)$$

Hence, for intact skin pathway (stratum corneum as a membrane) the flux per unit area as a function of time is given by:

$$J_{ISP} = -D_{SC} \left(\frac{dC_{SC}}{dx} \right)_{x=h_{SC}} = \frac{D_{SC}}{h_{SC}} C_v \left[1 + 2 \sum_{n=1}^{\infty} (-1)^n \cdot e^{\left(-\frac{t}{t_d}\pi^2 n^2\right)} \right] \quad (10.8)$$

and for microchannel pathway (dermis as a membrane) the analogous solution is:

$$J_{MCP} = -D_{VT} \left(\frac{dC_{VT}}{dx} \right)_{x=h_{VT}'} = \frac{D_{VT}}{h_{VT}} C_v \left[1 + 2 \sum_{n=1}^{\infty} (-1)^n \cdot e^{\left(-\frac{t}{t_d}\pi^2 n^2\right)} \right] \quad (10.9)$$

213

The above solutions are assumed to adequately describe drug transport through MN-treated skin in *in vitro* conditions. In the *in vivo* case an additional factor that needs to be considered is the microchannel closure process.

Module 2 – Microchannel closure

Upon formation of microchannels in the skin *in vivo,* the tissue repair process initiates. The fundamental assumption of this module about *in vitro* and *in vivo* microchannel pathway permeability is the following*: in vitro* microchannel pathway permeability is a constant and remains high indefinitely, while *in vivo* microchannel pathway permeability decreases as a function of time. Multiple studies demonstrated that after MN treatment of skin *in vitro* the permeability of microchannel pathway remains constant as manifested by achievement and maintenance of steady-state flux [6, 28, 255]. For simplicity, the permeability of the microchannel pathway can be interpreted in terms of the fractional skin surface area of microchannels that remains open. Such treatment is an obvious generalization, as behind the decreasing permeability of the microchannel pathway *in vivo* lays a cascade of biological processes related to wound healing, which ultimately leads to the complete repair of the injured skin [43, 44, 268]. These processes will affect both the drug diffusivity in the microchannel pathway and skin surface opening of microchannels. However, for the sake of drug delivery discussion, it is a compelling simplification. Another crucial assumption is that the skin electrical impedance measurements employed herein to study the time-dependent microchannel closure provide valuable information with respect to NTX•HCl permeability through the microchannel pathway. A report by P. Karande et al. demonstrated that even for non-MN-treated skin, in presence of chemical enhancers, the inverse correlation between

electrical impedance and permeability of hydrophilic solutes was good (R^2 = 0.8) [269]. Authors stated that permeability can be related to skin impedance through the porous pathway theory with the fundamental underlying hypothesis that polar uncharged solutes and ions (carrying current) migrate through the SC via identical pathways. With respect to drug transport through MN-treated skin, G. Yan et al. found a good linear correlation (R^2 = 0.94) between acyclovir flux and skin conductance [263]. This is not surprising since the presence of microchannels in the skin undoubtedly establishes the pathway of least electrical and diffusional resistance. Hence, the electrical impedance measurements can be expected to reliably probe the barrier domain for transport of NTX•HCl across MN-enhanced skin. The inverse of electrical impedance is electrical admittance, which is assumed herein to be directly proportional to permeability of the microchannel pathway. Hence, the equation that can adequately describe the total flux in *in vivo* situation is as follows:

$$J_{TOT,C} = f_{ISP}J_{ISP} + f_{OMF}f_{MCP}J_{MCP} \tag{10.10}$$

where $J_{TOT,C}$ is total flux corrected for microchannel closure, f_{OMF} stands for open microchannel surface area fraction, or more precisely for fraction of initial permeability of the microchannel pathway. It was found experimentally that the decrease in the admittance of the microchannel pathway follows an apparent exponential decrease in time (unpoulished human results by Nicole Brogden). The apparent first-order rate constant, k_Y, obtained from *in vivo* electrical impedance measurements was used directly as an estimate of k_{OMF} to describe the drop in time-dependant permeability of the microchannel pathway:

215

$$f_{OMF} = f_{OMF}^0 e^{-k_{OMF} t}$$

<div align="right">(10.11)</div>

where f_{OMF}^0 numerically equals the value of unity and corresponds to the initial open microchannel surface area fraction, or more precisely the initial permeability of the microchannel pathway obtained immediately after skin MN treatment. Implicitly it is assumed that in *in vitro* situation f_{OMF}^0 holds the value of unity and **Eq. 10.10** collapses to **Eq. 10.1**. Of note, in the strict sense the microchannel healing process causes time-dependant drop in the microchannel skin surface area which is accompanied by the same area increase in the intact skin around the microchannels. However, since f_{MCP} is typically very small (e.g. 0.025) as compared to f_{ISP} (e.g. 0.975), the time-dependant increase in f_{ISP} is minute and ignored in **Eq. 10.10**, as shown by lack of a time-dependant term in front of the $f_{ISP} \cdot J_{ISP}$ term. This simplification reduces the calculation work and does not negatively affect the results. Once drug has crossed viable skin tissue and reaches local microvasculature it is swept away by blood flow to find itself in the central pharmacokinetic compartment.

Module 3 – pharmacokinetic compartments

Through viable tissue drug is absorbed into systemic circulation, or central pharmacokinetic compartment. The experimental data reported herein demonstrated an apparent 3-exponential decrease in NTX•HCl concentration as a function of time after a bolus IV administration. In consequence, a 3-compartment mammillary model was chosen to describe NTX•HCl distribution and elimination from the body. The differential

equations that describe drug delivery to the central compartment, its distribution and elimination are as follows:

$$\frac{dC_1}{dt} = \frac{A \cdot J_{TOT,C}}{V_d} + \frac{k_{21}X_2}{V_d} + \frac{k_{31}X_3}{V_d} - k_{12}C_1 - k_{13}C_1 - k_{10}C_1 \qquad (10.12)$$

$$\frac{dX_2}{dt} = k_{12}C_1V_d - k_{21}X_2 \qquad (10.13)$$

$$\frac{dX_3}{dt} = k_{13}C_1V_d - k_{31}X_2 \qquad (10.14)$$

where A is the total skin area of hydrogel application, V_d is the initial volume of distribution; k_{12}, k_{13}, k_{21}, k_{31} are micro rate constants describing drug transport between central (#1) and peripheral (#2 and #3) compartments; and k_{10} is the elimination constant. The drug plasma concentration (central compartment) is a single major variable of interest.

10.4. Method of solution

Scientist® software (Micromath, Saint Louis, MO) was used to numerically solve model equations (**Eq. 10.8 - 10.14**) transformed into LaPlace domain. The inverse transformation was performed by software using Piessens and Weeks algorithms. Scientist® initially uses fast Weeks algorithm; however, in situation when this method is not applicable it automatically detects it and employs to a slower but more reliable Piessens algorithm. The accuracy of numerical solutions obtained from equations written in LaPlace domain was compared with those written in time domain for a case where

diffusion equations describing drug transport through MN-treated skin were replaced with true zero-order delivery. The agreement between two methods was excellent.

10.5. Parameter estimation

Estimation of naltrexone diffusion coefficient in water

The estimate of the NTX diffusion coefficient in water was obtained by the use of Stokes-Einstein equation:

$$D = \frac{kT}{6\pi\eta r} \qquad (10.15)$$

where k is the Boltzmann constant, T is the absolute temperature, η is the viscosity and r is the hydrodynamic radius of the solute. Using experimentally determined viscosity value of 1.03 cP determined at 32 °C [39] and assuming the hydrodynamic molecular radius of 4.6 Å [227] a diffusion coefficient value of $4.7 \cdot 10^{-6}$ cm^2 s^{-1} was calculated. This value is assumed to approximate well the diffusivity of naltrexone in microchannels filled with interstitial fluid. It has been formerly shown by McAllister et al. that MN-enhanced transdermal flux values for a variety of compounds of different sizes correlated well with prediction based on the Stokes-Einstein eq. [27]. It suggests that diffusivity of drug molecules in the microchannels resembles that seen in the bulk solution.

Estimation of naltrexone diffusion coefficient in the dermis

For the purpose of experimental assessment of drug diffusivity in the dermis, a study involving NTX•HCl permeation across skin devoid of epidermis was carried out. **Figure 10.2** demonstrates a representative graph of cumulative amount of naltrexone HCl plotted against time. As evident from the plot, the flux is very high, which caused depletion of drug in the donor solution. At the end of the 48 h study, experimentally measured NTX•HCl concentration in the donor solution dropped, on average, by 50 ± 18 %. Due to this fact, the plot lacks late steady-state portion and flux was estimated not from the terminal, but rather, early graph section. The slope of the plot in 6-12 h timeframe better approximates stead-state flux, in this case, as it allows for lag time but minimizes the effect of drug depletion in the donor solution. Flux values obtained by this method were plotted against the thickness of the dermis employed in the diffusion study. **Figure 10.3** summarizes data from all 14 cells. A clear trend is visible with thicker dermis corresponding to higher diffusional resistance of the barrier and decreased flux. The reciprocal relationship between flux and the thickness of the barrier (dermis) can be described by **Eq. 10.16**:

$$J = \frac{C}{\frac{h_{VT}}{D_{VT}}}$$
(10.16)

where J is steady-state flux, C is donor solution concentration of NTX•HCl, h_{VT} is thickness of the dermis (viable tissue) and D_{VT} is diffusion coefficient of NTX in the dermis. Since the values of all the above terms are known with exception of the NTX diffusion coefficient in dermis, it can be estimated by non-linear regression of flux on

dermis thickness by means of **Eq. 10.16**. The mean estimated value was found to be 3.46 10^{-7} cm^2 s^{-1}, 95 % confidence interval of (3.28 10^{-7}, 3.65 10^{-7}). This value is approximately 14-fold lower than the diffusion coefficient of NTX in water estimated in the former paragraph.

Estimation of effective microchannel diameter

Effective microchannel diameter was estimated from *in vitro* diffusion data. Former studies employed *in vitro* diffusion set-up consisting of 0.95 cm^2 of 1.8 mm-thick Yucatan minipig skin possessing 100 microchannels and donor solution of NTX•HCl in water at 110 mg/ml. The length of the microchannels in the skin was assessed to be approximately 650 μm (unpublished data). The steady-state flux through microchannel pathway alone ($J_{MCP-EXP}$) was measured to be 76.8 ± 11.7 nmol h^{-1} [39]. By comparison of this experimental flux value ($J_{MCP-EXP}$) to the calculated flux value ($J_{MCP-CAL}$), which corresponds to the same experimental conditions but with fractional skin surface area of microchannel pathway of unity ($f_{MCP-CAL} = 1$), the estimate of the effective microchannel pathway skin fractional surface area ($f_{MCP-EXP}$) can be obtained. The value of $J_{MCP-CAL}$ was estimated by use of the following parameter values: $D_{MC} = 4.70$ 10^{-6} cm^2 s^{-1}, $h_{MC} = 0.65$ mm, $D_{VT} = 3.46$ 10^{-7} cm^2 s^{-1}, $h_{VT'} = 0.115$ mm, $C = 290$ mM, and $f_{MCP-CAL} = 1$ according to **Eq. 10.17**:

$$J_{MCP-CAL} = f_{MCP-CAL} \frac{C}{\frac{h_{MC}}{D_{MC}} + \frac{h_{VT'}}{D_{VT}}} \qquad (10.17)$$

where $f_{MCP-CAL}$ is the microchannel pathway skin fractional surface area, C is NTX•HCl donor solution concentration, D_{MC} is NTX diffusivity in microchannels approximated by NTX diffusivity in water, h_{MC} is thickness of the microchannel layer, D_{VT} is NTX diffusivity in the dermis, and $h_{VT'}$ is the thickness of the underlying dermis layer. Numerically, $J_{MCP-CAL}$ was found to equal 3017 nmol cm^{-2} h^{-1}.

On the other hand, the $J_{MCP-EXP}$ of 76.8 nmol cm^{-2} h^{-1} corresponds to the following **Eq. 10.18**:

$$J_{MCP-EXP} = f_{MCP-EXP} \frac{C}{\frac{h_{MC}}{D_{MC}} + \frac{h_{VT'}}{D_{VT}}} \tag{10.18}$$

where $f_{MPC-EXP}$ is unknown. Since the numerical value of the ratio of drug donor solution concentration to the total microchannel pathway resistance is the same in **Eq. 10.17** and **Eq. 10.18**, the solution for $J_{MCP-EXP}$ can be simplified to **Eq. 10.19**:

$$f_{MCP-EXP} = \frac{J_{MCP-CAL} \cdot f_{MCP-EXP}}{J_{MCP-CAL}} \tag{10.19}$$

which yields the $f_{MCP-EXP}$ value of 0.025 or 2.5 %. This fractional skin surface area translates into an effective microchannel opening diameter of 176 µm. Noteworthy, this effective opening diameter is larger than the actual skin surface opening of the microchannel that is around 50-100 µm wide [270]. The likely reason for this difference is the inclusion of lateral diffusion within the "effective" microchannel diameter. While all the

equations presented herein are one-dimensional, in reality lateral diffusion will contribute to the overall flux, and it can be expected that "actual" microchannel diameter will not suffice to account for the flux obtained through microchannel pathway. Therefore, it will be the effective microchannel diameter that will be used for further calculations.

Estimation of microchannel pathway fractional skin area *in vivo*

The *in vivo* Yucatan minipig transdermal experiment involved application of 4 patches. Each patch had a diameter of 4 cm and covered 400 microchannels. Therefore, the total skin surface area involved in diffusion was 50.24 cm^2 and skin surface area of all microchannel openings was 0.39 cm^2, which gives the microchannel pathway fractional skin area f_{MCP} = 0.0077 or 0.77 % *in vivo*.

Estimation of the microchannel closure rate *in vivo*

The electrical impedance was used to evaluate the permeability of microchannel pathway *in vivo*. Skin impedance in the context of this study is understood as electrical resistance measured in presence of an AC signal. It measures the difficulty of electrical current (ionic) transport across skin. In the current experimental set-up, after MN treatment, three parallel and independent pathways for electric current transport can be distinguished: resistor box, skin around the microchannels and microchannels themselves. Alternatively, in the absence of microchannels in the skin, only two parallel pathways are available: resistor box and untreated skin. The latter case represents either a situation before MN treatment or a situation when microchannels are fully closed/healed after MN treatment. The resistor box and skin, with or without

microchannels, are truly unrelated pathways. However, in the strict sense, microchannels and skin are not since upon MN treatment microchannels take over a minute skin surface area. Practically, the drop in the intact skin surface area is negligible as a result of microchannel formation and the fractional area of skin before and after MN treatment remains close to unity $f_{MCP} \approx 1$. Based on earlier *in vitro* effective microchannel diameter estimates (167 µm), density of MN treatment (100/cm^2), and electrode surface area (0.95 cm^2) the fraction of microchannel pathway skin surface area f_{MCP} in *in vivo* microchannel closure studies also equals 2.5 %. Of note, the intact skin impedance value corrected for f_{MCP} establishes the upper limit for microchannel pathway. In other words, when the microchannel closure process is complete the microchannel pathway impedance values come back to the value corresponding to the intact skin. Overall, experimental electrical impedance measurements after skin MN-treatment provide a total impedance value Z_{TOT} that is a function of Z_{RB} (resistor box), Z_{ISP} (intact skin pathway) and Z_{MCP} (microchannel pathway) according to **Eq. 10.20**:

$$Z_{tot} = \frac{1}{\frac{1}{Z_{RB}} + \frac{1}{Z_{ISP}} + \frac{0.025}{Z_{MCP}}} \tag{10.20}$$

where the implicit assumption about a negligible drop in f_{ISP} as a result of MN-treatment is built in. In the absence of MN-treatment the total electrical impedance equals:

$$Z_{tot} = \frac{1}{\frac{1}{Z_{RB}} + \frac{1}{Z_{ISP}}} \tag{10.21}$$

Since Z_{TOT} and Z_{RB} are known, and Z_{ISP} can be independently estimated from an experiment employing untreated skin under occlusion, the electrical impedance of the microchannel pathway can be calculated. This approach allows elimination of the confounding variables, such as the influence of the resistor box settings and the hydration state of the skin. Moreover, to evaluate microchannel closure kinetics it is more intuitive to use inverse of the electrical impedance (Z), the electrical admittance (Y), which directly correlates with permeability or fractional skin surface area of open microchannels. The interpretation of electrical admittance values resembles another popular method – transepidermal water loss (TEWL) in the sense that high values signify compromise in the barrier integrity, while low, baseline values are typical under normal physiological conditions. Since no impedance microchannel closure data is available for Yucatan minipig at present, human impedance microchannel closure data (collected by Nicole Brogden, unpublished), were used instead. It is believed that human impedance microchannel closure data will provide an acceptable surrogate for its Yucatan minipig counterpart. The time-dependent changes of the microchannel pathway admittance values (normalized per initial admittance values obtained after microneedle treatment and after subtraction of baseline intact skin pathway value) followed an apparent exponential decrease. The subtraction of baseline intact skin pathway value from microchannel pathway admittance is necessary to assure that at long times the signal drops to zero as required by **Eq. 10.22.** To estimate the rate of microchannel closure the data was logarithmically transformed to obtain the apparent first-order microchannel closure rate constants (k_Y's) according to the following empirical model:

$$Y_{MCP} = Y_{MCP}^0 \cdot e^{-k_Y t} \tag{10.22}$$

where Y^0_{MCP} stands for the initial microchannel pathway admittance after microneedle treatment. The average estimate for k_Y obtained from human studies (data collected by Nicole Brogden, unpublished, n = 9) equaled 0.041 h^{-1}, corresponding to $t_{1/2}$ of 17 h, and was adopted as a surrogate k_Y value for Yucatan minipigs.

Adjustment of naltrexone diffusivity per formulation microviscosity

In **Chapter 7** the influence of propylene glycol on the MN-assisted NTX•HCl flux was discussed. It was demonstrated that the inclusion of PG in the aqueous donor solution caused a marked decrease in the transport rates *in vitro*. Hence, NTX diffusivity values corrected for the presence of 10 % propylene glycol in the formulation used in the current *in vivo* study are the following: $D_{MC} = 3.34 \ 10^{-6}$ cm s^{-1} and $D_{VT} = 2.46 \ 10^{-7}$ cm s^{-1}.

Estimation of naltrexone pharmacokinetic parameters

In order to assess parameter values related to NTX•HCl distribution and elimination from the body, IV bolus drug administration was carried out. The plasma levels of NTX•HCl in Yucatan minipig was observed to follow an apparent three-exponential decrease and can be adequately described by a three-compartmental model as shown in **Figure 10.4**. To obtain the pharmacokinetic parameter values the experimental data from three independent experiments with the following doses 1 mg/kg, 10 mg/kg, and 9 mg/kg were fitted simultaneously to the following differential equations:

$$\frac{dC_1}{dt} = \frac{k_{21}X_2}{V_d} + \frac{k_{31}X_3}{V_d} - k_{12}C_1 - k_{13}C_1 - k_{10}C_1 \qquad (10.23)$$

$$\frac{dX_2}{dt} = k_{12}C_1V_d - k_{21}X_2 \qquad (10.24)$$

$$\frac{dX_3}{dt} = k_{13}C_1V_d - k_{31}X_2 \qquad (10.25)$$

where at time zero the initial drug concentration in the central compartment (C_1) was calculated as dose/V_d. Such analysis resulted in parameter values summarized in **Table 1**. Given the preliminary nature of the IV bolus studies and limited number of repetitions the estimate values are to be taken with caution. Further studies will provide more certainty in the estimated parameter values. Systemic clearance of NTX•HCl defined as k_{10}•V_d equals 1.9 l min^{-1} or 47 ml min^{-1} kg^{-1}. Hence, weight-normalized systemic NTX•HCl clearance value is practically equivalent to its human counterpart of around 50 ml min^{-1} kg^{-1}.

10.6. Microneedle-enhanced naltrexone delivery in Yucatan minipig

Experimental data demonstrating NTX•HCl plasma levels in Yucatan minipig after a "poke and patch" method use are shown in **Figure 10.5.** No steady-state NTX•HCl plasma level is observed. Initially, the drug concentration increases quickly to reach C_{max} of approximately 2.5 ng/ml at 4 h. A sharp drop in the drug plasma level follows and within approximately 24 h NTX•HCl concentration becomes only half of C_{max}. Finally, at late 48-72 h timeframe the level seems to plateau at 0.6 ng/ml. After removal of the transdermal patches at 72 h NTX•HCl level drops rapidly below lower limit of quantification. No naltrexol was detected in the transdermal drug delivery study. The

overall goal of employing the mathematical model to describe the *in vivo* NTX•HCl plasma levels was to evaluate if recognition of two parallel flux and microchannel closure process would suffice to adequately describe plasma NTX•HCl profile, and obtain a reliable value of $h_{VT'}$ parameter. This estimate can be interpreted as a hypothetical thickness of the dermis that separates the microchannel from a dermis level at which an absolute clearance into the blood compartment exists (sink conditions). The knowledge of $h_{VT'}$ parameter can help better design *in vitro* experiments to reflect *in vivo* conditions as closely as possible. All the other parameter values are known from independent studies and summarized in **Table 10.1**. Of those, two parameter estimates are to be taken with caution: k_{OMF} and D_{SC}. The first was obtained through investigation of microchannel closure process in humans (Nicole Brogden's unpublished data) and is employed as a surrogate for its Yucatan minipig counterpart, which is lacking at present. The second, D_{SC}, obtained through a *in vitro* permeation study [39] turned out to be an overestimate. If its value held true in *in vivo* conditions a plateau observed at late times (48-72 h) in **Figure 10.5** would need to equal approximately 1.1 - 1.5 ng/ml. A possible reason for this mismatch is the negative effect of storage and freeze-thaw process on Yucatan minipig skin used in *in vitro* experiments. Transport of ionized species is expected to be very sensitive to even slightest defects in the skin which can cause a significant overestimate of permeation [66]. Such defects are not anticipated to play a major role in the transport of unionized and moderately lipophilic species for which SC lipid domain is the preferred route of permeation. Hence, the *in vivo* value of D_{SC} was re-estimated through regression analysis. Two parameter values $h_{VT'}$ and D_{SC} were fitted simultaneously through regression of NTX•HCl plasma concentration on time, while keeping all other parameter values, obtained independently, constant. The least-squares fit of the model equations to experimental data is denoted as solid line in **Figure 10.5**. In general, a good correlation indicates that the model presented herein can dependably

represent *in vivo* drug delivery conditions with a "poke and patch" method. The regression estimate of *in vivo* D_{SC} was found to be 4.02 10^{-12} cm^2 s^{-1}, or 95% CI (4.99 10^{-13}, 7.54 10^{-12}), suggesting a point estimate value about 3-fold lower as compared to the estimate obtained from the *in vitro* studies [39] but within a large confidence interval range. More importantly, though, the estimate for $h_{VT'}$ was found to be 0.74 mm, or 95% CI (0.64, 0.84). The accuracy of the $h_{VT'}$ estimate depends on the method of its estimation. Herein, as mentioned before, point estimates of all other parameters were fixed while performing the least-square fit. This approach assumes that these estimates were accurate and no uncertainty from their estimation was included in the fitting process. An alternative, more conservative, approach would include simultaneous fitting of individual parameters from independent experiments together with the herein described model, which would lead to a larger confidence interval for $h_{VT'}$. This approach was not used in the present analysis given the preliminary nature of the findings and the emphasis put on the recognition of the critical factors involved in the drug transport though closing microchannels *in vivo*. Yet another approach could involve simultaneous fitting of several parameters besides $h_{VT'}$ based on the transdermal data alone. However, such method was abandoned due to high correlation between parameters of interest and, hence, low credibility of the findings. The value of 0.74 mm may seem large, especially in the light of the fact that skin microvasculature is located in direct vicinity of the microchannel. For untreated skin, the distance that a permeating drug molecule needs to cross to reach cutaneous microcirculation is often assumed to be approximately 200 µm which anatomically corresponds to the thickness of avascular epidermis. Such approximation has been successfully used for a variety of cases. It could be expected then that the $h_{VT'}$ would be numerically even less than 200 µm; however, this is clearly not the case. There are at least a couple of factors that may rationalize this observation. Firstly, the assumption of an absolute clearance at a certain

depth of the dermis, although appealing by simplicity, may not be adequate to represent the drug transport process from a microchannel to the cutaneous blood vessels. It can be expected that a more complicated clearance distribution within the dermis would more realistically describe diffusion-clearance processes [271, 272]. Secondly, drug concentration in the microchannels is anticipated to be very high and it is likely that surrounding blood vessels do not provide true sink conditions. The existence of either the above phenomena would translate into a greater-than-expected $h_{VT'}$ value. *In vitro*, the $h_{VT'}$ value can be interpreted as an effective dermis thickness between a microchannel and a receiver solution, which provides true sink conditions. *In vivo,* this value can be understood as effective dermis thickness between a microchannel and a *hypothetical* dermis level at which an absolute clearance exists. It should be noted that a simple modeling approach used herein does not accommodate several other factors that may affect drug transport *in vivo,* such as microchannel shape, length, non-first order kinetics of microchannel closure, microvasculature spatial distribution, local blood flow, and others. More elaborate model would be required to address the above factors. For example, microneedle geometry may not only affect the fractional skin surface area of microchannel pathway but also the apparent value of $h_{VT'}$. This is due to the fact that the use one-dimensional diffusion modeling in *in vivo* situation may be an oversimplification. It can be anticipated that the area of the microchannel interior would better correlate with permeability rather than skin surface area of the opening. Such approach would be also robust enough to accommodate different length and shape of the microchannels. At this time, it was judged that the present approach was sufficient to elucidate key factors related to NTX•HCl delivery *in vivo*. The data analysis suggest that a single major obstacle for obtaining long-term, near steady-state drug profiles *in vivo* after the use of a "poke and patch" method is the relatively rapid closure of microchannels. Delaying the onset of microchannel closure or decreasing the rate of microchannel closure could

potentially greatly extend the timeframe of drug delivery via this route. All of the above discussion applies to a "poke and patch" method where the formulation is non-rate-limiting. Other uses of MN, e.g. inclusion of drug in polymeric dissolvable MN, would require a different treatment and optimization. An interesting discussion of the rate of drug release from drug-in-MN system was presented by Park et al. [273]. Authors presented biodegradable polymer microneedles that encapsulate drug for controlled release in skin. The rate of drug release was found to be determined by drug diffusivity in the polymeric matrix and could be controlled by selection of adequate polymer type. The release of the drug from polymeric MN showed an initial burst effect followed by gradual decrease in the rate of release. This represents a formulation-release-rate-limited drug delivery. Another option could involve polymeric MN that biodegrade very quickly, which would imply MN-erosion-rate-limited release of drug. The recognition of the rate-limiting step is critical. Within a broad notion of "MN drug delivery" several different delivery types may be distinguished with various rate-determining steps in drug transport.

Working under assumption that the present model is adequate, and employing parameter estimates obtained from the current study, a few meaningful simulations can be performed. First, it is instructive to compare the microchannel pathway flux J_{MCP} uncorrected (*in vitro* conditions) and corrected for microchannel closure process (*in vivo* conditions) through experimental skin surface area. **Figure 10.6** demonstrates how drastic the difference between *in vitro* and *in vivo* conditions is. Not only *in vivo* flux decreases sharply over time but also never quite reaches the steady-state flux level of almost 0.5 g of NTX•HCl per hour in absence of microchannel healing. The more advanced healing process is the greater limitation is drug transport via microchannel pathway exists. It is sometimes attempted to assign a "lifetime" to microchannels which

could be then employed to determine the time window for MN-assisted drug delivery. While this approach provides some very basic information with respect to timescale of the events it fails to recognize the time-dependent changes in permeability of the microchannels. The recognition of "open/close" microchannel state depends either on arbitrary assumptions (e.g. 5-10% "open" microchannel is considered "closed") or statistical difference in signal between MN-treated and untreated skin which, in turn, depends on the sensitivity and precision of the measurement technique (TEWL, electrical impedance, dye staining). Even more importantly, though, the consequence of microchannel transition between arbitrary "open" and "close" states seems to have little bearing on the drug transport. Adopting a 10% "open" mark as borderline between "open/close" state in the present study gives microchannels "lifetime" of around 56 h. However, it is evident from the graph that while the J_{MCP} keeps decreasing at 56 h there is no discontinuity in the flux at that time. The drop in J_{MCP} between 55 and 57 h is of lesser practical significance than at any time before 56 h, say, 12 and 14 h. What is of major importance is the apparent exponential decrease in permeability of the microchannels implying that, after achieving a maximum, flux will continue to decrease by half every 17 h. In the current study, within an "open" microchannel timeframe of 56 h, J_{MCP} will diminish as much as 8.6 times. Hence, the microchannel closure process cannot be successfully described by an on-off approach assigning either "open" or "closed" state, but rather gradual changes in the permeability must be recognized. Secondly, it can be visualized what are the contributions of intact skin pathway and microchannel pathway to the total flux *in vivo* across 50.24 cm^2 of skin area employed in the study. In the experiment reported herein J_{ISP} was so low that it could not be detected directly with analytical methods available (below LLOQ) and its value was inferred indirectly through least-squares fit to the model. **Figure 10.7** demonstrates that the total flux is almost synonymous with J_{MCP}, except for late times when microchannels are

231

almost completely healed and low J_{ISP} value comes into play. It is also evident from the comparison of **Figure 10.6** and **Figure 10.7** that the time needed to reach J_{ISP} steady-state is much longer as compared the time needed to reach J_{MCP} steady-state. Next, an interesting comparison can be made by allowing for changes in the microchannel closure half-life ($t_{1/2}$). Experimental $t_{1/2}$ was evaluated to be around 17 h, and is too short to provide a sustained delivery of drug over the period of several days. However, if the rate of microchannel healing can be slowed four times ($t_{1/2}$ of 69 h), a substantial improvement in the flux and drug plasma concentration can be anticipated as demonstrated in **Figure 10.8**. In such case, a drop of NTX•HCl plasma concentration from around 3 to 2 ng/ml can be expected instead of experimentally observed drop from 2.7 to 0.4 ng/ml during 72 h. Alternative solution could involve the delay in the onset of the healing process rather than the decrease in the rate of healing. The approaches that can be utilized to achieve these goals are beyond the scope of the present work. It should be noted, however; that attempts have been made to elongate lifetime of the microchannels. A recent publication by Banks et al. [264] and unpublished results of Nicole Brogden suggest that a topical use of diclofenac, a COX enzyme inhibitor, can slow down the microchannel healing process, possibly through reduction in the inflammatory response to the micro-injury. Other options are also being explored in our laboratory. Generally, the use of methods that can delay the onset or/and slow down rate of microchannel closure can have a vital effect on the delivery of therapeutic agents. It seems that besides suppression of local inflammation or lipid SC barrier synthesis, other approaches that could help extend microchannel lifetime include the agents that would interfere ad slow down the migration of keratinocytes and reepithalization of the micro-injury. Finally, **Figure 10.8** also presents the delivery profile of NTX•HCl anticipated in the absence of the microchannel closure process. This profile establishes the upper limit of *in vivo* drug delivery. As a result of the microchannel closure half-lives

extension from 17 h to 69 h to infinity (no healing) the shape of the drug delivery profile changes. While in the absence of the healing process the profile resembles a familiar shape of near 0-order delivery typically observed in classical transdermal drug delivery, with the microchannel closure process on, the shape gradually changes to resemble an oral delivery profile. Although the underlying processes behind the oral absorption processes and MN-enhanced percutaneous drug transport are different they manifest themselves in drug plasma concentration in a similar way. Depending on the overall goal of the delivery system this phenomenon can be desired or unwanted. When a sustained drug delivery over several days is sought for, the decrease in the rate of microchannel healing could provide an extended time window of high-flux NTX•HCl delivery.

10.7. Conclusions

In the present chapter NTX•HCl delivery in Yucatan minipig with a "poke and patch" method was investigated. After an initial spike in plasma drug concentration, a rapid drop and plateau followed. A mathematical model, which incorporated the concepts of two-pathway parallel drug transport, microchannel closure process, and drug disposition and elimination *in vivo,* was developed. With majority of the model parameters estimated independently, the overall fit of the model to experimental data was good implying that it accounted for key processes related to MN-enhanced drug delivery *in vivo*. Additionally, an estimate for hypothetical dermis thickness separating a microchannel from dermis level at which an absolute clearance exists, was obtained. Its relatively large value suggests that the effect of diffusional resistance of the dermis *in vivo* should not be ignored and must be accounted for in order to obtain a good in *vitro-in vivo* correlation. Based on the current study, it seems that the relatively fast rate of microchannel closure

is the single major hurdle for obtaining a sustained-delivery drug profiles *in vivo* after a "poke and patch" method. The application of the present model to other drugs delivered by MN-enhanced skin could shed some light on the generality of present findings. While the overall structure of the model should easily accommodate different diffusion coefficients of drugs, density of MN treatment, microchannel closure times and pharmacokinetic parameters, it would be very interesting to see if the value of the $h_{VT'}$ parameter remains approximately constant. The limitations of the present model include lack of explicit recognition of the microchannel length effect on the transport, ignorance of the possible dermal metabolism, protein binding, local blood flow, and microvasculature spatial distribution. A future project could address the above factors by expansion of the current model.

Table 10.1. Model parameters. All the parameters values (except for two which are denoted by asterisks) were obtained through independent experiments and were kept constant during performing a least-squares fit of the model to the *in vivo* transdermal data. The two fitted parameters (denoted by asterisks) are D_{SC} (*in vivo*) and $h_{VT'}$.

Parameter	Point estimate	95% CI	Unit
D_{SC} (*in vitro*)	$4.02 \ 10^{-12}$	n/a	$[cm^2 \ s^{-1}]$
D_{SC} (*in vivo*)*	$1.45 \ 10^{-12}$	$(4.99 \ 10^{-13}, 7.54 \ 10^{-12})$	$[cm^2 \ s^{-1}]$
h_{SC}	20	n/a	$[\mu m]$
D_{VT}	$2.46 \ 10^{-7}$	n/a	$[cm^2 \ s^{-1}]$
$h_{VT'}$*	740	(640, 840)	$[\mu m]$
A	50.24	n/a	$[cm^2]$
f_{ISP}	1	n/a	[-]
f_{MCP}	0.0077	n/a	[-]
$k_{OMF} = k_Y$	0.041	n/a	$[h^{-1}]$
V_d	43.86	n/a	[l]
k_{12}	3.192	n/a	$[h^{-1}]$
k_{21}	2.002	n/a	$[h^{-1}]$
k_{13}	0.098	n/a	$[h^{-1}]$
k_{31}	0.050	n/a	$[h^{-1}]$
k_{10}	2.596	n/a	$[h^{-1}]$

Figure 10.1.
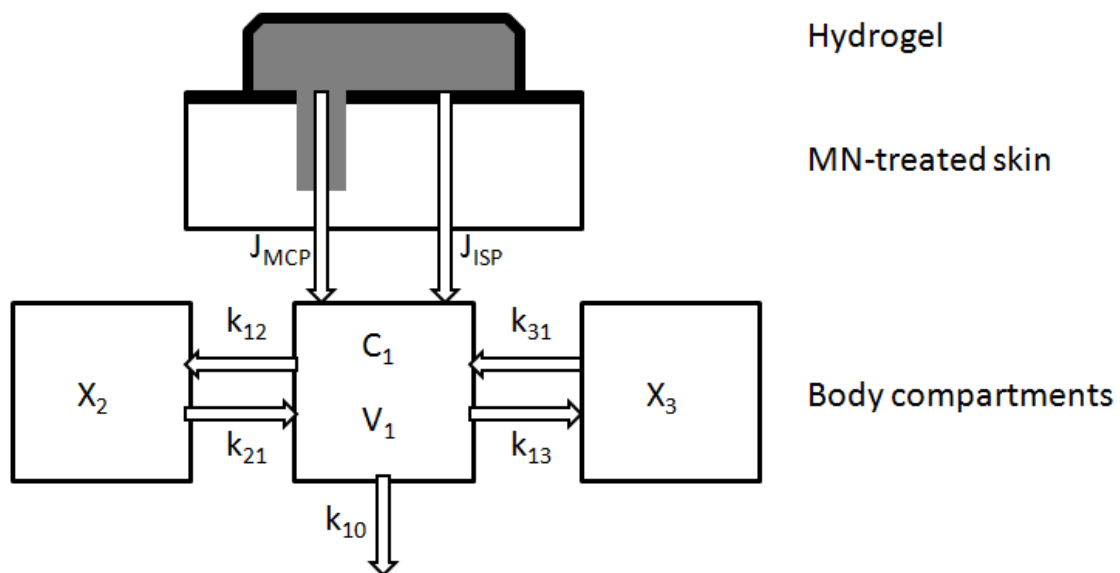
A schematic diagram of the model used to analyze the MN-assisted transdermal delivery of NTX•HCl in Yucatan minipig. Hydrogel drug formulation is placed on the MN-treated skin area. Skin allows drug transport through two parallel pathways. Drug is distributed amongst central and two peripheral compartments, and eliminated from the central compartment.

Figure 10.2.
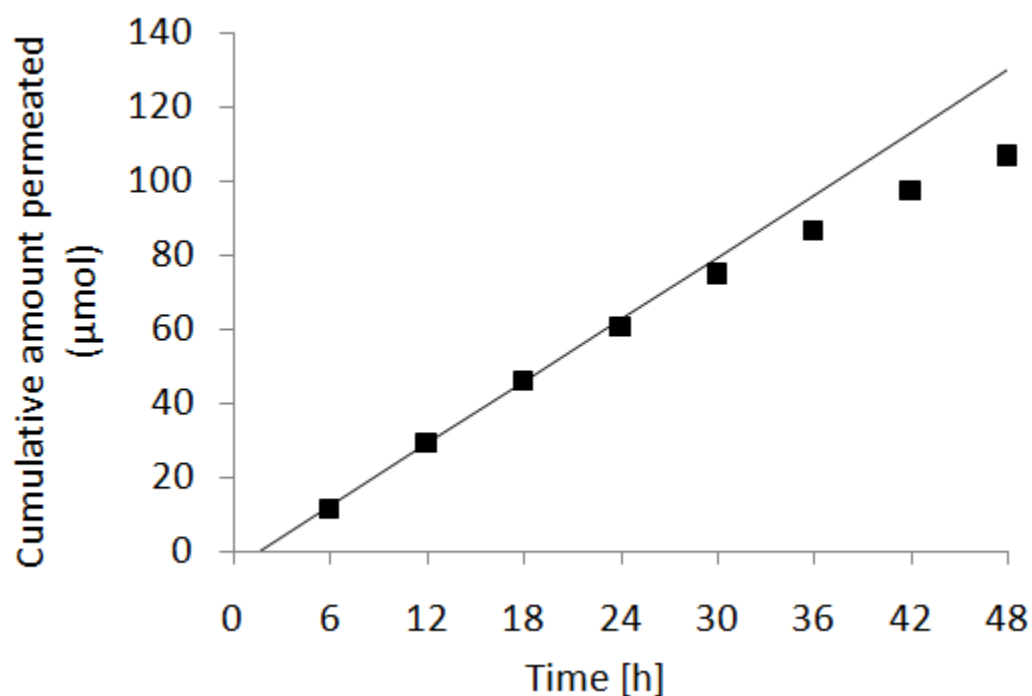
An individual (n = 1), representative permeation profile of NTX•HCl across dermis. Filled squares (■) denote experimental data points while solid line shows linear approximation of flux at 6-12 h timeframe extrapolated over the whole experiment duration. High flux resulted in approximately 50% drug depletion in the donor solution by the end of the 48 h study which manifests itself as a drop in flux at later time points.

Figure 10.3.
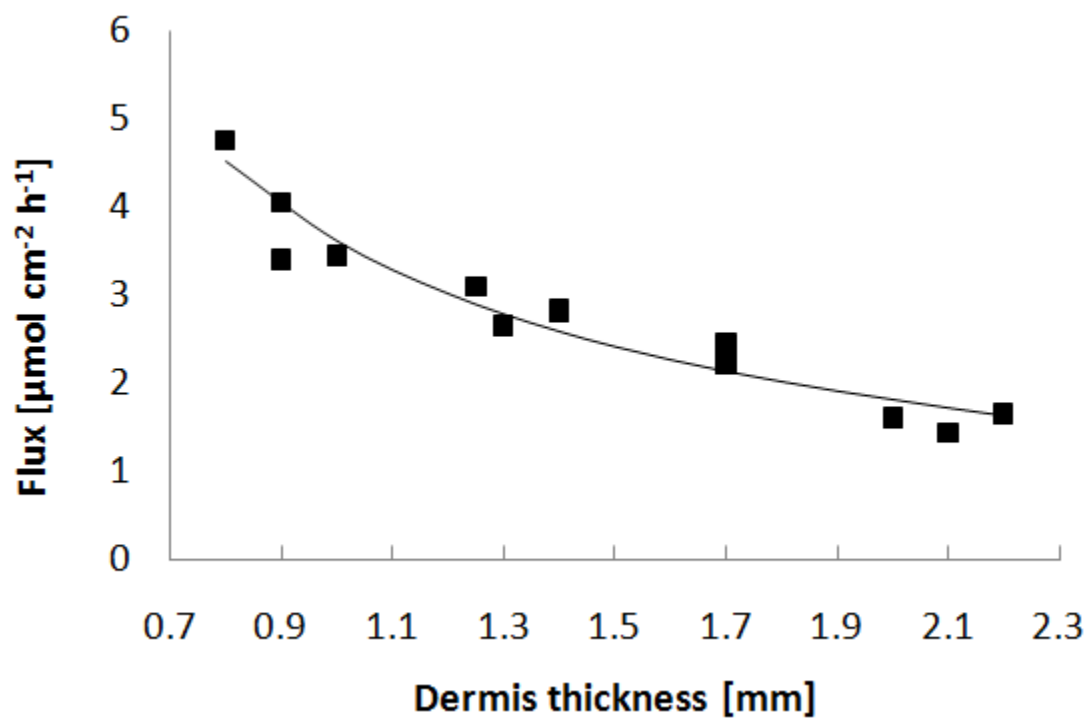
NTX•HCl flux across dermis. Fourteen (n = 14) individual flux values denoted as filled squares (■) are plotted against increasing thickness of the dermis. The solid line represents the least square fit to Eq. 10.3.

Figure 10.4.
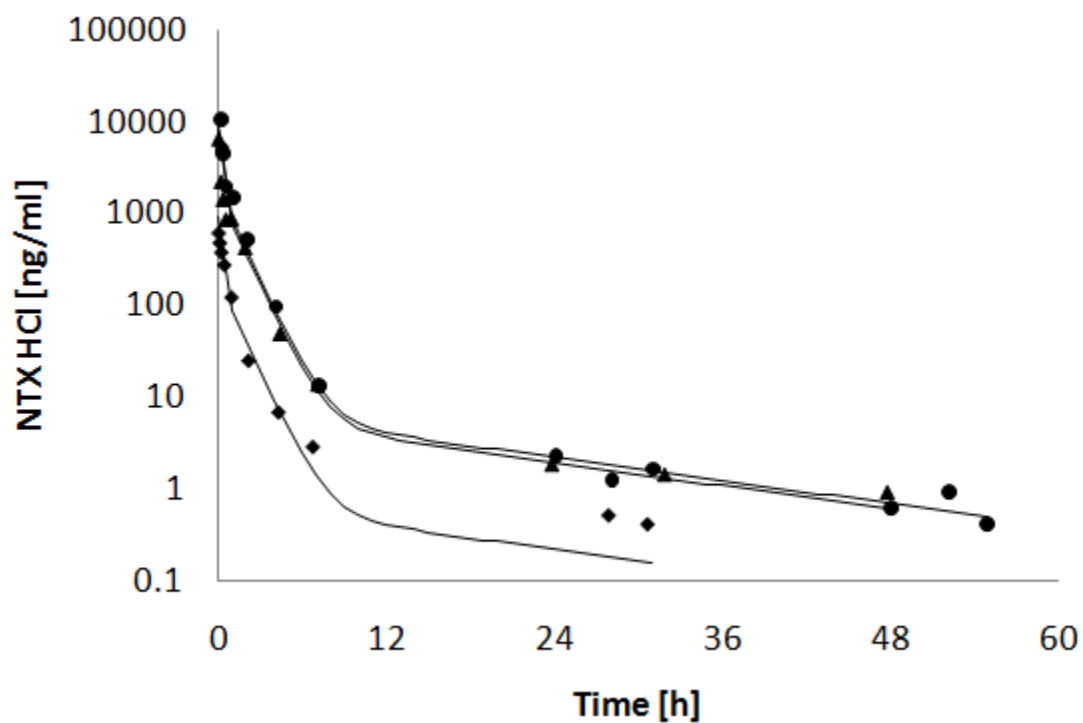
Yucatan minipig plasma NTX•HCl levels after IV bolus administration of 1 mg/kg dose (♦), 10 mg/kg dose (•), and 9 mg/kg dose (▲). Solid lines represent a least-squares fit according to Eq. 10.23-10.25.

Figure 10.5.
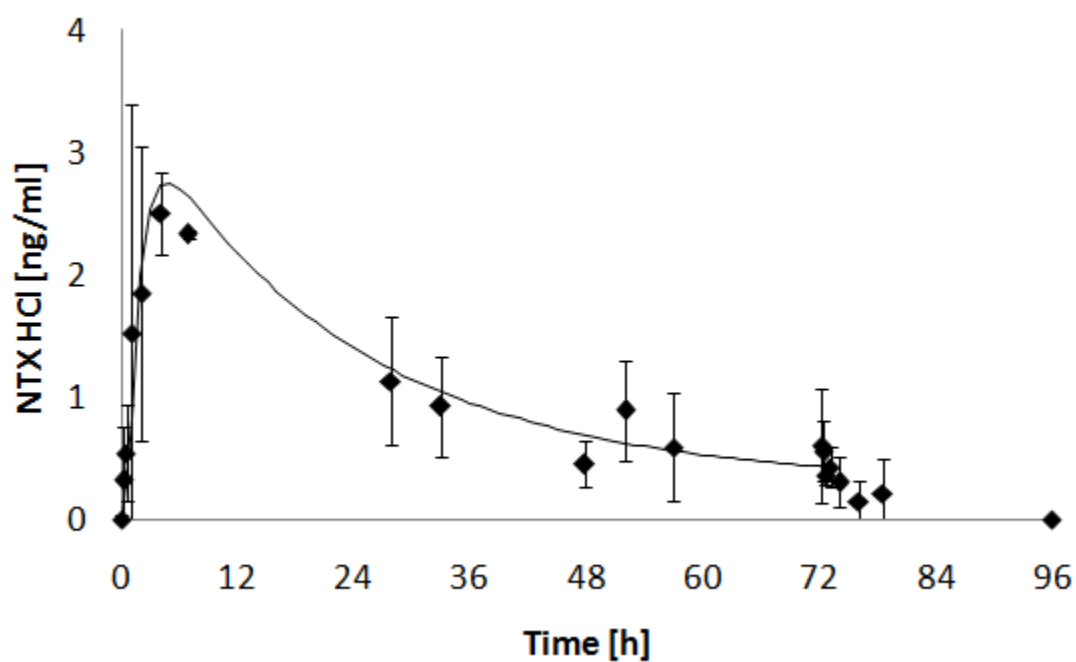
Yucatan minipig plasma NTX•HCl levels after a "poke and patch" method. At 72 h transdermal patches were removed. Points (♦) represent mean of three (n = 3) determinations, while solid line represent a least-squares fit according to Eq. 10.8-10.14 in the 0-72 h timeframe.

Figure 10.6.
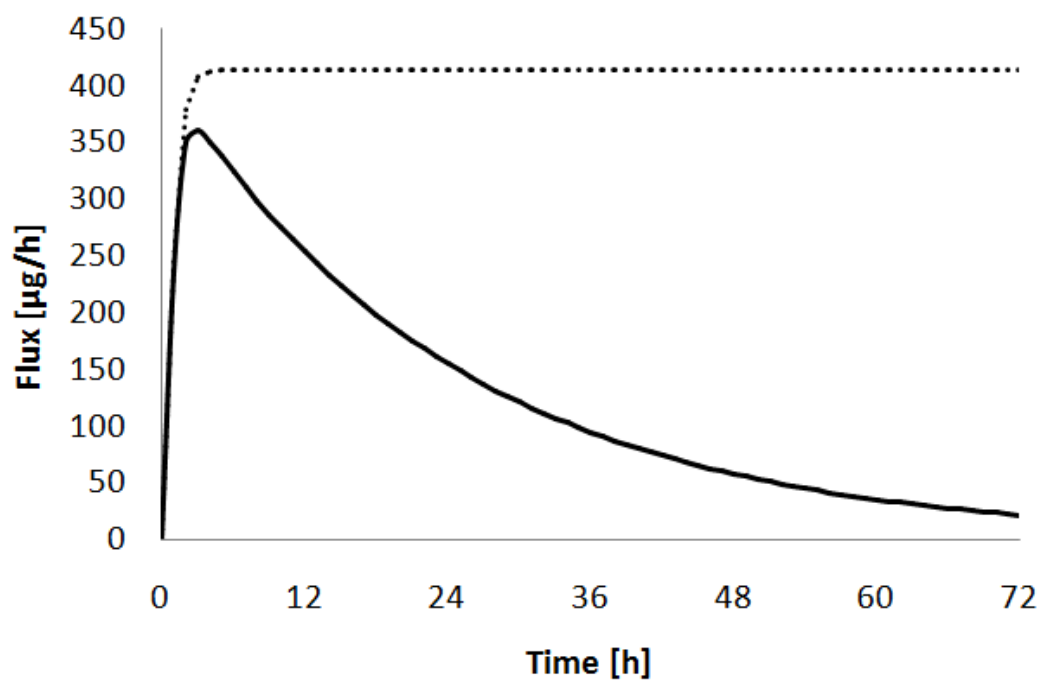
Simulation demonstrating time-dependent changes in microchannel pathway flux under *in vitro* (dotted line) and *in vivo* (solid line) conditions. Microchannel closure causes the drop in flux *in vivo*.

Figure 10.7.
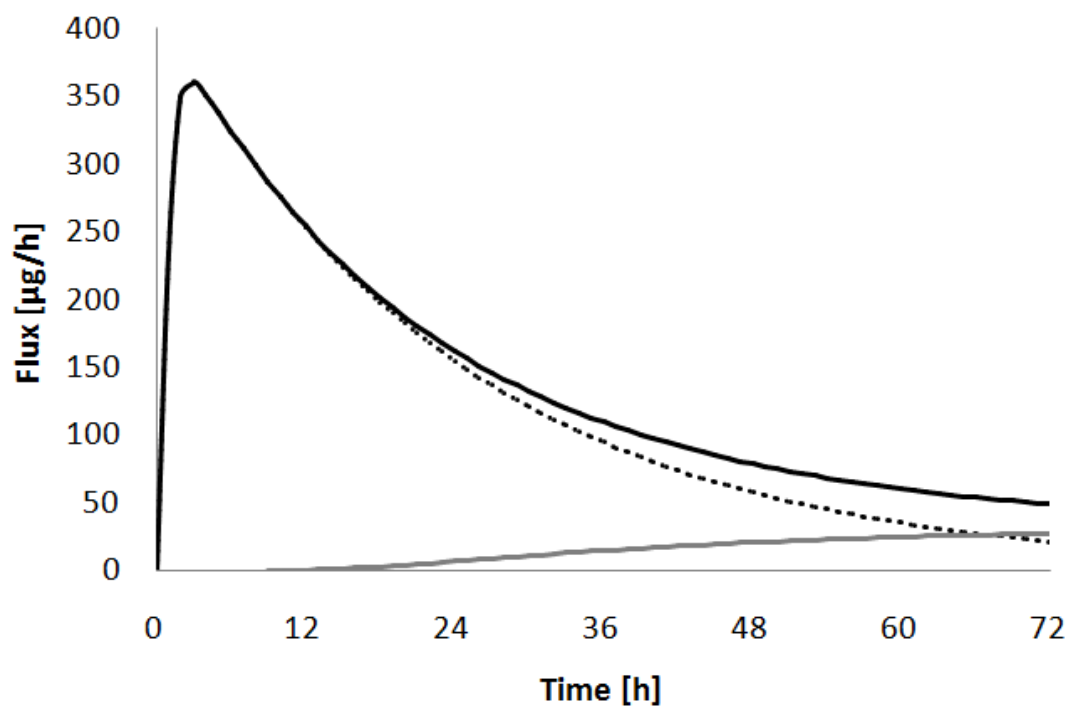
Simulation demonstrating contributions of intact skin pathway flux (gray line) and microchannel pathway flux (dotted line) to the total flux (solid black line) *in vivo*.

Figure 10.8.
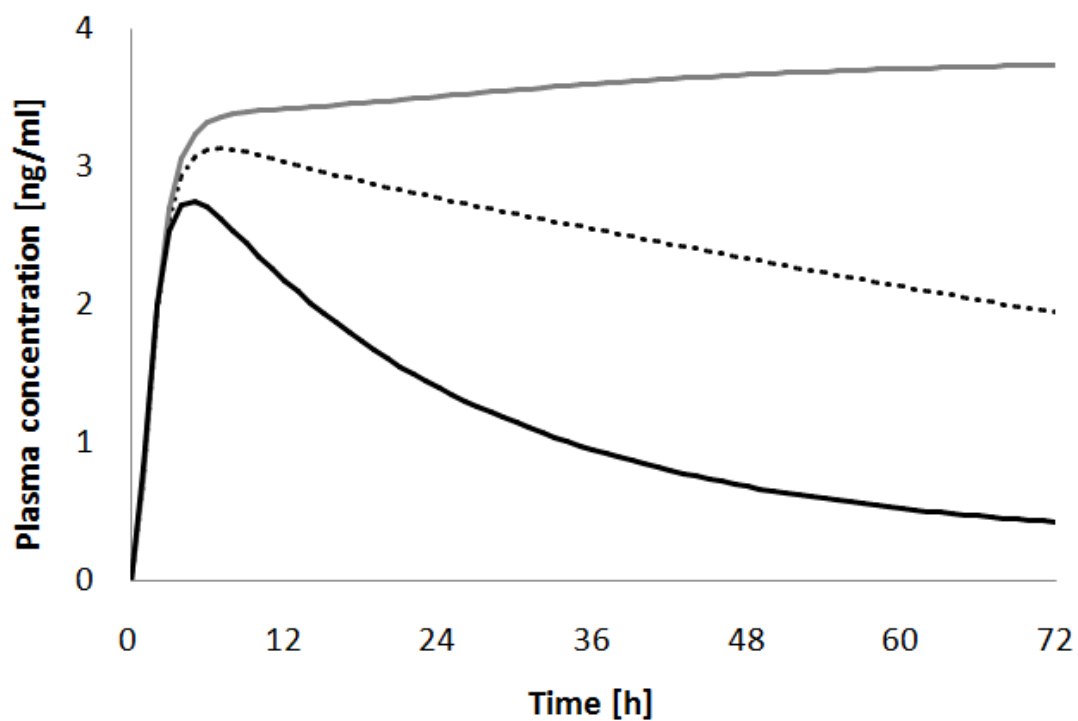
Simulation demonstrating an effect of the change in the microchannel closure time on the plasma concentration of NTX•HCl. Solid line corresponds to microchannel closure $t_{1/2}$ of 17 h (experimental), dotted line - $t_{1/2}$ of 69 h, and gray line - $t_{1/2}$ of infinity (no microchannel closure).

Chapter 11

Conclusions and future directions

The thesis project was based on two major objectives. The first, narrower in scope, was to increase the transdermal delivery rate of naltrexone from a transdermal patch through microneedle-enhanced skin. The second, wider in scope, is to gain better understanding of microneedle-enhanced transdermal drug delivery in terms of critical parameters governing the transport. Work reported herein can be seen as a continuation of pioneering NTX•HCl microneedle studies performed by Dr. S. Banks [274]. Naltrexone is a drug used primarily in the management of alcohol dependence and opioid dependence. Our interest in delivering naltrexone transdermally is well-founded and based on several drawbacks associated with the oral and injectable intramuscular dosage forms of naltrexone currently available on the market including significant first-pass effect, gastrointestinal side effects and poor patience compliance. Although NTX does not permeate skin at the rate sufficient to reach therapeutic concentrations in human plasma, novel flux enhancement methods such as microneedles can address this problem. The use of MN offers substantial increase in the rates of drug delivery though skin.

In fulfillment of the research goals, first, a simple mathematical model was developed for analysis of steady-state permeation data through MN-treated skin. The distinct feature of the model is that it recognizes the microchannels as a separate permeation pathway in parallel to the intact skin permeation pathway. Since the fractional skin surface area taken by the microchannel openings is very small the formation of microchannels practically does not affect the intact skin pathway. Hence, MN-treatment can be seen as a method of providing an additional permeation pathway through skin without affecting

an already existing one. *In vitro* diffusion studies with indomethacin demonstrated that the formation of microchannels increases percutaneous drug transport. The magnitude of flux enhancement depends on the donor solution solubility and permeability through both: intact skin pathway and microchannels pathway. The interplay between these factors determines the overall benefit of using MN. Former studies carried out with naltrexone and 6β-naltrexol provided similar results.

Secondly, the effect of formulation on the rate of transdermal transport of NTX•HCl through MN-enhanced skin *in vitro* was investigated. It was found that flux correlated well with changes in drug diffusivity caused by donor viscosity variations. Also, it is likely that the microchannel pathway flux rather than total flux (combined microchannel pathway and intact skin pathway flux) correlates with viscosity changes of donor solution through the Stokes-Einstein equation. Moreover, this work indicated that percutaneous flux of charged species across intact skin may become important when large skin area is exposed to the drug formulation. These findings suggested that when maximum flux through MN-treated skin is sought then the viscosity of the formulation should be kept as low as possible. However, that restriction does not hold with respect to high molecular weight polymeric systems which don't seem to increase the diffusional resistance of the microchannel pathway. The selection of water-rich sheet hydrogel formulation proved the most successful in conjunction with MN-assisted transdermal drug transport. Approximately 5-fold increase in the transdermal flux was achieved as compared to the formerly employed formulation in the first-in-human MN study [216].

Next, *in vitro* permeation of a PEGylated NTX prodrug across MN-treated skin was investigated. It has been found that the flux did not proportionally increase when high concentrations of the prodrug in the donor solution were utilized. In other words, the apparent permeability coefficient was not a concentration-independent proportionality

constant between flux and drug concentration. It was hypothesized that this non-linearity was caused, again, by elevated viscosity of the donor media. Calculations based on the Stokes-Einstein equation afford a reasonable explanation of the experimental data. The generalization of the results obtained from the current study will require further investigation. It is not expected that the type of behavior seen in the present study will be universal for all MN-involving transport experiments as different methods of MN application, MN design and formulation characteristics play a significant role in the drug transport across MN-treated skin. In consequence, the generality of the present *in vitro* findings may be limited to the studies involving, among others, water-based formulations, MN-pretreated skin with microchannels having similar nature to those obtained in this study and permeants which cross the skin mainly through microchannels and underlying dermis, rather than through the intact skin around microchannels. A great variety of other NTX prodrugs were tested in stability and solubility studies. The use of prodrugs to modify permeant physicochemical properties has been known to be a successful strategy to improve flux in a variety of cases. However, in the current project this goal was not achieved. Three major factors that have contributed to this result are the lack of adequate formulation stability, pronounced deviation from ideal behavior causing a non-linear flux increase as function of permeant concentration, and insufficient aqueous solubility.

In the following step, the permeation and skin irritation potential of several NTX salts was studied. Three NTX salts (acetate, lactate and glycolate) demonstrated improved aqueous solubility at practically-relevant skin surface pH of 5.0 over that of NTX•HCl. Increased solubility of NTX glycolate, despite the non-ideal behavior, can be used to achieve approximately 50% increase in permeation across MN-treated skin. Moreover, the skin irritation-potential of naltrexone glycolate and lactate were found to be not greater than that of NTX•HCl in the guinea pig model implying that they can be safely

246

used on human skin. Overall, a new NTX glycolate salt was demonstrated to be a promising candidate for further testing and inclusion in a *in vivo* transdermal drug delivery system in conjunction with microneedle skin treatment.

Finally, a mathematical model that would described *in vivo* NTX•HCl plasma profile after a "poke and patch" method application was developed. This was achieved through the use of a combined diffusion-compartmental model. The critical elements incorporated into the model were the recognition of two parallel pathways for drug permeation after MN skin treatment (intact skin pathway and microchannel pathway), the barrier thickness-dependant diffusional resistance of microchannel pathway, direct relationship between electrical admittance of the microchannels and their permeability to drugs, and classic pharmacokinetic compartmental module for description of drug disposition and elimination from the body. Experimentally, NTX•HCl delivery in Yucatan minipig with a "poke and patch" method was studied and demonstrated an initial spike in drug plasma concentration followed by a rapid drop and a plateau. With majority of the model parameters estimated independently, the overall fit of the model to experimental data was good implying that it accounted for key processes related to MN-enhanced drug delivery *in vivo*. A 0.74 mm estimate for hypothetical dermis thickness separating a microchannel from dermis level at which an absolute clearance exists was obtained. Its relatively large value suggests that the effect of diffusional resistance of the dermis *in vivo* should not be ignored and must be accounted for in order to obtain a good in *vitro-in vivo* correlation. Based on the current study, it seems that the relatively fast rate of microchannel closure is the single major hurdle for obtaining a sustained-delivery drug profiles *in vivo* after a "poke and patch" method.

From a practical perspective, it is envisioned that future research efforts will primarily focus on the extension of microchannel lifetime so that a wider time window for NTX•HCl

delivery becomes available. A method that would enable the delay of the healing process and/or substantially decrease the rate of the microchannel closure has a great potential to add more value to the sustained delivery of drugs via microchannel pathway. Based on the present study, the rate of microchannel closure *in vivo* makes the use of the MN skin enhancement to attain high, sustained drug delivery over the period of several days difficult. However, a more optimistic human study is also known, which demonstrated a milder drop in the NTX•HCl concentration over time after MN-treatment [32]. It is anticipated that future research efforts will ultimately lead to longer sustained delivery of NTX•HCl, which is the end therapeutic goal. Moreover, it should be emphasized that the time window for drug delivery through microchannels, available at present, may be sufficient for other therapeutic indications without any further modifications. In various instances including: delivery of bolus-like dose of drug, shorter drug delivery time, or permeation of large-molecular-weight drugs (proteins) that are impermeable to untreated skin, microneedles present a distinct advantage and major delivery option. Apart from the "poke and patch" method other modes of MN application have been described in details [7] and include MN coating, drug in MN, and injections through hollow MN. There is an array of clinical options for MN use [97]. For example, one of the most promising therapeutic areas employing MN, is vaccination [22, 23, 29, 210, 275]. Due to the high potency of vaccines and presence of immunologically-relevant Langerhans cells in skin microneedles provide a very convenient and hypodermic-needle-free medium for effective inoculation process. Likely, as research progress is made, even more clinical options will be unveiled. On the other hand, it is recognized that a more advanced mathematical model can further improve the understanding of the critical factors involved in the drug transport via "poke and patch" method. Overall, this work has introduced several concepts that may facilitate analysis of drug transport through MN-treated skin: parallel permeation pathways, relative

contributions of diffusional resistance of individual skin layers, influence of formulation viscosity on the rate of transport, recognition of link between electrical admittance and permeability of skin, and combination of the above factors with compartmental pharmacokinetic modeling to describe *in vivo* drug plasma levels. It is believed that these concepts can be further expanded and build upon to gain additional insight and increase the predictive power of the current model.

References

1. *Results from the 2009 National Survey on Drug Use and Health: Volume I. Summary of National Findings*. 2010.

2. *National Institute on Drug Abuse InfoFacts: Nationwide Trends*. 2007; Available from: http://www.nida.nih.gov/Infofacts/nationtrends.html.

3. Eap, C.B., et al., *Stereoselective block of hERG channel by (S)-methadone and QT interval prolongation in CYP2B6 slow metabolizers.* Clin. Pharmacol. Ther. (N. Y., NY, U. S.), 2007. **81**(5): p. 719-728.

4. Volpicelli, J.R., et al., *Naltrexone in the treatment of alcohol dependence.* Arch Gen Psychiatry, 1992. **49**(11): p. 876-80.

5. Staff, *PDR Generics. 1995. First Edition. Medical Consultant: Ronald Arky*. Vol. 39. 1996. 2278.

6. Banks, S.L., et al., *Flux Across Microneedle-treated Skin is Increased by Increasing Charge of Naltrexone and Naltrexol In Vitro.* Pharmaceutical Research, 2008. **25**(7): p. 1677-1685.

7. Prausnitz, M.R., *Microneedles for transdermal drug delivery.* Advanced Drug Delivery Reviews, 2004. **56**(5): p. 581-587.

8. Prausnitz, M.R. and R. Langer, *Transdermal drug delivery.* Nat. Biotechnol., 2008. **26**(11): p. 1261-1268.

9. Anton, R.F., et al., *Combined pharmacotherapies and behavioral interventions for alcohol dependence. The COMBINE study: a randomized controlled trial.* JAMA, J. Am. Med. Assoc., 2006. **295**(17): p. 2003-2017.

10. McCaul, M.E., et al., *Serum 6-beta-naltrexol levels are related to alcohol responses in heavy drinkers.* Alcohol Clin Exp Res, 2000. **24**(9): p. 1385-91.

11. O'Malley, S.S., *Opioid antagonists in the treatment of alcohol dependence: Clinical efficacy and prevention of relapse.* Alcohol Alcohol., 1996. **31**(Suppl. 1): p. 77-81.

12. O'Malley, S.S., et al., *Naltrexone and coping skills therapy for alcohol dependence. A controlled study.* Arch Gen Psychiatry, 1992. **49**(11): p. 881-7.

13. Volpicelli, J.R., *Naltrexone in alcohol dependence.* Lancet, 1995. **346**(8973): p. 456.

14. Honkanen, A., et al., *Alcohol drinking is reduced by a mu 1- but not by a delta-opioid receptor antagonist in alcohol-preferring rats.* Eur J Pharmacol, 1996. **304**(1-3): p. 7-13.

15. Hyytia, P., *Involvement of mu-opioid receptors in alcohol drinking by alcohol-preferring AA rats.* Pharmacol Biochem Behav, 1993. **45**(3): p. 697-701.

16. *Information for Healthcare Professionals: Naltrexone Injection Site Reactions [naltrexone for extended-release injectable suspension (marketed as Vivitrol).* 2008.

17. Prausnitz, M.R., S. Mitragotri, and R. Langer, *Current status and future potential of transdermal drug delivery.* Nat. Rev. Drug Discovery, 2004. **3**(2): p. 115-124.

18. Flynn, G.L., *Cutaneous and Transdermal Delivery: Processes and Systems of Delivery*, in *Modern Pharmaceutics*, C.T.R. G.S. Banker, Editor. 1990, Marcel Dekker: New York. p. 239 - 298.

19. Bos, J.D. and M.M.H.M. Meinardi, *The 500 Dalton rule for the skin penetration of chemical compounds and drugs.* Exp. Dermatol., 2000. **9**(3): p. 165-169.

20. Paudel, K.S., et al., *Transdermal delivery of naltrexone and its active metabolite 6-beta-naltrexol in human skin in vitro and guinea pigs in vivo.* Journal of Pharmaceutical Sciences, 2005. **94**(9): p. 1965-1975.

21. Stinchcomb, A.L., et al., *Straight-chain naltrexone ester prodrugs: diffusion and concurrent esterase biotransformation in human skin.* Journal of Pharmaceutical Sciences, 2002. **91**(12): p. 2571-2578.

22. Arora, A., M.R. Prausnitz, and S. Mitragotri, *Micro-scale devices for transdermal drug delivery.* Int. J. Pharm., 2008. **364**(2): p. 227-236.

23. Bal, S.M., et al., *In vivo assessment of safety of microneedle arrays in human skin.* Eur. J. Pharm. Sci., 2008. **35**(3): p. 193-202.

24. Coulman, S.A., et al., *Microneedle mediated delivery of nanoparticles into human skin.* Int J Pharm, 2009. **366**(1-2): p. 190-200.

25. Gill, H.S., et al., *Effect of microneedle design on pain in human volunteers.* Clinical Journal of Pain, 2008. **24**(7): p. 585-594.

26. Kalluri H, B.A., *Microneedles and transdermal drug delivery.* Journal of Drug Delivery Science and Technology, 2009. **19**(5): p. 303-310.

27. McAllister, D.V., et al., *Microfabricated needles for transdermal delivery of macromolecules and nanoparticles: Fabrication methods and transport studies.* Proceedings of the National Academy of Sciences of the United States of America, 2003. **100**(24): p. 13755-13760.

28. Qiu, Y., et al., *Enhancement of skin permeation of docetaxel: A novel approach combining microneedle and elastic liposomes.* J. Controlled Release, 2008. **129**(2): p. 144-150.

29. Gill, H.S. and M.R. Prausnitz, *Coated microneedles for transdermal delivery.* J. Controlled Release, 2007. **117**(2): p. 227-237.

30. Haq, M.I., et al., *Clinical administration of microneedles: skin puncture, pain and sensation.* Biomed Microdevices, 2009. **11**(1): p. 35-47.

31. Kaushik, S., et al., *Lack of pain associated with microfabricated microneedles.* Anesthesia and analgesia, 2001. **92**(2): p. 502-4.

32.   Wermeling, D.P., et al., *Microneedles permit transdermal delivery of a skin-impermeant medication to humans.* Proc Natl Acad Sci U S A, 2008. **105**(6): p. 2058-63.

33.   Collier, S.W., et al., *Maintenance of skin viability during in vitro percutaneous absorption/metabolism studies.* Toxicology and Applied Pharmacology, 1989. **99**(3): p. 522-33.

34.   Eggleston, T.A., et al., *Comparison of two porcine (Sus scrofa domestica) skin models for in vivo near-infrared laser exposure.* Comparative Medicine, 2000. **50**(4): p. 391-397.

35.   Fujii, M., et al., *Evaluation of yucatan micropig skin for use as an in vitro model for skin permeation study.* Biological & Pharmaceutical Bulletin, 1997. **20**(3): p. 249-254.

36.   Gore, A.V., A.C. Liang, and Y.W. Chien, *Comparative biomembrane permeation of tacrine using Yucatan minipigs and domestic pigs as the animal model.* Journal of Pharmaceutical Sciences, 1998. **87**(4): p. 441-447.

37.   Chuong, C.M., et al., *What is the 'true' function of skin?* Experimental dermatology, 2002. **11**(2): p. 159-87.

38.   Prausnitz, M.R., *Overcoming skin's barrier: the search for effective and user-friendly drug delivery.* Diabetes Technol. Ther., 2001. **3**(2): p. 233-236.

39.   Milewski, M. and A.L. Stinchcomb, *Vehicle composition influence on the microneedle-enhanced transdermal flux of naltrexone hydrochloride.* Pharm Res, 2011. **28**(1): p. 124-34.

40.   *Answers.com - skin.* 2011.

41.   Schiffman, H.R., *Sensation and Perception. An Integrated Approach.* 2001, New York: John Wiley and Sons, Inc.

42. Kanitakis, J., *Anatomy, histology and immunohistochemistry of normal human skin.* Eur J Dermatol, 2002. **12**(4): p. 390-9; quiz 400-1.

43. Coulombe, P.A., *Wound epithelialization: Accelerating the pace of discovery.* J. Invest. Dermatol., 2003. **121**(2): p. 219-230.

44. Martin, P., *Wound healing - aiming for perfect skin regeneration.* Science (Washington, D. C.), 1997. **276**(5309): p. 75-81.

45. Oudshoorn, M.H., et al., *Development of a murine model to evaluate the effect of vernix caseosa on skin barrier recovery.* Exp Dermatol, 2009. **18**(2): p. 178-84.

46. Yang, L., et al., *Topical stratum corneum lipids accelerate barrier repair after tape stripping, solvent treatment and some but not all types of detergent treatment.* Br J Dermatol, 1995. **133**(5): p. 679-85.

47. Foldvari, M., *Non-invasive administration of drugs through the skin: challenges in delivery system design.* Pharm. Sci. Technol. Today, 2000. **3**(12): p. 417-425.

48. Elias, P.M., *Stratum corneum defensive functions: an integrated view.* Journal of Investigative Dermatology, 2005. **125**(2): p. 183-200.

49. Elias, P.M., *Structure and function of the stratum corneum permeability barrier.* Drug Dev. Res., 1988. **13**(2-3): p. 97-105.

50. Wilkes, G.L., I.A. Brown, and R.H. Wildnauer, *The biomechanical properties of skin.* CRC Crit Rev Bioeng, 1973. **1**(4): p. 453-95.

51. Michaels, A.S., S.K. Chandrasekaran, and J.E. Shaw, *Drug permeation through human skin. Theory and in vitro experimental measurement.* AIChE J., 1975. **21**(5): p. 985-96.

52. Elias, P.M., et al., *Percutaneous transport in relation to stratum corneum structure and lipid composition.* J. Invest. Dermatol., 1981. **76**(4): p. 297-301.

53. Bouwstra, J.A., et al., *Structure of the skin barrier and its modulation by vesicular formulations.* Prog. Lipid Res., 2003. **42**(1): p. 1-36.

54. Flynn, G.L., S.H. Yalkowsky, and T.J. Roseman, *Mass transport phenomena and models. Theoretical concepts.* Journal of Pharmaceutical Sciences, 1974. **63**(4): p. 479-510.

55. Harding Clive, R., *The stratum corneum: structure and function in health and disease.* Dermatol Ther, 2004. **17 Suppl 1**: p. 6-15.

56. Johnson Anthony, W., *Overview: fundamental skin care--protecting the barrier.* Dermatol Ther, 2004. **17 Suppl 1**: p. 1-5.

57. Madison, K.C., *Barrier function of the skin: "La raison d'etre" of the epidermis.* J. Invest. Dermatol., 2003. **121**(2): p. 231-241.

58. Abraham, M.H., H.S. Chadha, and R.C. Mitchell, *The factors that influence skin permeation of solutes.* J. Pharm. Pharmacol., 1995. **47**(1): p. 8-16.

59. Kretsos, K., et al., *Partitioning, diffusivity and clearance of skin permeants in mammalian dermis.* Int. J. Pharm., 2008. **346**(1-2): p. 64-79.

60. Kasting, G.B., S.R. L., and A.B. D., *Prodrugs for dermal delivery: solubility, molecular size, and functional group effects*, in *Prodrugs: topical and ocular drug delivery*, K.B. Sloan, Editor. 1992, Marcel Dekker: New York. p. 117-161.

61. Scheuplein, R.J., *Mechanism of percutaneous absorption. II. Transient diffusion and the relative importance of various routes of skin penetration.* J Invest Dermatol, 1967. **48**(1): p. 79-88.

62. Scheuplein, R.J. and I.H. Blank, *Permeability of the skin.* Physiol Rev, 1971. **51**(4): p. 702-47.

63. Cross, S.E. and M.S. Roberts, *Subcutaneous absorption kinetics and local tissue distribution of interferon and other solutes.* J. Pharm. Pharmacol., 1993. **45**(7): p. 606-609.

64. Bonina, F.P., et al., *In vitro and in vivo evaluation of polyoxyethylene esters as dermal prodrugs of ketoprofen, naproxen and diclofenac.* European Journal of Pharmaceutical Sciences, 2001. **14**(2): p. 123-134.

65. Flynn, G.L., *Principles of route-to-route extrapolation for risk assessment*, in *Physicochemical determinants of skin absorption*, T.R.G.C.J. Henry, Editor. 1990, Elsevier: New York. p. 93-127.

66. Kasting, G.B., R.L. Smith, and B.D. Anderson, *Prodrugs for dermal delivery: solubility, molecular size, and functional group effects.* 1992. **53**(Prodrugs): p. 117-61.

67. Roberts, M.S., et al., *Epidermal permeability-penetrant structure relationships: 1. An analysis of methods of predicting penetration of monofunctional solutes from aqueous solutions.* Int. J. Pharm., 1995. **126**(1,2): p. 219-33.

68. Bouwstra, J.A., et al., *The lipid organisation in the skin barrier.* Acta Derm Venereol Suppl (Stockh), 2000. **208**: p. 23-30.

69. Guy, R.H. and J. Hadgraft, *Physicochemical aspects of percutaneous penetration and its enhancement.* Pharm Res, 1988. **5**(12): p. 753-8.

70. Kasting, G.B., et al., *Mobility of water in human stratum corneum.* J. Pharm. Sci., 2003. **92**(11): p. 2326-2340.

71. Wang, T.-F., G.B. Kasting, and J.M. Nitsche, *A multiphase microscopic diffusion model for stratum corneum permeability. II. Estimation of physicochemical parameters, and application to a large permeability database.* J. Pharm. Sci., 2007. **96**(11): p. 3024-3051.

72. Wallace, S.M. and G. Barnett, *Pharmacokinetic analysis of percutaneous absorption: evidence of parallel penetration pathways for methotrexate.* J Pharmacokinet Biopharm, 1978. **6**(4): p. 315-25.

73. Goldsmith, L.A. and Editor, *Biochemistry and Physiology of the Skin*. 1983. 1300 pp.

74. Benowitz, N.L., et al., *Intravenous nicotine retards transdermal absorption of nicotine: evidence of blood flow--limited percutaneous absorption.* Clin Pharmacol Ther, 1992. **52**(3): p. 223-30.

75. Flynn, G.L. and B. Stewart, *Percutaneous drug penetration: choosing candidates for transdermal development.* Drug Dev. Res., 1988. **13**(2-3): p. 169-85.

76. Bauerova, K., D. Matusova, and Z. Kassai, *Chemical enhancers for transdermal drug transport.* Eur J Drug Metab Pharmacokinet, 2001. **26**(1-2): p. 85-94.

77. Joshi, A. and J. Raje, *Sonicated transdermal drug transport.* J Control Release, 2002. **83**(1): p. 13-22.

78. Crank, J., *The Mathematics of Diffusion. 2d Ed.* 1975. 414 pp.

79. Bronaugh, R.L., H.I. Maibach, and Editors, *Percutaneous Absorption: Drugs-Cosmetics-Mechanisms-Methodology, Fourth Edition. [In: Drugs Pharm. Sci.; 2005, 155].* 2005. 878 pp.

80. *Vivitrol(R) Healthcare Professional Site.* 2011; Available from: www.vivitrol.com/hcp/Vivitrol_Info/adherence.aspx.

81. Mucha, R.F. and A. Herz, *Motivational properties of kappa and mu opioid receptor agonists studied with place and taste preference conditioning.* Psychopharmacology (Berl), 1985. **86**(3): p. 274-80.

82. Terenius, L., *Alcohol addiction (alcoholism) and the opioid system.* Alcohol, 1996. **13**(1): p. 31-4.

83. Volpicelli, J.R., et al., *Naltrexone and alcohol dependence. Role of subject compliance.* Archives of General Psychiatry, 1997. **54**(8): p. 737-742.

84. Di Chiara, G., E. Acquas, and G. Tanda, *Ethanol as a neurochemical surrogate of conventional reinforcers: the dopamine-opioid link.* Alcohol, 1996. **13**(1): p. 13-7.

85. *Low dose naltrexone (LDN).* 2009; Available from: www.lowdosenaltrexone.org/.

86. Kranzler, H.R., V. Modesto-Lowe, and J. Van Kirk, *Naltrexone vs. nefazodone for treatment of alcohol dependence. A placebo-controlled trial.* Neuropsychopharmacology, 2000. **22**(5): p. 493-503.

87. Terenius, L., *Rational treatment of addiction.* Curr Opin Chem Biol, 1998. **2**(4): p. 541-7.

88. Rothenberg Jami, L., et al., *Behavioral naltrexone therapy: an integrated treatment for opiate dependence.* J Subst Abuse Treat, 2002. **23**(4): p. 351-60.

89. Comer, S.D., et al., *Injectable, sustained-release naltrexone for the treatment of opioid dependence: a randomized, placebo-controlled trial.* Arch Gen Psychiatry, 2006. **63**(2): p. 210-8.

90. Galloway Gantt, P., et al., *Pharmacokinetics, safety, and tolerability of a depot formulation of naltrexone in alcoholics: an open-label trial.* BMC Psychiatry, 2005. **5**: p. 18.

91. Sullivan Maria, A., K. Vosburg Suzanne, and D. Comer Sandra, *Depot naltrexone: antagonism of the reinforcing, subjective, and physiological effects of heroin.* Psychopharmacology (Berl), 2006. **189**(1): p. 37-46.

92. Garbutt, J.C., et al., *Efficacy and tolerability of long-acting injectable naltrexone for alcohol dependence: a randomized controlled trial.* JAMA, 2005. **293**(13): p. 1617-25.

93. O'Brien, B. and C. Cody, *Analgesia and sedation in the presence of a naltrexone implant: a novel pharmacological challenge.* 2006: England: United Kingdom. p. 315-6.

94.   Kruptisky, E.M., et al., *Overcoming opioid blockade from depot naltrexone (Prodetoxon).* 2007, St Petersburg Regional Center in Addiction and Psychopharmacology affiliated with Pavlov State Medical University, St Petersburg, Russia: England: United Kingdom. p. 1164-5.

95.   Valiveti, S., et al., *In vivo evaluation of 3-O-alkyl ester transdermal prodrugs of naltrexone in hairless guinea pigs.* Journal of Controlled Release, 2005. **102**(2): p. 509-520.

96.   Vaddi, H.K., et al., *Human skin permeation of 3-O-alkyl carbamate prodrugs of naltrexone.* J. Pharm. Sci., 2009. **98**(8): p. 2611-2625.

97.   Paudel, K.S., et al., *Challenges and opportunities in dermal/transdermal delivery.* Ther Deliv, 2010. **1**(1): p. 109-131.

98.   Milewski, M., N.K. Brogden, and A.L. Stinchcomb, *Current aspects of formulation efforts and pore lifetime related to microneedle treatment of skin.* Expert Opinion on Drug Delivery, 2010. **7**(5): p. 617-629.

99.   Thong, H.Y., H. Zhai, and H.I. Maibach, *Percutaneous penetration enhancers: An overview.* Skin Pharmacol. Physiol., 2007. **20**(6): p. 272-282.

100.   Albery, W.J. and J. Hadgraft, *Percutaneous absorption: in vivo experiments.* J. Pharm. Pharmacol., 1979. **31**(3): p. 140-7.

101.   Tojo, K., *Random brick model for drug transport across stratum corneum.* J. Pharm. Sci., 1987. **76**(12): p. 889-91.

102.   Goffin, V., et al., *Penetration enhancers assessed by corneoxenometry.* Skin Pharmacol. Appl. Skin Physiol., 2000. **13**(5): p. 280-284.

103.   Barry, B.W., *Lipid-protein-partitioning theory of skin penetration enhancement.* J. Controlled Release, 1991. **15**(3): p. 237-48.

104. Karande, P., et al., *Design principles of chemical penetration enhancers for transdermal drug delivery.* Proc. Natl. Acad. Sci. U. S. A., 2005. **102**(13): p. 4688-4693.

105. Kogan, A. and N. Garti, *Microemulsions as transdermal drug delivery vehicles.* Adv. Colloid Interface Sci., 2006. **123-126**: p. 369-385.

106. Karande, P., A. Jain, and S. Mitragotri, *Discovery of transdermal penetration enhancers by high-throughput screening.* Nat Biotechnol, 2004. **22**(2): p. 192-7.

107. Karande, P., A. Jain, and S. Mitragotri, *Insights into synergistic interactions in binary mixtures of chemical permeation enhancers for transdermal drug delivery.* J. Controlled Release, 2006. **115**(1): p. 85-93.

108. Hamilton, J.G., *Needle phobia: a neglected diagnosis.* J Fam Pract, 1995. **41**(2): p. 169-75.

109. Burkoth, T.L., et al., *Transdermal and transmucosal powdered drug delivery.* Crit Rev Ther Drug Carrier Syst, 1999. **16**(4): p. 331-84.

110. Schramm, J. and S. Mitragotri, *Transdermal Drug Delivery by Jet Injectors: Energetics of Jet Formation and Penetration.* Pharm. Res., 2002. **19**(11): p. 1673-1679.

111. Bremseth, D.L. and F. Pass, *Delivery of insulin by jet injection: recent observations.* Diabetes Technol. Ther., 2001. **3**(2): p. 225-232.

112. Denne, J.R., et al., *A survey of patient preference for insulin jet injectors versus needle and syringe.* Diabetes Educ, 1992. **18**(3): p. 223-7.

113. Dean Hansi, J., D. Fuller, and E. Osorio Jorge, *Powder and particle-mediated approaches for delivery of DNA and protein vaccines into the epidermis.* Comp Immunol Microbiol Infect Dis, 2003. **26**(5-6): p. 373-88.

114. Spencer James, M., *Microdermabrasion.* Am J Clin Dermatol, 2005. **6**(2): p. 89-92.

115. Fang, J.Y., et al., *Enhancement of topical 5-aminolaevulinic acid delivery by erbium:YAG laser and microdermabrasion: a comparison with iontophoresis and electroporation.* Br J Dermatol, 2004. **151**(1): p. 132-40.

116. Fujimoto, T., K. Shirakami, and K. Tojo, *Effect of microdermabrasion on barrier capacity of stratum corneum.* Chem. Pharm. Bull., 2005. **53**(8): p. 1014-1016.

117. Gill, H.S., et al., *Selective removal of stratum corneum by microdermabrasion to increase skin permeability.* Eur. J. Pharm. Sci., 2009. **38**(2): p. 95-103.

118. Park, J.-H., et al., *The effect of heat on skin permeability.* International Journal of Pharmaceutics, 2008. **359**(1-2): p. 94-103.

119. Lee, W.R., et al., *Transdermal drug delivery enhanced and controlled by erbium:YAG laser: a comparative study of lipophilic and hydrophilic drugs.* J. Controlled Release, 2001. **75**(1-2): p. 155-166.

120. Nelson, J.S., et al., *Mid-infrared laser ablation of stratum corneum enhances in vitro percutaneous transport of drugs.* J Invest Dermatol, 1991. **97**(5): p. 874-9.

121. Gomez, C., et al., *Laser treatments on skin enhancing and controlling transdermal delivery of 5-fluorouracil.* Lasers Surg Med, 2008. **40**(1): p. 6-12.

122. Riviere, J.E. and M.C. Heit, *Electrically-assisted transdermal drug delivery.* Pharm. Res., 1997. **14**(6): p. 687-697.

123. Warwick, W.J., et al., *Evaluation of a cystic fibrosis screening system incorporating a miniature sweat stimulator and disposable chloride sensor.* Clin Chem, 1986. **32**(5): p. 850-3.

124. Squire, S.J., K.T. Kirchhoff, and K. Hissong, *Comparing two methods of topical anesthesia used before intravenous cannulation in pediatric patients.* J Pediatr Health Care, 2000. **14**(2): p. 68-72.

125. Patel, S.R., et al., *Controlled non-invasive transdermal iontophoretic delivery of zolmitriptan hydrochloride in vitro and in vivo.* Eur. J. Pharm. Biopharm., 2009. **72**(2): p. 304-309.

126. Nakamura, K., et al., *Transdermal administration of salmon calcitonin by pulse depolarization-iontophoresis in rats.* Int. J. Pharm., 2001. **218**(1-2): p. 93-102.

127. Pillai, O. and R. Panchagnula, *Transdermal delivery of insulin from poloxamer gel: ex vivo and in vivo skin permeation studies in rat using iontophoresis and chemical enhancers.* J. Controlled Release, 2003. **89**(1): p. 127-140.

128. Rastogi, S.K. and J. Singh, *Transepidermal transport enhancement of insulin by lipid extraction and iontophoresis.* Pharm. Res., 2002. **19**(4): p. 427-433.

129. Suzuki, Y., et al., *Prevention of bone loss in ovariectomized rats by pulsatile transdermal iontophoretic administration of human PTH(1-34).* J. Pharm. Sci., 2002. **91**(2): p. 350-361.

130. Nair, V. and R. Panchagnula, *Physicochemical considerations in the iontophoretic delivery of a small peptide: in vitro studies using arginine vasopressin as a model peptide.* Pharmacol. Res., 2003. **48**(2): p. 175-182.

131. Galinkin, J.L., et al., *Lidocaine iontophoresis versus eutectic mixture of local anesthetics (EMLA((R))) for IV placement in children.* Anesthesia and analgesia, 2002. **94**(6): p. 1484-1488.

132. Runeson, L. and E. Haker, *Iontophoresis with cortisone in the treatment of lateral epicondylalgia (tennis elbow) - a double-blind study.* Scandinavian Journal of Medicine & Science in Sports, 2002. **12**(3): p. 136-142.

133. Gupta, S.K., et al., *Fentanyl delivery from an electrotransport system: Delivery is a function of total current, not duration of current.* Journal of Clinical Pharmacology, 1998. **38**(10): p. 951-958.

134. Singh, J., et al., *Regional variations in skin barrier function and cutaneous irritation due to iontophoresis in human subjects.* Food and Chemical Toxicology, 2001. **39**(11): p. 1079-1086.

135. *Drugs at FDA.* Available from: http://www.accessdata.fda.gov/Scripts/cder/Drugsatfda/.

136. Prausnitz, M.R., *A practical assessment of transdermal drug delivery by skin electroporation.* Advanced Drug Delivery Reviews, 1999. **35**(1): p. 61-76.

137. Denet, A.R. and V. Preat, *Transdermal delivery of timolol by electroporation through human skin.* Journal of Controlled Release, 2003. **88**(2): p. 253-262.

138. Zewert, T.E., et al., *Creation of transdermal pathways for macromolecule transport by skin electroporation and a low toxicity, pathway-enlarging molecule.* Bioelectrochemistry and Bioenergetics, 1999. **49**(1): p. 11-20.

139. Mitragotri, S., *Effect of therapeutic ultrasound on partition and diffusion coefficients in human stratum corneum.* Journal of Controlled Release, 2001. **71**(1): p. 23-29.

140. Tang, H., et al., *An investigation of the role of cavitation in low-frequency ultrasound-mediated transdermal drug transport.* Pharmaceutical Research, 2002. **19**(8): p. 1160-1169.

141. Mitragotri, S., D. Blankschtein, and R. Langer, *Transdermal drug delivery using low-frequency sonophoresis.* Pharmaceutical Research, 1996. **13**(3): p. 411-420.

142. Mitragotri, S., D. Blankschtein, and R. Langer, *Ultrasound-mediated transdermal protein delivery.* Science, 1995. **269**(5225): p. 850-3.

143. Mitragotri, S., et al., *Mechanistic study of ultrasonically-enhanced transdermal drug delivery.* Journal of Pharmaceutical Sciences, 1995. **84**(6): p. 697-706.

144. Mitragotri, S., et al., *Determination of threshold energy dose for ultrasound-induced transdermal drug transport.* Journal of Controlled Release, 2000. **63**(1-2): p. 41-52.

145. Mikszta, J.A., et al., *Improved genetic immunization via micromechanical disruption of skin-barrier function and targeted epidermal delivery.* Nat Med, 2002. **8**(4): p. 415-9.

146. Arora, A., M.R. Prausnitz, and S. Mitragotri, *Micro-scale devices for transdermal drug delivery.* Int J Pharm, 2008. **364**(2): p. 227-36.

147. Prausnitz, M.R. and R. Langer, *Transdermal drug delivery.* Nat Biotechnol, 2008. **26**(11): p. 1261-8.

148. Davis, S.P., et al., *Insertion of microneedles into skin: measurement and prediction of insertion force and needle fracture force.* J Biomech, 2004. **37**(8): p. 1155-63.

149. Banga, A.K., *Microporation applications for enhancing drug delivery.* Expert Opin Drug Deliv, 2009. **6**(4): p. 343-54.

150. Verbaan, F.J., et al., *Improved piercing of microneedle arrays in dermatomed human skin by an impact insertion method.* J Control Release, 2008. **128**(1): p. 80-8.

151. Al-Qallaf, B. and D.B. Das, *Optimizing microneedle arrays to increase skin permeability for transdermal drug delivery.* Ann N Y Acad Sci, 2009. **1161**: p. 83-94.

152. Henry, S., et al., *Microfabricated Microneedles: A Novel Approach to Transdermal Drug Delivery.* Journal of Pharmaceutical Sciences, 1998. **87**(8): p. 922-925.

153. Sullivan, S.P., N. Murthy, and M.R. Prausnitz, *Minimally invasive protein delivery with rapidly dissolving polymer microneedles.* Adv. Mater. (Weinheim, Ger.), 2008. **20**(5): p. 933-938.

154. Lanke, S.S.S., et al., *Enhanced transdermal delivery of low molecular weight heparin by barrier perturbation.* Int. J. Pharm., 2009. **365**(1-2): p. 26-33.

155. Banks, S.L., et al., *Transdermal Delivery of Naltrexol and Skin Permeability Lifetime after Microneedle Treatment in Hairless Guinea Pigs In Vivo.* Journal of Pharmaceutical Sciences, 2010. **In press**.

156. Cross, S.E. and M.S. Roberts, *Physical enhancement of transdermal drug application: Is delivery technology keeping up with pharmaceutical development?* Current Drug Delivery, 2004. **1**(1): p. 81-92.

157. Kost, J., et al., *Synergistic effect of electric field and ultrasound on transdermal transport.* Pharmaceutical Research, 1996. **13**(4): p. 633-638.

158. Riviere, J.E., et al., *Pulsatile transdermal delivery of LHRH using electroporation - drug delivery and skin toxicology.* Journal of Controlled Release, 1995. **36**(3): p. 229-233.

159. Chang, S.L., et al., *The effect of electroporation on iontophoretic transdermal delivery of calcium regulating hormones.* Journal of Controlled Release, 2000. **66**(2-3): p. 127-133.

160. Chen, H., et al., *Iontophoresis-driven penetration of nanovesicles through microneedle-induced skin microchannels for enhancing transdermal delivery of insulin.* J Control Release, 2009. **139**(1): p. 63-72.

161. Kiptoo, P.K., et al., *In vivo evaluation of a transdermal codrug of 6-beta-naltrexol linked to hydroxybupropion in hairless guinea pigs.* Eur. J. Pharm. Sci., 2008. **33**(4-5): p. 371-379.

162. Kiptoo, P.K., et al., *Transdermal delivery of bupropion and its active metabolite, hydroxybupropion: a prodrug strategy as an alternative approach.* J. Pharm. Sci., 2009. **98**(2): p. 583-594.

163. Pillai, O., et al., *Physicochemical Evaluation, in Vitro Human Skin Diffusion, and Concurrent Biotransformation of 3-O-Alkyl Carbonate Prodrugs of Naltrexone.* Pharmaceutical Research, 2004. **21**(7): p. 1146-1152.

164. Vaddi, H.K., et al., *Human Skin Permeation of Branched-Chain 3-O-Alkyl Ester and Carbonate Prodrugs of Naltrexone.* Pharmaceutical Research, 2005. **22**(5): p. 758-765.

165. Qandil, A., et al., *Synthesis of piperazinylalkyl ester prodrugs of ketorolac and their in vitro evaluation for transdermal delivery.* Drug Development and Industrial Pharmacy, 2008. **34**(10): p. 1054-1063.

166. Kushnir, M., et al., *Transdermal delivery of a levodopa prodrug; a pilot clinical trial.* Movement Disorders, 2008. **23**: p. 592.

167. Thomas, J.D., S. Majumdar, and K.B. Sloan, *Soft alkyl ether prodrugs of a model phenolic drug: the effect of incorporation of ethyleneoxy groups on transdermal delivery.* Molecules, 2009. **14**(10): p. 4231-4245.

168. Potts, R.O. and R.H. Guy, *Predicting skin permeability.* Pharmaceutical Research, 1992. **9**(5): p. 663-669.

169. Yalkowsky, S.H. and S.C. Valvani, *Solubility and partitioning. I: Solubility of nonelectrolytes in water.* J. Pharm. Sci., 1980. **69**(8): p. 912-22.

170. Jain, N. and S.H. Yalkowsky, *Estimation of the aqueous solubility I: Application to organic nonelectrolytes.* Journal of Pharmaceutical Sciences, 2001. **90**(2): p. 234-252.

171. Bronaugh, R.L. and C.N. Barton, *Prediction of human percutaneous absorption with physicochemical data.* Health Risk Assess., 1993: p. 117-26.

172. Brown, S.L. and J.E. Rossi, *A simple method for estimating dermal absorption of chemicals in water.* Chemosphere, 1989. **19**(12): p. 1989-2001.

173. Cleek, R.L. and A.L. Bunge, *A new method for estimating dermal absorption from chemical exposure. 1. General approach.* Pharmaceutical Research, 1993. **10**(4): p. 497-506.

174. McKone, T.E. and R.A. Howd, *Estimating dermal uptake of nonionic organic chemicals from water and soil. 1. Unified fugacity-based models for risk assessments.* Risk Analysis, 1992. **12**(4): p. 543-557.

175. El Tayar, N., et al., *Percutaneous penetration of drugs - a quantitative structure-permeability realationship study.* Journal of Pharmaceutical Sciences, 1991. **80**(8): p. 744-749.

176. Fiserova-Bergerova, V., J.T. Pierce, and P.O. Droz, *Dermal absorption potential of industrial chemicals - criteria for skin notation.* American Journal of Industrial Medicine, 1990. **17**(5): p. 617-635.

177. Potts, R.O. and R.H. Guy, *A predictive algorythm for skin permeability - the effects of molecular size and hydrogen-bond activity.* Pharmaceutical Research, 1995. **12**(11): p. 1628-1633.

178. Vecchia, B.E., *Estimating the dermally absorbed dose from chemical exposure: data analysis, parameter estimation, and sensitivity to parameter uncertainties.* 1997, Colorado School of Mines: Golden, CO.

179. Lieb, W.R. and W.D. Stein, *Biological membranes behave as nonporous polymeric sheets with respect to the diffusion of nonelectrolytes.* Nature (London), 1969. **224**(5216): p. 240-3.

180. Diamond, J.M. and Y. Katz, *Interpretation of nonelectrolyte partition coefficients between dimyristoyl lecithin and water.* J. Membrane Biol., 1974. **17**(2): p. 121-54.

181. Bean, H.S., et al., *Advances in Pharmaceutical Sciences, Vol. 4.* 1974. 444.

182. Anderson, B.D. and P.V. Raykar, *Solute structure-permeability relationships in human stratum corneum.* Journal of Investigative Dermatology, 1989. **93**(2): p. 280-6.

183. Itoh, T., et al., *A method to predict the percutaneous permeability of various compounds - shed snake skin as a model membrane.* Pharmaceutical Research, 1990. **7**(12): p. 1302-1306.

184. Cohen, M.H. and D. Turnbull, *Molecular transport in liquids and glasses.* J. Chem. Phys., 1959. **31**: p. 1164-9.

185. Shroot, B., H. Schaefer, and Editors, *Pharmacology and the Skin, Vol. 1: Skin Pharmacokinetics.* 1987. 264.

186. Lieb, W.R. and W.D. Stein, *Non-Stokesian nature of transverse diffusion within human red-cell membranes.* J. Membrane Biol., 1986. **92**(2): p. 111-119.

187. Guy, R.H., J. Hadgraft, and Editors, *Transdermal Drug Delivery: Second Edition, Revised and Expanded. [In: Drugs Pharm. Sci., 2003; 123].* 2003. 383 pp.

188. Hildebrand, J.H., J.M. Prausnitz, and R.L. Scott, *Regular and Related Solutions. The Solubility of Gases, Liquids, and Solids.* 1970. 228 pp.

189. Fung, H.-L. and T. Higuchi, *Molecular interactions and solubility of polar nonelectrolytes in nonpolar solvents.* J. Pharm. Sci., 1971. **60**(12): p. 1782-8.

190. Hansen, C.M., *Hansen Solubility Parameters: A User's Handbook.* 2007. 519 pp.

191. Bustamante, P., et al., *Predicting the solubility of sulfamethoxypyridazine in individual solvents I: calculating partial solubility parameters.* J. Pharm. Sci., 1989. **78**(7): p. 567-73.

192. Abraham, M.H. and J. Le, *The correlation and prediction of the solubility of compounds in water using an amended solvation energy relationship.* J. Pharm. Sci., 1999. **88**(9): p. 868-880.

193. Kamlet, M.J., et al., *Linear solvation energy relationships: 36. Molecular properties governing solubilities of organic nonelectrolytes in water.* J. Pharm. Sci., 1986. **75**(4): p. 338-49.

194. Kuehne, R., et al., *Group contribution methods to estimate water solubility of organic chemicals.* Chemosphere, 1995. **30**(11): p. 2061-77.

195. Mitchell, B.E. and P.C. Jurs, *Prediction of aqueous solubility of organic compounds from molecular structure.* J. Chem. Inf. Comput. Sci., 1998. **38**(3): p. 489-496.

196. Magnusson, B.M., et al., *Molecular size as the main determinant of solute maximum flux across the skin.* J. Invest. Dermatol., 2004. **122**(4): p. 993-999.

197. Sloan, K.B., S.C. Wasdo, and J. Rautio, *Design for Optimized Topical Delivery: Prodrugs and a Paradigm Change.* Pharmaceutical Research, 2006. **23**(12): p. 2729-2747.

198. Majumdar, S., et al., *The effect of water solubility of solutes on their flux through human skin in vitro.* Int. J. Pharm., 2007. **329**(1-2): p. 25-36.

199. Juntunen, J., S. Majumdar, and K.B. Sloan, *The effect of water solubility of solutes on their flux through human skin in vitro: A prodrug database integrated into the extended Flynn database.* International Journal of Pharmaceutics, 2008. **351**(1-2): p. 92-103.

200. Scheuplein, R.J. and I.H. Blank, *Mechanism of percutaneous absorption. IV. Penetration of nonelectrolytes (alcohols) from aqueous solutions and from pure liquids.* J. Invest. Dermatol., 1973. **60**(5): p. 286-96.

201. Edwards, D.A. and R. Langer, *A Linear Theory of Transdermal Transport Phenomena.* J. Pharm. Sci., 1994. **83**(9): p. 1315-34.

202. Johnson, M.E., D. Blankschtein, and R. Langer, *Evaluation of Solute Permeation Through the Stratum Corneum: Lateral Bilayer Diffusion as the Primary Transport Mechanism.* J. Pharm. Sci., 1997. **86**(10): p. 1162-1172.

203. Talreja, P.S., et al., *Visualization of the lipid barrier and measurement of lipid pathlength in human stratum corneum.* PharmSci, 2001. **3**(2).

204. Frasch, H.F. and A.M. Barbero, *Steady-state flux and lag time in the stratum corneum lipid pathway: Results from finite element models.* J. Pharm. Sci., 2003. **92**(11): p. 2196-2207.

205. Higuchi, T., *Physical chemical analysis of percutaneous absorption process from creams and ointments.* Journal of the Society of Cosmetic Chemists, 1960. **11**: p. 85-97.

206. Kretsos, K. and B. Kasting Gerald, *A geometrical model of dermal capillary clearance.* Math Biosci, 2007. **208**(2): p. 430-53.

207. Sznitowska, M., B. Berner, and H.I. Maibach, *In vitro permeation of human skin by multipolar ions.* International Journal of Pharmaceutics, 1993. **99**(1): p. 43-9.

208. Cordero, J.A., et al., *A Comparative Study of the Transdermal Penetration of a Series of Nonsteroidal Antiinflammatory Drugs.* J. Pharm. Sci., 1997. **86**(4): p. 503-508.

209. Hadgraft, J. and C. Valenta, *pH, pKa and dermal delivery.* Int. J. Pharm., 2000. **200**(2): p. 243-247.

210. Gill, H.S. and M.R. Prausnitz, *Coated microneedles for transdermal drug delivery.* AIChE Annual Meeting, Conference Proceedings, San Francisco, CA, United States, Nov. 12-17, 2006, 2006: p. 543e/1-543e/2.

211. Banks S, P.K., Stinchcomb A, Loftin C, *COX enzyme inhibitor enables drug delivery through microneedle treated skin for seven days.* AAPS Journal, 2008. **10**(S2).

212. Kolli, C.S. and A.K. Banga, *Characterization of solid maltose microneedles and their use for transdermal delivery.* Pharm Res, 2008. **25**(1): p. 104-13.

213. Coulman, S.A., et al., *Minimally invasive cutaneous delivery of macromolecules and plasmid DNA via microneedles.* Current Drug Delivery, 2006. **3**(1): p. 65-75.

214. Meyer, M.C., et al., *Bioequivalence, dose-proportionality, and pharmacokinetics of naltrexone after oral administration.* J. Clin. Psychiatry, 1984. **45**(9, Sect. 2): p. 15-19.

215. Wall, M.E., D.R. Brine, and M. Perez-Reyes, *Metabolism and disposition of naltrexone in man after oral and intravenous administration.* Drug Metab. Dispos., 1981. **9**(4): p. 369-75.

216. Wermeling, D.P., et al., *Microneedles permit transdermal delivery of a skin-impermeant medication to humans.* Proceedings of the National Academy of Sciences of the United States of America, 2008. **105**(6): p. 2058-2063.

217. Badran, M.M., J. Kuntsche, and A. Fahr, *Skin penetration enhancement by a microneedle device (Dermaroller) in vitro: Dependency on needle size and applied formulation.* Eur. J. Pharm. Sci., 2009. **36**(4-5): p. 511-523.

218. Osborne, D.W. and J.J. Heneke, *Skin penetration enhancers cited in the technical literature.* Pharmaceutical technology 1997. **21**(11): p. 58-66.

219. Barry, B.W., *Mode of action of penetration enhancers in human skin.* J. Controlled Release, 1987. **6**: p. 85-97.

220. Goodman, M. and B.W. Barry, *Action of penetration enhancers on human skin as assessed by the permeation of model drugs 5-fluorouracil and estradiol. I. Infinite dose technique.* J. Invest. Dermatol., 1988. **91**(4): p. 323-7.

221. Megrab, N.A., A.C. Williams, and B.W. Barry, *Estradiol permeation through human skin and silastic membrane: effects of propylene glycol and supersaturation.* Journal of Controlled Release, 1995. **36**(3): p. 277-94.

222. Trottet, L., et al., *Effect of finite doses of propylene glycol on enhancement of in vitro percutaneous permeation of loperamide hydrochloride.* Int J Pharm, 2004. **274**(1-2): p. 213-9.

223. Herkenne, C., et al., *Effect of propylene glycol on ibuprofen absorption into human skin in vivo.* Journal of Pharmaceutical Sciences, 2007. **97**(1): p. 185-197.

224. Watkinson, R.M., et al., *Optimisation of Cosolvent Concentration for Topical Drug Delivery - II: Influence of Propylene Glycol on Ibuprofen Permeation.* Skin Pharmacol. Physiol., 2009. **22**(4): p. 225-230.

225. Hussain, M.A., et al., *Improvement of the oral bioavailability of naltrexone in dogs: a prodrug approach.* J. Pharm. Sci., 1987. **76**(5): p. 356-8.

226. Kaufman, J.J., N.M. Semo, and W.S. Koski, *Microelectrometric titration measurement of the pKa's and partition and drug distribution coefficients of narcotics and narcotic antagonists and their pH and temperature dependence.* Journal of Medicinal Chemistry, 1975. **18**(7): p. 647-55.

227. Sugano, K., et al., *Prediction of passive intestinal absorption using bio-mimetic artificial membrane permeation assay and the paracellular pathway model.* Int. J. Pharm., 2002. **241**(2): p. 241-251.

228. Zhao, G. and S.B. Chen, *Microviscosity of hydrophobically modified hydroxyethyl cellulose aqueous solutions.* J Colloid Interface Sci, 2008. **322**(2): p. 678-80.

229. Milewski, M., et al., *In vitro permeation of a PEGylated naltrexone prodrug across microneedle-treated skin.* Journal of Controlled Release, 2010. **146**(1): p. 37-44.

230. Elias PM, F.K., Fluhr JW, *Fitzpatrick's Dermatology in General Medicine*, E.A. Freedberg IM, Wolff K, Austen KF, Goldsmith LA, Katz SI, Editor. 2003, Mc-Graw Hill: New York.

231. Valiveti, S., et al., *In Vitro/in Vivo Correlation of Transdermal Naltrexone Prodrugs in Hairless Guinea Pigs.* Pharmaceutical Research, 2005. **22**(6): p. 981-989.

232. Bruckdorfer, T., *PEGylation - a key technology to improve solubility and pharmacokinetic of peptides, proteins and other biopharmaceuticals for superior drug delivery.* Biopolymers, 2009. **92**(4): p. 337-337.

233. Riley, T. and J. Riggs-Sauthier, *The benefits and challenges of PEGylating small molecules.* Pharmaceutical Technology, 2008. **32**(7): p. 88, 90-92, 94.

234. Basu, A., et al., *Structure-function engineering of interferon-beta-1b for improving stability, solubility, potency, immunogenicity, and pharmacokinetic properties by site-selective mono-PEGylation.* Bioconjugate Chemistry, 2006. **17**(3): p. 618-630.

235. Harris, J.M. and R.B. Chess, *Effect of PEGylation on pharmaceuticals.* Nature Reviews Drug Discovery, 2003. **2**(3): p. 214-221.

236. Veronese, F.M. and G. Pasut, *PEGylation, successful approach to drug delivery.* Drug Discovery Today, 2005. **10**(21): p. 1451-1458.

237. N'Da, D.D. and J.C. Breytenbach, *Synthesis of methoxypoly(ethylene glycol) carbonate prodrugs of zidovudine and penetration through human skin in vitro.* Journal of Pharmacy and Pharmacology, 2009. **61**(6): p. 721-731.

238. Yerramreddy, T.R., et al., *Novel 3-O-pegylated carboxylate and 3-O-pegylated carbamate prodrugs of naltrexone for microneedle-enhanced transdermal delivery.* Bioorg. Med. Chem. Lett., 2010. **20**(11): p. 3280-3283.

239. Wester, R.C., et al., *Human cadaver skin viability for in vitro percutaneous absorption: Storage and detrimental effects of heat-separation and freezing.* Pharmaceutical Research, 1998. **15**(1): p. 82-84.

240. Messager, S., et al., *Assessment of skin viability: is it necessary to use different methodologies?* Skin Research and Technology, 2003. **9**(4): p. 321-330.

241. Shaikh, N.A., J.I. Ademola, and H.I. Maibach, *Effects of freezing and azide treatment of in vitro human skin on the flux and metabolism of 8-methoxypsoralen.* Skin Pharmacology, 1996. **9**(4): p. 274-280.

242. Ahlstrom, L.A., S.E. Cross, and P.C. Mills, *The effects of freezing skin on transdermal drug penetration kinetics.* Journal of Veterinary Pharmacology and Therapeutics, 2007. **30**(5): p. 456-463.

243. Babu, R.J., et al., *The influence of various methods of cold storage of skin on the permeation of melatonin and nimesulide.* Journal of Controlled Release, 2003. **86**(1): p. 49-57.

244. Moody, R.P., A. Yip, and I. Chu, *Effect of Cold Storage on In Vitro Human Skin Absorption of Six 14C-Radiolabeled Environmental Contaminants: Benzo[a]Pyrene, Ethylene Glycol, Methyl Parathion, Naphthalene, Nonyl Phenol, and Toluene.* Journal of Toxicology and Environmental Health-Part a-Current Issues, 2009. **72**(8): p. 505-517.

245. Chilcott, R.P., B. Stubbs, and Z. Ashley, *Habituating pigs for in-pen, non-invasive biophysical skin analysis.* Lab Anim, 2001. **35**(3): p. 230-5.

246. Gendimenico, G.J., et al., *Evaluation of topical retinoids for cutaneous pharmacological activity in Yucatan microswine.* Arch. Dermatol. Res., 1995. **287**(7): p. 675-9.

247. Kanikkannan, N., et al., *Percutaneous permeation and skin irritation of JP-8+100 jet fuel in a porcine model.* Toxicol. Lett., 2001. **119**(2): p. 133-142.

248. Yosipovitch, G., et al., *Time-dependent variations of the skin barrier function in humans: transepidermal water loss, stratum corneum hydration, skin surface pH, and skin temperature.* J Invest Dermatol, 1998. **110**(1): p. 20-3.

249. Firooz, A., et al., *Comparison of hydration, sebum and pH values in clinically normal skin of patients with atopic dermatitis and healthy controls.* Clin Exp Dermatol, 2007. **32**(3): p. 321-2.

250. Buraczewska, I., *Outside and inside skin pH.* Dry Skin Moisturizers (2nd Ed.), 2006: p. 161-169.

251. Ohman, H. and A. Vahlquist, *The pH gradient over the stratum corneum differs in X-linked recessive and autosomal dominant ichthyosis: a clue to the molecular origin of the "acid skin mantle"?* J. Invest. Dermatol., 1998. **111**(4): p. 674-677.

252. Chirife, J. and M.P. Buera, *A Simple Model for Predicting the Viscosity of Sugar and Oligosaccharide Solutions.* Journal of Food Engineering, 1997(33): p. 221-226.

253. Dittert, H., *Rates of hydrolysis of carbamate and carbonate esters in alkaline solution.* J. Pharm. Sci., 1963. **52**: p. 852-857.

254. Milewski, M., N.K. Brogden, and A.L. Stinchcomb, *Current aspects of formulation efforts and pore lifetime related to microneedle treatment of skin.* Expert Opinion on Drug Delivery. **7**(5): p. 617-629.

255. Milewski, M. and A.L. Stinchcomb, *Vehicle composition influence on the microneedle-enhanced transdermal flux of naltrexone hydrochloride.* Pharm Res, 2010. **In press**.

256. Serajuddin, A.T.M., *Salt formation to improve drug solubility.* Advanced Drug Delivery Reviews, 2007. **59**(7): p. 603-616.

257. *Alpha Hydroxy Acids in Cosmetics.* 2009 [cited 2009; Available from: http://www.fda.gov/cosmetics/productandingredientsafety/selectedcosmeticingredients/ucm107940.htm.

258. Andersen, F., et al., *The hairless guinea-pig as a model for treatment of cumulative irritation in humans.* Skin Research and Technology, 2006. **12**(1): p. 60-67.

259. Andersen, F., et al., *The hairless guinea-pig as a model for treatment of acute irritation in humans.* Skin Research and Technology, 2006. **12**(3): p. 183-189.

260. Tenjarla, S.N., et al., *Evaluating the irritaiton potential of skin penetration enhancers in the hairless guinea pig.* Journal of Toxicology-Cutaneous and Ocular Toxicology, 1995. **14**(4): p. 299-307.

261. Birchall, J., et al., *Cutaneous DNA delivery and gene expression in ex vivo human skin explants via wet-etch microfabricated microneedles.* Journal of Drug Targeting, 2005. **13**(7): p. 415-421.

262. Li, G., et al., *In vitro transdermal delivery of therapeutic antibodies using maltose microneedles.* Int J Pharm, 2009. **368**(1-2): p. 109-15.

263. Yan, G., et al., *Evaluation needle length and density of microneedle arrays in the pretreatment of skin for transdermal drug delivery.* Int. J. Pharm., 2010. **391**(1-2): p. 7-12.

264. Banks, S.L., et al., *Diclofenac Enables Prolonged Delivery of Naltrexone Through Microneedle-Treated Skin.* Pharm Res, 2011.

265. So, J.-W., et al., *Effect of microneedle on the pharmacokinetics of ketoprofen from its transdermal formulations.* Drug Delivery, 2009. **16**(1): p. 52-56.

266. Kalluri, H. and A.K. Banga, *Formation and closure of microchannels in skin following microporation.* Pharm Res, 2011. **28**(1): p. 82-94.

267. Bal, S., et al., *In vivo visualization of microneedle conduits in human skin using laser scanning microscopy.* Laser Phys. Lett., 2009. **7**(3): p. 242-246.

268. Menon, G.K., K.R. Feingold, and P.M. Elias, *Lamellar body secretory response to barrier disruption.* J Invest Dermatol, 1992. **98**(3): p. 279-89.

269. Karande, P., A. Jain, and S. Mitragotri, *Relationships between skin's electrical impedance and permeability in the presence of chemical enhancers.* J. Controlled Release, 2006. **110**(2): p. 307-313.

270. Coulman, S.A., et al., *In vivo, in situ imaging of microneedle insertion into the skin of human volunteers using optical coherence tomography.* Pharm Res, 2011. **28**(1): p. 66-81.

271. Kretsos, K., G.B. Kasting, and J.M. Nitsche, *Distributed diffusion-clearance model for transient drug distribution within the skin.* J Pharm Sci, 2004. **93**(11): p. 2820-35.

272. Gupta, E., M.G. Wientjes, and J.L.S. Au, *Penetration kinetics of 2',3'-dideoxyinosine in dermis is described by the distributed model.* Pharm. Res., 1995. **12**(1): p. 108-12.

273. Park, J.H., M.G. Allen, and M.R. Prausnitz, *Polymer Microneedles for Controlled-Release Drug Delivery.* Pharm Res, 2006.

274. Banks, S.L., *Transdermal delivery of naltrexone by minimally invasive microneedle array application: Permeation enhancement of a water soluble compound across a lipophilic barrier.* 2008. p. 212 pp.

275. Birchall, J. and K.R. Brain, *Microneedle arrays as transcutaneous delivery devices.* Dermatologic, Cosmeceutic, and Cosmetic Development, 2008: p. 577-589.

Vita

Mikolaj Milewski

Pharmaceutical Sciences PhD candidate

University of Kentucky, College of Pharmacy

Born: August 27, 1979

Birthplace: Ostrow Wlkp., Poland

EDUCATION

University of Medical Sciences in Poznan, College of Pharmacy, ul. Fredry 10, 61-

701 Poznan, Poland

Master of Science in Pharmacy (October 1998 – March 2005)

prof. L. Zaprutko and Dr D. Olender

Master's thesis title: "Reduction reactions of 4,5-dinitroimidazole derivatives"

PROFESSIONAL EXPERIENCE

GlaxoSmithKline Pharmaceuticals, ul. Grunwaldzka 189, 60-322 Poznan, Poland

Analytical Chemist (May 2005 – April 2006)

AWARDS AND HONORS

- **Peter G. Glavinos Jr., Ph.D., Fall Travel Award** recipient 2010

- **American Chemical Society member** (2010 – present)

- **UKY Pharmaceutical Sciences Graduate Program representative** at GPEN

conference 2010

- **Graduate Student Congress** departmental representative (2009 – 2010)

- **Rho Chi Research Day poster session 1st award**: "Microneedle-enhanced transdermal delivery of naltrexone prodrugs" (2009)

- **Kentucky Opportunity Fellowship recipient** (2008-2009)

- **AAPS Dermatopharmaceutics Steering Committee Group member** (2008 – present)

- **University of Kentucky AAPS chapter officer**: historian (2007 – 2010)

- **American Association of Pharmaceutical Scientists (AAPS) member** (2006 – present)

- **Poznan College of Pharmacy scholarship** 2000 – 2001

PUBLICATIONS

- M. Milewski, A. L. Stinchcomb **"Vehicle composition influence on the microneedle-enhanced transdermal flux of naltrexone hydrochloride"** Published in Pharmaceutical Research (2011) Pharm Res 28(1): 124-134.

- M. Milewski, T. Yerramreddy, P. Ghosh, P. A. Crooks, A. L. Stinchcomb **"*In vitro permeation of PEGylated naltrexone prodrug across microneedle-treated skin*"** Published in Journal of Controlled Release (2010) 146(1):37-44

- M. Milewski, N. K. Brogden, A. L. Stinchcomb **"Current aspects of formulation efforts and pore lifetime related to microneedle treatment of skin"** Published in Expert Opinion on Drug Delivery (2010) 7(5):617-629

- T. Yerramreddy, M. Milewski, N. Penthala, A. L. Stinchcomb, Peter A. Crooks **"Novel 3-O-pegylated carboxylate and 3-O-pegylated carbamate prodrugs

of naltrexone for microneedle-enhanced transdermal delivery" Published in Bioorganic & Medicinal Chemistry Letters 2010 Jun 1;20(11):3280-3

- Kalpana S. Paudel, M. Milewski, S. L. Courtney, N. K. Brogden, P. Ghosh, A. L. Stinchcomb **"Challenges and Opportunities in Transdermal Delivery"** Published in Therapeutic Delivery (2010) Jul;1(1):109-131

Mikolaj Milewski

Student's signature

March 23rd, 2011

Date